INVESTIGATION OF MICROWAVE LOSSES AND MINIATURIZATION PARAMETERS OF GARNET FERRITE COMPOSITES FOR ANTENNA APPLICATION

Thesis Submitted For the Award of the Degree of

DOCTOR OF PHILOSOPHY

in

PHYSICS

By

Anjori Sharma

(Reg. No. 11916735)

Supervised By

Dr. A.K. Srivastava

LOVELY PROFESSIONAL UNIVERSITY

PUNJAB

2022

DECLARATION BY THE CANDIDATE

I hereby declare that the thesis entitles "**Investigation of microwave losses and miniaturization parameters of garnet ferrite composites for antenna application"** submitted for award of degree of Doctor of Philosophy in Physics, Lovely Professional University, Phagwara, is my own original work conducted under the supervision of Dr. A. K. Srivastava (Supervisor), Professor in Department of Physics at School of Chemical Engineering and Physical Science, Lovely Professional University, Phagwara, Punjab, India. I further declare that the thesis does not contain any part of any work which has been submitted for the award of any degree in this university or in any other University/Deemed University without proper citation.

Author: **Anjori Sharma**

Reg. number: 11916735

Supervisor: **Dr. A. K. Srivastava**

(Professor)

Lovely Professional University

Phagwara-144411

Punjab, India

CERTIFICATE

This is to certify that the work entitled "**Investigation of microwave losses and miniaturization parameters of garnet ferrite composites for antenna application"** is a piece of research work done by Miss Anjori Sharma under my guidance and supervision for the degree of Doctor of Philosophy in Physics, Lovely Professional University, Phagwara (Punjab) India.

To the best of my knowledge and belief, the thesis:

1. Embodies the work of the candidate herself.
2. Has duly been completed.
3. Fulfils the requirements of the ordinance related to the Ph.D. degree of the university.
4. Is up to the standard both in respect of contents and language for being referred to the examiner.

Supervisor: **Dr. A. K. Srivastava**

(Professor)

Lovely Professional University

Phagwara-144411

Punjab, India

ACKNOWLEDGEMENT

All thanks and glory to Lord Rama, most benevolent and merciful, for giving me the health and financial resources to complete my PhD research. I would like to express my sincere gratitude to my Ph.D. supervisor **Dr. A. K. Srivastava**, Professor, School of Computer Science and Engineering, Lovely Professional University, for accepting me as his student and giving me all the necessary scientific guidance and support required to complete my Ph.D. research. My mother Smt. Kamla Rani has been a vital part of my life right from the moment I came into this world. She has been more than a mother to me, sacrificing her comfort, so that I can achieve greatness in the academic world and beyond. No amounts of words could express my appreciation to you. I just pray to the God to give us more time to spend together so that I can do my best in putting some endless smile on your face. My father Sh. Manoj Kumar has been my backbone at every difficult situation. He has been supportive throughout my entire PhD endeavours. I will be thankful to him. My brother Khushwant Dutt Sharma has always supported me and encouraged me through out by Ph.D. With the blessings of my grandfather Late Sh. Bhagwat Dutt Sharma who has always motivated me to do hard work to achieve big in life. A special thanks to my uncle, Sh. Manish Sharma, aunty, Smt. Raj Sharma, grandmother, Smt. Pushpa Sharma, my cousins Amisha and Arunima. I would like to express my sincere and profound appreciation to my colleagues, Dr. Dipesh, Shakra, Mehar Jyoti, Seema Sharma, Shaveta Sharma, Hamnesh Mahajan, Ibrahim Mohammed, and Owais Amin. A special thanks to my friend Dr. Dipesh without whom it would have really been impossible to carry out this task. He has supported me unconditional over all these years.

A big thanks to the entire staff of Department of Physics, Lovely Professional University for giving words of encouragement. I would like to mention Dr. Kailash Juglan (HOS) for his sincere support and encouragement. My sincere appreciation goes to Dr. Pradip K. Maji (Department of Polymer and Processing Engineering, IIT Roorkee, Saharanpur Campus, U.P. India), Dr. Sachin Kumar Godara (Department of Chemistry, GNDU, Amritsar, India) and Neha Aggarwal (Department of Electronics and Communication, GNDU, Amritsar, India) for providing various supports in characterization.

Author: **Anjori Sharma**

Registration number: 11916735

List of Figures

List of Tables

Abstract

In this era of technology, the researchers are interested to synthesize such nanocomposites that may resolve the major problems of antenna efficiency and miniaturization. The existing materials that are being used for antennas have low efficiency, impedance mismatching, low miniaturization, high dielectric losses and magnetic losses. Many researchers have used and synthesized the dielectric materials with high permittivity in order to tackle with problems related to antennas. But such materials have some problems like the wave present at surface got excited due to which radiation efficiency decreases. Further there is an impedance mismatch between material and signal. Most of the composites that have been used for antenna applications either showed very good results for dielectric properties or either for magnetic properties. But for the better efficiency and miniaturization of antennas, both magnetic as well as dielectric properties must be excellent. Ferrites are ceramic oxides that have good magnetic and dielectric properties. Garnet ferrites are best suitable materials for antenna applications because, it has least dielectric and magnetic loses with high permittivity and permeability. In this research we have synthesized and characterized nanocomposites of garnet ferrites and soft ferrites in order to study the losses and miniaturization parameters for antenna applications. We have also studied the different properties such as structural, optical, dielectric and magnetic properties for garnet ferrites and its composites. In the present research work, the sol-gel auto-combustion method is adopted to synthesize the ferrites. The following mentioned samples of garnet ferrites and its composites have been synthesized and characterized:

- $Gd_3Al_xFe_{5-x}O_{12}$ (x = 2)
- $Gd_3Fe_5O_{12}$ (x) / $MgFe_2O_4$ (1-x) (x = 1.0, 0.5, 0.75)
- $Gd_3Fe_5O_{12}$(x) / $MgFe_2O_4$(1-x) (x = 0.75)
- $Y_{0.2}Bi_{0.2}La_xGd_{2.6-x}Fe_5O_{12}$ (x = 0, 0.2, 0.4)
- ErIG(x) / YIG(1-x) (x = 0.5)
- $Y_3Fe_5O_{12}$(*x*) / $Mg_{0.4}Cd_{0.4}Co_{0.2}Fe_2O_4$ (1-*x*) (*x* = 0.3, 0.6, 0.9)
- $Pr_xGd_{3-x}Fe_5O_{12}$ (x = 0.5,1.0,1.5)

All the prepared samples in the thesis have some specific results at different conditions. These prepared samples have their application for electronic communication devices.

For the study of temperature variation on the garnet ferrites, $Gd_3Al_xFe_{5-x}O_{12}$ (x=2) sample has been chosen and characterized. The research work explores the effect of sintering temperature on morphology and magnetic properties of aluminium substituted gadolinium iron garnet $Gd_3Al_xFe_{5-x}O_{12}$ (x=2). Sol-gel auto combustion method was adopted to prepare $Gd_3Al_xFe_{5-x}O_{12}$, and further sintered at 900°C, 1000°C and 1100°C. X-ray diffraction (XRD) confirms the formation of garnet phase structure. Fourier Transformation Infrared (FTIR) further stands with result of XRD which reveals the presence of garnet phase. Field emission scanning electron microscope (FESEM) analysis shows the formation of average grain size 4, 6 and 13 nm for 900°C, 1000°C and 1100°C for respectively. Vibrating sample magnetometer (VSM) results show that the coercivity decreases with increases in temperature which indicates that this material can be used in switching devices. The calculated value of microwave operating frequency reveals that these materials can be used in Ultra high frequency region.

To study the effect of composition variation on garnet ferrite composites, $Gd_3Fe_5O_{12}$ (x)-$MgFe_2O_4$ (1-x) with x=1, 0.75, 0.5 has been chosen. Sol-gel auto-combustion method was used to prepare $Gd_3Fe_5O_{12}$ and $MgFe_2O_4$. Mechanical blending was used to form the composites of $Gd_3Fe_5O_{12}$ (x)-$MgFe_2O_4$ (1-x) (x = 1.0, 0.5, 0.75 in wt%). X-ray diffraction (XRD) study reveals the pure phase formation of $Gd_3Fe_5O_{12}$ and $MgFe_2O_4$ and the presence of both phases in composites. The average crystallite size lies in the range of 26-56 nm. Field emission scanning electron microscope (FESEM) study reveals that the grains of $Gd_3Fe_5O_{12}$ have a spherical morphology and its composites show agglomeration due to presence of magnetic interaction between ferrites nanoparticles. The dielectric study reveals that the real and imaginary parts of complex permittivity of the composites vary with the change in the composition of $Gd_3Fe_5O_{12}$ and $MgFe_2O_4$. For x = 0.5, the low dielectric tangent loss ($\tan\delta$) ~ 0.35 with high dielectric constant (ε') ~ 612 was obtained at 1 MHz frequency. This suggests the use of these composites for dielectric substrate antennas. Further, the magnetic property reveals that the magnetic parameter of $Gd_3Fe_5O_{12}$ composites varies by addition of $MgFe_2O_4$ i.e., at x = 0.5 and 0.75. The values of microwave operating frequency (ω_m) are 3.5 GHz and 2.5 GHz for x = 0.5 and x = 0.75 respectively. These values suggest that the composites can be used in S-band.

To study the effect of temperature variation on garnet ferrite composites, ($Gd_3Fe_5O_{12}$(x)/$MgFe_2O_4$(1-x) at x=0.75 has been characterized. The composite of gadolinium iron garnet and magnesium ferrite ($Gd_3Fe_5O_{12}$(x)/$MgFe_2O_4$(1-x) at x=0.75)) was successfully prepared by mechanical blending method and sintered at different temperatures (900°C,

1300°C). X-ray diffraction (XRD) study suggests that both the phases of ferrites are present independently in composite without impurity. The crystallite size for both the samples is in the range of 39-44 nm. Field emission scanning electron microscopy (FESEM) images suggest the change in microstructure with temperature. Energy dispersive X-ray (EDX) study explains about the composition present in the composites. Impedance analyser study reveals that heat treated samples have higher value of dielectric constant (ε'_r) with dielectric losses values lesser than 0. From Vibrating sample magnetometer (VSM) study, it has been observed that saturation magnetization is high for the sample heated at 1300°C. This suggests the use of these composites for microwave devices. The microwave operating frequency (ω_m) value for both the sample is in the range of 1-2 GHz suggesting the use of these composites in devices operate in L band.

The samples of $Y_{0.2}Bi_{0.2}La_xGd_{2.6-x}Fe_5O_{12}$ (x=0, 0.2 and 0.4) were successfully prepared by sol-gel auto combustion method to study the effect of substitution on garnet ferrites. X-ray diffraction (XRD) study reveals that garnet phase is dominant in all prepared samples. The crystallite size of the samples is in 33-54 nm range. The crystallite size varies with varying La^{3+}substitution in the samples. The calculated grain size of the samples is in 0.100 to 0.116μm range. Energy dispersive X-ray (EDX) mapping confirms the presence of all elements in the formed samples. From Ultraviolet- Visible (UV-VIS) spectroscopy it has been found that the samples have wide band gap (3.7 eV to 3.9 eV) which suggests that such materials can be operated in higher temperature, voltage and frequency. This makes these materials suitable in military application. From vibrating sample magnetometer (VSM) it has been clear that addition of La^{3+} changes the value of coercivity (H_c) and magnetic saturation (M_s) which make these materials suitable for switching devices and for antenna applications. The value of operating microwave frequency (ω_m) suggests the use of such materials in devices operated in Ultra High frequency region.

The composite of yttrium iron garnet (YIG) and erbium iron garnet (ErIG) (i.e., ErIG(x)/YIG(1-x) (x=0.5)) was prepared by facile mechanical blending method to study the dielectric losses in the composites. X-ray diffraction study (XRD) reveals the pure phase formation of YIG, ErIG and ErIG(x)/YIG(1-x). Field emission scanning electron microscope (FESEM) micrographs were used to calculate grain size of the samples. Impedance analyser was used to study dielectric property of YIG, ErIG and ErIG(x)/YIG(1-x). The composite ErIG(x)/YIG(1-x) has larger values of dielectric constant and lower values of tangent losses~0.05 at 1MHz.

Calculated ac conductivity of ErIG(x)/YIG(1-x) composite is low which implies its resistive nature. The value of coercivity (Hc) is lesser and value of magnetic saturation (Ms) is high for composite as compare to parent YIG and ErIG. The calculated value of microwave operating frequency (ω_m) for composite was found to be 4.5GHz. The good dielectric property, low dielectric losses and enhanced magnetic property of ErIG(x)/YIG(1-x) composite suggest a better option over parent garnet ferrites to be used in microwave devices such as dielectric antennas.

Herein we report the synthesis and enhanced magnetodielectric properties of $Y_3Fe_5O_{12}$(*x*) and $Mg_{0.4}Cd_{0.4}Co_{0.2}Fe_2O_4$ (1-*x*) (*x* = 0.3, 0.6, 0.9) composites for miniaturized antenna applications. X-ray diffraction spectra confirm that the spinel ferrite phase dominates over the garnet ferrite phase for the *x*=0.3 composites whereas it is the opposite for *x*=0.6 and x=0.9 composites. The grains are spherical for the garnet phase and cubic for the spinel ferrite phase. Magnetic study reveals that the composite with *x* = 0.3 has the highest coercivity value of 99.2 Oe and magnetization value of 41 emu/g. The composite with *x* = 0.3, also has the highest permittivity value of ∼19.5, permeability value of ∼ 2.8 but low dielectric and magnetic losses of ∼0.009 and ∼0.002 respectively. These low losses and a high miniaturization factor of ∼7.2 at 14.5 GHz make it a potential candidate for high-speed antenna applications.

Praseodymium doped gadolinium iron garnet ($Pr_xGd_{3-x}Fe_5O_{12}$ for x=0.5,1.0 and 1.5) was synthesised by adopting sol-gel auto-combustion process to study the effect of substitution on garnet ferrite. The structural properties of the Pr^{3+} substituted GdIG were examined with X-ray diffraction (XRD) pattern. It has been observed that with variation of Pr^{3+} content from x= 0.5 to 1.5 the crystallite size value ranges from 52nm to 41nm. The value of lattice constant, micro strain and dislocation density varies with Pr^{3+} substitution. The obtained micrographs from the field emission scanning electron microscope (FESEM) explains about the morphological changes in samples. It has been observed that with increase in Pr^{3+} content, agglomeration was found. The average grains size calculated from micrographs lies between 0.27 micrometre to 0.401 micrometres. The calculated band gap from Ultraviolet-visible spectroscopy also varies with increases in Pr^{3+} content. The band gap of the samples lies in insulator materials region i.e., between 4.5 eV- 4.7 eV. From fluorescence spectroscopy it has been found that the prepared garnet ferrites emit emission in red light region i.e., at 650 nm. This suggests the use of materials in red LEDs. It has been found that emission spectra vary with Pr^{3+} substitution in GdIG which means such materials are good candidate to be use in optical devices.

There are five chapters in this thesis. The first chapter provides an overview of the research, as well as an analysis of crystal structure, phenomena of magnetic materials as well as the theory underpinning antenna application. The critical review of literature is presented in chapter two, while the research methodology is covered in chapter three. The experimental data for each of the compositions is discussed in detail in Chapter four. The fifth chapter contains the summary and conclusion.

Table of Contents

Dedicated to my father

Sh. Manoj Kumar

May God rewards him with good health

Chapter 1

Introduction

1.1 Preface

Today we are living in 21st century, a century of technology where everyone is using high-tech gadgets like mobile phones, smart watches, laptops and televisions. The communication devices are ruling the industries, for an example mobile phone that have become the basic need of all human beings. All we needed are highly efficient, compact sized wireless communication devices with low signal loss **[1]**. Compact sized devices are very easy to carry from one place to another. The main drawback of any communication device is its efficiency. Because as the size tends to decrease, the efficiency of the device gets affected. Without antennas, communication devices are of no use **[2]** and without suitable substrate material for antennas are of no work. No doubt that there are lot antennas working in our surroundings but still they are having some limitations like low power, low efficiency, high losses, impedance mismatching, narrow bandwidth, large size, and selection of inexpensive materials **[3] [4] [5]**. There is a dire need to synthesize and characterize such materials that have low losses and good magneto-dielectric properties that can replace the traditional antennas. A larger number of attempts have been made to strengthen the performance of the antennas. The materials like $Li_{0.43}Zn_{0.27}Co_xTi_{0.13}Fe_{2.167-x}Bi_{0.003}O_4$ **[6]**, $NiZnFe_2O_4/BaFe_{12}O_{19}$ **[7]**, $SrFe_{12}O_{19}/Li_2MoO_4$ **[8]**, Bi_2O_3 doped $MgCdFe_2O_4$ **[9]**, $Ba_3Co_{2+x}Ir_xFe_{24-2x}O_{41}$ **[10]**, $BaSrCo_{2-x}Ni_xFe_{12}O_{22}$ **[11]**, $Gd_3Fe_5O_{12}/Y_3Fe_5O_{12}$ **[12]**, $Ni_{0.95-x}ZnxCo_{0.05}Fe_{1.90}Mn_{0.02}O_4$ **[13]**, $Y_{3-x}Dy_xFe_5O_{12}$ (x=0,0.2,04, 0.6) **[14]**, $Y_{3-x}Gd_xFe_5O_{12}$ (x= 0, 1, 2,3, 4) **[15]**, $Ni_{0.5}Zn_{0.3}Al_{0.2}Fe_2O_4$ and $Y_{2.8}Al_{0.2}Fe_5O_{12}$ **[16]**, $NiZnFe_2O_4/BaFe_{16}O_{27}$ **[17]**, $Ba_2Co_2Fe_{12}O_{22}/NiFe_2O_4$ **[18]**, $Ba_3Co_2Fe_{24}O_{41}$/glass composite **[19]**, $SrCo_{1.5}Ti_{1.5}Fe_9O_{19}/B_2O_3$/glass **[20]**, LiZnTiMn/polydimethylsiloxane **[21]**, $Co_{80}Ni_{20}$ **[22]**, $BaFe_{12}O_{19}/CoFe_2O_4$ **[23]**, $Ni_{0.368}Cu_{0.2}Zn_{0.432}Fe_{1.96}O_{3.94}/TiO_2$ **[24]**, $Ba_3Co_2Fe_{24}O_{41}$ **[25]**, $Ni_{0.4}Zn_{0.6}Fe_2O_4$ **[26]** have been investigated for replacements in the antennas. No doubt that all these materials have showed some interesting properties for antennas but, they did not provide the all-necessary requirements for excellent efficiency and miniaturization of antennas at higher frequency range. For the antenna applications, materials should have good magnetic and dielectric properties with least dielectric and magnetic losses. The miniaturization and losses in antennas are dependent on the real and imaginary parts of permeability and permittivity. Ferrites are ceramic oxides that have applications in memory devices, microwave devices, antenna, transformer core and many more

[27]. Ferrites are very promising materials for antenna miniaturization and for high efficiency antennas **[28]**. Composites of the ceramic oxides have gained the attention of researchers for their use in high frequency operating devices such as antennas. Nanocomposites of ferrites are very useful to enhance the individual properties like dielectric, structural and magnetic properties of ferrites. The addition of two different ferrites in the form of composites (having distinct phases) leads to exchange bias. As a result, the superparamagnetic limit rises, which is a very crucial parameter for device miniaturization **[29, 30]**. The composites of ferrites exhibit excellent properties like: magneto-dielectric, low losses, chemical stability, and high resistivity **[31]**. Ferrites are of three types: hexagonal ferrite, spinel ferrite and garnet ferrites. Hexaferrites possess very good magnetic properties and have a higher value of imaginary part of complex permittivity, which provides higher losses in the material **[32]**. High losses are the biggest drawback of their use in antenna applications. Garnet ferrites are the best choice for antenna applications. The reason is their excellent magnetic property, electromagnetic property, dielectric property and low magnetic and dielectric losses **[33-37]**. Among garnet ferrites, yttrium iron garnet (YIG) is one of the renowned magneto-dielectric materials for microwave devices.

In general, different preparation methods have been adopted for the preparation of ferrites. The preparation method is the key to obtain desirable properties in the ferrites. The synthesis method can tailor the morphology of the materials. Many researchers have adopted solid-state reaction method **[38, 39]**, hydrothermal ball milling **[40]**, sol-gel method **[41-43]** and co-precipitation method **[44-46]** for the preparation of soft ferrites. These methods have some disadvantages such as requirement of higher sintering temperature, higher sintering time, presence of inhomogeneity, presence of impurity phases and costly precursors. Sol-gel auto combustion is the most appropriate and portable method for the synthesis of garnet ferrites. This method needs inexpensive precursors, less temperature and less time to prepare ferrite. This method provides homogeneity in the structure and formation of single phase **[47-49]**.

In the present research work, sol-gel auto-combustion method has been employed for the preparation of garnet ferrite and spinel ferrite. The composites of ferrites were selected after review of literature by keeping in mind the improvements required for the antenna applications like good magnetic and dielectric properties. The effect of variation of composition (in composites) on the structural, dielectric and magnetic properties of garnet ferrite have been studied. The effect of temperature on the structural, magnetic and dielectric properties of the prepared composites of garnet ferrites have been carefully investigated. The miniaturization

parameters and losses in the composites of the garnet ferrites has been studied in details for antenna applications.

1.2 Antenna Theory

Antennas are the devices that transmit and/or receive the electromagnetic signal. In terms of radio engineering, an antenna is a device which is interface between radio wave and electric current that passes through free space and metal conductors respectively. The demand of compact size antenna with matching impedance is large in communication industry. But it cannot be ignored that impedance bandwidth of small electric antenna is directly proportional to volume of antenna at wavelengths. Which clearly indicates that if size of antenna is less then impedance, bandwidth has to suffer. So, the best technique to obtain compact size of antenna is to load or substitute different materials. It has been noticed that the material which is going to be loaded inside antenna must have the properties that can make antenna compact, highly efficient, and low lossy. The material must also provide high bandwidth and impedance matching with free space. Many researchers have used such dielectric materials that have high permittivity in order to miniaturize antenna. But such materials have some problems like the wave present at surface got excited due to which radiation efficiency decreases as well as impedance mismatching is also created.

Figure 1.1 represents the traditionally used TV antennas that were having very low efficiency. Such TV antennas were facing the biggest problem of poor signals at that time and gave worst results during bad weathers. In 1950's antenna was firstly introduced, after that it has gained a huge interest in telecommunication industries. Initially the antenna was fabricated with material having dielectric properties. Till now many antennas contains dielectric substrate for better application. Such antenna was bigger in size and their efficiency was lower. Many scientists have worked on many dielectric materials to alter the properties of antenna. So, after conducting a large number of researches, scientists investigated a material with high dielectric constant. Such materials were capable to reduce the size but on the cost of impedance mismatching which further decreases the efficiency of antennas **[50-52]**. The second and important problem of the dielectric antennas is that in high permittivity region the field gets concentrated and further it adversely affects the efficiency of the signals. **Figure 1.2** represents the modern dielectric antennas. To overcome the problems faced by existing antennas, ferrites-based antenna was fabricated in 1980's by using NiCo and YIG. This research was performed to overcome the problems faced by dielectric material-based antennas. After larger number of researches, it has been concluded that the materials with good magnetic as well as good dielectric properties

(magneto-dielectric materials) are best suitable for substrate in antennas. **Figure 1.3** represents the compact and good efficiency antennas used in wireless communication.

Figure 1.1 Large size and low efficiency TV antenna used earlier

Figure 1.2 Modern dielectric antennas

Figure 1.3 Compact antennas use in wireless communication

1.2.1 Permittivity and Permeability

The miniaturization and microwave losses in antennas are related to permeability and permittivity of the material. So, it is very important to understand the magnetic and dielectric parameters before studying antenna parameters. A material is said to be electrically insulator when it does not have any free charge carriers to conduct electric current. Such materials are known as dielectric materials. **Figure 1.4** represent the polarization of charges in dielectric material, when exposed to electric field. The flow of field is restricted in the material and charges are slightly shifted from their mean position. When electric field is provided to the dielectric material, the positive charges are displaced in the direction of the field. Whereas negative charges are displaced in the opposite direction. This is known as polarization. Due to polarization, the internal field is generated that opposes the external field. In general terms, the study of dielectric properties of a material means the analysis of storage and loss in the electric and magnetic field.

The amount of resistance produced in presence of an electric field in a vacuum is known as permittivity. The complex permittivity (ε^*) is described as the potential of the material to store electric energy in the presence of external applied field. The complex permittivity is written in terms of real and imaginary part of permittivity, which is given as:

$$\varepsilon^* = \varepsilon' - j\varepsilon'' \quad (1.1)$$

Herein ε' represents the dielectric constant and ε'' represents the dissipation or loss of electric field. The dielectric constant is written as the ratio of permittivity of material to the permittivity in vacuum. The dielectric constant (ε') is dependent on the dielectric polarization which always opposes the electric field. The dielectric constant for all materials is greater than that of free space and hence is always greater than 1.

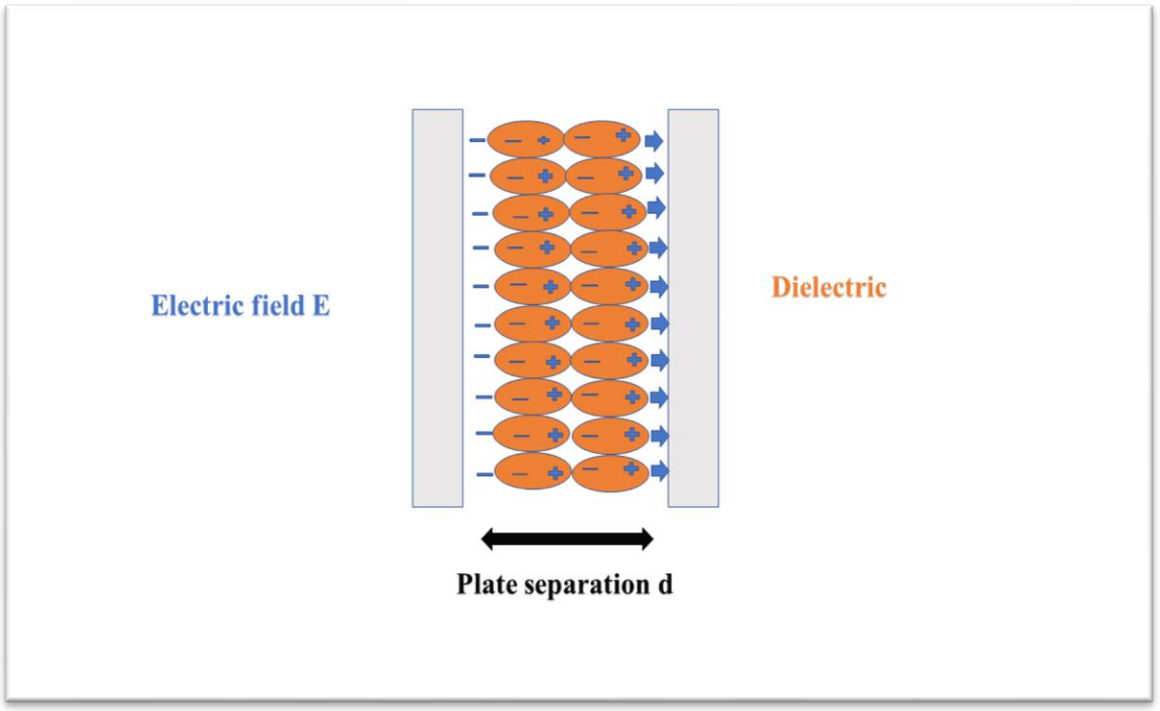

Figure 1.4 Polarization of charges in dielectric material

When the electromagnetic field is applied to the material, the amount of electromagnetic flux it allows to pass through itself is termed as magnetic complex permeability (μ^*). Magnetic permeability is explained as the magnetic flux density (B) produced within a material by a magnetizing field divided by the magnetic field strength (H). The permeability is given as the combination of real and imaginary parts of permeability:

$$\mu^* = \mu' - \mu'' \quad (1.2)$$

Herein μ' represents permeability and μ'' represents the attenuation in magnetic field in the

material.

1.2.2 Miniaturization

The miniaturization factor of antenna is related to refractive index which further depends upon permeability and permittivity and is given as:

$$\eta = \sqrt{\epsilon\mu} \tag{1.3}$$

Here n is refractive index of ferrite material, μ' is real permeability and ε' is real permittivity of material.

1.2.3 Microwave Losses in Antennas

For antenna application, losses in the material plays an important role because high losses mean low efficiency.

The dielectric loss tangent of a material is given as:

$$tan\delta_{\varepsilon} = \frac{\varepsilon''}{\varepsilon'} \tag{1.4}$$

Herein δ_{ε} is the dielectric loss angles. If loss tangents are higher, then the wave will experience higher attenuation while passing through the materials.

The magnetic loss tangent is given as:

$$tan\delta_{\mu} = \frac{\mu''}{\mu'} \tag{1.5}$$

Herein δ_{μ} is the magnetic loss angles. If loss tangents are higher, then the wave will experience higher attenuation while passing through the materials.

The higher value of magnetic losses implies absorption of signal inside the materials and attenuation of the wave as it moves through material. Both of the components contribute to wavelength compression inside the material. Additionally, due to the coupled electromagnetic wave, loss in either the magnetic field or electric field will attenuate the energy of the wave. In coupled electromagnetic wave, the values of complex permittivity (ε^*) and complex permeability (μ^*) are dimensionless.

1.3 Magnetism and Magnetic Materials

Magnetic materials are present on earth from many decades, and mankind is using them since, 500 years ago. Neolithic man was the first who used ferrite as loadstone for navigation. But at that time the concept behind these magnetic materials i.e., magnetism was unknown. As human got aware with the magnetism, a revolution of new technologies based on these magnetic

materials has started. Now the question arises that how a material is classified as magnetic or non-magnetic.

The magnetism originates from the spin and orbital motion of the electrons. In spin and orbital motion, electrons interact with other electrons while pertaining their spins. The major contribution to the magnetism came from the spin of valence unpaired electron that produces permanent magnetic moments in the material. Based on the response of materials to the magnetic field, they are classified into different categories that are: diamagnetism (diamagnetic material), para-magnetism (paramagnetic material), ferromagnetism (ferromagnetic materials), anti-ferromagnetism (antiferromagnetic materials) and ferrimagnetism (ferrimagnetic materials).

Diamagnetism is usually very weak phenomena and the fundamental characteristic of all materials. It occurs due to lack of unpaired electrons and have no permanent magnetic moments. The alignment of all the magnet moments in the materials is always in opposite direction to applied field. The revolving electron in an orbit consists of electric current. When exposed to some magnetic flux, the disturbance in the electric current occurs. According to the Lenz's law, the current is induced in such direction so that it can oppose the altered flux in the circuit. In diamagnetic materials, the produce magnetic field in the material is opposite to the applied magnetic field and therefore susceptibility (χ) is negative and values ranges from -5×10^{-9} for Si to -1.6×10^{-4} for Bi. For diamagnetic materials, χ is always temperature independent. The materials such as Ge and Si are non-magnetic but show diamagnetism.

Para-magnetism phenomena emerges from atoms, ions and molecules that have unpaired electrons (odd number of electrons). Paramagnetic behaviour is present in free ions or atoms that have partially filled inner shell or atoms having even number of electrons but have non vanishing spins for e.g., actinides, transition elements (Fe^{2+}, Mn^{2+}) and rare earth elements (Gd^{3+}). These unpaired electrons cause some non-zero total spin. Such materials have permanent magnetic moments which are randomly oriented. Due to randomness in magnetic moments, no magnetization is formed in the absence of field. When paramagnetic materials are exposed to magnetic field, the magnetic moments align in the direction of field and hence magnetization occurs. These materials exhibit linear relationship of magnetization (M) versus applied magnetic field (H) with positive values of magnetization and slopes. The value of susceptibility (χ) is greater than zero and is temperature dependent. The Langevin theory explains about the para-magnetism phenomena.

Ferromagnetism effect is similar to para-magnetism because it also has permanent magnetic moments. The only difference is that ferromagnetic materials have non zero magnetic moment because of fine alignment of atoms in the lattice. So, the magnetic moments can easily interconnect with each other, and therefore in the absence of magnetic field the materials have magnetization. This type of magnetization is known as spontaneous magnetisation and this exists below curie temperature (T_c). The ferromagnetism is best defined only if the all-magnetic moments are parallel or aligned in the direction of applied field and add contribution to entire magnetization. In 1907, Weiss proposed the classical theory that estimated the existence of molecular field in the ferromagnetic substances. But Heisenberg proposed a model according to which alignment of magnetic moment in same direction is because of exchange interactions among the neighbour magnetic moments. Ferromagnetic materials have very large χ that changes with magnetic field strength. Below T_c, M-H curve exhibits hysteresis and above this temperature the substance changes into para-magnetism because of large thermal agitation. Elements like Fe, Co and Ni are the only ones that show ferromagnetism above room temperature.

Anti-ferromagnetism is the extreme case in which zero net magnetizations occurs despite the fact that some magnetic moments are aligned orderly. The reason is that in such materials the neighbouring magnetic moments are aligned antiparallel and exchange interactions are negative. The magnetic moments cancelled out each other effect in the absence of applied field. In antiferromagnetic materials, the crystal has two sub-lattices A and B. In one of the two sub-lattices, the magnetic moments are aligned parallel to the fields whereas opposite for the other sub-lattice. The anti-alignment in ferromagnetic materials occurs below the Neel temperature (T_N) which is counterpart of T_c. For ferromagnets and ferrimagnets it occurs below T_c. Anti-ferromagnetism shifted to para-magnetism above T_N. Chromium is the only existing element that shows anti-ferromagnetism at room temperature with T_N =37°C. The value of χ is small and positive of antiferromagnetic materials.

The important magnetic behaviour which is similar to anti-ferromagnetism to some extent is ferrimagnetism. Ferrites (Fe_2O_3) are one of the examples of ferrimagnetism, that consist of Fe. This effect occurs in the compounds that exhibits complex crystal structure. In such materials the magnetic moments are alignment in one sub lattice ‘A’ due to exchange interaction. Whereas in sublattice ‘B’ the magnetic moments are aligned in opposite direction. But unlike to anti-ferromagnetism, ferrimagnetic materials have some net magnet moments. The reason for this is that the magnitude of the magnetic moments in ‘A’ sublattice is larger than that of

the magnetic moments in 'B' site. In some extent, ferrimagnetism and ferromagnetism are similar as they become paramagnetic above T_c. But the difference is that ferrimagnetic materials have smaller value of saturation magnetization.

The permeability of magnetic materials can also be used to classify them. The constant relative permeability of a diamagnetic substance is somewhat less than 1. The permeability of diamagnetic substance, such as bismuth, depends on magnetic field. If the external field is partly reduced, the magnetic flux density within the material is also slightly reduced and hence in turn permeability is reduced. The relative permeability of a paramagnetic substance is somewhat higher than 1. When a magnetic field is applied to a paramagnetic material, such as platinum, it becomes somewhat magnetised in the direction of the external field. The relative permeability of a ferromagnetic substance, such as iron, is not constant. The greatest relative permeability of purified iron and many magnetic alloys is 100,000 or more.

1.3.1 Garnet Ferrites

Based on structure, ferrites can be categorized into two types: cubic structure ferrites which are spinel and garnets, hexagonal structure ferrites which is hexaferrite. All these ferrites consist of Fe_2O_3 as basic formula. These ferrites are different from each other by not only structure but also differ by properties and applications.

Garnet ferrite has attracted the focus of many researchers because of its huge range of applications in high frequency region. Basic rare earth yttrium iron garnet has very good resistivity, good dielectric property, large faraday rotation, high initial permeability, high thermal and chemical stability, high remanence, low propagation losses. These properties can be tailored by substitution in particular site and by mode of preparations.

1.3.2 Crystallographic Structure of Garnet Ferrites

The structure of garnet ferrite is very complicated and its 2-D representation is very difficult to draw. Garnet ferrites have cubic symmetry with stoichiometric formula $C_3A_2D_3O_{12}$, where C, A, D are cations in dodecahedral, octahedral and tetrahedral sites in crystal structure. **Figure 1.5** represents the basic cubic crystal structure of garnet ferrites. The cations of ferrites occupy the interspace of oxygen (O^{2-}). For total of 160 atoms, there are 8 formula units. In general way, the distribution of ions can be understood with formula: $\{R_3\}\,[Fe_2]\,(Fe_3)\,O_{12}$. Herein 'R' is used to represent rare earth metal, in general yttrium (Y). The different brackets represent different sites. The bracket '{}' symbolizes 24c i.e., dodecahedral 'c' site, bracket '[]' symbolizes 16a

i.e., octahedral ‘a’ site and bracket ‘()’ symbolize 24d tetrahedral ‘d’ site. Iron has smaller size as compare to that of rare earth metals so, rare earth metals occupy dodecahedral site and the interspace of these sites are occupied by iron. The magnetic moment of entire garnet ferrite is mainly due to Fe^{3+}, and Fe^{2+} ions exist in ‘a’ and ‘d’ sites with ratio 3:2. Whereas rare earth ions (R^{+3}) exist in ‘c’ site have very less magnetic moment. The ferrimagnetic behavior of garnet ferrite is due to antiparallel alignment of iron ions in ‘d’ and ‘a’ site to that of ‘c’ site ions. The arrangement of these ions is as shown in figure below:

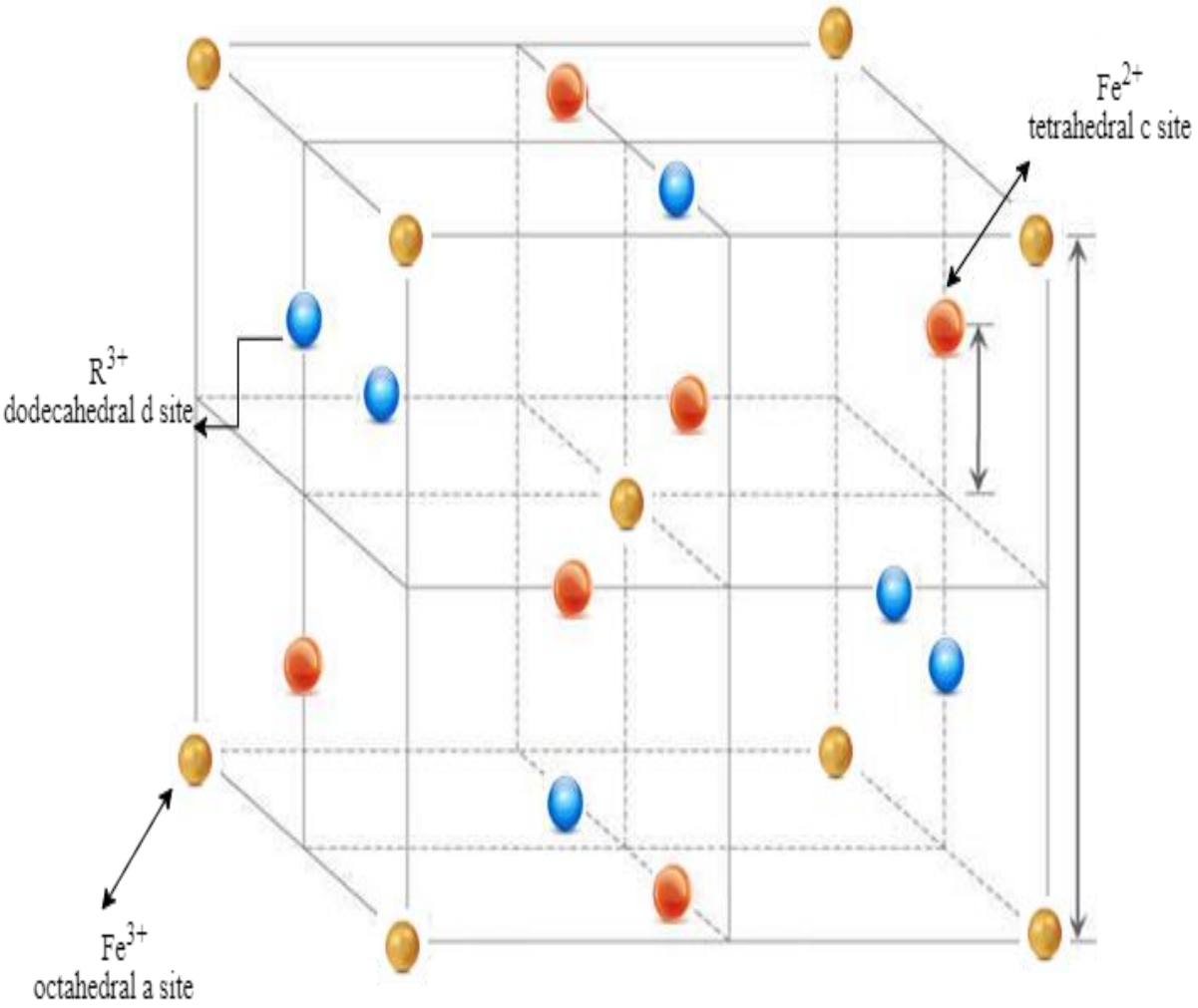

Figure 1.5 Cubic crystal structure of garnet ferrite

Addition to this, the magnitude of exchange interaction between two sub-lattices (c, a and d) totally depends on the angle between the magnetic ions. If an angle of 180° is formed, or nearer to it, there is high exchange interaction and at angle 90° and near there is very poorer interaction. An angle of 126.6° represents strong interaction between Fe^{3+} (a) – O^{2-} – Fe^{3+}(d) (a-d). For the second strongest interaction, angle between Fe^{3+} (d) – O^{2-} – R^{3+}(c) is 122.2°. The garnet ferrite is when substituted with trivalent metals (Me: Al, Ga), the angel between Me^{3+} – O^{2-} – Fe^{3+}(a) shifted to 100° and interaction between neighboring cations become least.

1.3.3 Properties of Garnet Ferrites

Permeability:

The relation between magnetic flux density B and magnetic field strength H is given as:

$$\vec{B}=[\mu]\,\vec{H}$$

Where μ is permeability tensor.

For non-magnetic materials, permeability becomes scaler quantity i.e., B= μ H.

Whereas, for ferrite μ becomes a tensor quantity.

$$\mu= \mu_0 [1+ \omega_0 \omega_m/ (\omega_0)^2(\omega_m)^2]$$

$$\kappa= \mu_0(\omega \omega_m/ \omega_0^2- \omega^2)$$

Where ω_0 is the Larmor frequency or precession frequency and written as: $\omega_0 = \mu_0\gamma H_0$

H_0 is the bias field or applied field, γ is gyromagnetic ratio which is given as:

γ = spin magnetic moment/ spin an angular moment

When bias field is applied to the ferrites, magnetic dipoles align themselves in direction of magnetic field. As the bias strength keeps on increasing, all dipoles align and a saturation point is attained which is known as saturation magnetization M_s.

$$\omega_m= \mu_0\gamma M_s$$

When bias is applied in z direction then

$$[\mu] = \begin{bmatrix} \mu & -j\kappa & 0 \\ j\kappa & \mu & 0 \\ 0 & 0 & \mu_0 \end{bmatrix}$$

From above matrix equation, it is clear that permeability tensor gives antisymmetric conditions which make ferrites important for non-reciprocal device.

The permeability of garnet ferrites varies with porosity. As magnetic field is applied, magnetic poles are formed on the surface. After that, there is decrease in permeability due to demagnetization field. These magnetization field is somehow interconnected with grain size and grain boundary **[53]**. The initial permeability of YIG ferrites is large. The permeability of YIG can be increased by addition of Indium by 50% **[54]**.

Hysteresis Loops:

The shape of hysteresis loop is very important in order to calculate coercive force 'H_c' and remanence ratio 'R'. In garnet ferrites, saturation magnetization is moderate, coercive force is less and remanence is high. This is due to dependence of H_c and R on following factors:

(a) Microstructure (b) Anisotropy

(a) Microstructure: The porosity, morphology of grains, agglomeration, and phases that may be seen through micrographic study are referred to as microstructure. Generally, porosity (that consist of nonmagnetic secondary-phase material) increases H_c and decreases R. Because, the ability of 180°domain-wall motion when the material changes from one magnetic state to the other determines the coercive force, pores and grain boundaries have a propensity to increase coercivity by obstructing wall motion **[55]**. As a result, the size of any spike domains will directly cause R to decrease **[56]**. These microstructures are also related with production of demagnetization effect. Material that gets easily demagnetized are soft magnet. By a complex substitution of Ca^{2+}, In^3 and V^{5+}, the porosity of polycrystalline garnets can be decreased **[57]**.

(b) Magneto-crystalline Anisotropy: As garnet has cubic structure so, magneto-crystalline anisotropy energy is obtained by series expansion of angle between the magnetization direction and cube axes. The anisotropy energy can be considered by arbitrary direction in terms of series expansion. The effective anisotropy field is given as:

$H_a = 2k_1 / M_s$

Here k_1 is the 1^{st} term of series expansion, which is also known as magneto crystalline anisotropy constant. It is the energy requirement to rotate magnetization from an easy axis to hard axis.

Effective anisotropy field depend upon angle 'θ' that forms between direction of applied magnetic field as well as single crystal axes **[58].**

In general anisotropy of garnet ferrites is very small. This is mainly due to presence of Fe^{3+} ion **[59]**. The magnetic moments of ions in garnet ferrites are only due to of Fe^{3+} ion (present in excess in tetrahedral site) rather than Fe^{2+} ion (in octahedral site). The magnetic crystalline anisotropy for YIG is 82 Oe. The garnet ferrites have low magnetic crystalline anisotropic and therefore exhibits least losses.

The coercive force is directly proportional to anisotropy and porosity but inversely proportional to grain size **[60]**. Whereas remanence goes on decreasing with increase in anisotropy. Coercivity of ferrites can be increased by minimizing or by reducing the size of particle **[61]**.

Anisotropy constant is given by the relation:

Anisotropy constant = $H_c \times M_s / 0.96$

Where M_s is saturation magnetization and H_c is coercivity.

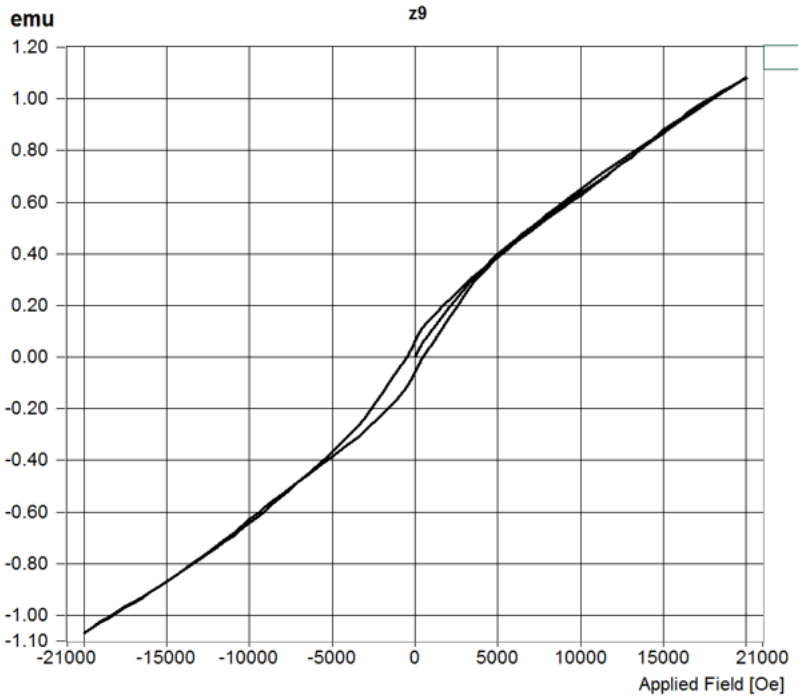

Figure 1.6 Magnetization versus applied field curve (Hysteresis loop) of ferrites

Loss Mechanism in Garnet:

(a) Dielectric Loss:

Garnet ferrites are the best dielectric materials and have dielectric properties that are dependent on resistivity. Such dielectric material possesses some sort of EM losses due to flow of charges. During dielectric losses in the materials the energy dissipates. The charges are associated with dipole moments. When these dipoles moment vibrates and generates dielectric loss, vibration arises from imaginary part of permittivity can be written as:

$\epsilon = \epsilon'$-j ϵ''

For conducting medium, loss tangent is given as:

$\tan\delta = \frac{\epsilon'' \omega + \sigma}{\omega \epsilon'}$

For insulator or for poor conducting medium, loss tangent is given as:

$\tan\delta = \frac{\epsilon''}{\epsilon'}$

Where ϵ'' is dielectric loss.

For media having less loss:

$\epsilon = \epsilon_0 \epsilon_r (1 + j \tan\delta)$

Where $\epsilon_r = \epsilon'/\epsilon_0$ is dielectric constant.

(b) Conduction Loss:

The conduction loss occurs due to imperfection in lattice. The electric displacement is given by: D= ϵE, where E is the electric field. By using Maxwell curl equation for 'H' we get:

$\nabla \times H = \frac{\partial D}{\partial t} + J = j \omega D + \sigma E$

Putting the value of 'D' in above equation, we get :

$= j \omega \epsilon E + \sigma E$

$= j \omega [\epsilon' - j(\epsilon'' + \sigma/\omega)]E$

From above equation it is clear that dielectric losses (ϵ'') and conduction losses (σ) cannot be distinguish easily.

(c) Total Loss:

The net or total loss in a material is related with ferromagnetic resonance (FMR) due to magnetic damping **[62]**. FMR is the phenomena in which EM wave couples with the magnetization of ferrite. In such process the power of EM wave got absorbed by the material and as a result there is loss in signal. In garnet ferrites especially in single crystal ferrites the FMR line width (width of resonance peak) is narrow subsequently the magnetic losses are least. But if we consider the case of polycrystalline ferrites along with intrinsic losses (i.e., related to fundamental interaction) extrinsic losses are also there. These extrinsic losses occur due to polycrystalline anisotropy, fast and slow relaxation impurities (i.e., hopping, Fe^{2+}, Fe^{3+}, rare earth ions etc), grain boundaries, surface roughness and porosity.

The magnitude of FMR linewidth (ΔH) is very crucial if we want to calculate the external losses in the microwave devices that do not work on resonance phenomena. ΔH is the sum of four independent effect **[63,64]** that are mentioned below:

- In the presence of microwave field, the magnetic spin transfers its energy to the crystal lattice by vibrations or by thermal energy. This entire process is known as spin lattice relaxation.
- Another factor which broadens the line width is porosity which produces demagnetization effects. Due to this effect, resultant resonance line width is directly related to saturation magnetization i.e., $4\pi M_s$ and become proportional to volume fraction of porosity i.e., P_{eff}.
- Magneto-crystalline anisotropy is the third and most important effect. In this effect there are different crystallographic directions of each grain i.e., there is random demagnetization. This demagnetization produces broadening of line width, which is further proportional to anisotropy energy and magnetization constant.
- The surface conditions also bother the linewidth. If the surface of grains is rough, then the demagnetization effect occurs in the material. The demagnetization of magnetic moments further decreases the value of line width. In general, $\Delta H_{eff} = 2n/\gamma$, where γ is gyrometric ratio. The value of ΔH_{eff} increases with grain size and hence losses also increase. The anisotropy of YIG generally found to be low. Therefore, the line width of garnet ferrites is less and hence losses are less.

Saturation Magnetization:

Saturation magnetization is a property of ferrites and ferromagnetic materials in which increase in the applied magnetic field becomes unable to increase magnetization beyond certain limit. Garnet ferrites have saturation limit about 1950 Gausses. For microwave devices, a material must have temperature stability for saturation. In general, it has been seen that at higher temperatures, the value of magnetic saturation starts decreasing and therefore losses occur in the form of heat. The heat in the material further raises the temperature and hence magnetic saturation again decreases. So, in order to get stability between magnetic saturation and higher temperatures, garnet ferrites are used. Garnet ferrites basically have higher Curie's temperature (T_c), which means the nature of ferrite material do not change to paramagnetic and therefore stable saturation will be obtained.

YIG has saturation value of 1790 Gausses. It can be further decreased by addition of rare earth or by substitution of Al and Ga in octahedral site. It's value decreases to 1200 to 300 Gausses. If In (Indium) or Ca-Zr is substituted in YIG then saturation can be increased upto1900 Gausses. Basically, substitution in octahedral site may enhances the value of saturation magnetization **[65].**

Temperature Dependence of Spontaneous Magnetization:

Spontaneous magnetization is a property of ferromagnetic and ferrimagnetic materials in which some of the magnetic domains have order spin under zero magnetic field. In garnet ferrites, the spontaneous magnetization of c sub-lattice decreases more than a & d, with increase in temperature. Here compensation of magnetization occurs where c has equal magnetization to that of a-d sublattice. As temperature rises the magnetization of the a-d sublattice dominates over entire material. If we talk about the sub lattices of iron in garnet ferrites, their magnetic moment varies with temperature. The value of magnetization changes with substitution. Magnetization can be lowered by tetrahedral substitution **[66]**. Gadolinium garnet iron oxide ($Gd_3Fe_5O_{12}$) has compensation temperature value approx. 295K and that for erbium, it is 80K **[58].**

1.3.4 Applications of Garnet Ferrites

As garnets possess low dielectric losses, low linewidth, high retentivity, high faraday rotation, high initial permeability, good thermo-optical properties, magnetic and optical properties. So, these materials have a large number of applications. These all properties can be achieved

because of super exchange interactions in garnet ferrites **[67].** YIG is the most studied soft ferrite till now, after their discovery in 1956 **[68].** YIG shows very good application in microwave region. There are three lattice sites in garnet ferrites. By the substitution of particular ion in YIG, it can be operated in different frequency ranges. The rare earth substituted garnets are very good for microwave and communication purposes because of very low eddy current losses, high saturation magnetization, low propagation losses and high remanence **[69]**. Garnet ferrites are used in microwave devices such as in: phase shifter, filters, circulator, faraday devices in laser**,** resonator antenna and tuneable antenna **[70-84]**. As garnet ferrites are cytotoxic so, they are used in biotechnological applications **[85-86]**.

1.3.5 Spinel Ferrites

Spinel ferrites are also a type of soft ferrite with the general formula MFe_2O_4, where M represents divalent ions like Fe^{+2}, Mg^{+2}, Mn^{+2} $Ni^{+2,}$ or Co^{+2}. Spinel ferrites have good magnetic and dielectric properties with very less value of $\varepsilon^{"}$ at higher frequency i.e., losses are very low in these ferrites **[87]**. The crystal structure of spinel ferrite is given in **Figure 1.7**. These cations are placed according to two alternative crystallographic sites (tetrahedral sites and octahedral sites). One MFe_2O_4 unit consists of 32 densely packed oxygen atoms of 64 divalent tetrahedral sites and 32 trivalent octahedral sites. Specific, M^{2+} and Fe^{3+} typically occupy 8 tetrahedral and 16 octahedral sites, respectively, to maintain an electrically balanced state between the anions in the structure.

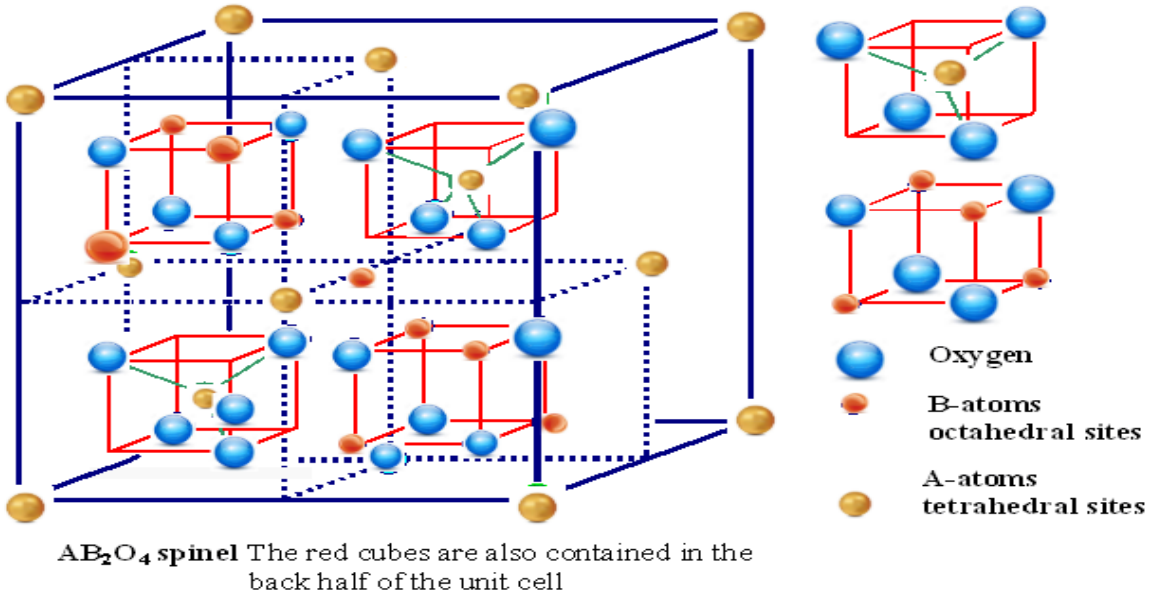

Figure 1.7 Cubic crystal structure of spinel ferrites

Chapter 2

Literature Review

2.1 Literature Review

Haitao et al., in 2008 have studied magnetic properties of YIG substituted with Ce, Gd substituted Y_{3-x-y} $Ce_xGd_yFe_5O_{12}$ (x=0-0.1 and y= 0.1). The samples were synthesized via sol gel method. From XRD analysis it was observed that at 800°C crystallization start and at 850°C single phase of garnet was obtained. From XRD analysis it was concluded that there was only peaks of garnet and the size ranges from 42 to 65. Magnetization of garnet was increased with Ce substitution while substitution of Gd^{3+} lead to decrease the value. Also, with increase in particle size saturation magnetization increased **[88]**.

Fechine et al., in 2009 have studied the microwave antenna property of ($Gd_3Fe_5O_{12}$) GdIG(x) – ($Y_3Fe_5O_{12}$) YIG(1-x) ferrimagnetic composite prepared by ball milling method. Magnetic measurement and dielectric measurement were done by Hakki-Coleman's procedure at microwave frequency using Ansoft's high frequency structure simulator. Good agreement was found between numerical and experimental data. The result proves that by varying composition of material of resonator, GdIG(x) / YIG(1-x) can be operated as magnetodielectric antenna and at frequency range of 4.4-5.3 GHz, bandwidth of antenna ranges from 7.5-11% **[12]**.

Qureshi et al., 2009 have synthesized YIG by mechanochemical method. The composite of YIG with PMMA was examined for electrical and dielectric studies. With increases in YIG content in the composites the dielectric constant and electrical conductivity increases. This is because of increasing of polarization in the composites. The effect of temperature on the dielectric properties of the composites has also been examined. The dielectric loss and constant increases with rise in temperature **[89]**.

Mallmann et al., in 2013 have worked on $Y_3Fe_5O_{12}$ and $Gd_3Fe_5O_{12}$ and further investigated their electrical and magnetic behavior at RF and microwave range. YIG and GdIG were prepared by solid state method and mechanically milled at high energy. The result shows that the ferrimagnetic garnets are very good for antenna application as there is control in antenna radiation and tuning was enhanced **[90]**.

Zheng et al., 2013 have worked on Z type hexaferrite for antenna application. NiZn / Co_2Z composites were synthesized via solid state reaction method. XRD analysis for the composites showed proper formation of ferrite phase. SEM results show good agreement with XRD result

and also it has been observed that while changing the composition from 55 wt.% to 70 wt.% there is no change in densification and in average grain size. From VNA it was found that permeability is strongly dependent on NiZn and there is increase in μ' from 10 to 19 at low frequencies **[91]**.

Varouti et al., in 2014 have prepared aluminum substituted YIG via standard solid-state reaction method by varying composition in $Y_3Fe_{5-x}Al_xO_{12}$ (x= 0, 0.25, 0.5, 0.7, 0.8 and 0.9). After measurement of isothermal magnetization at T=295° K, samples show ferrimagnetic behavior and there is diminishing of ferromagnetism. Saturation magnetization varies linearly with x. Further measurement of ferromagnetic resonance was done, it proves that Al substituted YIG has very low losses as compare to pristine YIG. As a result, YIG-Al can be used as tunable UWB antenna which operates in 1.7-8 GHz region. Also, YIG-Al based antenna has formed isolated stop bands. Whereas in such stopbands, antenna is reflective as well as inefficient **[92]**.

Akhtar et al., in 2014 have examined the comparison between magnetic, structural and morphological properties of YIG prepared via different methods. Sol-gel, self- combustion and modified conventional mixed oxide methods were used for synthesis of the samples. The sintering temperature for sol gel used was 950°C, for self-combustion was 1150°C and for modified conventional mixed oxide is 1300°C. XRD showed the difference in particle size and cell volume by different synthesis methods, also it revealed formation of single-phase structure. There was increase in grain size from 40 nm to 100 nm by increasing sintering temperature, which was calculated by FESEM and TEM. From impedance network analyzer it has been seen that by using sol gel method initial permeability is high and losses are less for YIG. The reason is increase in grain size and large densification. Also, magnetic properties of YIG prepared by sol- gel method was increased. As a result, it was concluded that sol gel method is best method for preparation of garnet ferrites **[93]**.

Zhang et al., in 2015 have worked on Z type hexaferrite for antenna miniaturization and impedance matching of antenna. Synthesis of Z type hexaferrite $(Ba_{0.5}Sr_{0.3})_3\ Co_2Fe_{24}O_{41}$ + $xSnO_2$ (x= 0, 0.1, 0.2, 0.4, 0.6 wt.%) was done via conventional solid-state reaction process. It was observed that with the addition of SnO_2 in ferrite lead to high refractive index ($\eta = \sqrt{\varepsilon\mu}$) 0.99) on frequency range from 3-300 MHz but sample has higher dielectric loss which make the material to limited in 3-300 MHz range **[94]**.

Hasan et al., in 2015 have worked on Yttrium Iron Garnet (YIG) thick film to investigate it's uses for microstrip patch antenna. It was observed that the overall bandwidth and return loss has improved. Also, it has been proved that by using YIG thick film, the main limitation of

antenna i.e., bandwidth can be enhanced **[95]**.

Fechine and Fontgalland, in 2016 have studied the dielectric properties of GdIGxYIG1-x composite (x=1, 0.75, 0.5, 0.25 and 0) for miniaturization of magneto-dielectric antennas. GdIGxYIG1-x was prepared by ball milling method. It was observed that the formed material has stability as very less change in function of temperature and in frequency range has been observed. Further investigation with FRAs gave very satisfactory results because it showed control antenna radiation and good tuning **[96]**.

Andreou et al., in 2017 have examined the magneto-dielectric properties of YIG/Epoxy composite for reconfigurable microstrip antenna. The effect of dielectric losses on the efficiency of the antenna has been studied. The fabrication of YIG/Epoxy substrate has been done with improved properties of antenna having less losses and high efficiency **[97]**.

Akhtar et al., in 2018 have worked on the composite of Bismuth Iron Garnet with composition $Bi_{3-x}R_xFe_5O_{12}$ for x= 1.5 (R symbolize rare earth element, like Y, Gd, Pr, Ho, Yb). Composites of BIG have been successfully synthesized via sol-gel method and investigated further. XRD analysis show that there is formation of single-phase garnet structure and crystallite size was calculated for different composites. From SEM, grain size was calculated. From FTIR analysis, vibrational bands were obtained which is withstand with XRD result, that there is presence of garnet phase. From VNA analysis detailed magnetic as well as dielectric properties was calculated at 6 GHz. These calculated magnetic and dielectric properties show that these rare earths doped garnet ferrites have good application for high frequency range i.e., in GHz range **[98]**.

Aakansha et al., in 2018 have reported the dielectric and magnetic propertied of samarium doped YIG ($Y_{3-x}Sm_xFe_5O_{12}$ x=0 to 0.3). Solid state reaction was used to prepare samples. It has been observed that with increase in Sm content in the samples the value of magnetic saturation decreases due to antiferromagnetic behavior. The value of dielectric constant increases with substitution and from Nyquist plot the contribution of both grain and grain boundaries has been observed **[99]**.

Bhalekar and Singh, in 2020 have worked on the pure YIG and its composite of YIG by doping of Al and La and further studied the structural and magnetic properties. YIG and it's $Y_{2.8}La_{0.2}Fe_{5-x}Al_xO_{12}$ (x= 0.0, 0.1, 0.2and 0.3) was synthesized via sol gel auto combustion route at sintering temperature of 900 C for 3 hours. From XRD and FTIR (due to Fe-O vibrations) analysis it was proved that there is formation of garnet phase. From XRD analysis it was found that there is decreased in value of d- spacing, X-ray density, lattice parameter(a), reason is

addition of small size of Al^{3+} in tetrahedral site. From SEM analysis it has been found that agglomerated and branched morphology was present also branch length was ranging 537-437 nm and average branch width ranges from 90-140 nm. From VSM it was found that there was enhancement in saturation magnetization of sample containing 6.7% of La^{3+} ion at place of Y^{3+} ions. Whereas decreased in value of saturation magnetization with addition of Al^{3+} because it tends to weaken the super exchange interaction. As a result, it was found that composites of rare earth garnet are very useful in high frequency microwave devices **[100]**.

Shafiee et al., in 2020 have studied the application of Gadolinium Iron Garnet by variation with particle size in potential patch antennas. Ball milling method has been used to synthesized GdIG, at 3,6,9 and 12 hours of sintering at 1200°C. From STEM analysis it has been found that with changing milling time from 3,6,9 and 12 hours the average particle size also change from 36.9, 27.2, 19.2 and 20.8 nm respectively. The grain size was calculated for single phase gadolinium iron garnet i.e., 0.66, 0.67, 0.72 and 0.69 μm respectively and further from VSM it was calculated that initial permeability and magnetic losses were less when applied in low frequency. This result was in favor of using of GdIG as potable patch antenna **[101]**.

Musa et al., in 2020 have studied microstructure, electrical, dielectric and electromagnetic properties of Al substituted YIG. YIG was successfully prepared by sol-gel auto-combustion route. The composition taken was $Y_3Al_xFe_{5-x}O_{12}$, whereas x= 0.4, 0.8, 1.2. 1.6 and 2.0. FESEM analysis was done to study microstructural analysis, from which grain size was calculated. Grain size show decreasing trend from 0.46 μm to 0.33 μm at x=0.4 and x=2.0 resp. From Agilent Impedance Analyzer it has been concluded that with Al concentration resistivity decreases. With Al substitution and increasing frequency loss tangent decreases. At x= 0.4 the real permeability is 1263.12 which further decrease at x = 1.2 with 11.74. it was concluded that low loss values, high dielectric constant of these composites of YIG doped Al can be used as miniaturization of antenna, filter resonator and for radio frequency devices **[102]**.

Akhtar et al., in 2020 have studied the structural, morphological and magnetic properties of Ce doped garnet ferrite i.e., $Ce_xGd_{3.5-x}Fe_{4.5}O_{12}$ (x=0.0, 0.4, 0.8, 1.2, 1.6, 2.0 and 2.4). Ce doped garnet ferrite was synthesized by sol gel self-combustion method. From XRD analysis single phase structure of Ce^{3+} doped garnet ferrite was revealed. Further study of XRD showed crystallite size of garnet decreases with Ce^{3+}. From XRD bond length, ionic radii, radii were calculated. From FTIR analysis study of stretching band was done. Using FESEM results, grain size morphology of Ce^{3+} doped garnet was examined. From VSM it was found that with increased in saturation, remanence and coercivity. As a result, it was concluded that as Ce^{3+}

doped garnet showed very good magnetic properties so it can be a better material for use as miniaturization of devices for various application **[103]**.

Khalifeh et al., in 2020 synthesized $Y_{2.8-x}Dy_xCe_{0.10}Bi_{0.10}Fe_5O_{12}$ (x=0, 0.2 to 0.6) and YIG by conventional solid-state method. The effect of substitution of yttrium by dysprosium ions on the structural and magnetic properties of $Y_{2.8-x}Dy_xCe_{0.10}Bi_{0.10}Fe_5O_{12}$ (x=0, 0.2 to 0.6) has been reported. The XRD results reveals that in samples the garnet phase formed with some impurities of CeO_2. The Raman spectroscopy also support the formation of garnet phase in the samples. The XPS study reveals that the yttrium, dysprosium, bismuth and iron ions present in +3 valence state. The magnetic saturation increases with substitution and coercivity decreases. The reported samples are good for microwave devices **[104]**.

Gao et al., in 2021 synthesized $Y_{3-x}Ca_xIn_{0.6}Ge_xFe_{4.4-x}O_{12}$ (x=0-0.6) by adopting conventional solid-state reaction process. The structural, magnetic and dielectric properties were studied for Ca-Ge substituted YInIG. XRD study reveals that Ca-Ge substitution did not affect the phase of the garnets. The Ca-Ge substituted samples result in enhanced magnetic properties and dielectric properties with high saturation magnetization, small coercivity, narrow ferromagnetic resonance, low dielectric loss and low dielectric constant. The properties of the samples, make the materials proper candidate for microwave devices applications **[105]**.

Li et al., in 2021 fabricated indium (In) doped YIG ($Y_3Fe_{5-x}In_xO_{12}$ x= 0-0.75 with step size 0.15) by solid state reaction method. XRD study reveals that 'In' doping did not distort the garnet crystal structure and bulk density increases. SEM study indicates that with substitution grain size changes. From VSM study it has been found that saturation magnetization value increases with 'In' content from 25.98 emu/g to 28.2 emu/g. The modified structural and magnetic properties imply that 'In' doped YIG is appropriate candidate of antenna applications and high frequency devices **[106]**.

Sibi et al., in 2021 have tailored magnetodielectric properties of the composite of natural garnet/$Ni_{0.5}Zn_{0.5}Fe_2O_4$/$LiFe_5O_8$ mixed with B_2O_3. XRD study implies that proper diffusion of two phases in the composites. The morphological study of the composites reveals that the grains are tightly packed in the composites. The calculated dielectric and magnetic losses for 0.5 natural garnet and 0.5 $Ni_{0.5}Zn_{0.5}Fe_2O_4$ are 0.02 and 0.49, whereas for 0.5 natural garnet and $LiFe_5O_8$ composite the values are 0.001 and 0.05 at GHz frequency. The obtained results indicates that the composites of natural garnet with spinel ferrites are good candidate for wireless applications in GHz range **[107]**.

Dewi et al., in 2022 synthesized lanthanum-doped YIG ($Y_{3-x}La_xFe_5O_{12}$ for x = 0, 0.1, 0.3, 0.5)

with solid state ball-milling method. With increase in lanthanum content, the value of lattice constant increases and crystallite size decreases. It has been reported that due to doping the value of saturation magnetization and remanence increases as compare to pure YIG. The improved properties of the samples suggest their use for microwave applications **[108]**.

Ji et al., in 2022 synthesized praseodymium, zinc and zirconium doped YIG ($Pr_xY_{3-x}Zn_{0.1}Zr_{0.1}Fe_{4.8}O_{12}$ (x=0, 0.1, 0.15 and 0.2). From XRD it has been clear that the Pr ion is properly doped in YIG. With Pr doping the lattice constant and grain size increases. The magnetic parameter like saturation magnetization, magnetic anisotropy and ferromagnetic resonance increases with the Pr content. The dielectric parameters like real and imaginary part of the permittivity have highest value at x=0.15. The Pr doping in YIG has enhanced the structural, dielectric and magnetic properties **[109]**.

Fu et al., in 2022 synthesized low temperature $Bi_{1.4}Y_{1.3-x}Ca_{0.3+x}Zr_{0.3}Sn_xFe_{4.5-x}O_{11.7}$ by using solid state method. The variation in structural, magnetic and dielectric properties under the effect of Ca, Sn, Co substitution. From 1MHz to 0.5 GHz the dielectric constant for all samples is high (~ more than 30) The and dielectric losses are less ($\sim 10^{-3}$). With increases in substitution the lattice constant increases and density decreases. The prepared samples possess very good magnetic properties. The present results indicates that low temperature sintered YIG is best for miniaturized and high-performance microwave communication devices **[110]**.

Karilainen et al., in 2011 have suggested that dielectric or magneto-dielectric materials could be utilized to miniaturize antennas, there are a number of crucial factors that must be taken into account. The authors talk about these merit statistics and a scientific way to contrast antennas with various material fillings. Fe-SiO2 sheets with a mylar substrate produce the magneto-dielectric material. The material's permeability measurement results are reported. The meandering PIFA's radiation process is investigated, and the ideal placement for dielectric and magneto-dielectric filling is explored and determined. At the same resonance, the degree of miniaturization of the provided magneto-dielectric fills and commercial dielectric is measured and compared **[198]**.

Bolivar et al., in 2003 have used time-domain spectroscopy to examine low-loss, high-dielectric-constant materials in the THz frequency band. Steatite, alumina, titania-loaded polystyrene, and zirconium-tin-titanate dielectric constants and loss tangents are provided and compared to tests on high-resistivity silicon. The real component of the dielectric constant for these materials ranges from 6 to 90. The samples were all discovered to have acceptable low-loss tangents. Applications as terahertz frequency antenna photonic crystal substrates are

anticipated **[199]**.

Huitema et al., in 2013 have reported ultracompact antenna design for DVB-H (digital video broadcasting-handheld) receiving devices. The 49 channels of 8 MHz that make up the DVB-H frequency range span 470 to 862 MHz. It is substantially downsized (λ_0 /49, λ_0/71, λ_0/160 at 470 MHz) and made to fit inside a tablet, and by using a magneto-dielectric material, it can cover every channel. Additionally, the incorporation of a varactor diode allows the working frequency to be continually tuned across the whole DVB-H band. The behavior of this varactor diode has been accurately described and predicted to match that of the antenna. The behavior of this varactor diode inside the antenna has been accurately described and modelled. Limitations on the amount of power the diode will accept are highlighted. Subsequently, the antenna design is integrated into the DVB-H receiver device along with magneto-dielectric material and a varactor diode **[200]**.

2.2 Motivation and Research Gap

The literature survey on various papers based on garnet ferrites and its composites has been done. From literature survey it has been found that till now the focus of research is oriented mostly on YIG and its composites for antenna applications, where as many of the other rare earth doped garnet ferrites are less exploded for antenna application. Some researchers have discussed the application of garnet ferrites at different frequency range. In literature it has been found that mostly garnet ferrites are prepared by conventional solid- state method and other methods, very less researchers have synthesized garnet ferrites by sol-gel auto combustion method. Also, miniaturization factor found in literature is low. The problems of impedance mis-matching, and low bandwidth are further needed to improve along with low losses in garnet ferrite for antenna application. To attain specific application of ferrite, different substitution of ions has been done. Substitution of ions results in the modification in grains size, hysteresis and electromagnetic properties which are useful for numerous technological applications.

2.3 Objectives of the Study

1 Effect of temperature and composition variation on structural, magnetic and dielectric properties of garnet ferrites composite.

2 To study the miniaturization parameters of garnet ferrites composites for antenna application.

3 To study the losses of garnet ferrites composites for antenna application.

Chapter 3

Research Methodology

3.1 Introduction

In this research, we have adopted sol-gel auto combustion method to synthesize garnet ferrite and spinel ferrite. Structural, magnetic and dielectric properties of garnet ferrites and rare earth, metal, non-metal ions substituted spinel ferrites composites with composition and temperature variations have been investigated. Nanocomposites of pure and metal ion substituted garnet ferrites with other ferrite that has been synthesized and characterized in order to study miniaturization and losses in the composites for antenna application.

3.2 Synthesis Method

3.2.1 Sol – Gel Auto-Combustion Method

For the preparation of nanosized oxides of the ferrites, sol-gel auto combustion method is used. In the preparation process an exothermic reaction takes place between fuels and oxidized, it is wet chemical method. In the present work, nitrates are used as oxidant and citric acid as fuel. This method is most appropriate method to synthesized ferrites over other synthesis methods like solid state method, hydrothermal method, ceramic method and co-precipitation method. Sol-gel auto combustion method provides controlled morphology, homogeneity in the samples, time saving, required low temperature and is the cheapest method because the precursors are nitrates and do not require costly equipment. The first step in this process is to transform monomers or starting materials into colloidal solution (sol), which serves as a precursor for the subsequent gel formation. The raw material, such as metal nitrates or alkoxides, is usually dispersed in a particular solvent, such as ethylene glycol, water, or a suitable acid, to form a "sol," which is then aged and heated to form a "gel," which is then dried or heated at higher temperatures to evaporate the liquid medium and transform the gel into a "precursor." A sol is a colloid suspended in a liquid, whereas a gel is a suspension that maintains its shape, hence the name "sol-gel". **Figure 3.1** represents the formation of different phases during sol-gel process and the steps followed for the preparation of ferrites.

(a)

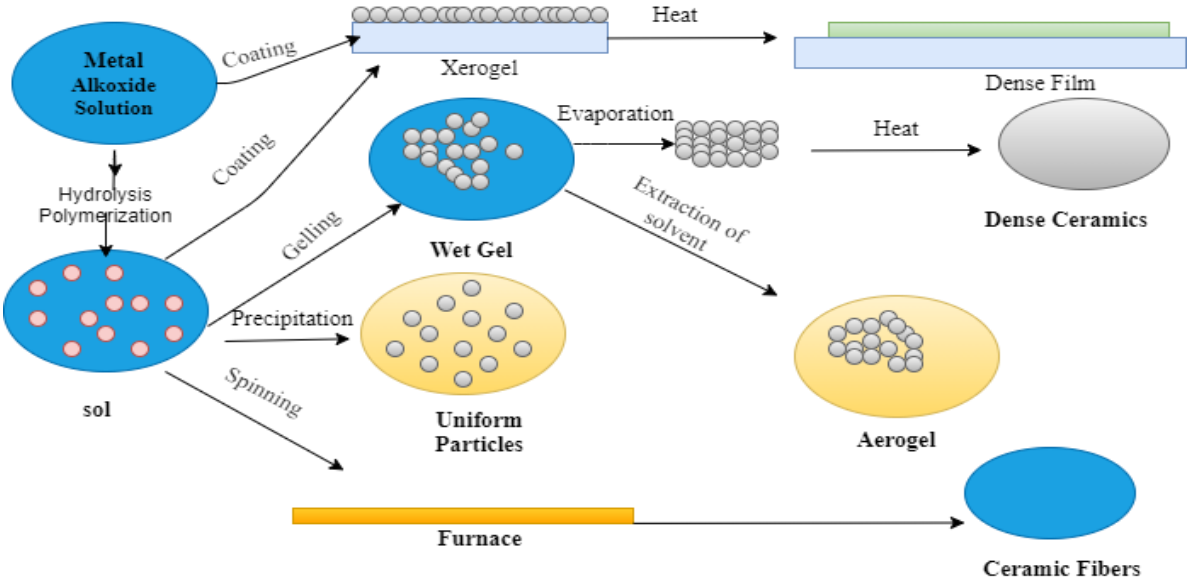

(b)

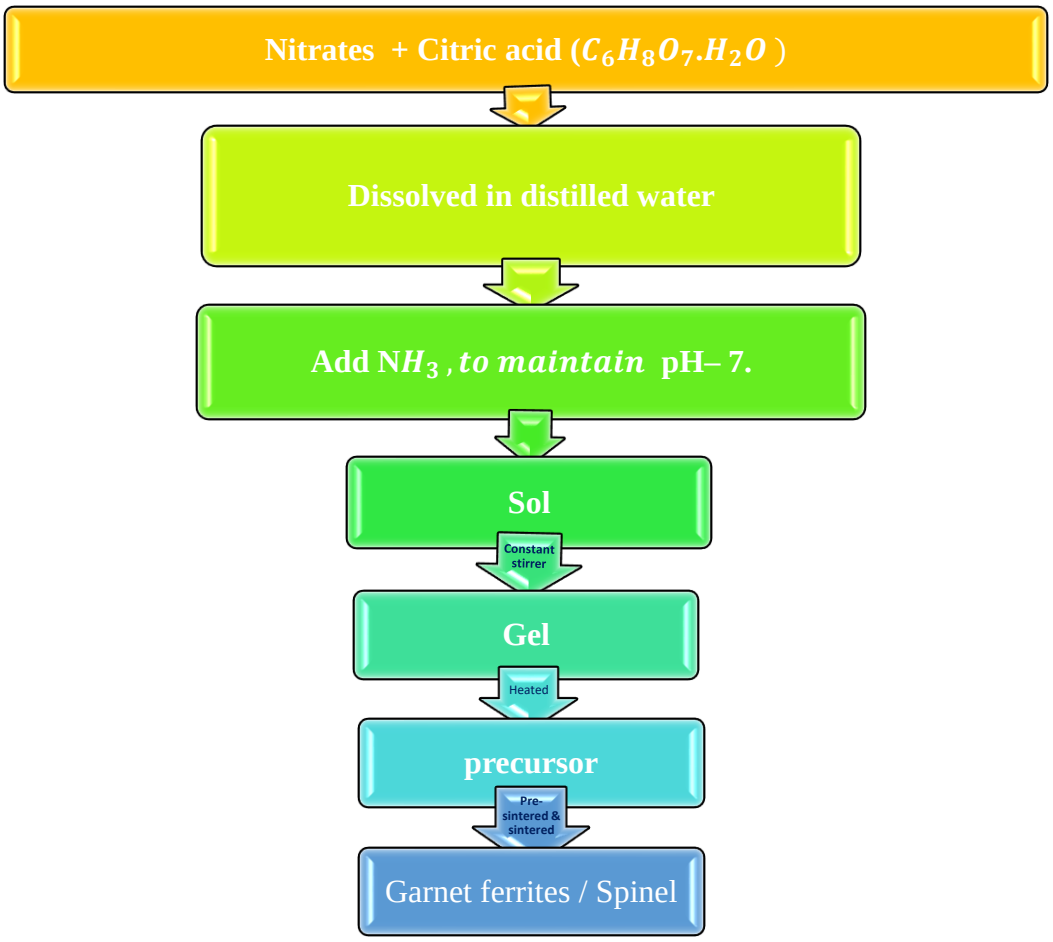

Figure 3.1 (a) Sol-gel auto-combustion process and (b)steps of the preparation of ferrites

The hydrolysis, condensation, and polymerization of monomers to create particle and particle agglomeration, followed by the creation of a network that expands across the liquid media, culminates in the formation of gel in the beginning of sol-gel auto-combustion process. When a substance reacts with water, it undergoes hydrolysis, whereas condensation is the transformation of a gas or vapour into a liquid.

3.2.2 Synthesis of Al^{3+} substituted gadolinium iron garnet ($Gd_3Fe_5O_{12}$)

The method adopted to prepare $Gd_3Fe_3Al_2O_{12}$ is sol gel auto combustion method. Gadolinium (III) nitrate [$Gd(NO_3)_3.6H_2O$], ferric (III) nitrate [$Fe(NO_3)_3.9H_2O$], aluminium (III) nitrate [$Al_3(NO_3)_3.6H_2O$] and citric acid ($C_6H_8O_7.H_2O$) of AR grade were used as precursors to form sample.

Formation of garnet ferrite started with weighing of these nitrates according to stoichiometric ratio mention in the equation below:

$$3Gd(NO_3)_3.6H_2O + 3Fe(NO_3)_3.9H_2O + 2\ Al_3(NO_3)_3.6H_2O \longrightarrow Gd_3Fe_3Al_2O_{12}$$

These nitrates along with citric acid are then put together in 100 ml of distilled water with metal to citric acid ratio of 1:0.5 and then keep on magnetic stirrer for half an hour stirring until clear solution was obtained. After half an hour stirring, pH of 7 of the solution was balanced by adding ammonium drop wise into the solution. After that, solution was kept for stirring along with heating of around 70°C, until gel was formed. The gel was heated at 200-250°C for an hour to get dark brown powder. Finally, powder was fined by using mortar pastel. And then sintered the sample at different temperature that is 900°C, 1000°C and 1100°C for 5 hours in muffle furnace.

3.2.3 Synthesis of gadolinium iron garnet, magnesium spinel ferrite and their composite ($GdIG/MgFe_2O_4$)

Gadolinium iron garnet ($Gd_3Fe_5O_{12}$) and magnesium ferrite ($MgFe_2O_4$) were prepared using the sol-gel auto- combustion method separately. For the preparation of $Gd_3Fe_5O_{12}$ (GdIG), gadolinium (III) nitrate [$Gd(NO_3)_3.6H_2O$], ferric (III) nitrate [$Fe(NO_3)_3.9H_2O$], and citric acid ($C_6H_8O_7.H_2O$) of Sigma Aldrich and LOBA company with AR grade were used as precursors. For the preparation of $MgFe_2O_4$, magnesium (II) nitrate [$Mg(NO_3)_2.\ 6H_2O$], ferric (III) nitrate [$Fe(NO_3)_3.9H_2O$], and citric acid ($C_6H_8O_7.H_2O$) of LOBA company with AR grade were used as precursors. According to stoichiometric, these salts of metals were added in 100 ml of

distilled water by using different beakers for the preparation of GdIG and magnesium ferrite (MF) and kept for stirring for half an hour on a magnetic stirrer in order to dissolve these salts in distilled water properly. After that pH of the solution was made 7 by adding ammonia solution dropwise. Then the solutions were kept for stirring and heated at 70°C until the solution reduces and the gel was obtained. The gel of both the solutions was heated at 200-250°C for an hour. The gel starts drying up, swelling up and burning in presence of air. Finally, the powder was obtained. The sintering of GdIG was done at 1200°C for 6 hours in a muffle furnace. The sintering of the MF was done at 900°C for 6 hours in a muffle furnace. The sintered samples were ground using mortar pastel for half an hour to obtain a fine powder. Finally, the obtained samples were used to form composites. The GdIG sample was divided into three parts in order to make composites with MF. The composites were formed according to wt% using the equation $mx = m(1 - x)$ where x is weight percent, m is the total weight of material used to prepare composites. The weighted sample were then mixed together by mechanical blending for 45 minutes to prepare composes with wt% x= 1.0 (GdIG), 0.5 (GdIG 50% and MF 50%) and 0.7 (GdIG 75% and MF 25%).

3.2.4 Synthesis of gadolinium iron garnet, magnesium spinel ferrite and their heat-treated composite (GdIG/$MgFe_2O_4$)

Sol-gel auto-combustion method was used to prepare gadolinium iron garnet ($Gd_3Fe_5O_{12}$) and magnesium ferrite (spinel ferrite). Gadolinium (III) nitrate [$Gd(NO_3)_3.6H_2O$], ferric (III) nitrate [$Fe(NO_3)_3.9H_2O$], and citric acid ($C_6H_8O_7.H_2O$) of AR grade were used as precursors for the preparation of $Gd_3Fe_5O_{12}$ (GdIG). Magnesium (II) nitrate [$Mg(NO_3)_2.6H_2O$], ferric (III) nitrate [$Fe(NO_3)_3.9H_2O$], and citric acid ($C_6H_8O_7.H_2O$) of AR grade were used as precursors for the preparation of $MgFe_2O_4$ (MF). Both GdIG and MF was prepared separately. The precursors of ferrites weighted according to stoichiometric were added to 100 ml of distilled water. To dissolve these precursors properly, solutions was kept for stirring on magnetic stirrer for half an hour. After half an hour clear solution was obtained. To maintain the pH of solutions, ammonia solution was added drop wise until pH is equal to 7. These solutions were kept for stirring with heating at 70°C until sol reduces and gel formed. In order to dry, swell the gel and to initiate combustion process the temperature around 200-250°C was provided for an hour. The heat was provided in order to dry the obtained powder properly. After that a light weight powder was obtained for both ferrites. These obtained fined powders were ground with the help of pestle mortar. These fine powders were then sintered according to required temperatures.

GdIG powder was treated at 1200°C for 6 hours. MF powder was treated at 1000°C for 6 hours in muffle furnace.

These sintered powders of GdIG and MF were used to form composite. Powder of GdIG and MF were weighted according to weight percent of 0.75 ((GdIG)x-MF(1-x) GdIG 75% and MF25% of total powder) and then mixed with the help of pestle mortar (mechanical blending) to form composite. The composite is divided into two parts. One part is sintered at 900°C and other at 1300°C for 3 hours in order to check the effect of temperature on properties of garnet ferrite composite.

3.2.5 Synthesis of Y^{3+}, Bi^{3+}, La^{3+} substituted gadolinium iron garnet (GdIG)

Sol-gel auto-combustion method was adopted for preparation of Y^{3+}, Bi^{3+} and La^{3+} substituted $Y_{0.2}Bi_{0.2}La_xGd_{2.6-x}Fe_5O_{12}$ (x=0, 0.2 and 0.4). Gadolinium (III) nitrate [$Gd(NO_3)_3.6H_2O$], Yttrium (III) nitrate [$Y(NO_3)_3.6H_2O$], Bismuth (III) nitrate [$Bi(NO_3)_3.6H_2O$], Lanthanum (III) nitrate [$La(NO_3)_3.6H_2O$], ferric (III) nitrate [$Fe(NO_3)_3.9H_2O$] and citric acid ($C_6H_8O_7.H_2O$) were used as precursor. Substituted garnet ferrite samples (x=0,0.2,0.4) was prepared by weighing of these nitrates according to stoichiometric ratio and put into three different beakers, carrying 100 ml of distilled water. These different composition solutions were then kept on magnetic stirrer for half an hour in order to obtain clear solutions. After that ammonia solution was added drop wise in each solution with continuous stirring to obtain pH∼7. Then these three solutions were kept on magnetic stirrers in order to give continuous stirring and heating at 70°C until gel formed. Then the obtain gel for three sample as kept for heating at 200°C to 250°C for an hour. This gel gets swell dry and burn in presence of air. The obtain powder of the samples dried completely. The obtained powder for sample x=0 ,0.2 and 0.4 is firstly grounded finely and then sintered at 1200°C in different muffle furnace of 6 hours.

3.2.6 Synthesis of yttrium iron garnet, erbium iron garnet and their composite (YIG/ErIG)

Sol-gel auto- combustion method was adopted to prepare yttrium iron garnet ($Y_3Fe_5O_{12}$) and erbium iron garnet ($Er_3Fe_5O_{12}$). $Y_3Fe_5O_{12}$ was prepared by using yttrium (III) nitrate [$Y(NO_3)_3.6H_2O$] with 99.999% trace of Sigma-Aldrich company, ferric (III) nitrate [$Fe(NO_3)_3.9H_2O$] with 98% purity of LOBA company and citric acid ($C_6H_8O_7.H_2O$) with purity of 98% of LOBA company as precursors. $Er_3Fe_5O_{12}$ (ErIG) was prepared by using erbium (III) nitrate [$Er(NO_3)_3.6H_2O$] with 99.999% trace of Sigma-Aldrich company, ferric (III) nitrate [$Fe(NO_3)_3.9H_2O$] with 98% purity of LOBA company, and citric acid ($C_6H_8O_7.H_2O$) with 98%

purity of LOBA company as precursors. By weighing these salts according to stoichiometric ratio i.e., citric acid to metal (cation) ratio in 1:1 all salts were added in 100 ml of distilled water one by one. For easy understanding first write the molecular weights (MW) of all cation's nitrates (written on the chemical box), for e.g. $Y(NO_3)_3.6H_2O$, $Fe(NO_3)_3.9H_2O$ in case of $Y_3Fe_5O_{12}$. Then multiply the MW with number of cations like for Y^{3+} with 3 and for Fe^{3+} with 5. Now in order to know the amount of citric acid to be added firstly sum up the total number of cations in formula like for our case it is 8. Then multiply the total number of cations with citric acid to metal ratio.

Finally multiply the obtain number with MW of citric acid. Just for simplification divide all the obtain amounts individually with some common factor like 100, 200 and so on. Beakers containing salts of YIG and ErIG were kept for stirring for half an hour on magnetic stirrer to make homogenous clear solution. In order to maintain pH around 7 ammonia solution was added drop wise in solutions with continuous stirring. These solutions were than provided with continuous stirring and heating around 70°C until solutions turn to gel. After that stirring has been stopped and gels were kept for heating at 200-250°C until it swells up and burnt in presence of air. After proper drying the required powders were obtained. Finally, the prepared powders were sintered at 1200°C for 7 hours in muffle furnace.

3.2.7 Synthesis of yttrium iron garnet, Cd^{3+}- Co^{3+} substituted magnesium ferrite and their composite YIG/MgCdCoFe

The sol-gel auto combustion method was adopted to prepare yttrium iron garnet ($Y_3Fe_5O_{12}$) and magnesium substituted spinel ferrites ($Mg_{0.4}Cd_{0.4}Co_{0.2}Fe_2O_4$). The precursors, yttrium (III) nitrate [$Y(NO_3)_3.6H_2O$], cadmium (III) nitrate [$Cd(NO_3)_3.6H_2O$], cobalt (III) nitrate with 99.999% traces were procured from Sigma-Aldrich whereas ferric (III) nitrate [$Fe(NO_3)_3.9H_2O$], magnesium (III) nitrate [$Mg(NO_3)_3.6H_2O$] and citric acid ($C_6H_8O_7.H_2O$) with a purity of 98% were procured from Loba Chemie. The weighted amount these salts were taken according to the stoichiometric ratio of citric acid to metal cation in 1:1 and added to 100 ml of distilled water. The solution was magnetically stirred for half an hour to get a homogenous clear solution. Ammonia solution was then added slowly to maintain the pH 7. The solution was then continuously stirred and heated simultaneously at 70°C until it turns to gel. The obtained gels were kept for heating at 200°C -250°C until it swells up and burnt in presence of air to get the dried powders. Finally, the prepared powders were sintered at 1200°C for 7 hours in a muffle furnace. The powders of YIG and MgCdCoFe were ground finely by using a mortar

pestle. These fine powders were used to prepare the composites. The powders of the synthesized YIG and MgCdCoFe were weighed according to the weight per cent and then blended by facile mechanical/ physical blending for 45 minutes with the help of a mortar pestle to prepare the composites of YIG(x)/MgCdCoFe(1-x) with wt%, x = 0.3, 0.6 and 0.9.

3.2.8 Synthesis of Pr^{3+} substituted gadolinium garnet ferrite (GdIG)

Praseodymium doped Gadolinium iron garnet ($Pr_xGd_{3-x}Fe_5O_{12}$ for x=0.5,1.0 and 1.5) was prepared using sol- gel auto-combustion method. Gadolinium (III) nitrate [Gd $(NO_3)_3.6H_2O$], ferric (III) nitrate [Fe $(NO_3)_3.\ 6H_2O$], Praseodymium (III) nitrate [Pr $(NO_3)_3.\ 6H_2O$] and citric acid ($C_6H_8O_7.H_2O$) of AR grade were used as precursors. The precursors were weighed according to stoichiometric formula and add into 100ml of distilled water. Then the beakers containing salts were kept for stirring for thirty minutes in order to form clear solution. In order to maintain the pH approximately 7 ammonia solution was added into the solutions with constant stirring. Then the solution kept for stirring and heating until gel form. After that heat is increase to $200 - 250^{\circ}$C until gel swells and auto combustions starts. Finally, powders were obtained after proper drying of samples. These obtained samples were finely ground. The obtained powder was sintered in muffle furnace for 6 hours at 1200° C temperature.

3.3 Characterization Techniques

3.3.1 Introduction

In order to investigate and to study the variation in structural, optical, morphological, magnetic, dielectric, microwave losses and miniaturization parameters of garnet ferrites (substituted or pure) and its composites different characterization has been caried out. Characterization techniques are very useful tools for the contribution of new research. X-ray diffraction (XRD), Field emission scanning electron microscope (FESEM), Energy dispersed x-ray (EDX), Fourier transform infra-red (FTIR), Ultraviolet visible (UV-Vis), Vibrating sample magnetometer (VSM), Impedance spectroscopy, Fluorescence spectroscopy and Vector network analyzer (VNA) were used for the study of different properties of the synthesized samples.

3.3.2 X-ray Diffraction (XRD)

For the characterization of the sample, X-Ray diffraction is a commonly used technique. X-ray diffractogram is generally use to study the crystallographic changes such as phase identification in the material. The basic principle of the characterization technique is based on the constructive interference that occurs in cathode ray tube and produces the monochromatic beam of X-rays from the crystalline sample. XRD method is non-destructive and deals with the interaction of

X-rays with matter. Elastic diffusion, also known as Rayleigh diffusion, occurs when a monochromatic X-ray beam interacts with the object and scatters in random directions with the same energy as the input photons. This characterizations procedure only works on crystalline or semi-crystallized matter. As a result, if the sample to be examined has a regular arrangement of atoms, dispersed light is oriented in specified directions that is determined by the X-ray wavelength, crystal lattice dimensions, and orientation.

X-rays are the bundle of electromagnetic energy, that are originates from electron clouds of atoms. For the production of X-ray, a high-speed electron from the cathode strikes on the atom of anode. After bombardment, an electron from the cathode got ejected and a vacancy is created. The electron presents in higher shell jump from its shell to lower shell in order to fill the vacancy, and therefore while jumping the X-rays photon of particular energy releases. When this X-ray is bombarded on the sample the atoms scatter the incident ray. While interacting with the regular array of electrons in the atom, arrays of spherical waves produce. Due to destructive interference a large number of waves got cancel in major of the directions. On the other side in some directions some waves added up constructively as explained by Bragg's law mentioned as follow:

$$2dsin\theta = n\lambda$$

Where 'd' is spacing between diffraction planes, 'λ' is the wavelength of X-ray and 'θ' is angle of incidence. All the attainable diffraction direction of the lattice are scanned by the angles 2θ. Hence the XRD spectra is recorded in the form of diffraction peaks representing the definite miller indices values (hkl). The sample identification is done with the help of diffraction peaks that are transform to d-spacing, and every material has its unique d-spacing.

3.3.3 Fourier Transforms Infrared Spectroscopy (FTIR)

The technology of FTIR spectroscopy was used to investigate the interactions between infrared and sample. It is the most recently developed form of dispersive spectrometer and is favored over the others. Its excellent precision, accuracy, speed, increased sensitivity, ease of use, and sample non-destructiveness all contribute to its success. Infrared spectroscopy technology is based on the atomic vibrations of a molecule that absorbs only specified frequencies and energy of infrared radiation. Because various compounds have different infrared spectrums, FTIR could be used to detect and classify them. Its work is to investigate the vibrational properties of molecules in matter. This method can be used to identify the various functional groups and residues present in a sample. The IR region, which extends from (0.7-1) to (200-350) μm and can be categorized into three ranges that are as follow: Near IR 13000 -4000 cm^{-1} 400-10 cm^{-1},

Mid IR between 4000-400cm^{-1} Far infrared between 400-10 cm^{-1}. The far-infrared has low energy so it is used to study the fundamental and rotational vibrations. Mid infra-red having moderate energy is used to study coupled rotational – vibrational structure. Far infra-red has high energy so it is used to for the excitement of overtone vibrations. For the characterization purpose mid-infrared spectrum is used. Infrared radiation is passed through the material to be absorbed by the molecules it contains in FTIR spectroscopy. The vibration frequencies of the molecules must be equal to those of radiation so that matter can absorb energy. When light strikes a sample, one part of it is reflected, another is absorbed, and the third is transmitted. The exact frequencies of energy absorbed by the specimen match to the vibrational energy of the functional group in the sample. A detector collects the transmitted light that carries the sample's molecular information.

Figure 3.2 represent the basic principle of FTIR technique. The mid-infrared frequencies in FTIR are measured by the interferometer with in few seconds. The interferometer is used to analysis the energy that is transmitted through the material. The interferometer contains a beam splitter, stable mirror and moving mirror. that split the falling IR radiation in two parts. One beam is set so that it can retains fixed path length and create a path difference for the other beam that is varying according to moving mirror. These two beams interfere constructively and a beam is emitted out from the interferometer which is known as interferogram. The emitted beam consists of all the information about the sample. With the help of mathematical technique software name as Fourier transformation, all the information is decoded from the individual frequencies. Nicolet FTIR interferometer IR prestige-21 with model-8400S was used for FTIR spectrometer.

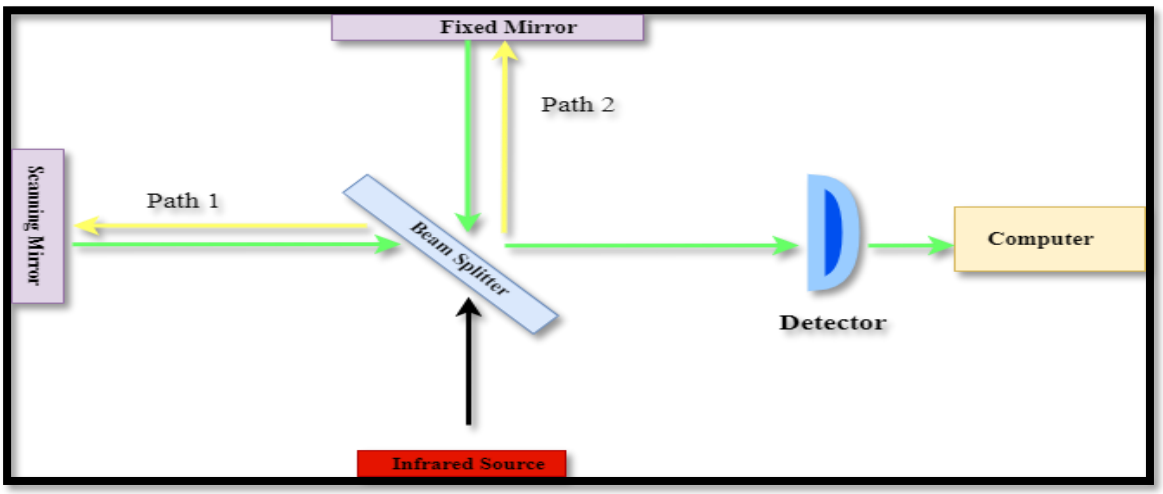

Figure 3.2 Principle of FTIR technique

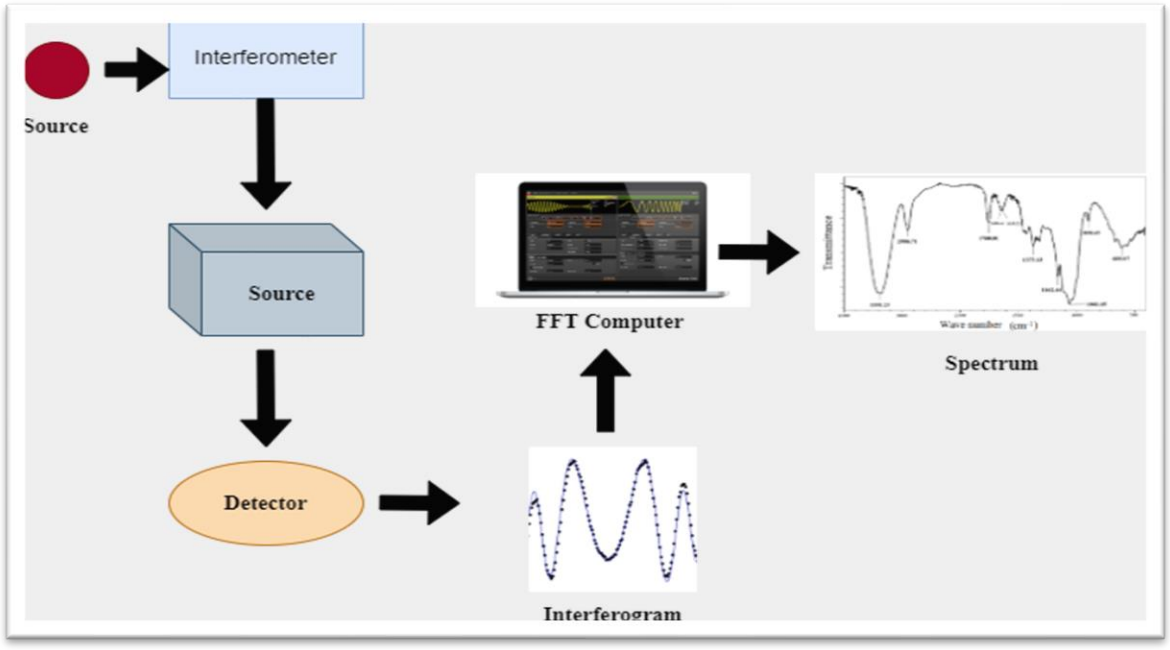

Figure 3.3 Working of FTIR technique

3.3.4 Ultraviolet-visible (UV-vis) Spectroscopy

This method is mostly used to identify chemical species in a sample. This approach is unique in that it studies atoms' electronic transitions. Generally, excitation of electron from lower energy state to higher energy state has been observed when the atoms or molecules absorb the ultraviolet (UV) and visible radiations. The quantum energy levels of atoms implies that only that radiation is absorbed that have specific amount of energy and is capability to make transition from one state to another. The basic principle of the spectroscopy is accordance to Beer-Lambert's law. According to this law **(Equation 3.1)** the absorbance (α) is directly proportional to the path length of the absorbing medium (b) and quantity of the sample (c).

$$\alpha = log_{10}\left(\frac{I_0}{I}\right) = \varepsilon bc \qquad (3.1)$$

Herein I_0 represents the intensity of the reference beam, I represent the intensity of the beam of sample and ε is proportionality constant. The UV radiation have energy between 200 to 400 nm which is more enough capable of electronic excitations with in molecular orbitals (ΔE). ΔE is the energy difference between the highest occupied molecular orbital (HOMO) and lowest unoccupied molecular orbital (LUMO). Which means if the value of ΔE is small than the energy requires for the excitation of an electron will also be small. The incident photon must have ΔE greater than or equal to the energy of the excited electron only than it can get absorb and able to excite the electron.

This method makes use of monochromatic radiation, which can be UV, visible, or near infrared. When radiation strikes a sample, it can cause the molecule to undergo an electronic transition. The colour of a material is linked with its electronic structure. This spectroscopy allows for the evaluation of all electronic transitions as well as the determination of certain sample properties such as band gap energy, which allows for the classification of the sample as an insulator, semiconductor, or conductor. When light (energy) falls on a sample, it is usually absorbed. The absorbed energy encourages electrons to move from the ground state to excited state orbital or to anti-bonding orbitals. **Figure 3.4** represents the all-possible transitions, when photon get absorb (σ-σ^*, π-π^*, σ-π^*, π-σ^*, n-σ^*, n-π^*). But in UV- vis spectroscopy σ-σ^*, π-π^*, σ-π^*, n-σ^*, n-π^* transitions are possible, whereas σ-σ^* and n-σ^* transition requires high energy and π-π^* and n-π^* require less energy.

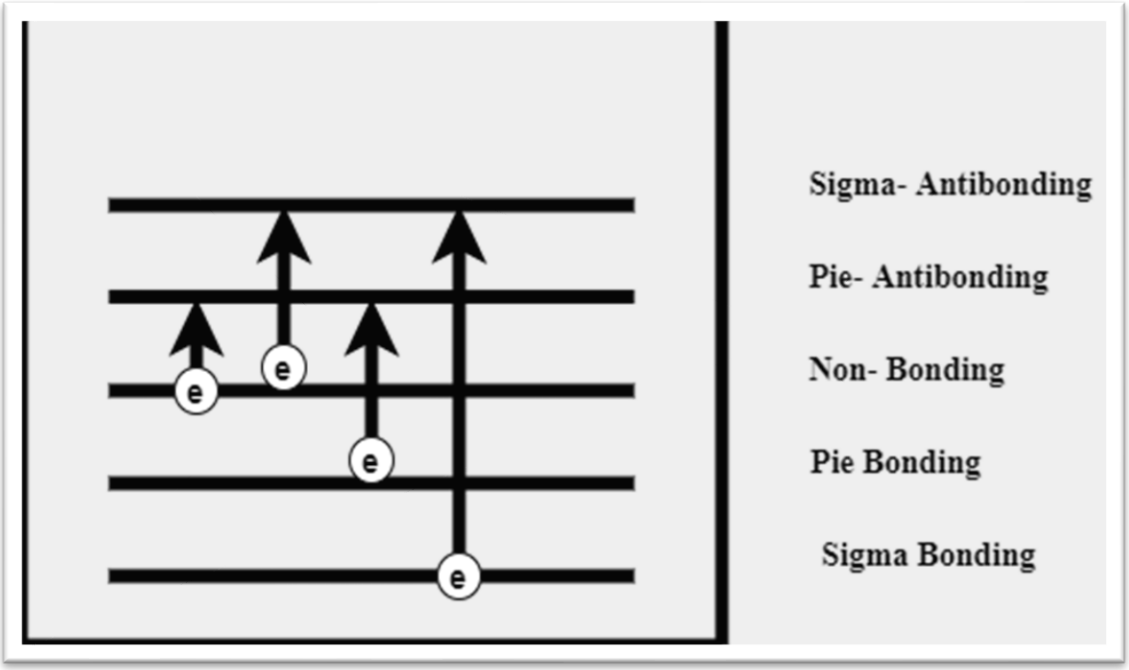

Figure 3.4 All possible transitions after absorption of photon.

3.3.5 Field Emission Scanning Electron Microscope (FESEM)

FESEM is a useful electron microscopic technique for analyzing the micrographs and examining structural information of micro-structured materials in high resolution specimens almost 10 times to 300,000 times with depth. FESEM rules over scanning electron microscope (SEM) in terms of high resolution that is three to six times better. More-over, smaller contamination spots can be investigated using electron accelerating voltages tuned with Energy Dispersive X-ray Spectroscopy (EDX) The interaction of electron beams with a target emits a

variety of radiation, including X-rays. An EDX detector is worked to separate the characteristic X-rays of different elements into an energy spectrum, which is then examined with software to calculate the number of individual elements in the sample.

The basic principle of FESEM is to scan the samples with the help of electron rather than a of light. This method is based on the interactions between electrons and matter. Electrons are generated by electron gun or field emission source and further accelerated with the help of field gradient. To make the beam more focused it is pass through electromagnetic less, and then it allows to fall on the samples. Various sorts of electrons are emitted from the sample as a result of this focusing. A detector captures the secondary electrons, and an image of the sample's surface is formed by comparing the intensity of the secondary electrons to the intensity of the scanning primary electron beam. At last, the image is then displayed on a computer monitor. Indeed, electrons are emitted by an X-ray tube are utilized to evaluate object size and morphology. Backscattered electrons and secondary electrons, X-ray, heat, and even transmitted electrons are all produced when incident electrons strike the material's surface. However, secondary and backscattered electrons, in particular, are responsible for the majority of information about the sample's surface shape (topological contrast). The test specimen is first earthed to prevent the collection of spatial charge, which could ruin FESEM micrographs. The electron beam scans the specimen's surface, then displays the particles contained within as a reaction.

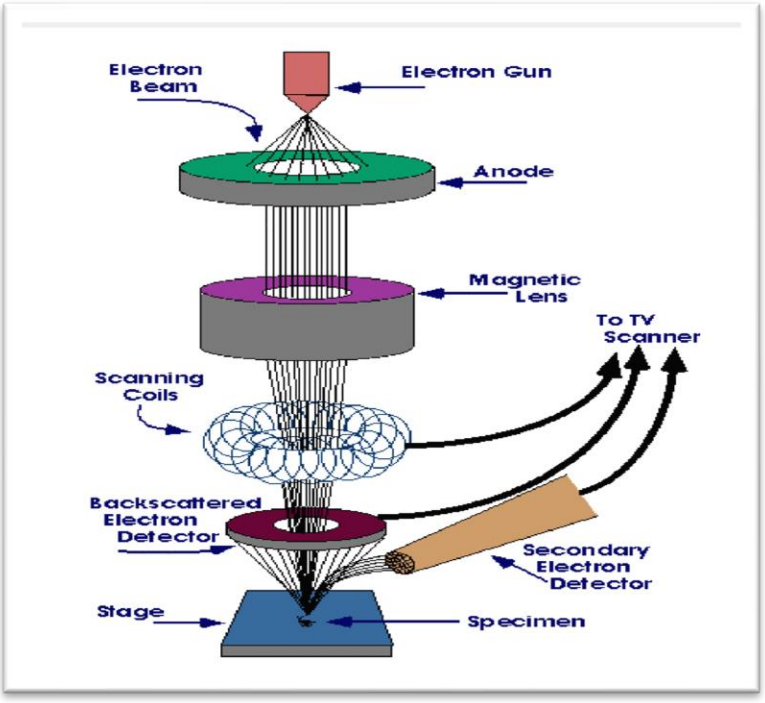

Figure 3.5 Working of FESEM technique

3.3.6 Impedance Analyzer

An impedance analyzer is a component of electrical devices that examines impedance and admittance. When voltage is provided to a circuit or device, the overall opposition offered to the flow of periodic current (AC test signal) is called impedance. The real and imaginary components are part of the periodic current. The impedance can be written as **Equation 3.2** when the connection is made in series.

$$Z = R + jX \tag{3.2}$$

Where X is the reactance (which is the imaginary component of impedance), R is the resistance (which is the real component of impedance), and j is an imaginary number. By plotting the resistance on the x-axis and the reactance on the y-axis, the calculations of the impedance can be done. In general, the device under test (DUT) has been provided with AC voltage, and impedance (Z) and capacitance (C) are used to assess the DUT's response. The angle (θ) formed by the impedance (Z) with the x-axis is also measured. Various dielectric parameters such as real part of permittivity (ε), imaginary part of permittivity (ε$^{'}$), dielectric tangent loss (tanδ), and AC conductivity can be calculated using the acquired data such as impedance (Z), capacitance (C), and angle (θ).

3.3.7 Vibrating Sample Magnetometer (VSM)

A VSM can be used to determine the material's magnetic characteristics. Simon Forner discovered this approach in 1955. The basic principle is based on Faraday's law of electromagnetic induction. According to the law a change in magnetic field generates an electric current. Magnetic characteristics such as coercivity (Hc), remanence (Mr), saturation magnetization (Ms), and squareness ratio (Mr/Ms) can be calculated using this technique.

The experimental sample is placed in a sample holder, which is then sandwiched between two sets of pick-up coils connected to an electromagnet. Because of the uniformity of the electromagnet's magnetic field, magnetization will be induced in the sample. The sample holder, carrying the sample inside, is designed to vibrate mechanically in a sinusoidal pattern. When a vibrating component produces a change in the magnetic field of the sample, Faraday's law of electromagnetic induction generates an electric field corresponding to the magnetization. Variations in magnetic flux cause a voltage in the pickup coils that is proportional to the sample's magnetization. These changes are converted into a graph of magnetization (M) against the applied magnetic field by software in a computer connected to the VSM equipment (H).

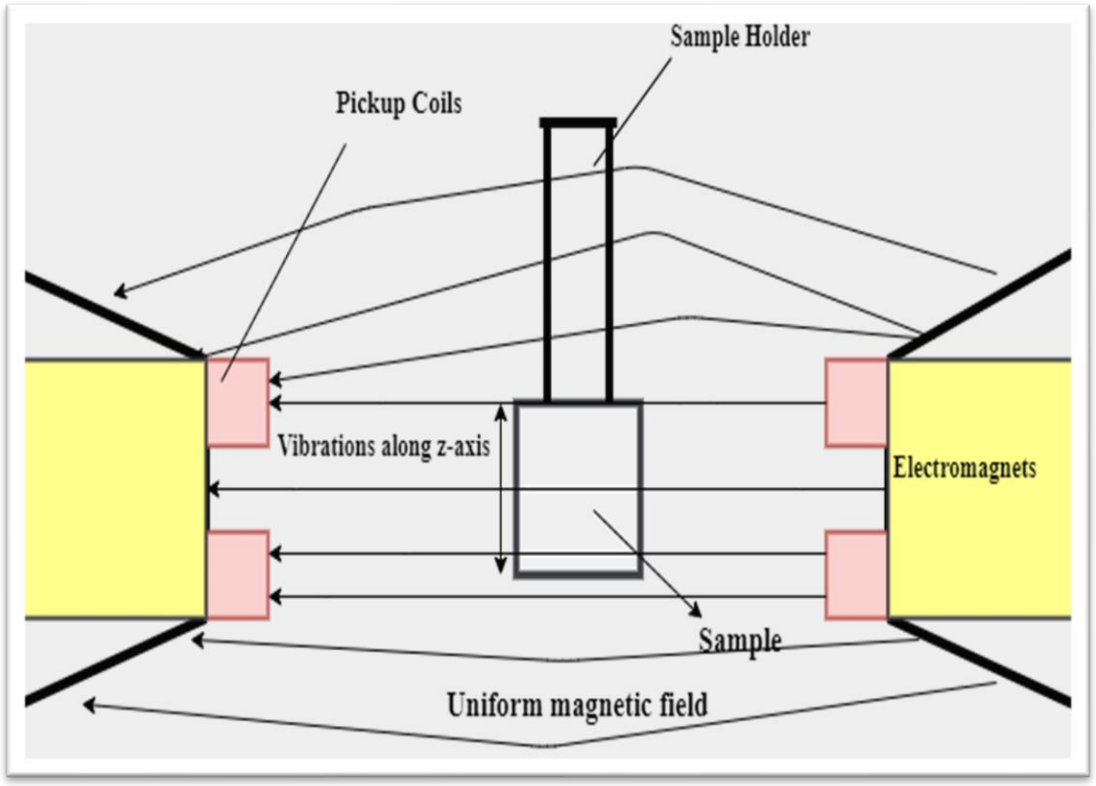

Figure 3.6 Principle of VSM technique

3.3.8 Vector network analyzer

The VNA is a tool for determining the network parameters of an electrical network in radio frequency range. When a signal travels through a device under test, it employs the principle of measuring transmitted and reflected waves (DUT). The S-parameters, which reflect the distribution properties of the cell (DUT), in module and phase, over a wide frequency range, can be obtained using the VNA instrument. The S-parameters (S_{11}, S_{22}, S_{12}, S_{21}) in reality, represent the electromagnetic energy distribution and connect incoming and outgoing waves.

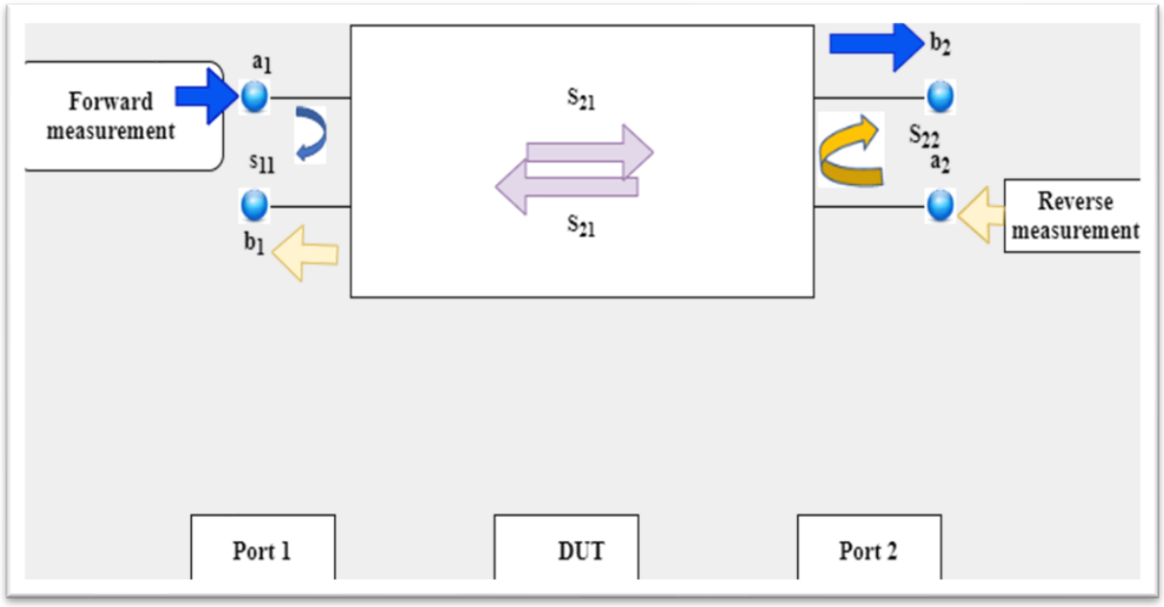

Figure 3.7 Working of VNA technique

A brief detail of the samples prepared and characterized in the presented thesis is as per the table below:

Sample	Study Purpose	Characterization
$Gd_3Fe_{5-x}Al_xO_{12}$ (x=2)	Temperature Variation 900°C, 1000°C, 1100°C	XRD, FTIR, FESEM, VSM
$(Gd_3Fe_5O_{12})x/(MgFe_2O_4)1-x$	Composition Variation x=0, 0.5, 1.0	XRD, FESEM, EDX, Impedance Analysers, VSM
$(Gd_3Fe_5O_{12})0.7/(MgFe_2O_4)0.3$	Temperature Variation 900°C, 1300°C	XRD, FESEM, EDX, Impedance Analysers, VSM
$Y_{0.2}Bi_{0.2}La_xGd_{2.6-x}Fe_5O_{12}$	Substitution Variation x=0, 0.2, 0.4	XRD, FESEM, EDX, VSM
(YIG)x-(ErIG)1-x	Losses Study for Antenna x=0.5	XRD, FESEM, EDX, Impedance Analysers
(YIG)x-$(Mg_{0.4}Cd_{0.4}Co_{0.2}Fe_2O_4)1-x$	Losses and Miniaturization Study for Antenna x=0.3, 0.6, 0.9	XRD, FESEM, EDX, VSM, VNA
$Pr_xGd_{3-x}Fe_5O_{12}$	Substitution Variation X=0.5, 1, 1.5	XRD, FESEM, UV, Fluorescence Spectroscopy

Chapter 4

Results and Discussions

4.1 Al^{3+} substituted gadolinium iron garnet ($Gd_3Fe_5O_{12}$)

4.1.1 XRD

The XRD pattern of $Gd_3Al_2\ Fe_3\ O_{12}$ sintered at different temperature range (900°C, 1000°C, 1100°C) is as shown in **Figure 4.1**. The XRD pattern of powder sample sintered at 900°C showed that there is presence of garnet ferrite phase with some extra phases mainly due to $GdFeO_3$(orthoferrite) and γ-Fe_2O_3(maghemite), indexed to JCPDS no. of 77-1888, 47-0067 and 33-0664 respectively. Further increasing sintering temperature to 1000°C leads to form more garnet phase with orthoferrite phase, also the intensity peak with hkl value (420) increases and became sharper. The impurities obtained in the sample is due to that these temperatures are uncapable to provide enough energy to excite reaction between the materials. Another reason of formation of orthoferrite may be diffusion process which might not be completed properly **[110]**. Further rising temperature to 1100°C leads to formation of higher amount of garnet phase with very little amount of orthoferrite phase, with sharper peak at maximum intensity value. This orthoferrite phase still remains at this temperature range might due to stoichiometry modification, that is presence of Al^{+3} in tetrahedral site of garnet phase.

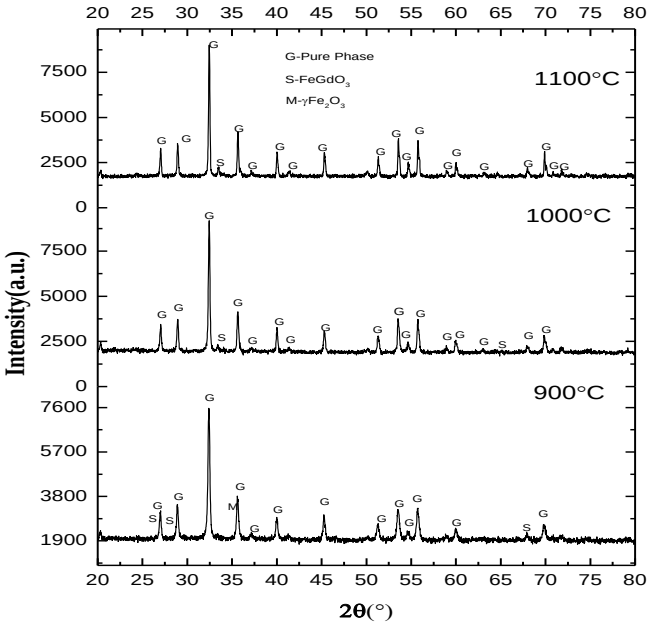

Figure 4.1. XRD pattern of $Gd_3Al_2\ Fe_3O_{12}$ at different sintering temperatures

The crystallite size, full width half maxima (FWHM), peak position, lattice constant, micro strain and dislocation density were calculated from XRD data and given in **Table 4.1**. The crystallite size of the sample sintered at different temperatures was calculated by using Scherrer **Equation (4.1) [34]**.

$$D = \frac{K\lambda}{\beta \cos\theta} \tag{4.1}$$

Where D is crystallite size, K=0.9(Scherrer constant), λ=0.15406 nm (wavelength of X-ray sources), β= FWHM radians, θ= peak position (radians). FWHM show decreasing trend with increase in temperature. This decrease in FWHM value is the sign of growth in grain, as well as the crystallite size increases with increase in temperature **[111]**. At higher temperature motion of the atom increases which further increases the growth of grain and with this crystallinity of the sample enhances. With temperature, crystallite size increases may be attribute to coalescence process **[112]**. The crystallite size corresponds to maximum intensity peak (420) found to be maximum (39 nm) for 1100°C. Akhtar et al., have reported that Ce substituted GdIG samples have crystallite size in range 20.1 to 38.4 nm, with substitution crystallite size decreases **[98]**. Sattar et al., have reported that Gd substituted YIG prepared via standard ceramic method have crystallite size in between 113nm to 150nm **[34]**. As the sample is garnet ferrites, and structure of garnet ferrite is cubic so lattice constant of the samples was calculated by using **Equation (4.2) [113]**. The calculated value of lattice constant is near to cubic YIG as reported by Azis et. al **[114]** and Praveena et. al **[37]**.

$$\frac{1}{d^2} = \frac{h^2+k^2+l^2}{a^2} \tag{4.2}$$

Where 'd' is interplanar spacing, a is lattice constant, miller indices (hkl) value used correspond to higher intensity peak that is (420). The interplanar spacing was calculated using Bragg's **Equation (4.3)**.

$$d_{spacing}(\text{Å}) = \frac{n\lambda}{2\sin\theta}\ , n = 1 \tag{4.3}$$

Lattice constant value goes on decreasing with increasing temperature, the change is very much little i.e., the difference of only 0.01. Temperature do not affect lattice constant to greater extent.

Micro strain and dislocation density of the samples was calculated by using **Equation (4.4)** and **Equation (4.5)** respectively.

$$\varepsilon = \frac{\beta}{4\tan\theta} \tag{4.4}$$

$$\delta = \frac{1}{d^2} \quad (4.5)$$

Here ε is micro strain and δ is dislocation density. Both micro strain and dislocation density values were found to be decreased from 900°C to 1000°C and become maximum at temperature (1100°C). Due to inward contraction of the atoms present at surface there is decrease in micro strain and maximum micro strain at 1100°C maybe due to expansion of atoms present at the surface of crystal. Also, dislocation density firstly decreases from 900°C to 1000°C and then became maximum at 1100°C.

Table 4.1 The hkl, peak position, FWHM, Lattice constant (a), crystallite size (D), dislocation and micro strain of $Gd_3Al_2Fe_3O_{12}$ at 900°C, 1000°C and 1100°C

Temperature(°C)	hkl	Peak position(°)	FWHM(°)	a(Å)	D (nm)	δ	ε
900	420	32.41	0.28	12.34	28.9 nm	1.32	3.51
1000	420	32.44	0.23	12.33	36.2 nm	0.89	3.07
1100	420	32.48	0.21	12.32	39.0 nm	2.06	3.83

4.1.2 FTIR

FTIR spectra of samples sintered at different temperature is as shown in **Figure 4.2**. Generally, in garnet spectrum the Fe-O stretching vibrations is seen in IR region. In region 550-650 cm^{-1} the Fe-O vibration of FeO_4 tetrahedra takes place. The peaks obtained at 575, 660 cm^{-1} is corresponded to formation of garnet phase. This result is with good agreement to XRD. At the range of 500-900 cm^{-1} the strongest bands have been observed. These bands are corresponded to intrinsic stretching vibration in the ions of metals and ions of oxygen present throughout the length of the octahedral and tetrahedral site **[115, 116]**. The band present at 1513 cm^{-1} is corresponded to stretching vibration due to NO_3. Also, the peaks present at 660 cm^{-1} and 2360 cm^{-1} is corresponded to the stretching band of ions of Fe_2O_3. However, there is peak at 3390 which is corresponded to O-H stretching bond, which might be due to presence of water molecule in sample. The peak corresponded to 1350 cm^{-1} found at sintering temperature 900°C and 1000°C is due to bending of O-H bonds. This deformation of bonds represented the absorption of water at the surface of sample and it has been seen that at 1100°C it become very weaker **[117, 118]**.

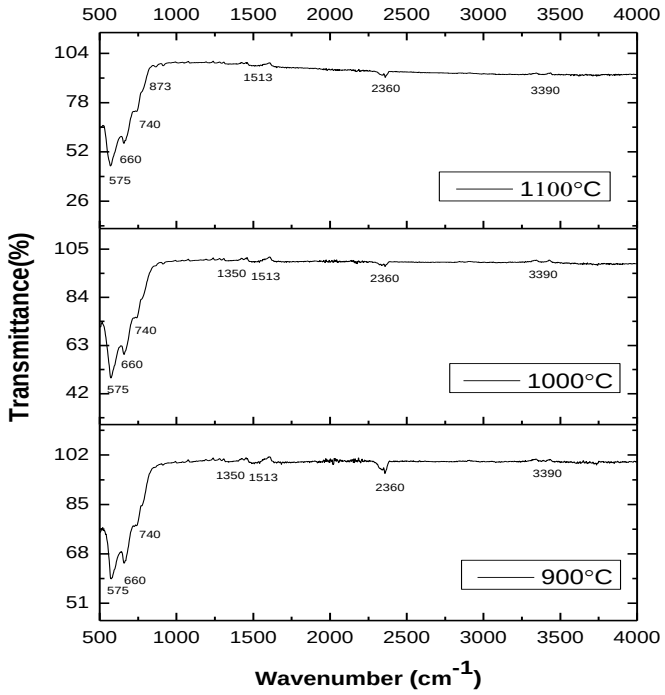

Figure 4.2 FTIR spectra of $Gd_3Al_2Fe_3O_{12}$ sintered at 900 °C, 1000 °C and 1100 °C

4.1.3 FESEM

The morphology of the samples sintered at different temperature is as shown in **Figure 4.3**. For each sample two micrographs are given at different magnification range in order to view both far and closer view of the sinterted samples. From microgrphs it is clear that with rise in temperature there is evolution in morphology. Micrograph (a) for sample sintered at 900°C reveals that elongated shape is present with agglomeration and large number of pores. As the sintering temperature increase further to 1000°C the micrograph (b) represents that the grain become irregular and rounded. At 1100°C the micrograph (c) obtained reveals that at this temperature particles come very closer to each other and pores almost vanishes. The spherical shaped grains with smooth surface obtained. The pores decrease at this temperature and at very slower rate get removed by diffusion of vacancies from pores towards the boundaries of grain **[115]**. From the obtained micrographs it may be trusted that mass transport mechanism initiated with atomic surface diffusion at relatively low temperature and carry on by occurring grain boundaries diffusion which results in the formation of necking, growth in contact, elimination of pores, and growth of particle size **[118]**.

The average grain size of the samples increases with increase in sintering temperature which was also reported by Ramesh et al., **[119]** and Mousavi Ghahfarokhi et al., **[120]**, and is calculated using line intercept method given in **Equation (4.6) [121]** and is given in **Table 4.2**.

$$grain\ size = \frac{1.5\,L}{mn} \tag{4.6}$$

Where m, n and L represents magnification, line intersecpt and length of line drawn on micrograph of sintered sample respectively. The grain size distribution of samples is represented by histogram given in **Figure 4.4**.The distribution of grain size of sample sintered at temperature 900°C is symmetric (Gaussian) at 75nm with grain size ranges from 25-450 nm, peaking at 80 nm. For sample sintered at 1000°C the distribution of grain size is symmetric (Gaussian) and peak ranges 10-125nm, the maximum number of grains lies between 32-72 nm. Similarly, for sample sintered at 1100°C the grain size ranges from 13-73 nm and maximum number of grains lies between 26-48nm. It can be said that one ferrite affects the growth of other ferrite which further limits the grain boundaries motions.

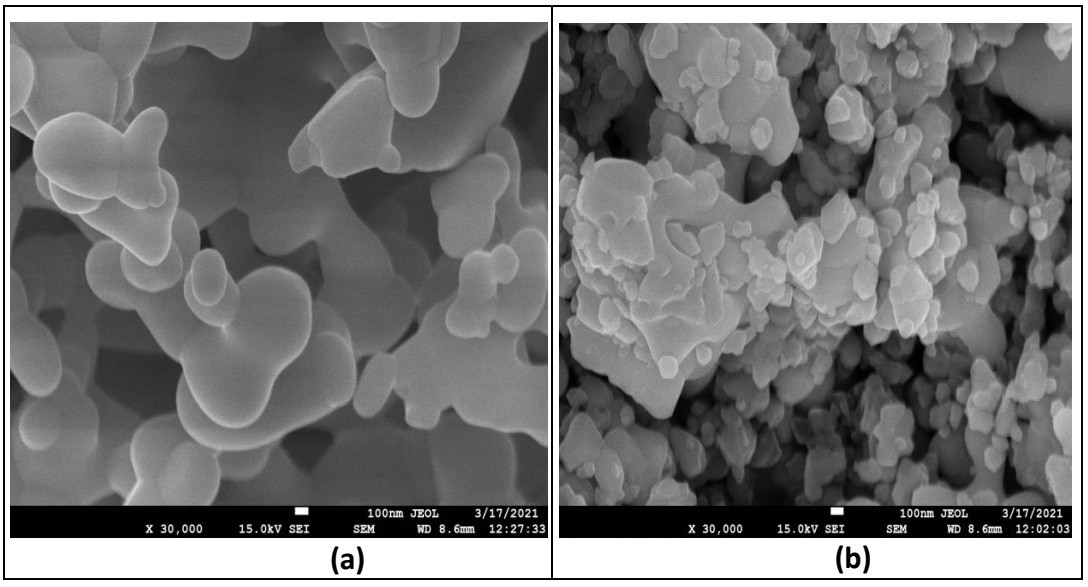

(a) **(b)**

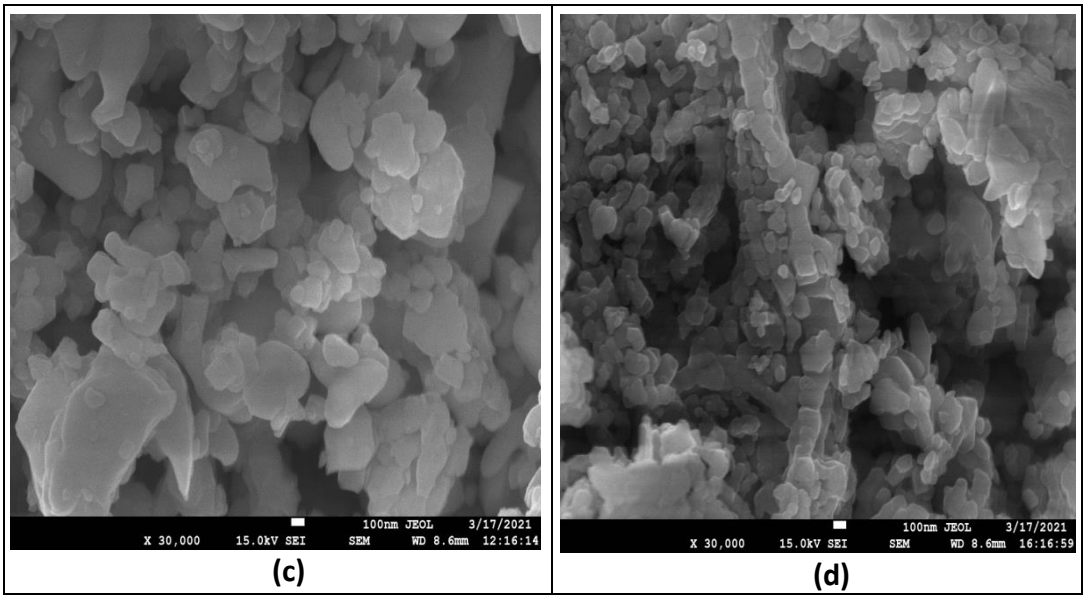

Figure 4.3 FESEM micrographs of (a) x=1.0 (GdIG), (b) x=0.5, (c) x=0.75 and (d) $MgFe_2O_4$

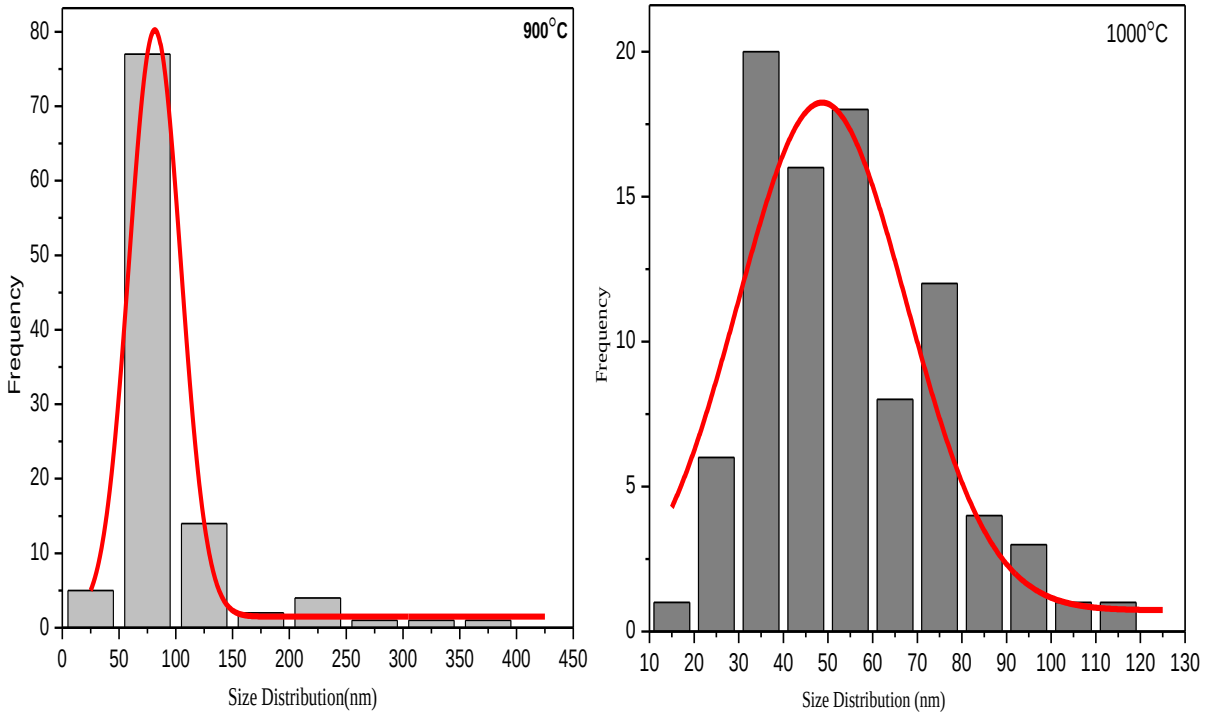

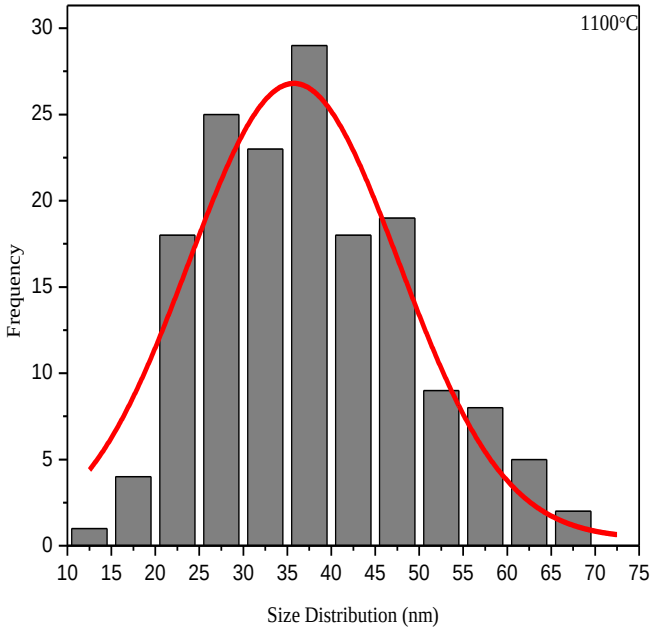

Figure 4.4. Size distribution of $Gd_3Al_2Fe_3O_{12}$ from FESEM images sintered at temperature (a) 900°C (b) 1000°C (c) 1100°

Table 4.2 Average grain size at sintering temperature 900°C, 1000°C and 1100°C

Sintering temperature (°C)	900	1000	1100
Grain Size(nm)	4	6	13

4.1.4 VSM

The magnetization-field (M-H) curves of samples sintered at different temperature is shown in Figure 5. Smooth BH loop signifies the presence single phase structure of Al substituted garnets with strongest coupling interaction. The value of saturation magnetization (M_s), coercive field (H_c), remanence (M_r) squareness ratio (Mr/M_s) of the sample sintered at different temperature are given in **Table 4.3**. It has been concluded that M_s for sample sintered at 900°C is maximum and that for sample sintered at 1000°C is minimum. This decreasing in value of M_s can be explained on the basis that as the temperature increases the chance of substitution of non-magnetic Al is more, which further weaken a-d super exchange interaction **[100]**. Both value of H_c and M_r is maximum for sample sintered at 900°C. The value of H_c goes on decreasing with increase in temperature which was also reported by Su et al., **[122]**, and value of M_r firstly

decreases from 900°C to 1000°C and increases little at 1100°C. This change in H_c and M_r can be explained by change in microstructure **[122]**. The sample sintered at 1100°C is the softest ferrite because of least value of H_c. As, it revealed from FESEM **(Figure 4.3)** that with increase in sintering temperature grain size also increased. The presence of multi-domain structure is more probable in larger grains and reversal of magnetization attained by displacement of domain walls is easier than by spin rotation **[123]**. The value of squareness ratio of sample sintered at different temperature ranges between 0.007-0.055 which is less than 0.5 signifies about superparamagnetic nature of the sintered samples, and also signifies about the presences of multi-domains in the structure. The anisotropy constant (K) and Bohr magnetization value is calculated by **Equation (4.6)** and **Equation (4.7)** respectively and tabulated in **Table 4. 3**. The magnetic properties get altered by intrinsic as well extrinsic properties and it has been found that also, sintering temperature can tailor magnetic variations **[124]**.

$$Anisotropy\ Constant = \frac{H_c \times M_s}{0.96} \tag{4.6}$$

$$Bohr\ Magnetization(\mu B) = \frac{\mathrm{M} \times \mathrm{M_S}}{5585} \tag{4.7}$$

The anisotropy constant decreases with increase in temperature might be due to the chance of presence of Al ion in tetrahedral site is more at higher temperature which further decrease the spin orbital interaction between ions of iron **[125, 126]**. Ansari et al., have reported that anisotropy constant of $CoFe_2O_4$ increases with particle size, which implies that surface constituents do not play major role. Calculated anisotropy constant decreases with increase in grain size.

Further in order to check the microwave operation frequency at which these sintered samples can be operated, which is depend upon saturation magnetization of nano ferrites and can be calculated using **Equation (4.8) [127, 128]** and value is given in **Table 4.3**.

$$\omega_m = 8\pi^2 \gamma M_s \tag{4.8}$$

Where, ω_m is microwave operating frequency, γ is gyromagnetic ratio of ferrites in microwave region and is equal to 2.8MHz/O_e, and M_s is saturation magnetization. The value ω_m for all sintered samples lie in Ultra high frequency range.

Table 4.3. H_c, M_r, M_s, anisotropy constant(K), Bohr magneton, SQR and ω_m calculated from BH loop at 900°C, 1000°C and 1100°C

temperature(°C)	H_c(Oe)	M_r(emu/g)	M_s(emu/g)	M	K (erg/cm^3)	Bohr Magneton(μB)	SQR	ω_m
900	491.8	0.19	3.46	1.076	551.3	0.175	0.055	764
1000	137.5	0.02	2.61	1.092	156.5	0.178	0.007	576
1100	62.9	0.08	2.46	0.714	46.9	0.116	0.032	543

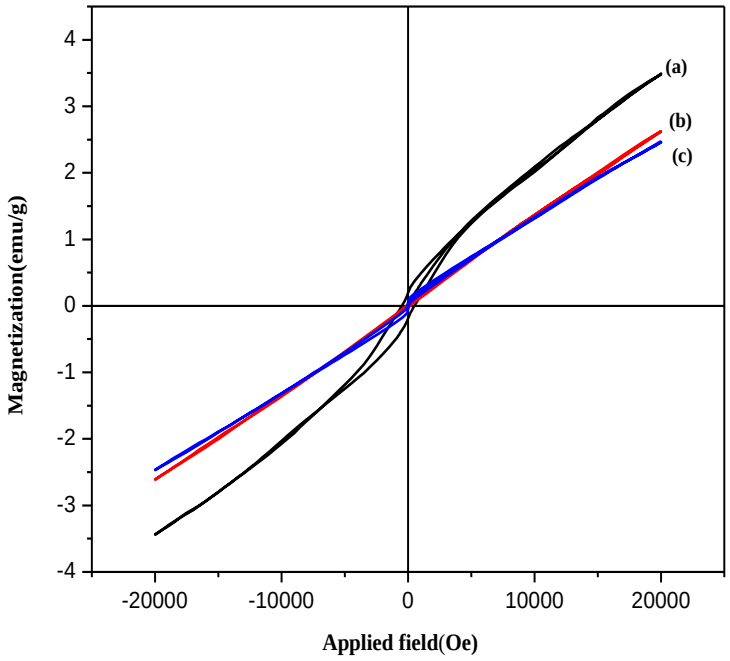

Figure 4.5 The magnetization-field (M-H) curve of $Gd_3Al_2Fe_3O_{12}$ sintered at 900 ℃, 1000 ℃ and 1100 ℃

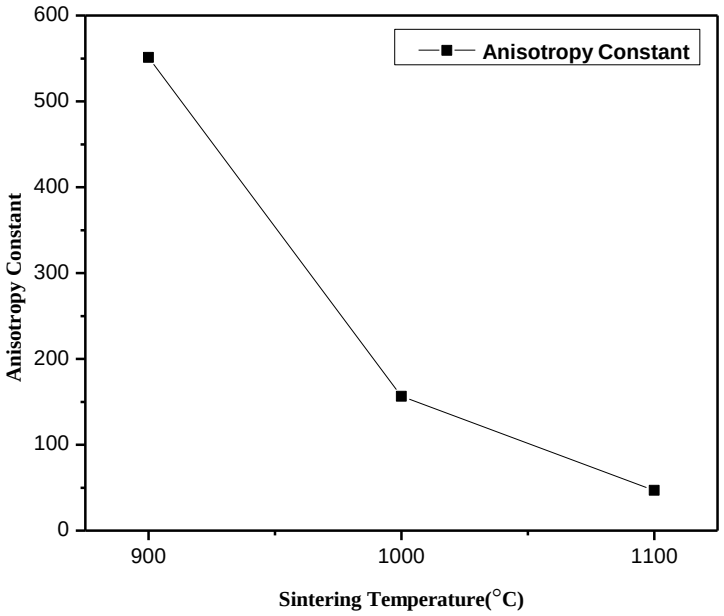

Figure 4.6 Dependence of anisotropy constant on sintering temperature

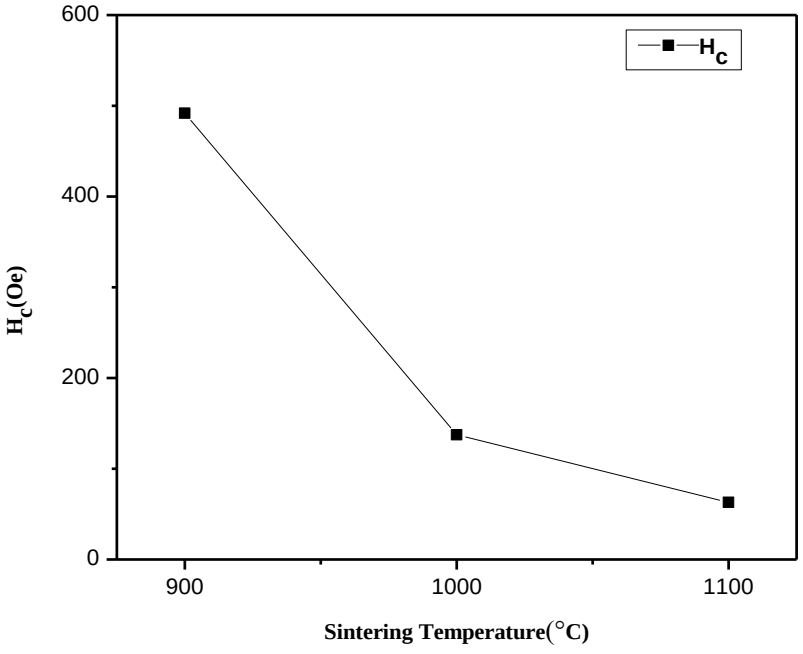

Figure 4.7 Dependence of H_c on sintering temperature

4.2 Synthesis of gadolinium iron garnet, magnesium spinel ferrite and their composite (GdIG/$MgFe_2O_4$)

4.2.1 XRD

The XRD patterns of garnet ferrite ($Gd_3Fe_5O_{12}$) and spinel ferrites ($MgFe_2O_4$) are shown in **Figure 4.8**. From the XRD pattern of both gadolinium garnet ferrite (GdIG) and magnesium spinel ferrites (MF), it has been clear that the single-phase is formed, which was confirmed from the JCPDS no. 720141 for GdIG and 711232 for MF. A little amount of secondary phase (JCPDS no. 47-0067) has been observed in the samples. **Figure 4.8** also represents the XRD pattern of composites of GdIG(x)/MF(1-x) with x (wt%) 1 (Pure garnet ferrite), 0.5 and 0.75. It has been observed from the pattern that at x = 0.5 both garnet and spinel phases are present with sharper peaks corresponding to hkl values of (420) and (311) respectively. This ensures that two independent phases of both ferrites exist in the composite without any chemical reaction **[129]**. But by a further increase in the amount of GdIG in composites that is at x= 0.75, many peaks of MF got surpassed, and the intensity of the peaks also decreases. The intensity and number of peaks formed in XRD are dependent on the number of corresponding phases present in the sample **[130]**. This decrease in intensity of the characteristic peak of MF implies that MF starts absorbing on the surface of GdIG and also indicates that the adhesion force between both ferrites at x= 0.75 is very strong. **Figure 4.9** represent the refined XRD pattern of the samples done by using Rietveld Refinement.

Table 4.4 represents the values of crystallite size, lattice constant, micro strain, of pure GdIG i.e., x= 1.0, MF and GdIG(x)/MF(1-x) composites at x= 0.5 and 0.75. The average crystallite size of the composites was calculated by using Scherrer **Equation (4.9)**.

$$D = \frac{K\lambda}{\beta \cos\theta} \tag{4.9}$$

Where D is crystallite size, K is Scherrer constant with value 0.9, λ is the wavelength of X-ray sources with value 0.15406 nm, β is full-width half maxima (FWHM) (in radians). The value of β was calculated from given XRD data using origin software. Where θ is the peak position (radians) and its value was also calculated from given XRD data using origin software. It has been seen that the average crystallite size of composites was found to be in the range of 33 -55 nm. The average crystallite size of GdIG composite first increases from x = 1.0 to x = 0.5 and then decreases at x = 0.75. At x = 0.5 both GdIG and MF are present in equal quantity and the increase in crystallite size reveals that MF is contributing towards the change in crystallite size

of GdIG. Further decrease in crystallite size at x = 0.75 is due to the dominance of GdIG on MF. Here MF present in lesser amount. Also, a decrease in crystallite size at x = 0.75 can be correlated with peak broadening, which can be clearly seen from **Figure 4.9**. The average crystallite size of the Pure GdIG (x = 1) is least and that for composite x = 0.5 (50% GdIG and 50% MF) is largest due to nanocomposites **[131]**. Reason for the lesser value of crystallite size at x = 1% is that D is inversely proportional to β and 2 θ and it has been found that the value of 2θ for x = 1% is largest which implies that the value of D is small.

As the structure of both garnet ferrite and spinel ferrite is cubic so lattice constant for the composites was calculated using **Equation (4.10)**.

$$\frac{1}{d^2} = \frac{h^2+k^2+l^2}{a^2} \tag{4.10}$$

Where a is lattice constant, hkl are the miller indices which is taken corresponded to maximum intensity peak, d is interplanar spacing calculated by using Bragg's law **(Equation 4.11)**.

$$d_{spacing}(\text{Å}) = \frac{n\lambda}{2\sin\theta}\ , n = 1 \tag{4.11}$$

The lattice constant for GdIG and MF single phase is well-matched with the literature. The lattice parameter of composites of GdIG increases slightly due to the effect of strain at the interface between GdIG and MF **[132]**. The modification that came due to the strain effect at the interface of composites also brings changes in the physical properties of composites. The variation in lattice constant is also because of dissimilarity in reciprocal solubility of soft ferrites phases. The micro strain of the GdIG and its composites is calculated using **Equation (4.12)**.

$$\varepsilon = \frac{\beta}{4\tan\theta} \tag{4.12}$$

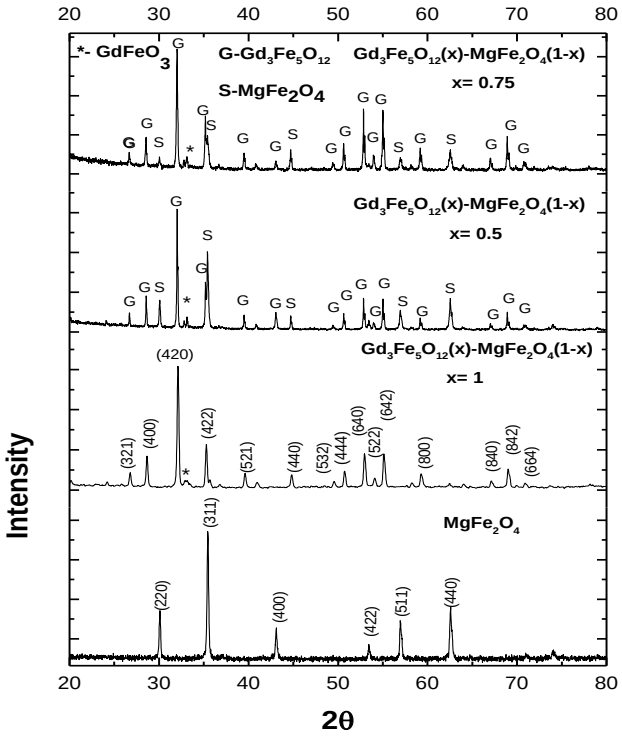

Figure 4.8 XRD spectra of $MgFe_2O_4$, ($Gd_3Fe_5O_{12}$) x=1.0, x=0.5, x=0.75

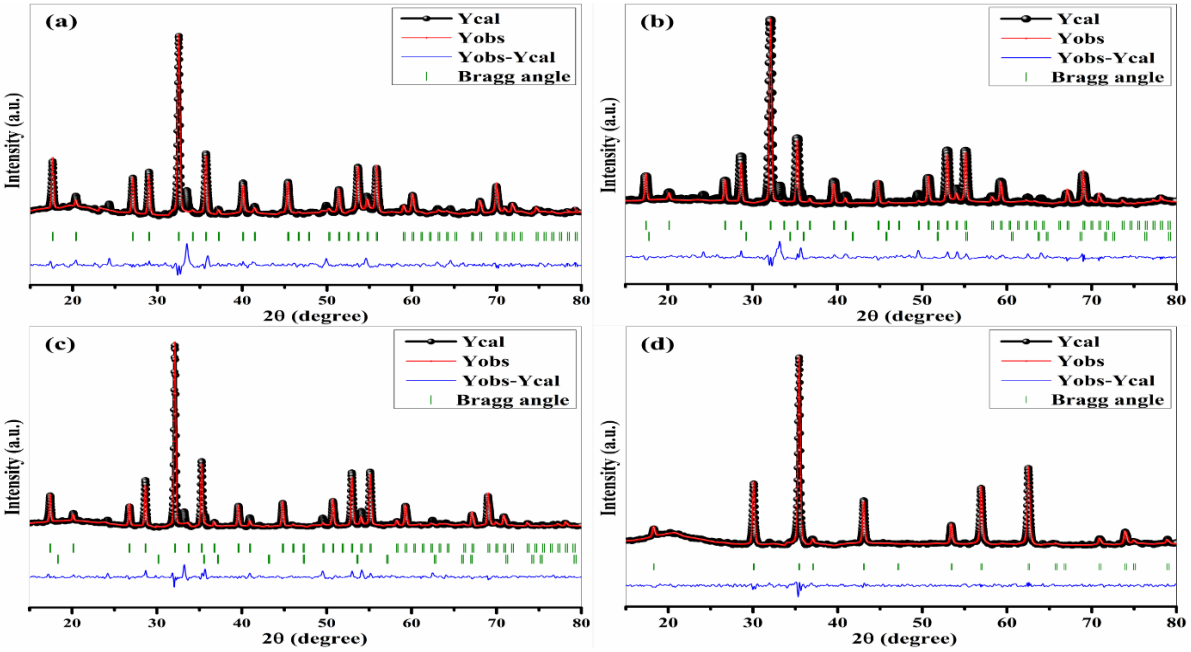

Figure 4.9. Refined XRD patterns of prepared samples a) $Gd_3Fe_5O_{12}$, b) $(Gd_3Fe_5O_{12})_{0.5}/(MgFe_2O_4)_{0.5}$, c) $(Gd_3Fe_5O_{12})_{0.75}/(MgFe_2O_4)_{0.25}$, and d) $MgFe_2O_4$

Table 4.4 Crystallite size, lattice parameter (a), and micro strain calculated for GdIG and its composites

Composition Code	Garnet%-Spinel%	Crystallite Size	Lattice Parameter(a)	Micro Strain
x=1. 0	Garnet only (GdIG)	33.1 nm	12.45	0.5
x=0.5	50%-50%	54.7 nm	12.48	2.28
x=0.75	70%-25%	45.7 nm	12.50	2.25
MF	$MgFe_2O_4$	26.7nm	8.37	-

4.2.2 FESEM

Figure 4.10 shows the morphology of pure GdIG (x = 1.0) and its composites. The micrograph (a) shows the presence of the spherical structure of GdIG. The micrographs of GdIG composites (b) and (c) show the presence of agglomeration of grains. Micrograph (d) shows the presence of rough cube-shaped grains of $MgFe_2O_4$ (MF). The agglomeration increases with an increase in GdIG in the composites i.e., at x=0.75 (GdIG is 75% and MF is 25%) i.e., here agglomeration is more. This is related with magnetic attraction in nanoparticles, which is due to the contribution of soft ferrite garnet **[133, 134]**. The grains of spinel ferrite (MF) seemed to be distributed over the micrographs for both composites. The micrograph shows some big and small grains, which indicates the presence of both GdIG and MF in composites. The cube (MF grains) like grains seemed to be present on the surface of some spherical grains (GdIG grains). This implies that the grains of MF get absorbed on the surface of GdIG in their composites. This adsorption of spinel ferrite (MF) on garnet ferrite (GdIG) is because of similarity in the structure **[135]**.

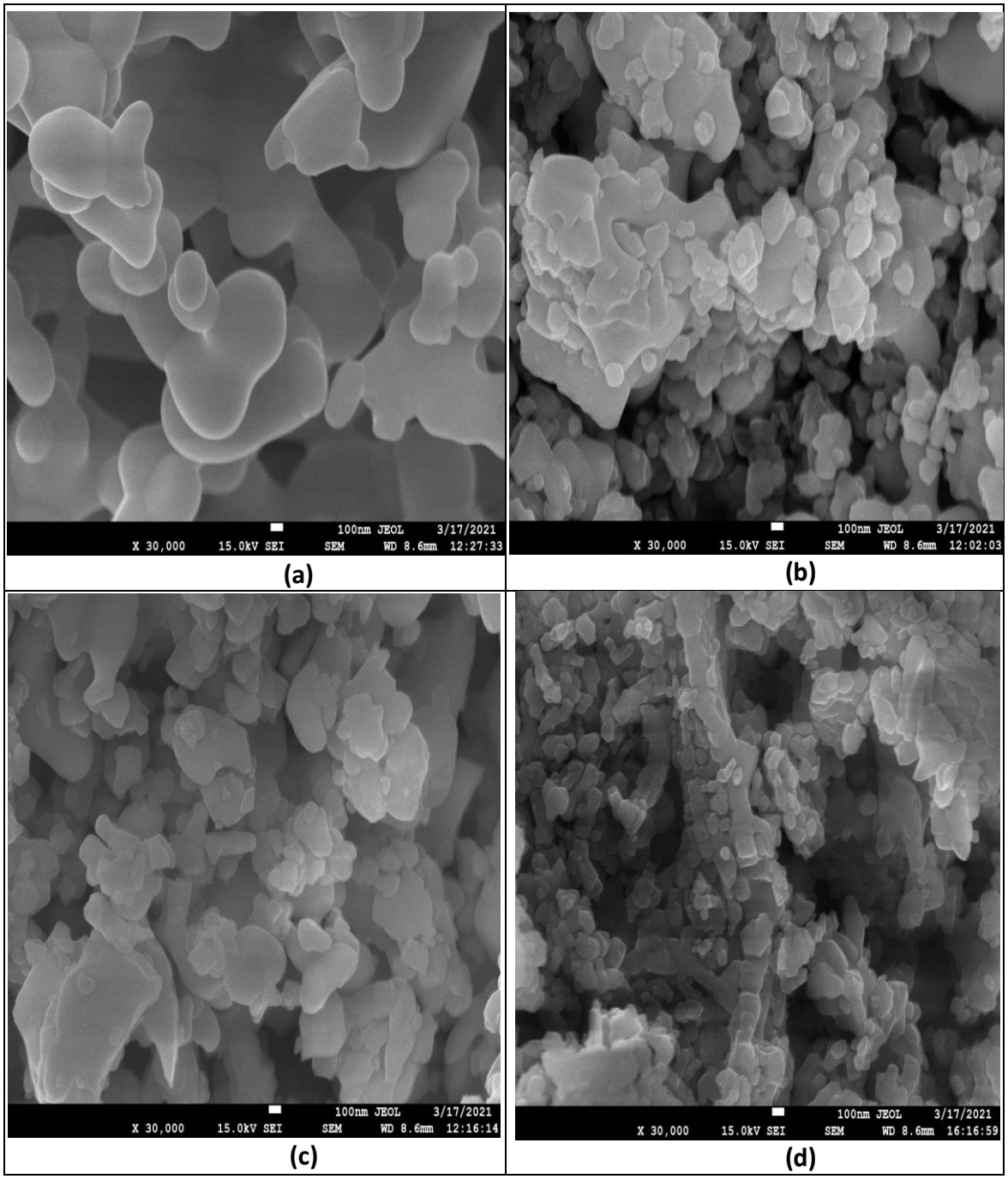

Figure 4.10 FESEM micrographs of (a) x=1.0 (GdIG), (b) x=0.5, (c) x=0.75 and (d) $MgFe_2O_4$

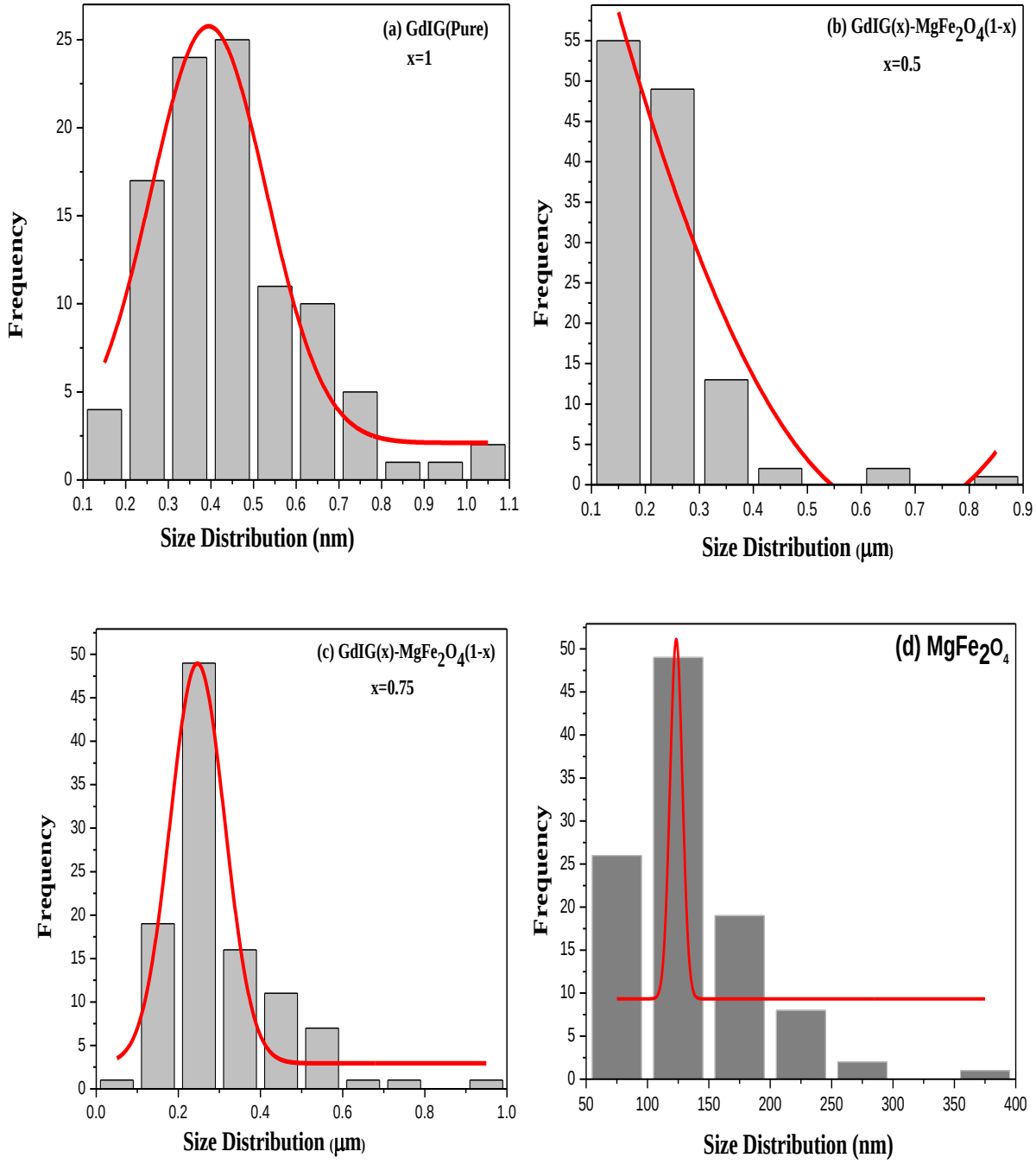

Figure 4.11 The Histograms representing size distribution of (a) x=1.0, (b) x=0.5, (c) x=0.75 and $MgFe_2O_4$

4.2.3 EDX

The EDX spectra with chemical composition of the prepared composite is as shown in **Figure 4.12**. It has been observed that the desire amount of the elements is present in the composites, with no extra sign of other elements. This implies that synthesized method and temperature is efficient. It has been observed that with change in composition of composites the change in chemical composition in EDX spectra is also observed.

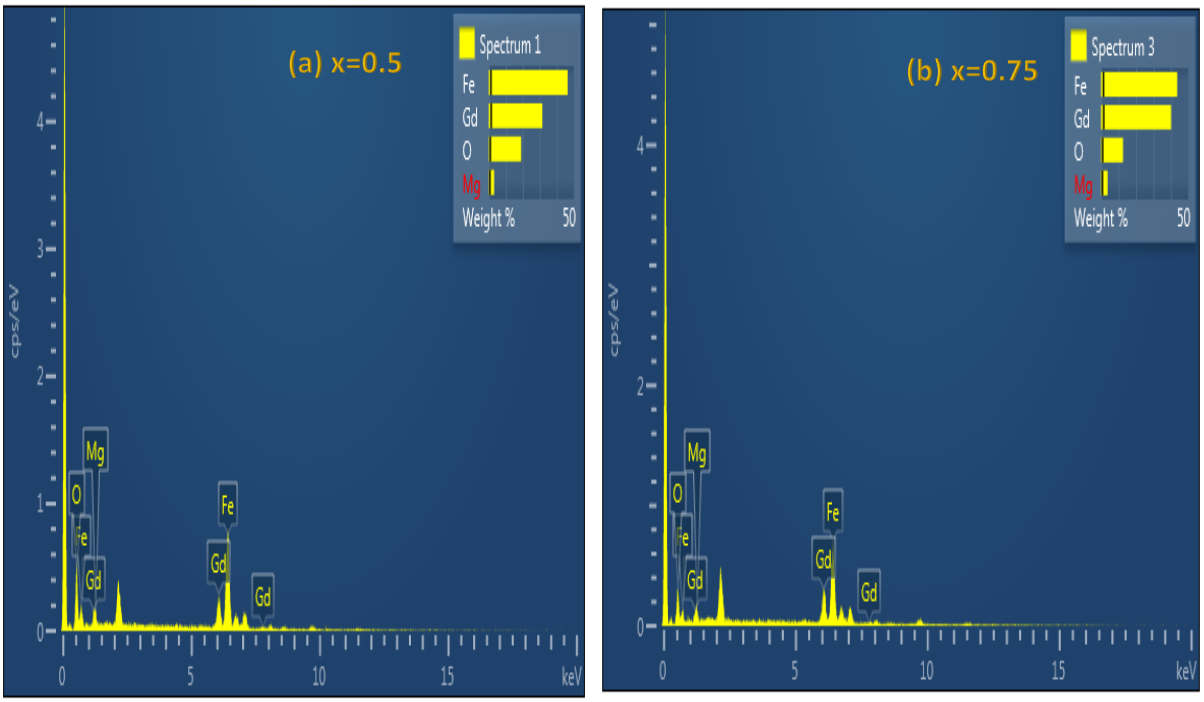

Figure 4.12 EDX spectra of composites (a) x=0.5 and (b) x=0.75

4.2.4 Impedance Analyser

The amount of resistance produced in presence of an electric field in a vacuum is known as permittivity. The complex permittivity (ε^*) has two parts i.e., real (ε') and imaginary (ε'') as given in **Equation (4.15) [134]** and which are further related with impedance (Z^*) as given in **Equation (4.16)**. The real part and imaginary part of complex permittivity can be calculated from impedance value and is given in **Equation (4.17)** and **Equation (4.18)** respectively **[137-143]**.

$$\varepsilon^* = \varepsilon' + \varepsilon'' \qquad (4.15)$$

$$\varepsilon^* = \frac{1}{j\omega C_0 Z^*} \quad (4.16)$$

$$C_0 = (\frac{\varepsilon_0 A}{t})$$

Where C_0 is geometrical capacitance, ε_0 is the permittivity of free space having value 8.85* 10^{-12} F/m, A is the area of pellet, t is the thickness of pellet measured using a vernier calliper.

$$\varepsilon' = Z"/2\pi f C_0(Z'^2 + Z"^2) \quad (4.17)$$

$$\varepsilon" = Z'/2\pi f C_0(Z'^2 + Z"^2) \quad (4.18)$$

Where f is frequency, $Z'$and $Z"$ are real and imaginary parts of the impedance, these values are already given in the data of electro-chemical spectroscopy.

The dielectric constant (ε') versus frequency variation for the composites and GdIG and MgFe2O4 is as shown in **Figure 4.13**. **Figure 4.13** has two parts (a) and (b) which rep the variation of ε' at different frequency ranges. **Figure 4.13** (a) represents the variation from 1MHz to 10MHz (10^6 to 10^7) range (higher frequency range) and (b) represents a variation from 1Hz to 100KHz (10^2 to 10^5) range (lower frequency range. The dispersion of the dielectric curve can be explained using the theory given by Koop's **[144]** which is based on the model of Maxwell-Wagner which explains about in-homogeneous double structure **[145]**. The structure of dielectric material was assumed to be formed by a double layer as stated by the model. Materials are well conducting in the first layer (grains) and materials are poor conductors in the second layer (grain boundaries). These layers are separated by each other. At higher frequency, grains of ferrites were effectual whereas, at a lower frequency, grain boundaries are more effectual. In garnet ferrites only Fe^{+3} ions are present and in spinel ferrite both Fe^{+3} and Fe^{+2} ions are present. This means that in composites Fe^{+3} is dominant as compared to Fe^{+2}. These two ions offer dipolar to the ferrite's composites. The grains and grain boundaries are present in higher amounts in the ultrafine region as compared to the bulk, due to this, a complex phenomenon arises. Also, there is additional probability in nanomaterials to have a larger dielectric constant as individual grains have a larger surface area which further provides large polarization at the surface. The dielectric properties for ferrites can be more accurately determined by this surface polarization in a low-frequency region rather than ionic or electronic polarization.

It has been observed that GdIG (x=1) show almost constant value for ε' from 1Hz to 100KHz (lower frequency region) shown in **Figure 4.13** (b) which means it is showing frequency-independent behaviour whereas, in high frequency (**Figure 4.13** (a)) region its value varies slightly. By the addition of MF to GdIG i.e., at x = 0.5 gives the maximum value of ε' near 1MHz and there is a decrease in value of ε' after this frequency range i.e., up to 10MHz. It shows more prominent decrease than x = 1 and x = 0.75. Further at x=0.75 i.e., on increasing GdIG ratio more, the values of ε' shows no variation with frequency from 1Hz to 1MHz. In the higher frequency region, it (x=0.75) follows the same trend as x=1. It has been observed that a large value of dielectric constant ~612 is obtained for x = 0.5 at 1MHz. It has been noticed that values of dielectric constant decrease by decreasing MF content (spinel ferrite) in GdIG i.e., at x=0.75, here the value of dielectric constant become almost independent of frequency up to 1MHz such variations have also been observed in pure GdIG. At a higher frequency, the value of the dielectric constant decreases which is a very obvious behaviour of ferromagnetic materials. In ferrites, the polarization mechanism can be understood similarly as conduction phenomena. As the Fe^{+3} ions and Fe^{+2} ions of composites exchange their electrons, the electron tends to displace in the direction of the field which is applied and hence polarization occurs. The decrease observed in the dielectric constant can be attributed to the fact that these charge caring ions need some fixed time to align themselves in the direction of the applied AC field. The charges get disabled to align themselves in the applied field due to the high reversal frequency **[146]**. Here the applied frequency increases continuously and at some points, polarization has started to proceed so that no reverse field opposes their motion, but unable to provide any contribution to polarization and further there is no dielectric constant. So, in general, grain boundaries defect, oxygen vacancies, presence of Fe^{+2} enhances the dielectric constant at lower frequencies whereas when polarization and applied field lags out there is a decrease in dielectric constant at higher frequency.

The imaginary part (ε'') of dielectric constant for the composites, GdIG and $MgFe_2O_4$ is as shown in **Figure 4.14**. Further variation of ε'' is also measured in 10^6 to 10^7 and 10^2 to 10^5 range as given in (a) and (b) of **Figure 4.14**. It can be seen that in lower frequency range GdIG (x=1), x=0.5, x=0.75 shows no variation in ε''. This implies that GdIG and its composites are independent of frequency in a lower frequency range. Whereas with the addition of MF in GdIG i.e., at x=0.5 the value of ε'' decreases near 1MHz and then increases near 7MHz. The value of ε'' is maximum for x=0.5 near about 7 MHz.

The dielectric tangent loss of samples is as shown in **Figure 4.15** and is calculated using **Equation (4.19)**. Dielectric loss is simply the loss of the energy induced by the applied field. It has been observed that for all composites the losses are almost zero in the high-frequency region (up to 5MHz) and not getting affected by frequency. But near 6 MHz variations in losses are there. The value of loss tangent is least for x=0.75 composite and become maximum for x=0.5 composite at this frequency range. Whereas in the low-frequency region as shown in **Figure 4.15** (b), x=0.75 composite has a larger value of dielectric loss tangent nearly at 1Hz frequency which further decreases with an increase in frequency. For x=1 no such variation in the value of dielectric loss in the lower frequency region is there. The dielectric loss is caused by the resonance obtained at the walls of the domains. And also, when charge carries transport from grain-grain boundaries of ferrites and direction of polarization changes in presence of applied field which cause dissipation in energy **[147]**. These domain wall motions are restricted at the higher frequency where magnetization causes the change in rotation so the losses are low at higher frequencies **[148]**.

$$\tan \delta_{\varepsilon} = \frac{\varepsilon''}{\varepsilon'} \qquad (4.19)$$

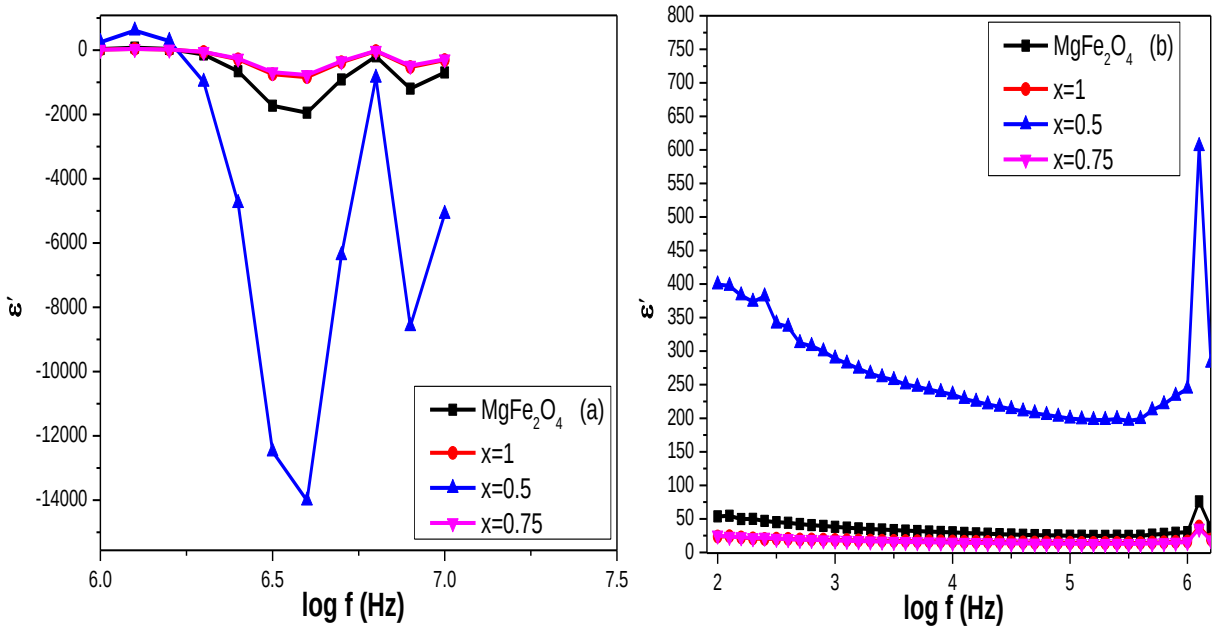

Figure 4.13 representing variation of dielectric constant (ε') of $MgFe_2O_4$ and x=1.0,0.5,0.75 at (a) 1MHz to 10 MHz (b) 1Hz to 100KHz frequency

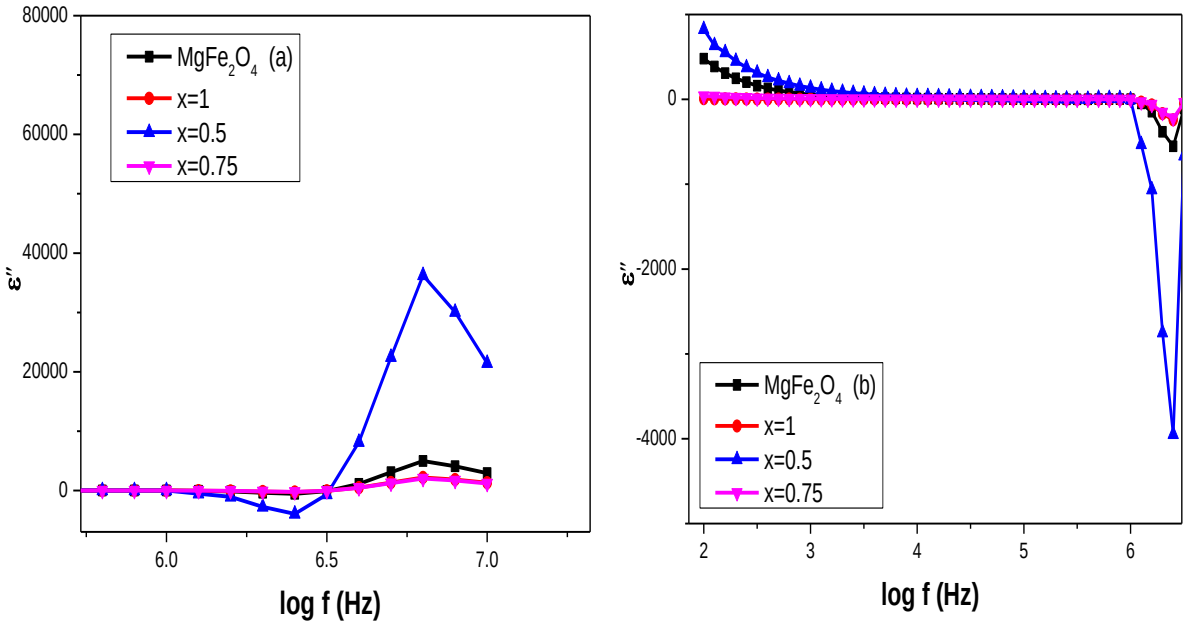

Figure 4.14 represent variation imaginary part (ε") of dielectric constant with frequency for $MgFe_2O_4$ and x=1.0,0.5,0.7 at (a) 1 MHz to 10 MHz (b)1 Hz to 100KHz frequency range

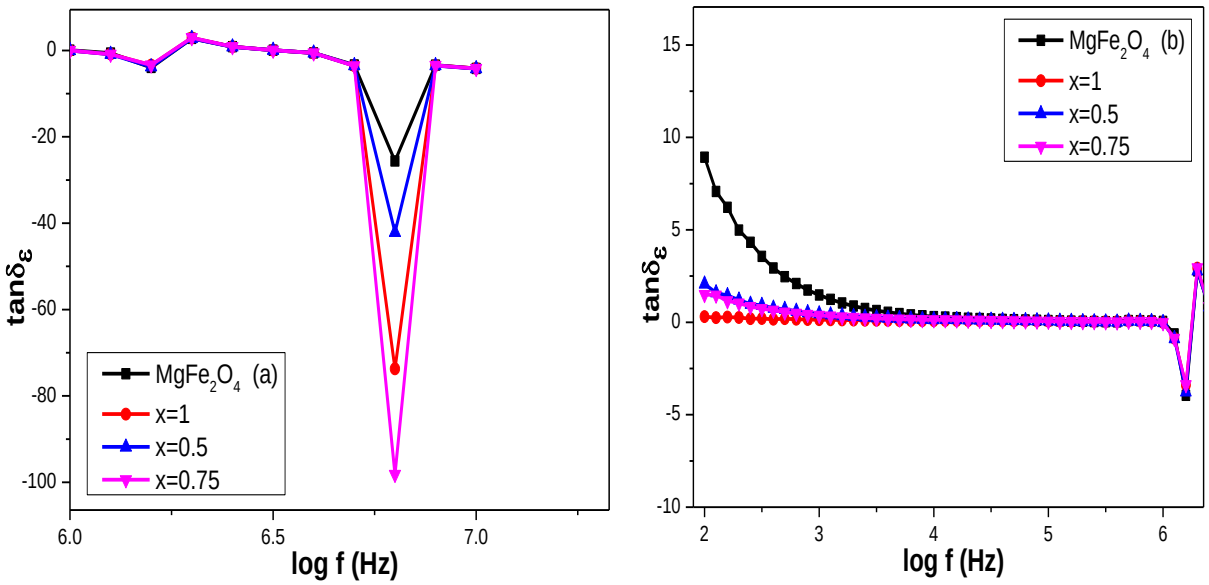

Figure 4.15 The variation of dielectric tangent loss with frequency for $MgFe_2O_4$ and x=1.0, 0.5, 0.75 at (a) 1 MHz to 10 MHz (b) 1Hz to 100 KHz

4.2.5 VSM

Figure 4.16 represents the magnetization vs applied field curve (M-H) of $MgFe_2O_4$ (MF), GdIG (x = 1) and their composites (x=0.5,0.75). The S-shaped curves signify the superparamagnetic nature of the samples. Single-phase magnetic nature has been observed by the addition of MF to GdIG. This suggests the exchange coupling between these two ferrites, which give rise to magnetization switching between the phases of ferrites present in composites. The magnetic parameter coercivity (H_c), retentivity (M_r), saturation magnetization (M_s), squareness ratio (SQR) deduces from the M-H curve and the value of anisotropy constant (K_{eff}), magneto crystalline anisotropy (H_a), microwave operation frequency (ω_m) is tabulated in **Table 4.5**. The value of K_{eff}, H_a, and ω_m have been calculated using **Equation (4.20)**, **Equation (4.21)** and **Equation (4.22)** respectively.

$$K_{eff} = \frac{H_c \times M_s}{0.96} \tag{4.20}$$

$$H_a = \frac{2K_{eff}}{Ms} \tag{4.21}$$

$$\omega_m = 8\pi^2 \gamma M_s \tag{4.22}$$

It has been observed that M_s value is least for x=1 (GdIG), maximum for x=0.5 (GdIG 50% and MF 50%) and moderate for x=0.75. The larger value of M_s is attributed to the addition of MF in GdIG, which is due to disorder in spin, morphology at the surface and anti-phase disorder **[149]**. The single-phase magnetization curve of ferrites is present despite two-phase nanocomposite which shows exchanged couple which is the reason for the enhancement in the value of M_s. If such behaviour of curve is not present then there is superimposition between the two curves of ferrites, and at interphase, the spin arrangement is non collinearly, which tends to reduce the value of M_s **[150]**. H_c is maximum for x=1, and by the addition of soft ferrite (MF) in soft ferrite (GdIG) in nanocomposites, the value of H_c decreases for x = 0.5, 0.75. As by the addition of MF in GdIG, dipolar interaction becomes very important. Due to dipolar interaction nucleation field reduces and further permit the reversal of domain in the soft ferrite phase in order to nucleate easily in presence of a low field so as a result of which value of H_c decreases **[151, 152]**. The lower value of coercivity for composites signifies that the composites have soft nature. This means that composites easily get magnetized as compare to parent ferrites. While the trend observed of M_r can be understood by magneto crystalline anisotropy (H_a) **[153]**. The value of H_a is larger for GdIG (x = 1), which means it is very difficult to reverse magnetization by providing a low field. But by the addition of soft ferrite in GdIG, the value of

H_a decreases. The ability of alignment of magnetization of ferrites in direction of applied field increases if dipolar interaction is more that it totally suppresses exchange-coupled interaction and hence M_r increases. The value of SQR for GdIG and its composites lies in the range 0.15 to 0.24 which is less than 0.5 signifies that all the samples have multi-magnetic domain structures. From the value of ω_m (microwave operating frequency), it is clear that only GdIG (x = 1) can be operated in 284 MHz range but with the addition of MF into GdIG, this microwave operation frequency jumps into the GHz range i.e., for x=0.5 nanocomposites can provide operation in 3.5 GHz range whereas for x=0.75 the range lies at 2.5 GHz. This implies that these nanocomposites can be operated at the S-band.

Table 4.5 H_c, M_r, M_s, anisotropy constant, magneto crystalline anisotropy, SQR and ω_m calculated from MH for x=0, 0.5, 0.75 and $MgFe_2O_4$

Composition	H_c (Oe)	M_r (emu/g)	M_s(emu/g)	M	K_{eff} (erg/cm^3)	H_a	SQR	ω_m
x=1.0	444.5	0.19	1.29	0.025	597.3	926	0.15	284 (MHz)
x=0.5	65.4	3.82	16.2	0.325	1103.6	136	0.24	3.5 (GHz)
x=0.75	73.7	2.68	11.63	0.233	892.8	153	0.23	2.5 (GHz)
$MgFe_2O_4$	220.2	10.5	31.04	0.6	7119	458	0.34	6.8 (GHz)

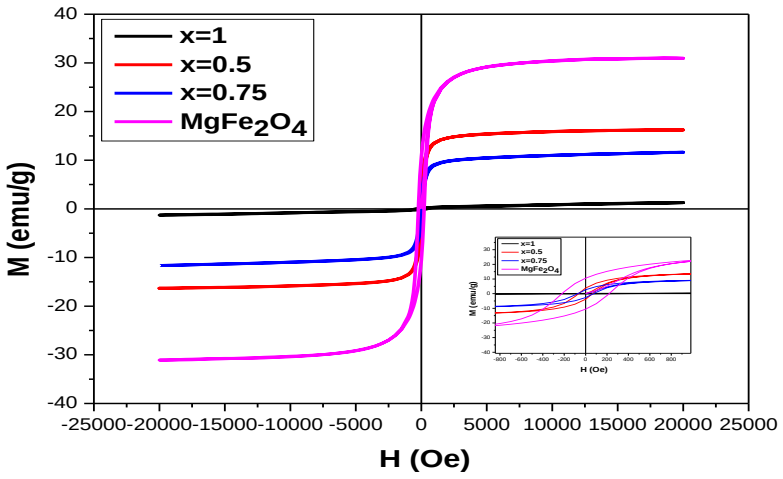

Figure 4.16 Magnetization hysteresis loops x=1, x=0.5, x=0.75 and $MgFe_2O_4$ composites

4.3 Gadolinium iron garnet, magnesium spinel ferrite and their heat-treated composite ($GdIG/MgFe_2O_4$)

4.3.1 XRD

The XRD pattern for composite of gadolinium iron garnet (GdIG) and magnesium iron ferrite (MF) with weighted ratio of GdIG (75%)/MF (25%) is represented in **Figure 4.17. Figure 4.17** (a) and (b) represent the XRD pattern of composite treated at 900°C (GM9) and 1300°C (GM13). It can be concluded from the patterns that peaks of both GdIG and MF are present in composites with no other phases. Which was confirmed from the JCPDS no. 720141 for GdIG and 711232 for MF. Also, it has been observed that with variation in temperature, both phases are present independently in composite. With increase in temperature the intensity of the major peak decreases and same happens for other peaks. This decrease in intensity might be due to presence of strong adhesion force between soft ferrites in composites at high temperature. The calculated value of crystallite size, lattice constant and micro strain for highly intense peak of GdIG and MF are tabulated in **Table 4.6**.

The crystallite size for sample GM9 and GM13 is calculated using Scherrer's **Equation (4.33)**.

$$D = \frac{K\lambda}{\beta \cos\theta} \tag{4.33}$$

In the equation D represent the crystallite size, λ represents the wavelength of X-ray source having values 0.15406 nm, K represents Scherrer constant having value 0.9, β is the full width half maxima (FWHM) which is computed from given XRD data. θ is the peak position which is also computed from XRD data. The values of 2θ and β are taken corresponding to major peaks of GdIG and MF, and are tabulated in **Table 4.6**. It has been noticed that the crystallite size decreases with increase in temperature. Which can be linked with broadening of peak. Also, crystallite size varies inversely to β and $2\,\theta$ and for sample GM13 value of β is larger and therefore crystallite size is lesser.

Because structure of both garnet ferrite and spinel ferrite is cubic so lattice constants for the composites GM9, GM13 were calculated using **Equation (4.34)**.

$$\frac{1}{d^2} = \frac{h^2+k^2+l^2}{a^2} \tag{4.34}$$

Where a is lattice constant, hkl is the miller indices which is taken corresponded to maximum intensity peak, d is interplanar spacing calculated by using Bragg's law **Equation (4.35)**.

$$d_{spacing}(\text{Å}) = \frac{n\lambda}{2\sin\theta}\ , n = 1 \tag{4.35}$$

The value of "a" for GdIG and MF in the composites slightly increases with increase in temperature. The lattice parameter of composites of GdIG increases slightly due to effect of strain, acting at interface between GdIG and MF **[154]**. Micro strain for GdIG and MF is more at higher temperature and is calculated using **Equation (4.36)**.

$$\varepsilon = \frac{\beta}{4\tan\theta} \tag{4.36}$$

Table 4.6 calculated 2θ, β, hkl, crystallite size(D), lattice parameter(a), micro stain for differently sintered samples

Composite	Sample Code	Ferrite	2θ	β(°)	hkl	D(nm)	a (Å)	Micro Stain
$(Gd_3Fe_5O_{12})x$-$(MgFe_2O_4)1$-x x = 0.75 at 900°C	GM9	GdIG	32.05	0.19	440	43.5	12.47	2.9
		MF	35.3	0.49	311	16.8	8.4	6.8
$(Gd_3Fe_5O_{12})x$-$(MgFe_2O_4)1$-x x = 0.75 at 1300°C	GM13	GdIG	32.01	0.21	440	39	12.49	3.2
		MF	35.4	0.54	311	15.3	8.44	7.4

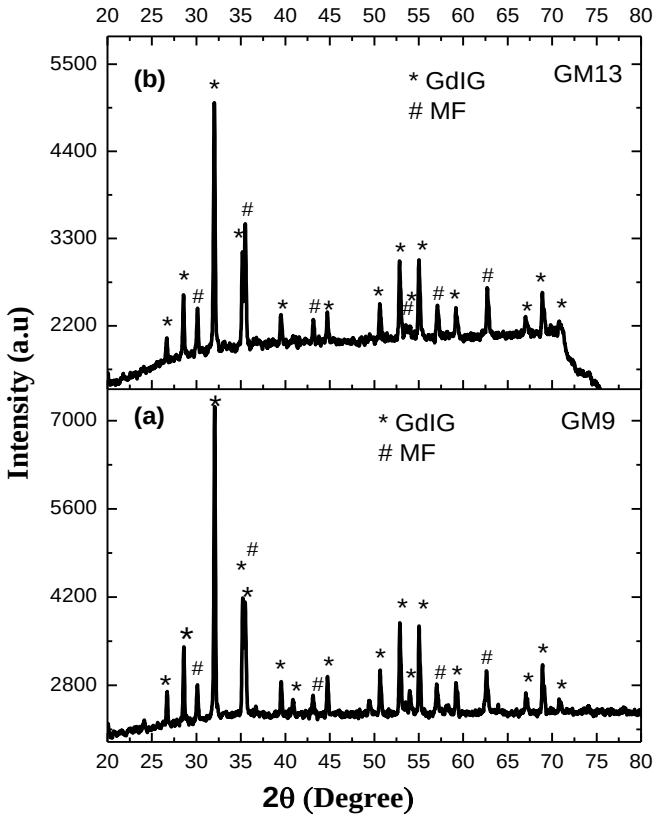

Figure 4.17 XRD pattern of (a) GM9 and (b) GM13 sample

4.3.2 FESEM

For better understanding of effect of temperature on microstructure of composite treated at different temperatures, FESEM was used. **Figure 4.18** represent the micrograph of GM9 and GM13 samples. It is clear from the micrographs that two different sizes of grains are present. These grains are corresponded to GdIG and MF. On very deep view it was examined that GdIG grains are present in larger amount as compare to MF in both samples. We have observed the spherical shaped grains for GdIG and roughly cubical shaped grains for MF. In both the micrograph (a) of sample GM9 and (b) of sample GM13 agglomeration of grains is present. But this agglomeration increases with increase in temperature i.e., more agglomeration is observed for GM13. This can be related to magnetic attraction in nanocomposite, made up of soft ferrite **[147]**. Micrograph (a) shows low densification with porosity. Whereas micrograph (b) shows larger densification of GdIG grains, which seemed to be connected with each other with very less porosity. This significant change with temperature proves that temperature

influences the grain growth. As a conclusion it can be said that temperature has great role in formation of better microstructure. This better microstructure further effects the dielectric and magnetic properties of composites **[155]**.

The gausian distributed histogram which represent size distribution of the composites is as shown in **Figure 4.19.** The particle size of the composites come out be 48 nm and 700 nm for GM9 and GM13 respectively. This means that particle size increases with increase in temperature.

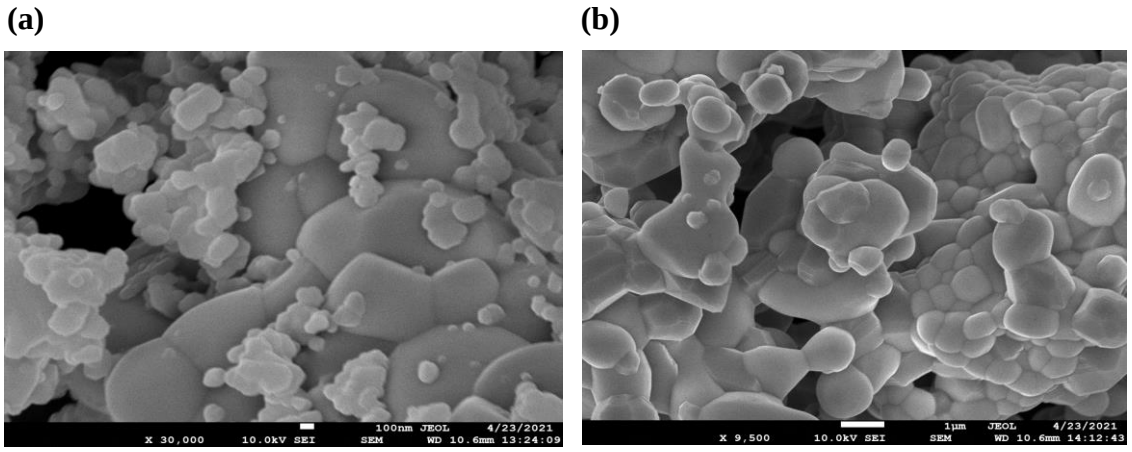

Figure 4.18 Micrographs of (a) GM9 and (b) GM13

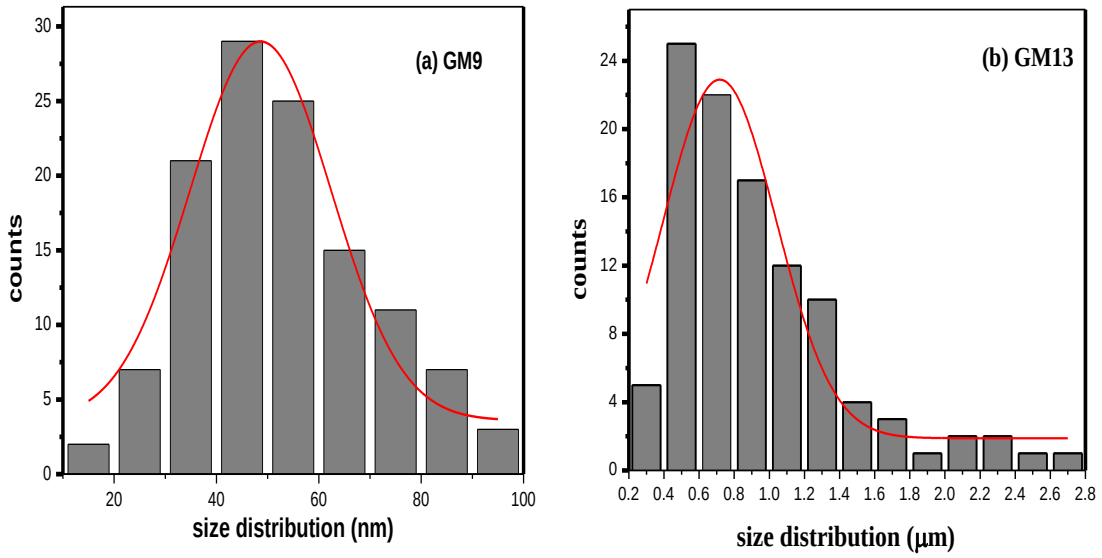

Figure 4.19 Histogram representing the particle size distribution of (a) GM9 (b) GM13

4.3.3 EDX

Figure 4.20 represent the EDX spectra and **Figure 4.21** represent elemental mapping of composites. From EDX analysis it is clear that all the required elements and desired composition is present in formed samples. There are no extra traces of other elements. This implies that preparation method is efficient. In EDX spectra some characteristic peak is appearing close to 2KeV, which is un identified. The reason for the presence of such peak is EDX underestimates the real content of residual impurities. This is due to the surface sensitivity of the FESEM/EDX analysis. From **Figure 4.20** (a-b) it can be analyse that all the elements are spread over entire region for GM13 sample, whereas for GM9 sample the elements are not dispersed homogenously. This might be due to high temperature which provide better microstructure. The weight percent and atomic percent for elements are also tabulated in **Table 4.7** and **Table 4.8**.

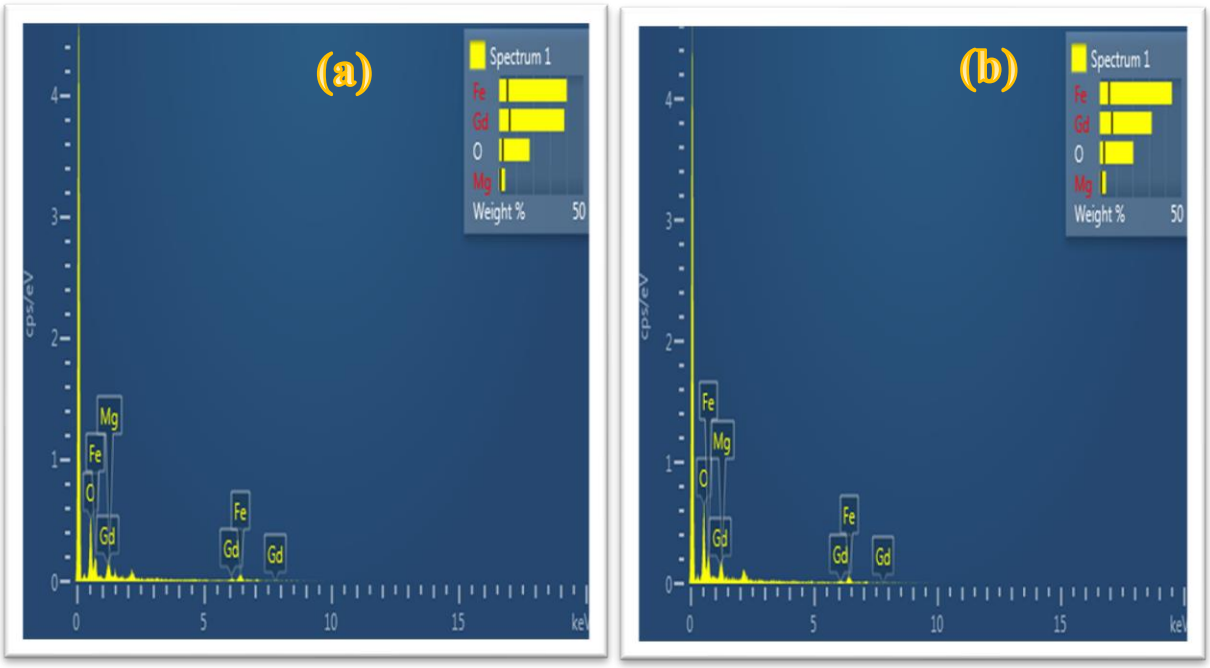

Figure 4.20 EDX spectra of (a) GM9 and (b) GM13 sample

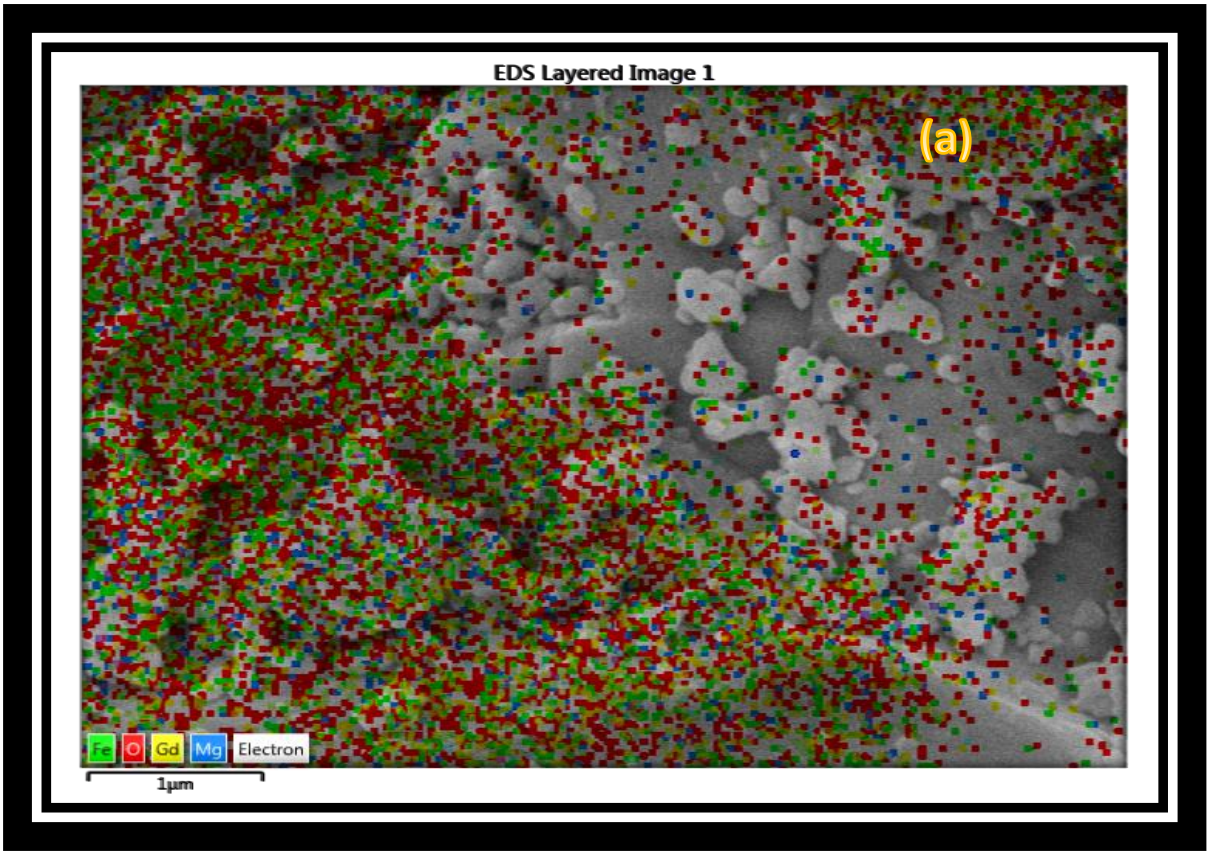
EDS Layered Image 1
(a)
Fe
O
Gd
Mg
Electron
1µm

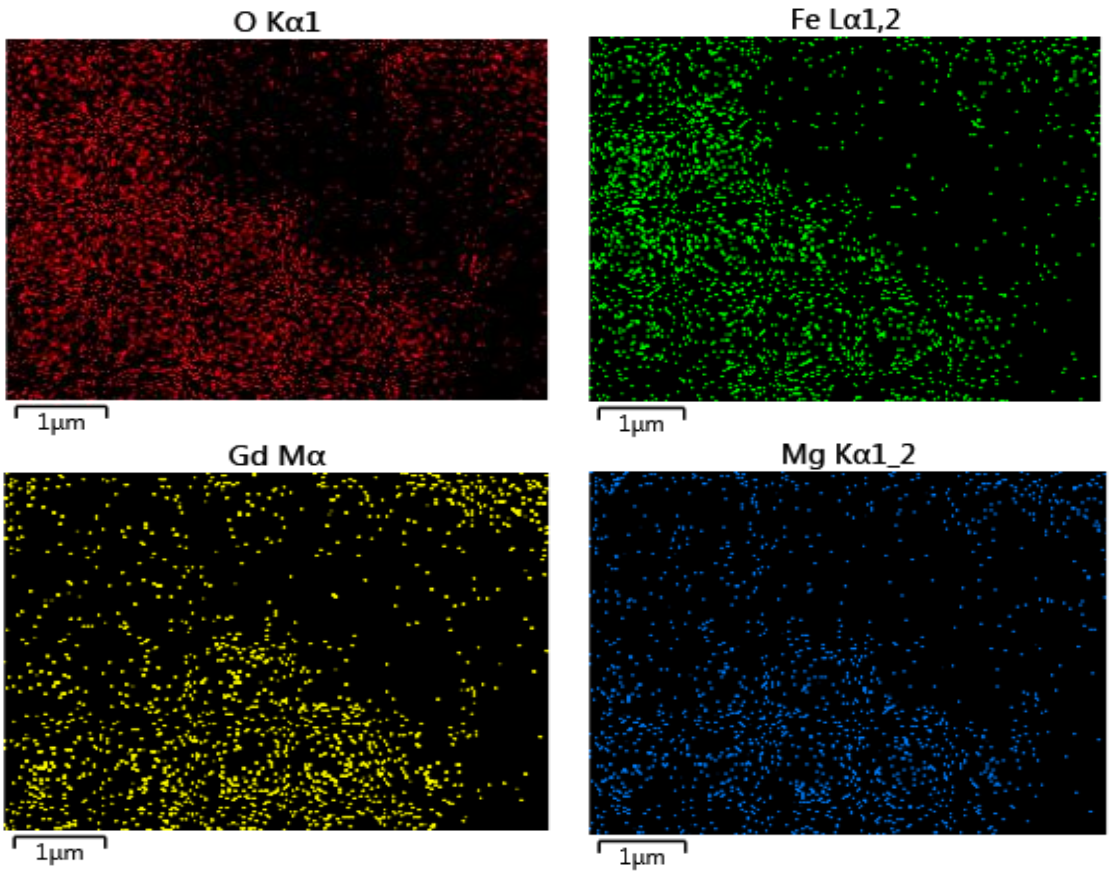
O Kα1
1µm
Fe Lα1,2
1µm
Gd Mα
1µm
Mg Kα1_2
1µm

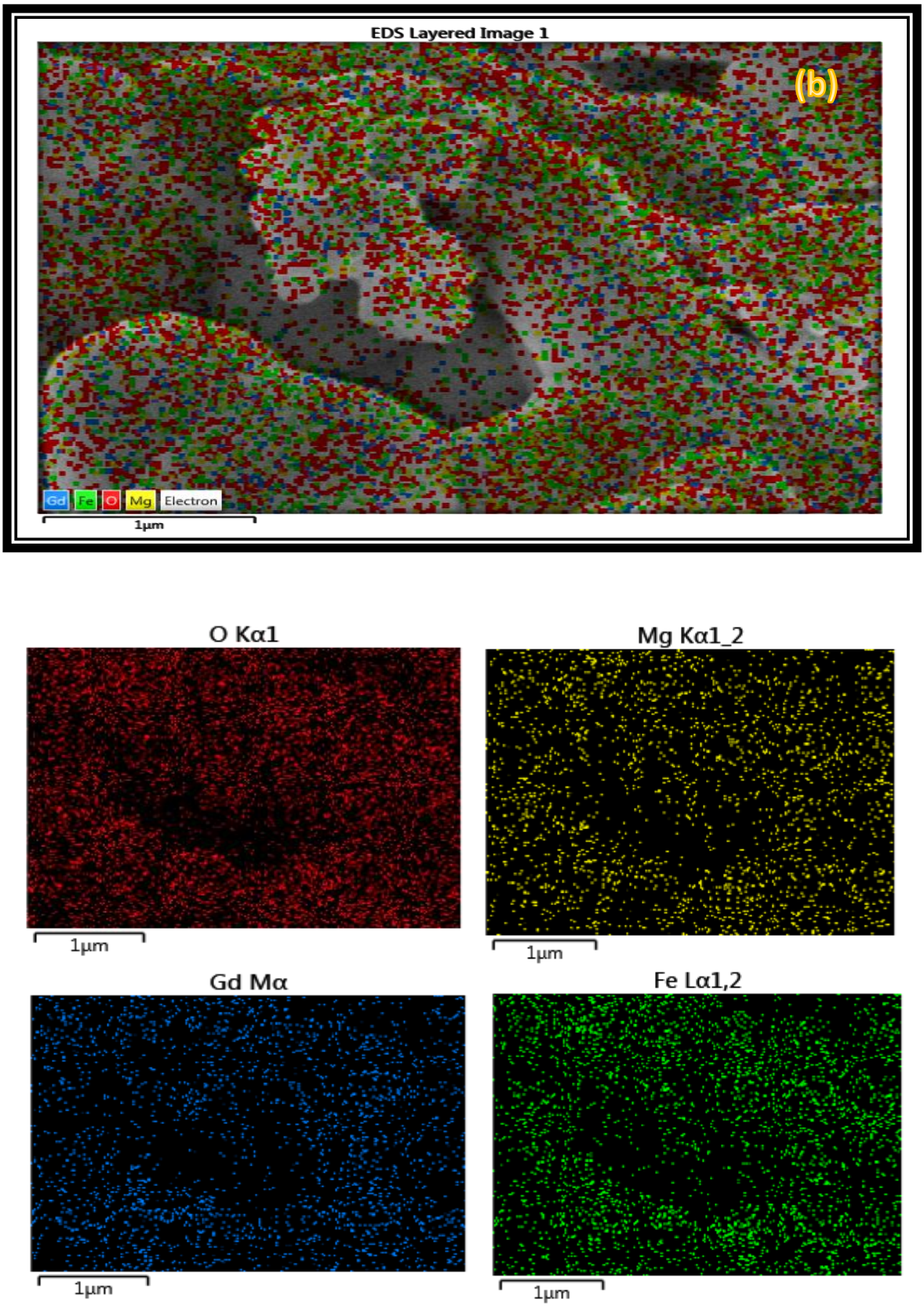

Figure 4.21 Images of elemental mapping of (a) GM9 and (b) GM13

Table 4.7 and Table 4.8 represent experimental value of wt% and atomic % for elements present in GM9 and GM 13 samples

GM9

Elements	Wt%	Atomic%
O	17.94	50.42
Mg	3.42	6.32
Fe	40.02	32.22
Gd	38.62	11.04
Total	**100.00**	100.00

GM13

Elements	Wt%	Atomic %
O	20.45	52.78
Mg	3.70	6.28
Fe	44.11	32.61
Gd	31.74	8.33
Total	100.00	100.00

4.3.4 Impedance Analyser

To understand the influence of temperature on dielectric behaviour of samples, impedance analyser technique has been caried out. **Figure 4.22** represent the variation of dielectric constant with frequency ranges from 1Hz to 10MHz for the sample sintered at different temperatures. Dielectric constant can be understood as, it is an ability of material to store electric charge in presence of electric field. The dielectric constant for samples is calculated using **Equation (4.37).**

$$\varepsilon_r' = \frac{\varepsilon'}{\varepsilon_0} \tag{4.37}$$

Where ε' is real part of complex permittivity and ε_0 is permittivity of free space. Stress must be given on the point that dielectric constant is affected by some factors like methods of preparation, distribution of cations, homogeneity in structure, size of the grain and sintering temperature **[156]**. It has been seen from **Figure 4.22** (a) and (b) that, dielectric constant fluctuates at lower frequency, whereas at high frequencies ranges, dielectric constant has negative value. The dispersion in dielectric constant value with frequency is because of Maxwell-Wagner sort of interfacial polarization which is accordance to the theory of Koop's. Both samples have large values of dielectric constant at different frequency. The reason can be that in nanomaterials the surface area of individual grains is large which further increases surface polarization and hence increase in dielectric constant. At lower frequency temperature is playing its role to enhance the value of dielectric constant. This temperature dependence of dielectric constant can be described on the basis of thermal energy **[157]**. Production of thermal

energy is large at higher temperature. This large thermal energy further contributes to increase the mobility of ions and also enhances the hopping rate. But at lower temperature this thermal energy is not that much capable to increase the rate of mobility of ions. Therefore, at higher temperature dielectric polarization increases. The negative value of dielectric constant at higher frequency has been seen for both the samples implies that at higher frequency ions tries to align in the direction of applied field but lags behind, even though temperature treatment is also disable to align them.

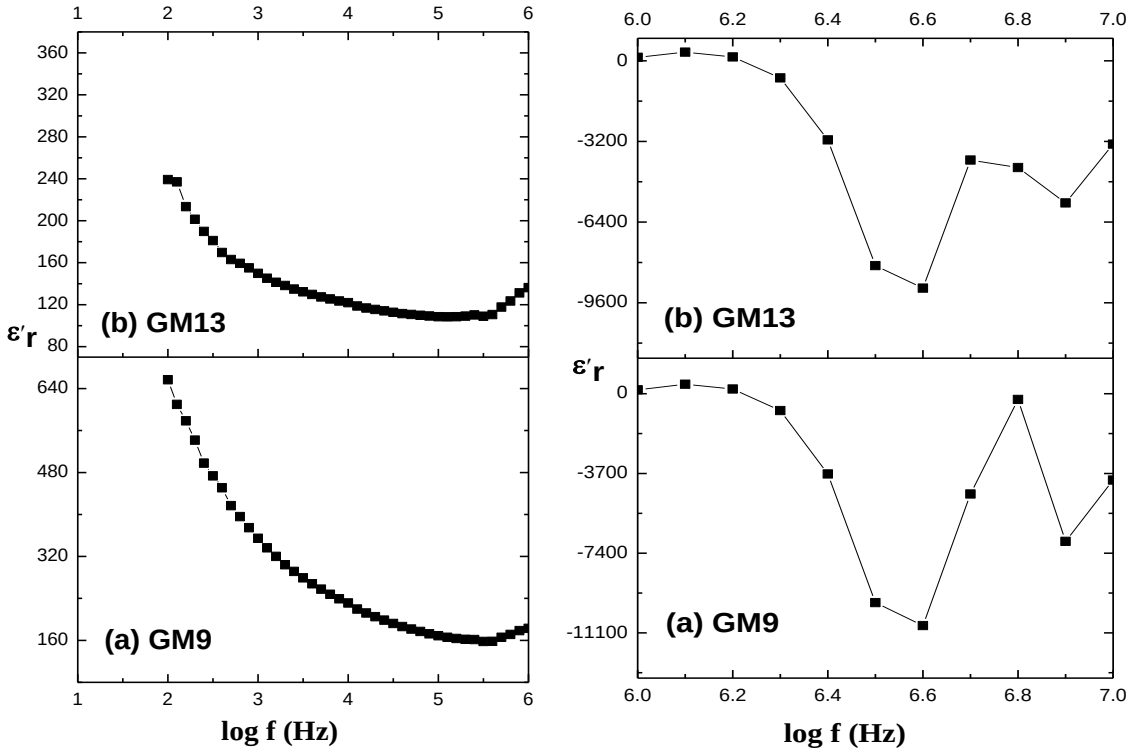

Figure 4.22 Dispersion in dielectric constant with frequency (100Hz to 10 MHz) for (a) GM9 and (b) GM13 sample

The variation in $\tan\delta_\varepsilon$ with frequency for both the samples is as shown in **Figure 4.23**. The loss in energy induced by applied field is dielectric loss. The dielectric loss tangent $(\tan\delta_\varepsilon)$ is calculated using **Equation (4.38)**.

$$\tan\delta_\varepsilon = \frac{\varepsilon''}{\varepsilon'} \tag{4.38}$$

Here ε'' is the imaginary part of the complex permittivity.

From **Figure 4.23** (a) and (b) it can be seen that at lower frequency range i.e., from 1Hz to 100 KHz the value of $\tan\delta_\varepsilon$ is almost zero that is independent of frequency. The sample GM9 treated at lower temperature show least value of $\tan\delta_\varepsilon$ at high frequency range. Whereas the sample GM13 treated at higher temperature has larger value of $\tan\delta_\varepsilon$ as compare to GM9. This variation of $\tan\delta_\varepsilon$ with frequency and further by different sintered sample can be explained by space charge conduction. The space charge conduction is associated with movements of defects like vacancies of oxygen to the interface of the dielectric electrode **[158]**. In general, the dielectric loss increases with decline in relaxation time. So, as the temperature increases, the relaxation time decreases and hence $\tan\delta_\varepsilon$ increases **[159]**.

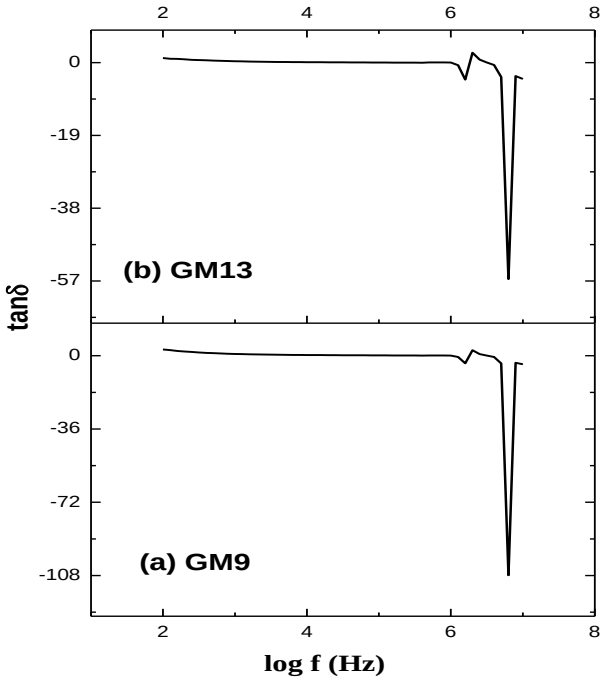

Figure 4.23 Variation of dielectric loss tangent with frequency (100Hz to 10 MHz) for (a) GM9 and (b) GM13 sample

In order to understand exact reason for the dependency of dielectric constant on temperature, the Nyquist plots for both samples are given in **Figure 4.24**. As it can be seen from the plot that arc is present in both the samples. In general, the arc present on the side of lower frequency is because of grain boundary conduction and that present on the side of high frequency is because of grain conduction. But from **Figure 4.24** (a) and (b) it is clear that only one arc is present for entire frequency range for both samples sintered at different temperatures. The change in arc for both the sample sintered at different temperature has been observed. Which reveals that the

temperature affects the diameter of the arc of both the samples. This evolution in the arc with temperature gives computable information about the grain boundary and grain resistance. With increase in temperature i.e., for sample GM13, it can be observed from plots that the arc at higher frequency range is diminishes. This means that the contribution is due to bulk of grain not from grain boundaries.

Further, complex impedance fitting of the plots has been done by using ZSimpwin Software. It has been seen properly that the experimental values are in good match with calculated values (obtain after fitting) for both the samples. The ideal equivalent circuit consist of both capacitor (C) and resistor (R) is best to examine experimental impedance plot **[160-162]**. The circuit used is as shown in **Figure 4.25**. In this circuits there are series of two sub circuit, one corresponds to grain effect and other to grain boundary effect. Let us assume grain resistance (R_g), grain boundary resistance (R_{gb}), grain capacitance (C_g) and grain boundary capacitance. The complex impedance (Z*) for the circuit is given by **Equation (4.39) [156]** which is related to real (Z') and imaginary (Z") part of impedance. This real and imaginary part is further related to R_g, R_{gb}, C_g and C_{gb} which is as given in **Equation (4.40)** and **Equation (4.41)**.

$$Z^* = \frac{1}{{R_g}^{-1} + j\omega C_g} + \frac{1}{{R_{gb}}^{-1} + j\omega C_{gb}} = Z' + Z'', \tag{4.39}$$

Here

$$Z' = \frac{R_g}{1+(\omega R_g C_g)^2} + \frac{R_{gb}}{1+(\omega R_{gb} C_{gb})^2} \tag{4.40}$$

$$Z'' = \frac{\omega {R^2}_g C_g}{1+(\omega R_g C_g)^2} + \frac{\omega {R^2}_{gb} C_{gb}}{1+(\omega R_{gb} C_{gb})^2} \tag{4.41}$$

From above mention equations we can accurately find that either contribution is from grain, grain boundary or either because of both. For the arc, the higher value of frequency or peak frequency is large for grain as their capacitance and resistance value is small and smaller for that of grain boundary **[163]**. So, in impedance plot the arc present on the side of higher frequency is correspond to grain and that present on lower frequency is correspond to grain boundary. The value of R_g, C_g, R_{gb}, C_{gb} obtain from fitting of plot is given in **Table 4.9**. The value of R_g decreases with increase in temperature, whereas the value of R_{gb} increases with temperature. Variation in the value of C_g is large as compare to C_{gb}. This implies that, the increase in value of ε'_r (dielectric constant) is totally due to grain (C_g).

Table 4.9 value of R_g, C_g, R_{gb} and C_{gb} calculated from complex impedance fitting for GM9 and GM13

Sample	R_g	C_g	R_{gb}	C_{gb}
GM9	293.5 Ω	0.504 µF	64.7 M Ω	15.33 pF
GM13	1.78 E-22 Ω	5.5 E4 F	2 E18 M Ω	12.43 pF

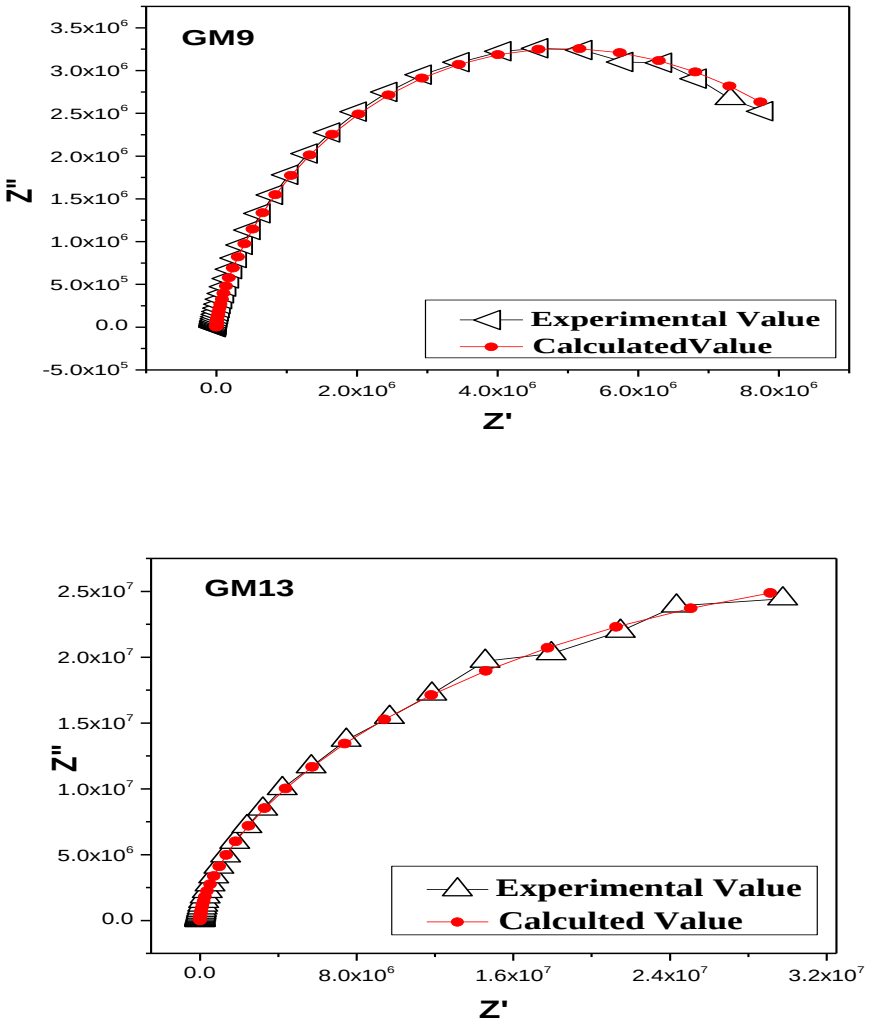

Figure 4.24 The impedance plot for (a) GM9 and (b) GM13 samples

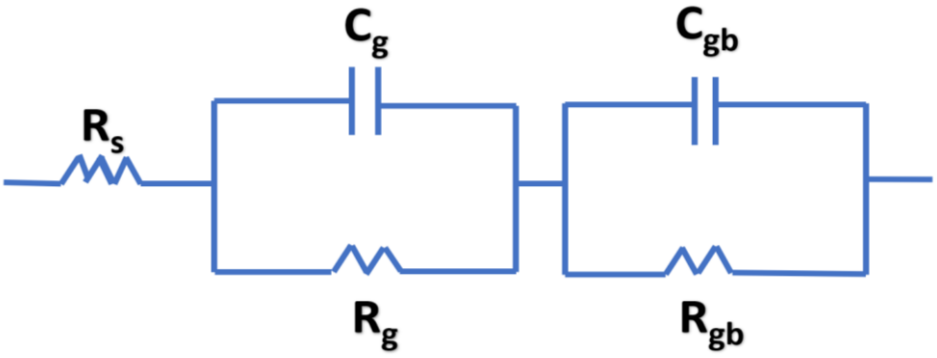

Figure 4.25 Equivalent Circuit

4.3.5 VSM

The magnetization versus applied field (M-H) plot for both the samples sintered at different temperatures is as shown in **Figure 4.26**. For both the samples the curve obtained is almost smooth. This smoothness of curve increases with increase in temperature. The curves are S shaped, which suggests the superparamagnetic nature of samples. From M-H loop the values of important magnetic parameters like coercivity (H_c), retentivity (M_r), saturation magnetization (M_s) and squareness ratio (SQR) are calculated and are given in **Table 4.10**. The values of anisotropy constant (K_{eff}), anisotropy field (H_a) and microwave frequency are calculated using **Equation 4.42**, **Equation 4.43** and **Equation 4.44 [164]** and tabulated in **Table 4.10**.

$$K_{eff} = \frac{H_c \times M_s}{0.96} \tag{4.42}$$

$$H_a = \frac{2K_{eff}}{Ms} \tag{4.43}$$

$$\omega_m = 8\pi^2 \gamma M_s \tag{4.44}$$

It has been seen that the value of M_s varies for both samples, i.e., with increases in temperature the value of M_s increases. But H_c decreases with increase in temperature. The lesser value of H_c suggests the superparamagnetic nature of sintered composites. It can be clearly seen that both H_c and M_s are depending on temperature. The variation in temperature brings microstructural changes **[165]** which further effect the magnetic properties of the samples. Microstructure plays a very vital role at high temperature. As with increase in temperature grain size increases and porosity in samples decreases **[166]**. In present work, with increase in temperature grain size increase and therefore decrease in porosity. But lesser value of M_s at lower temperature (for GM9) might be due to presence of pores. The magnetic circuits present

between grains breakout due to presence of pores, and therefore porosity in sample increases. The decrease in H_c with temperature is obvious and can be explained by **Equation (4.45)**.

$$H_c = \frac{0.96\,K_1}{M_s} \tag{4.45}$$

Where K_1 is the constant. It is clear from above equation that H_c varies inversely to M_s. Therefore, decrease in value of M_s has been observed. The decrease in K_{eff} is obvious with increase in temperature. The SQR value for both samples is 0.3 and 0.07 which is less than 0.5 signifies that the samples have multi-magnetic domain structure. Whereas calculated values of ω_m for both the samples suggest that the value increases from 1 GHz (for GM9) to 2 GHz (for GM13) with increase in temperature.

Table 4.10 H_c, M_r,M_s, K_{eff}, H_a, SQR, and ω_m value for GM9 and GM13

Sample	H_c (Oe)	M_r(emu/g)	M_s(emu/g)	K_{eff}(erg/cm^3)	H_a	SQR	ω_m
GM9	278.2	1.5	4.9	1431	579.7	0.3	1GHz
GM13	80.9	0.7	9.1	770	168.5	0.07	2GHz

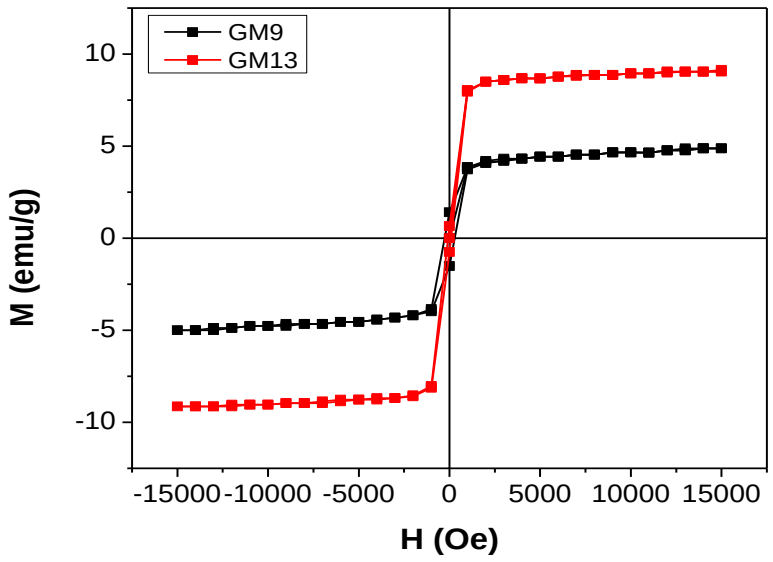

Figure 4.26 Magnetization hysteresis loops for GM9 and GM13

4.4 Y^{3+}, Bi^{3+}, La^{3+} substituted gadolinium iron garnet (GdIG)

4.4.1XRD

The XRD pattern of the $Y_{0.2}Bi_{0.2}La_xGd_{2.6-x}Fe_5O_{12}$ samples for x=0, 0.2, 0.4 is as shown in **Figure 4.27**. From the pattern it can be clearly seen that the garnet phase is present in majority for all samples. JCPDS no. 72-0141 also confirmed the presence of garnet phase in majority. The peaks at (321), (400), (420), (422), (521), (532), (444), (640), (642), (800), (840), (842), and (664) represents the diffraction pattern of garnet ferrite having cubic structure with space group Ia3d **[167]**. The occurrence of a greater number of pure phases in the samples suggests that the methods, temperature, and time were adequate for the samples. All of the strong peaks in the samples suggest that crystallisation was completed at 1200°C. The strongest peak, which corresponds to "hkl" value (420), has migrated somewhat towards lower 2 value with increased La^{3+} content in the samples. The greater ionic radii of La^{3+} (r=1.061) compared to Gd^{3+} (0.938) cause this change **[168]**. From obtained XRD data the values of lattice constant, crystallite size and micro strain for samples were calculated and are tabulated in **Table 4.11**.

As structure of garnet ferrite is cubic so lattice constant for the samples was calculated using **Equation (4.46)**.

$$\frac{1}{d^2} = \frac{h^2+k^2+l^2}{a^2} \tag{4.46}$$

Here “a” represents lattice constant, “hkl” represents miller indices, corresponds to maximum intensity peak, “d” represents interplanar spacing calculated by using Bragg’s law **Equation (4.47)**.

$$d_{spacing}(\text{Å}) = \frac{n\lambda}{2\sin\theta} \quad n = 1 \tag{4.47}$$

The lattice constant with addition of La^{3+} increases from x=0 to 0.2 and further decreases slightly at x=0.4. Both the samples with La^{3+} ion i.e., for $C_{0.2}$ and $C_{0.4}$ shows higher value of lattice constant as compare to sample which do not have La^{3+} ion. This behaviour of lattice constant can be explained on the basis of Bragg’s law. As the value of angle “θ” decrease the value of “d” increases so as the value of lattice constant increases. Larger La^{3+} ion substitution in dodecahedral site tends to distort the unit cell of cubic GdIG and therefore the value of lattice constant increases. The change in lattice constant is not only because of rare earth substitution but also depend upon condition of preparations, methodology, exerted stress and strain **[169]**.

By using Scherrer **Equation (4.48)** the crystallite size of the samples was calculated.

$$D = \frac{K\lambda}{\beta \cos\theta} \tag{4.48}$$

Here “D” represents crystallite size, “K” represents Scherrer constant having value 0.9, λ represent wavelength of X-ray sources having value 0.15406 nm, "β" represents full width half maxima (FWHM) in radians and "θ" represents peak position (radians). The value of crystallite size is large for sample C_0 (x=0). By addition of La^{3+} the crystallite size decreases from x=0 to x=0.2, and by further addition of La^{3+} at x=0.4 the crystallite size increases further. For sample C_0 the value of crystallite size is maximum. This variation of crystallite size can be understood by the presence of secondary phase which settle at grain boundaries and further impedes the growth of the crystal **[170]**. And another cause of variation in crystallite size is presence of stress and strain which produces defects in lattice **[171]**. For sample C_0 (x=0) there is less micro strain in lattice due to presence of Y^{3+} and Bi^{3+} ion in GdIG, with no secondary phase (Fe_2O_3, YFe_2O_3, etc). With increases in La^{3+} i.e., for sample $C_{0.2}$ (x=0.2) there is decrease in crystallite size. This can be attributed to presence of secondary phase into the sample. For sample $C_{0.4}$ (x=0.4) the crystallite size increases this is because the crystallite size also depends upon peak width or we can say on FWHM (according to **Equation (4.48)**). For $C_{0.4}$ the value of FWHM decrease due to which there is increase in crystallite size.

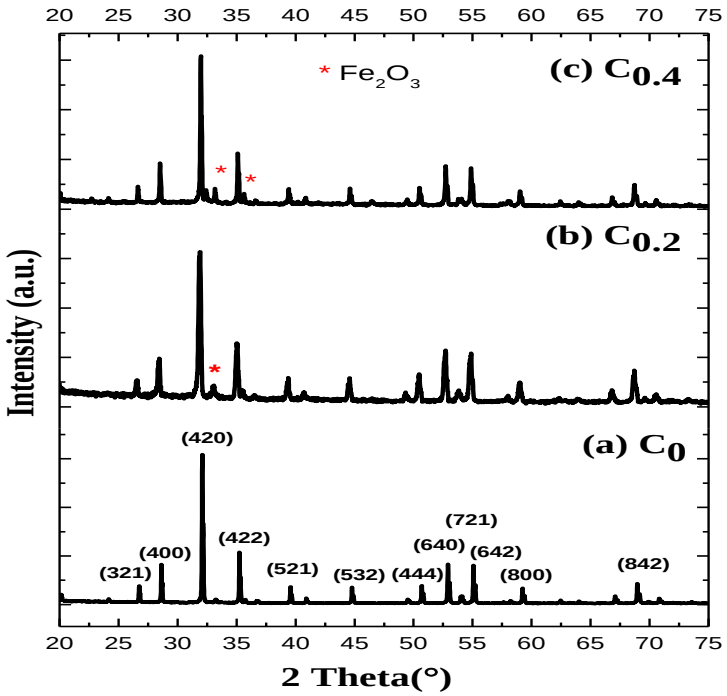

Figure 4.27 XRD pattern of $Y_{0.2}Bi_{0.2}La_xGd_{2.6-x}Fe_5O_{12}$ samples with (a) x=0,(b) x=0.2 and (c) x=0

Table 4.11 Variation in 2θ, β, crystallite size, lattice constant and micro strain by changing La^{3+} in C_0, $C_{0.2}$ and $C_{0.4}$ samples

Sample	Sample Code	2θ (°)	β(°)	hkl	D(nm)	a (Å)	Micro Stain
$Y_{0.2}Bi_{0.2}La_xGd_{2.6-x}Fe_5O_{12}$ x = 0	C_0	32.11	0.15	420	54	12.45	2.32
$Y_{0.2}Bi_{0.2}La_xGd_{2.6-x}Fe_5O_{12}$ x = 0.2	$C_{0.2}$	31.87	0.24	420	33.7	12.54	3.74
$Y_{0.2}Bi_{0.2}La_xGd_{2.6-x}Fe_5O_{12}$ x=0.4	$C_{0.4}$	31.98	0.16	420	50.8	12.50	2.47

4.4.2 FESEM

The micrograph images of samples of $Y_{0.2}Bi_{0.2}La_xGd_{2.6-x}Fe_5O_{12}$ (x=0, 0.2 and 0.4) obtained from FESEM are as shown in **Figure 4.28**(a-c). The shape of grains is roughly spherical for all samples. All the samples show agglomeration of grains which is due to magnetic attraction between ions present in samples **[172]**. In order to calculate grain size, line intercept method was used which is as given in **Equation (4.49)**. and value is tabulated in **Table 4.12**.

$$grain\ size = \frac{1.5\,L}{mn} \tag{4.49}$$

Here "L" represent length of line drawn in micrograph, "m" represent magnification given in micrographs and "n" represent number of intercept come under the line. The average grain of the samples depend upon the value of ionic radii of rare earth and doped elements, porosity, sintering temperature and methodology.

Table 4.12 Calculated grain size of the sample C_0, $C_{0.2}$ and $C_{0.4}$

Sample	Grain Size (μm)
C_0	0.100
$C_{0.2}$	0.116
$C_{0.4}$	0.108

The average grain size distribution of the samples is represent by histogram and is as shown in **Figure 4.29** (a-c). From the size distribution curve of the sample C_0 it is clear that maximum number of grains lie between 0.41µm to 0.58 µm range. For sample $C_{0.2}$ the maximum number of grains lies between 0.61µm to 0.78 µm range. The maximum number of grains for sample $C_{0.4}$ lies between 0.61 µm to 0.92 µm range.

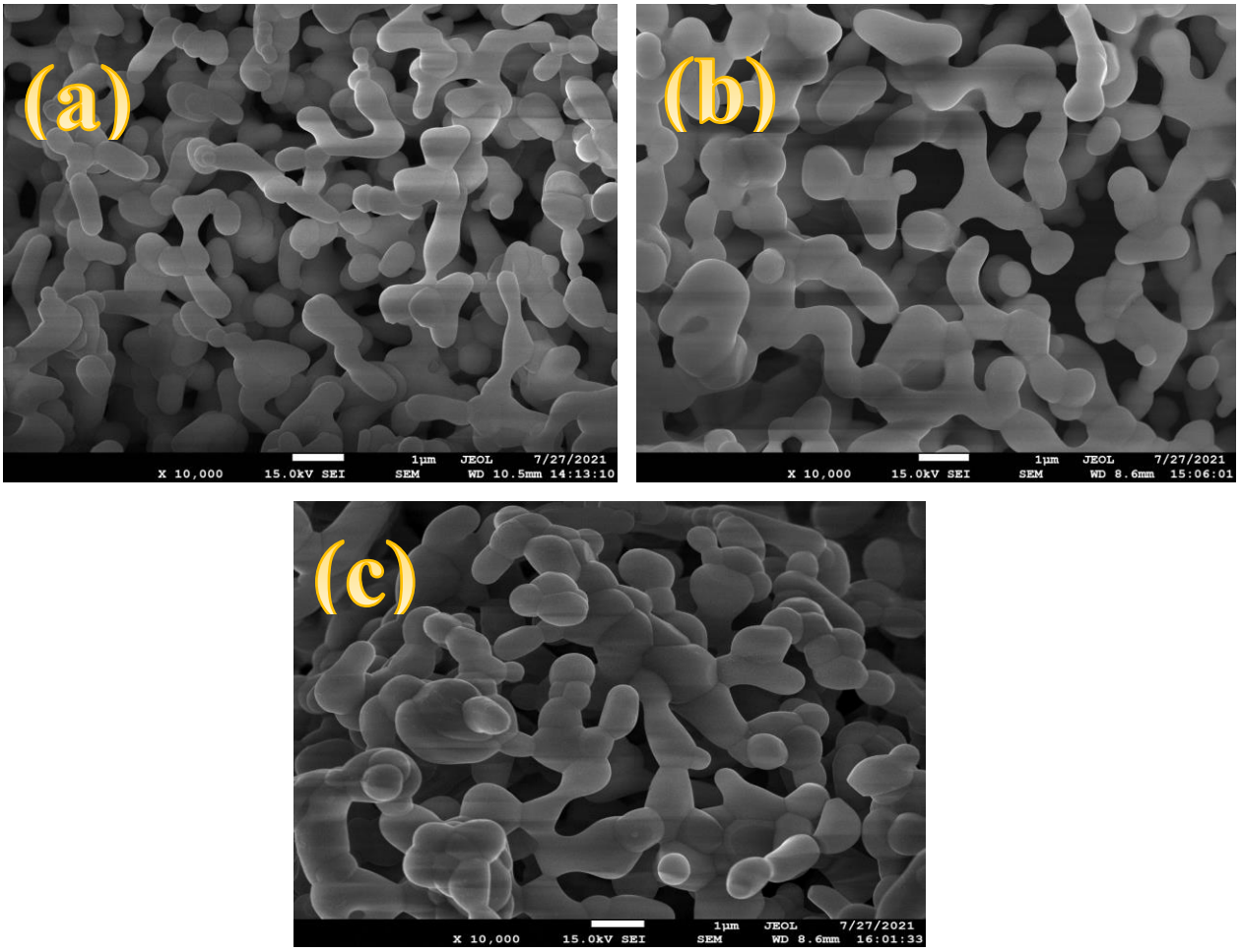

Figure 4.28 The Micrograph obtained from FESEM for (a) C_0, (b) $C_{0.2}$ and (c) $C_{0.4}$ samples

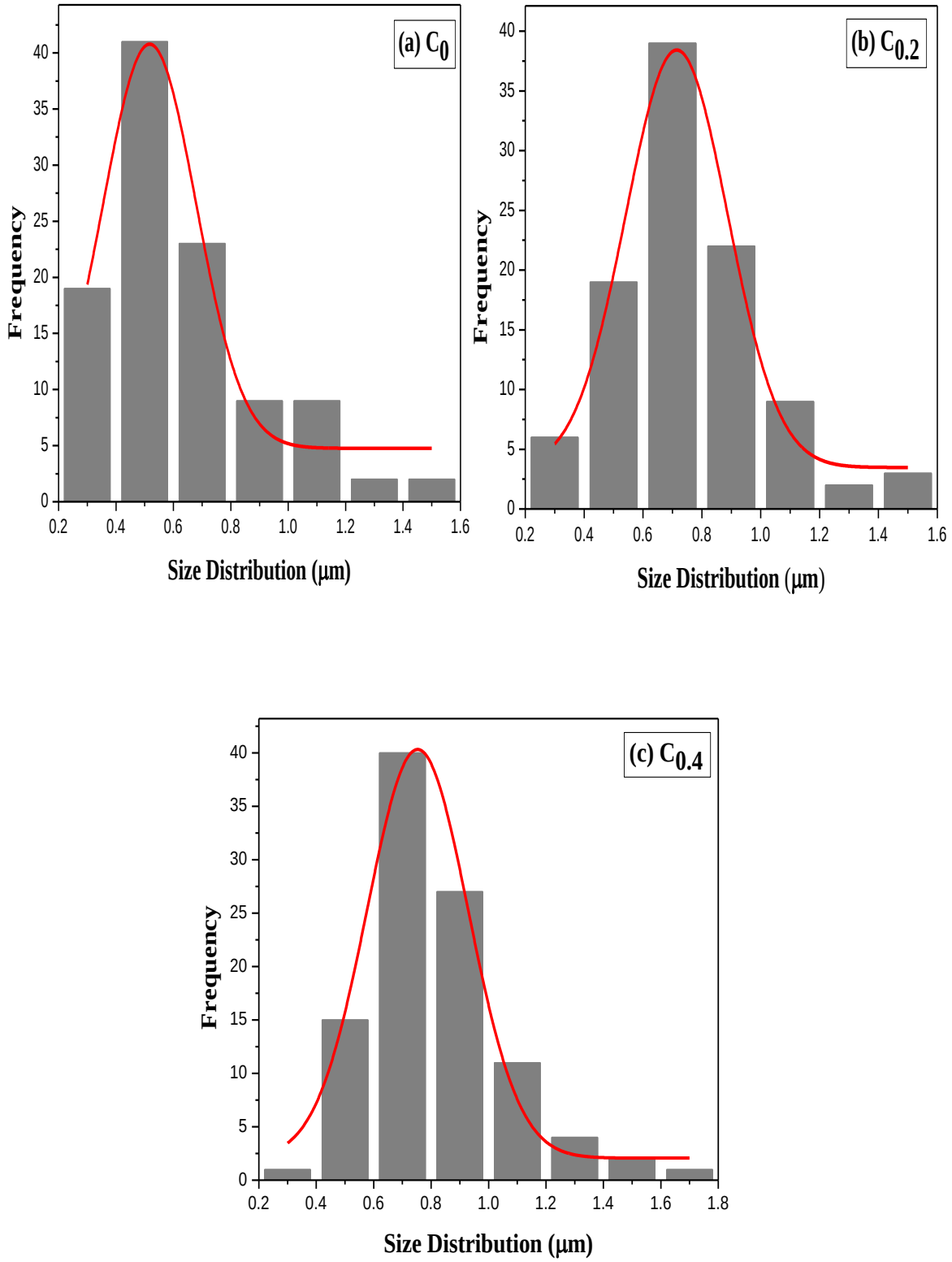

Figure 4.29 Histogram representing size distribution of sample (a) C_0, (b) $C_{0.2}$ and (c) $C_{0.4}$

4.4.3 EDX

The elemental mapping of samples is as shown in **Figure 4.30** (a-c). From EDX analysis it is clear that all the required elements are distributed properly and desired composition is present in formed samples. No extra traces of other elements have been observed in images. This means that preparation method is efficient. Y^{3+} is dispersed uniformly which means that very less chance of presence of secondary phase ($YFeO_2$) in the samples. The mapping images also show the presence of La^{3+} for the samples $C_{0.2}$ and $C_{0.4}$ which properly supports the presence of La^{3+} in the samples. This means that preparation method is efficient.

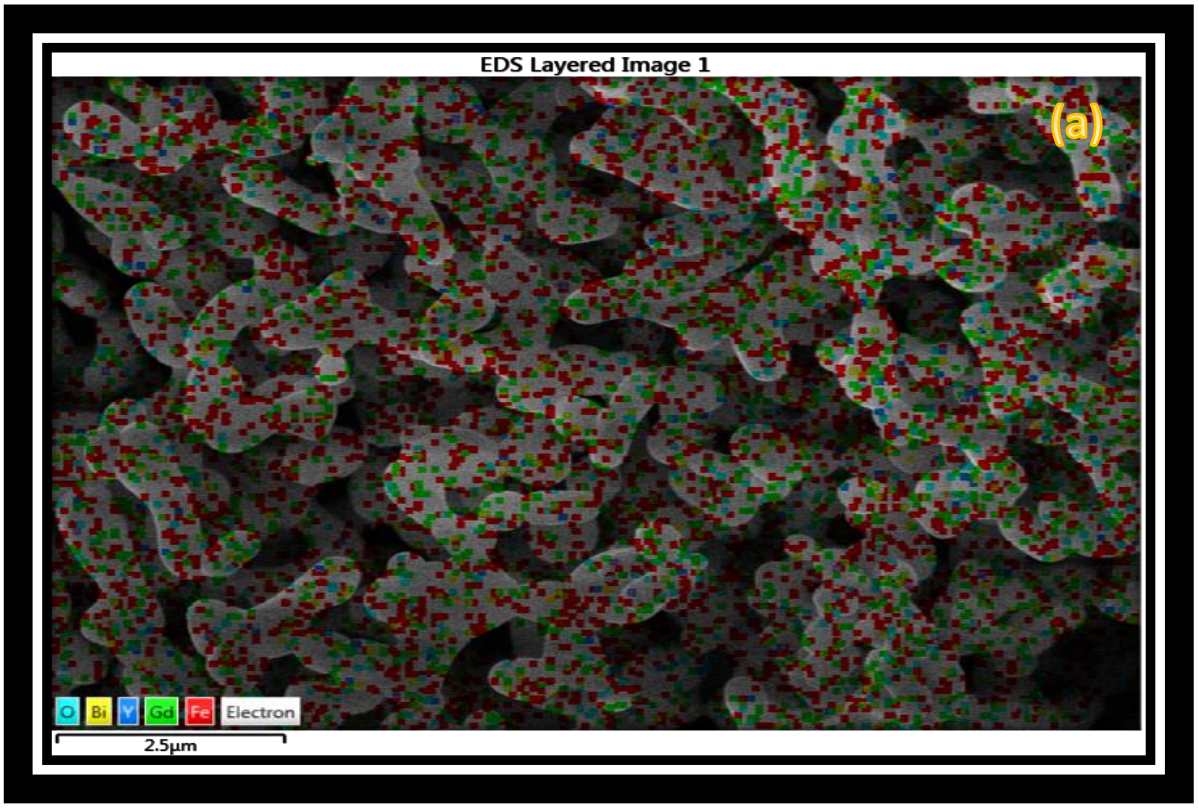

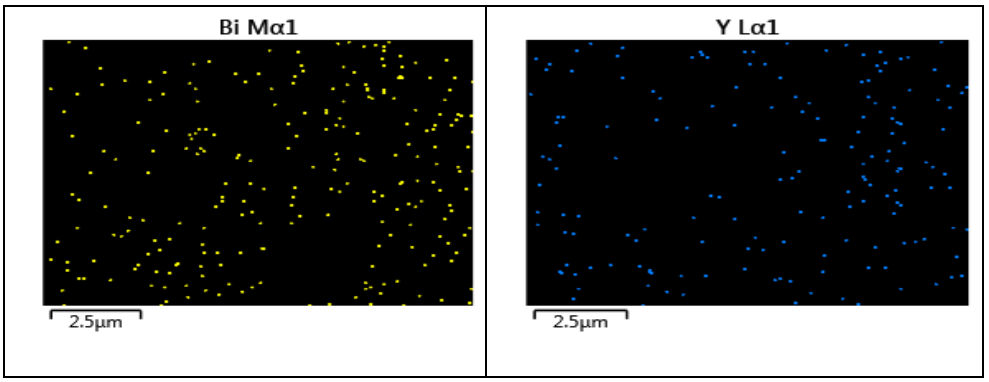

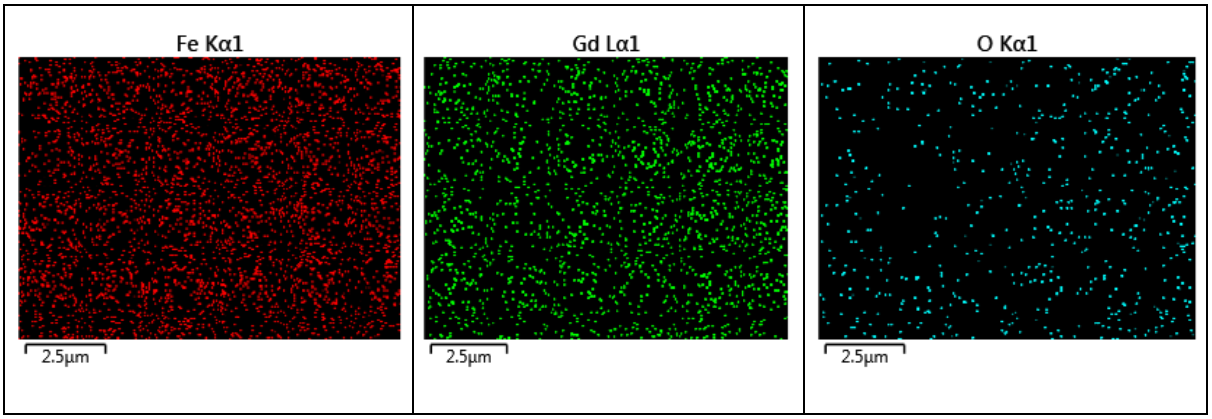
Fe Kα1
2.5µm
Gd Lα1
2.5µm
O Kα1
2.5µm

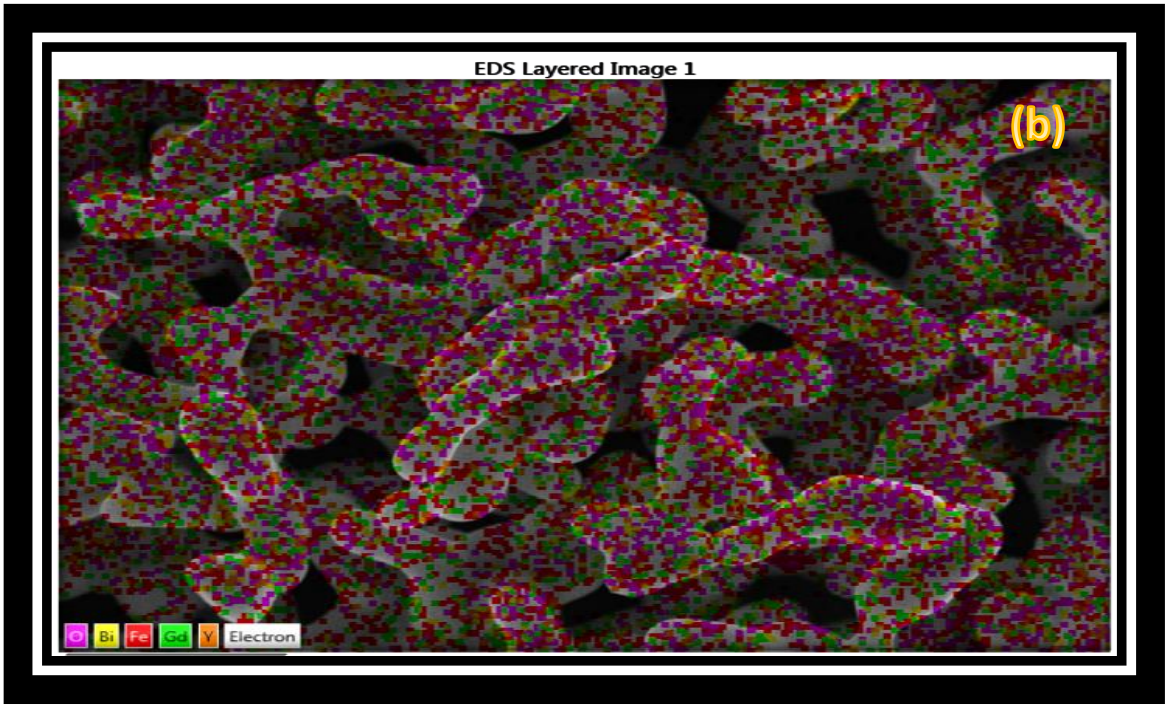
EDS Layered Image 1
(b)
O
Bi
Fe
Gd
Y
Electron

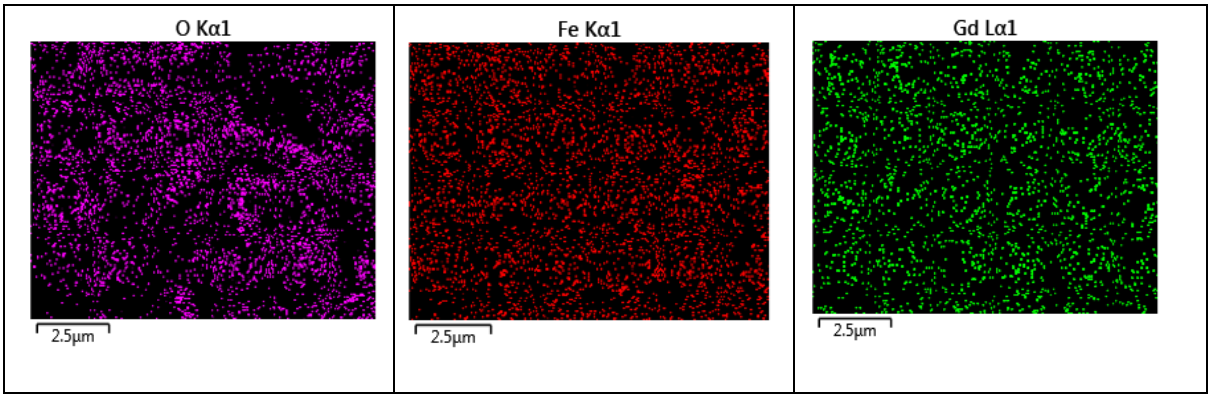
O Kα1
2.5µm
Fe Kα1
2.5µm
Gd Lα1
2.5µm

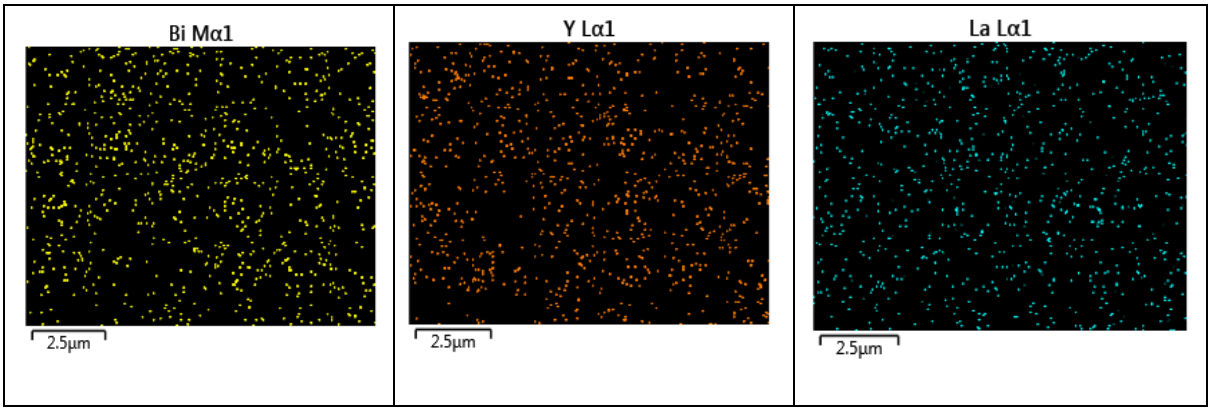
Bi Mα1
2.5µm
Y Lα1
2.5µm
La Lα1
2.5µm

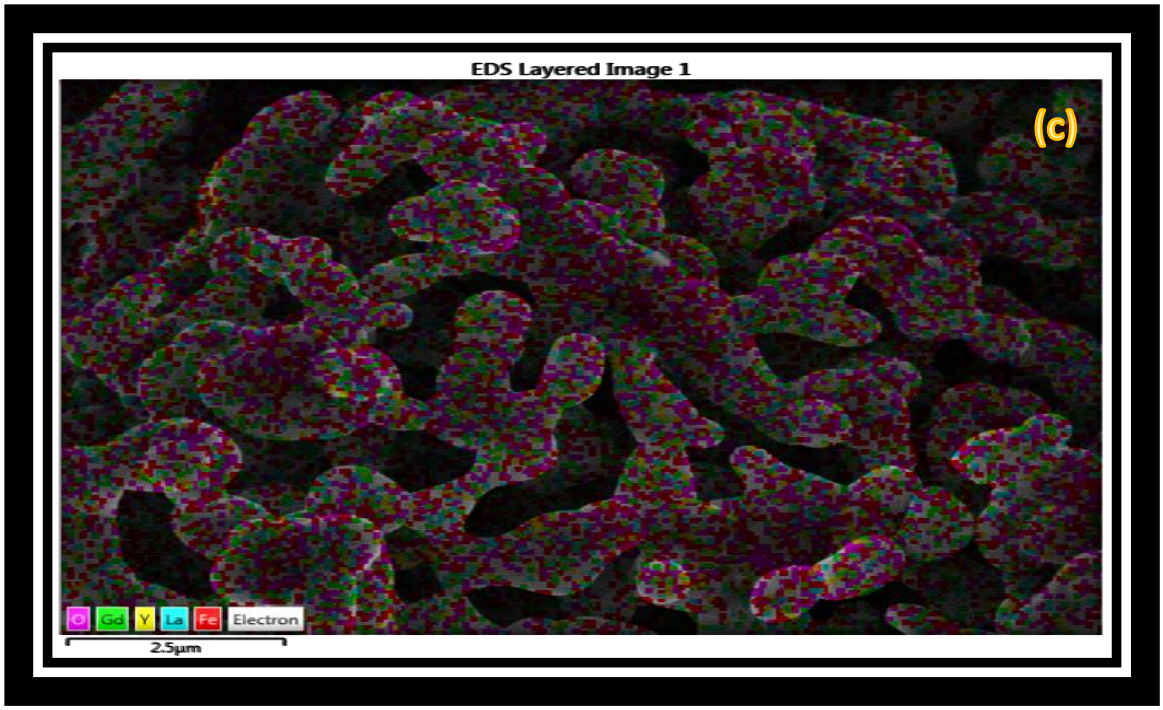
EDS Layered Image 1
(c)
O
Gd
Y
La
Fe
Electron
2.5µm

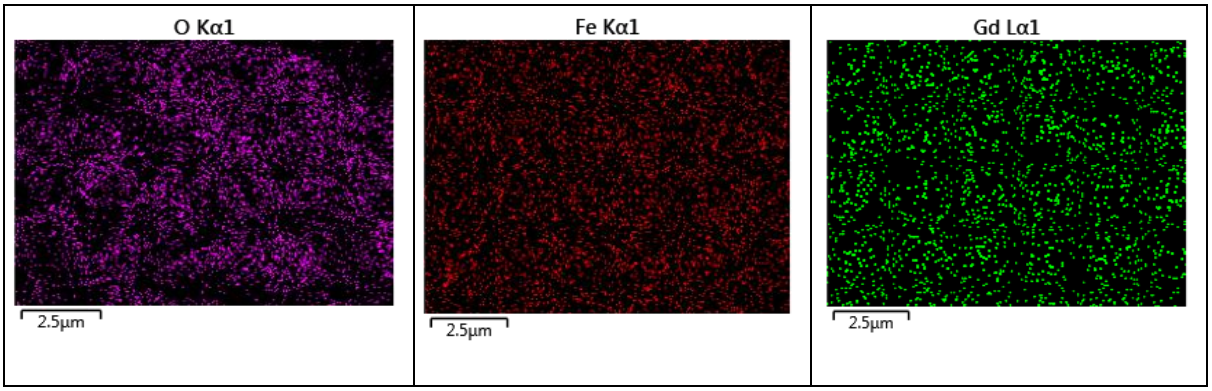
O Kα1
2.5µm
Fe Kα1
2.5µm
Gd Lα1
2.5µm

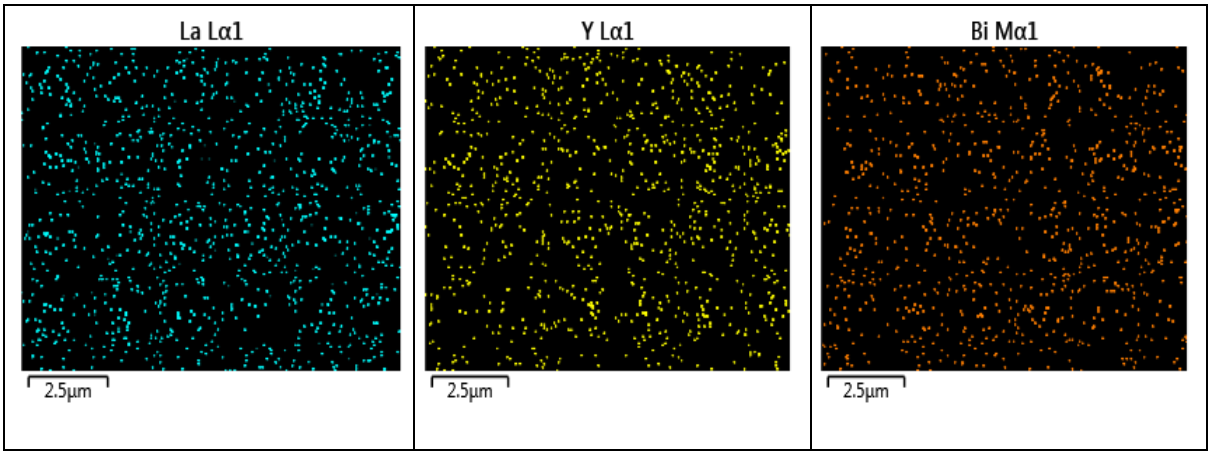

Figure 4.30 The images of elementary mapping of samples (a) x=0, (b) x=0.2 and (c) x=0.4

4.4.4 UV-vis

The optical property of the samples of $Y_{0.2}Bi_{0.2}La_xGd_{2.6-x}Fe_5O_{12}$ (x=0, 0.2 and 0.4) is observed by using UV-VIS spectroscopy. The absorbance versus wavelength plot is as shown in **Figure 4.31A** (a-c) from the range 200 to 800 nm. The different peaks have been observed in 200 to 350 nm range for all samples, which represent absorption. This is related to electronic transition between anion and cations present in $Y_{0.2}Bi_{0.2}La_xGd_{2.6-x}Fe_5O_{12}$ (x=0, 0.2, 0.4) samples. From 400 to 800 nm the samples show transmittance. It has also been observed from **Figure 4.31 B** (a-c) that there is shift in value of absorbance as the composition of $Y_{0.2}Bi_{0.2}La_xGd_{2.6-x}Fe_5O_{12}$ varies. From the obtained data the bandgap analysis has been done for all samples which is as shown in **Figure 4.32** (a-c). The band gap obtained after drawing tangent is in range 3.7 eV to 3.9 eV.

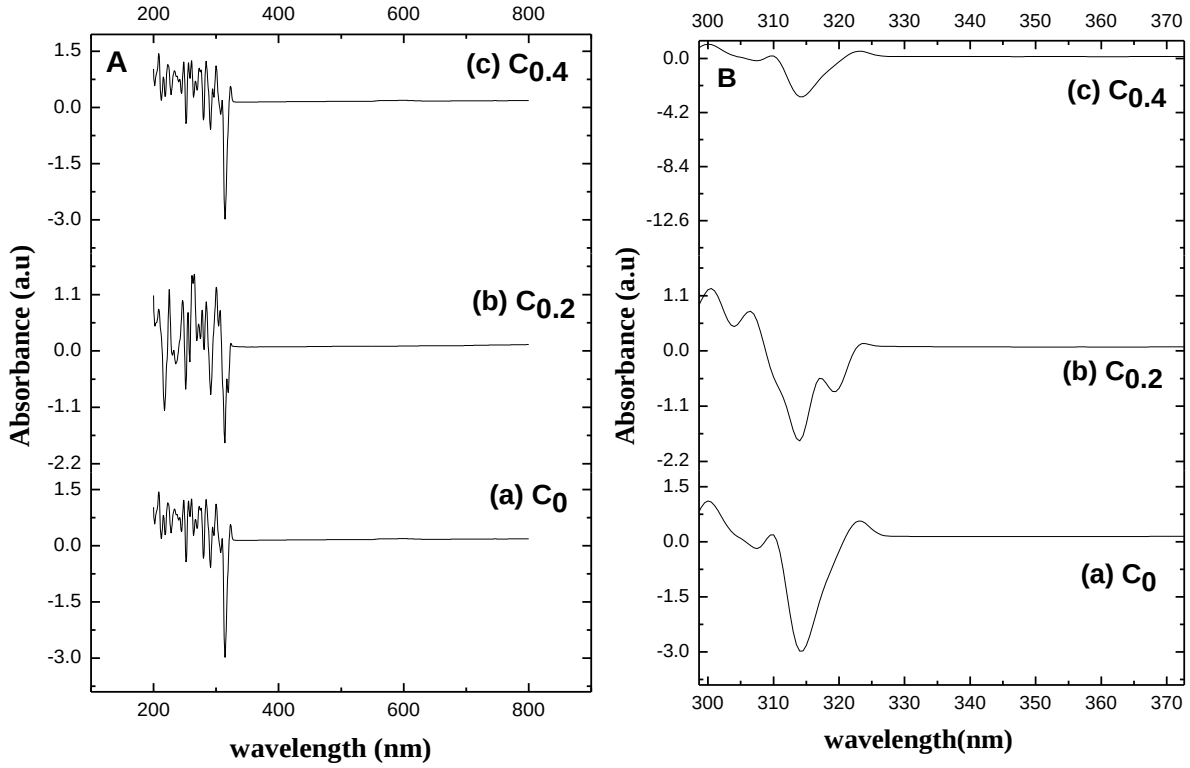

Figure 4.31 (A) represent the absorbance v/s wavelength graph and Figure 4.31 (B) represent shift in absorbance value in 300 to 370 nm wavelength for (a) C_0, (b) $C_{0.2}$ and $C_{0.4}$ sample

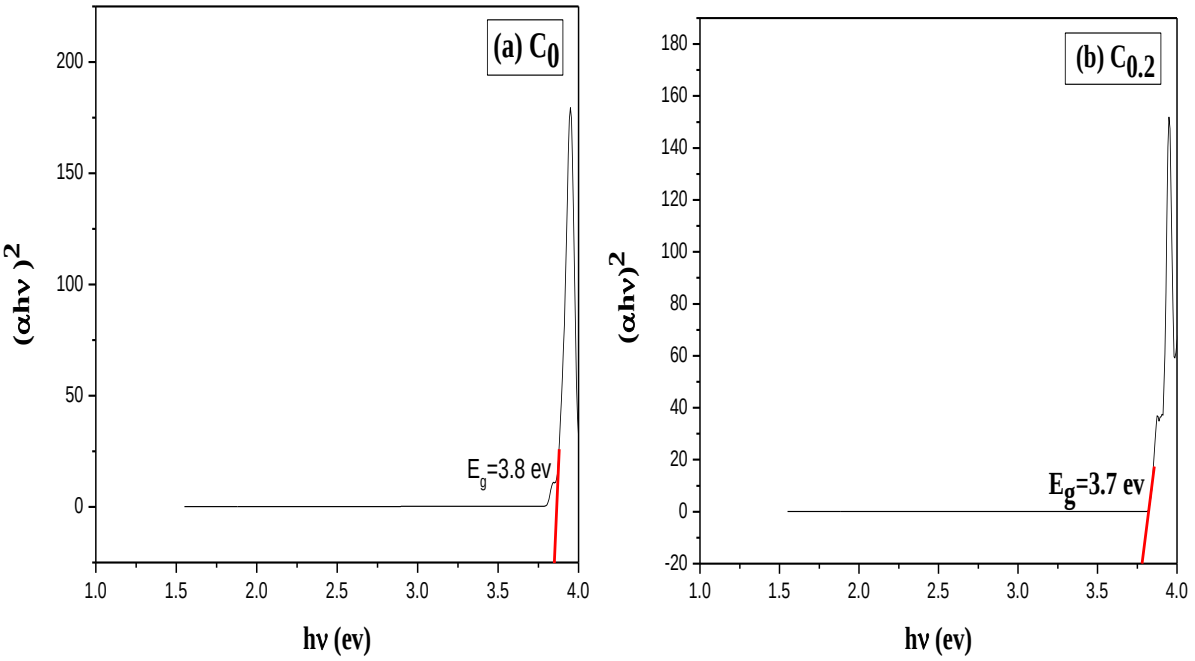

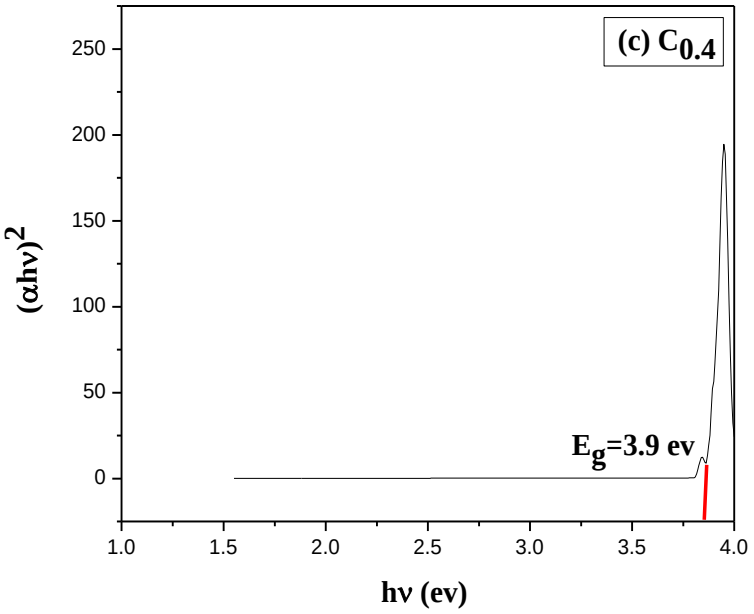

Figure 4.32 Calculated Optical band gap of (a) C_0, (b) $C_{0.2}$ and (c) $C_{0.4}$

4.4.5 Vibrating Sample Magnetometer

The Magnetization (M) versus applied field (H) curve measured at room temperature for $Y_{0.2}Bi_{0.2}La_xGd_{2.6-x}Fe_5O_{12}$ samples is as shown in **Figure 4.33**. Smooth S shaped curve has been obtained for all samples which signified about superparamagnetic nature of samples and strong exchange coupling between ions of garnets. The values of important magnetic parameters like coercivity (H_c), retentivity (M_r), magnetic saturation (M_s) and Squareness ratio (SQR) obtained from VSM data is tabulated in **Table 4.13**.

The value of Bohr Magneton (μB), anisotropy constant (K_{eff}), magneto-crystalline anisotropy (H_a) and microwave operating frequency (ω_m) is calculated using **Equation (4.50)**, **Equation (4.51)**, **Equation (4.52)** and **Equation (4.53)** respectively. And the values are tabulated in **Table 4.13**.

$$\mu B = \frac{M \times M_s}{5585} \tag{4.50}$$

$$K_{eff} = \frac{H_c \times M_s}{0.96} \tag{4.51}$$

$$H_a = \frac{2K_{eff}}{Ms} \tag{4.52}$$

$$\omega_m = 8\pi^2 \gamma M_s \quad (4.53)$$

Here "M" represents the molecular weight and γ is gyromagnetic ratio having value 2.8MHz/Oe.

The value of H_c decreases with increase in La^{3+} in samples. The value of H_c is lesser for sample $C_{0.4}$ suggesting its soft nature as comparison to other samples. The decrease in value of H_c can be understood as, with addition of La^{3+} in sample leads to change in grain size which is as mention in **Table 4.12**. obtained from FESEM. It has been observed that the value of grain size is least for sample having no La^{3+} i.e., for C_0, so for this coercivity is large. This effect can be explained as with decrease in grain size the shrinkage in magnetic domain wall occurs. This shrinkage further rises the magnetic hardness of the samples **[173]**. The value of coercivity for all prepared samples are less than 100 which suggest the soft magnetic nature of the samples. Also, it is clear that substitution is changing the value of H_c.

The value of M_s for pure GdIG noted by Akhtar et al., was 3.56 emu/g. It has been noticed that with substitution of both diamagnetic Y^{3+} and Bi^{3+} in dodecahedral site increases the value of M_s. But according to Neel theory, diamagnetic ions additions in materials cannot increase the magnetization **[174]**. Then the reason of increase in value of magnetic saturation for C_0 (x=0) is that, the ionic radii of Bi^{3+} is much larger than that of Gd^{3+}. This substitution of Bi^{3+} in the sample leads to distort the dodecahedral site. With distortion in lattice the super-exchange interaction energy changes as there is change in distance and angles between cations. This further increase the value of magnetic saturation. With addition of diamagnetic La^{3+} i.e., for sample $C_{0.2}$ (x=0.2) the value of M_s increases further for the same reason as La^{3+} ion has larger ionic radii as compare to Gd^{3+}. But by further increase in La^{3+} in $C_{0.4}$ sample (x=0.4) the value of magnetic saturation decreases. This decrease is because of secondary phases present in sample. The unwanted phase like Fe_2O_3 is more in sample $C_{0.4}$. This secondary phase (Fe_2O_3) has poor ferromagnetic property and further reduces the value of M_s **[175]**. In general, it can be concluded that the magnetic properties of material depend upon intrinsic and extrinsic properties like composition, grain size, pores, magnetic anisotropy field, domain wall motion, sintering temperature, presence of impurities and reversal in magnetic moments **[176]**.

The value of H_a is larger for C_0 (x = 0), this means it is very difficult to reverse the magnetization by providing low field. The value of H_a decreases by addition of La^{3+} in $Y_{0.2}Bi_{0.2}Gd_{2.6-x}Fe_5O_{12}$. This means that at very less field the magnetization can be reverse and therefore the value of Mr decreases. The value of squareness ratio is in the range 0.31 to 0.41 which is less than 0.5.

This reveals that the samples have multi-magnetic domain structure. Also, from the calculated value of operating microwave frequency it is clear that substituted samples with x=0 and 0.2 can work in 558 MHz to 1.1GHz range i.e., in ultra-high frequency range.

Table 4.13 Variation of magnetic parameters with substitution of La^{3+} in sample (a) C_0, (b) $C_{0.2}$ and $C_{0.4}$

Sample	H_c (Oe)	M_r(emu/g)	M_s(emu/g)	μB	K_{eff}(erg/cm^3)	H_a	SQR	ω_m
C_0	52.05	2.00	4.93	939.6	267.32	108.3	0.41	1.1 GHz
$C_{0.2}$	40.42	1.63	4.94	935.9	208.06	84.2	0.33	1.1 GHz
$C_{0.4}$	39.14	0.80	2.53	900.8	103.16	81.5	0.31	558 MHz

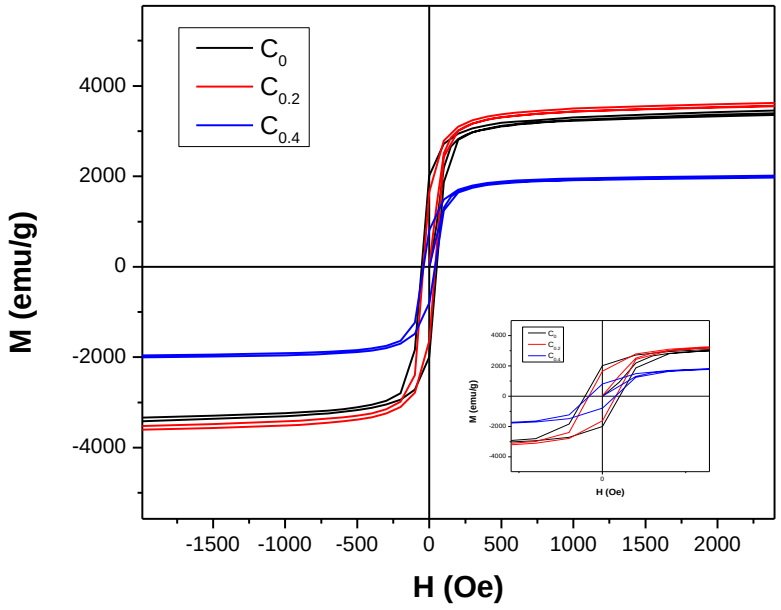

Figure 4.33 M-H loop for the samples C_0, $C_{0.2}$ and $C_{0.4}$

4.5 Yttrium iron garnet, erbium iron garnet and their composite (YIG/ErIG)

4.5.1 XRD

Structural analysis of yttrium iron garnet (YIG), erbium iron garnet (ErIG) and their composite has been carried out by x-ray diffraction. **Figure 4.34** represent the XRD diffractograms of YIG, ErIG and their composite. From Joint Committee on Powder Diffraction Standards **(**JCPDS) no. 430507 (for YIG) and 230240 (for ErIG) it has been concluded that prepared garnet ferrites are pure without any impurities. Also, both phases of garnets are present in the

YIG(1-x)-ErIG(x) composite. This implies that the method of preparation and sintering temperature are appropriate for garnet ferrites and for their composite. The values of 2 θ, Full width half maxima (β), miller indices (hkl), crystallite size (D), lattice parameter (a) and micro strain correspond to highly intense peak are tabulated in **Table 4.14**.

The crystallite size for sample YIG, ErIG and $YE_{0.5}$ is calculated using Scherrer's **Equation (4.54)**.

$$D = \frac{K\lambda}{\beta \cos\theta} \tag{4.54}$$

In above equation "K" represents Scherrer constant having value 0.9, "λ" is the wavelength of X-ray source with value 0.15406 nm, "β" is the FWHM and "θ" is the peak position.

As garnet ferrite has cubic structure so the lattice constants for the samples were calculated using **Equation (4.55)**.

$$\frac{1}{d^2} = \frac{h^2+k^2+l^2}{a^2} \tag{4.55}$$

In **Equation 4.55** "a" is lattice constant, "hkl" is the miller indices corresponded to highly intense peak, "d" symbolizes interplanar spacing calculated by using Bragg's law **Equation (4.56)**.

$$d_{spacing}(\text{Å}) = \frac{n\lambda}{2\sin\theta}\ , n = 1 \tag{4.56}$$

Micro strain is calculated using **Equation 4.57**.

$$\varepsilon = \frac{\beta}{4\tan\theta} \tag{4.57}$$

From Table 1 it can be concluded that there is no such variation of crystallite size of parent YIG, ErIG and $YE_{0.5}$ composite this might be due to the fact that crystallite size depends upon the values of "β" and "θ".

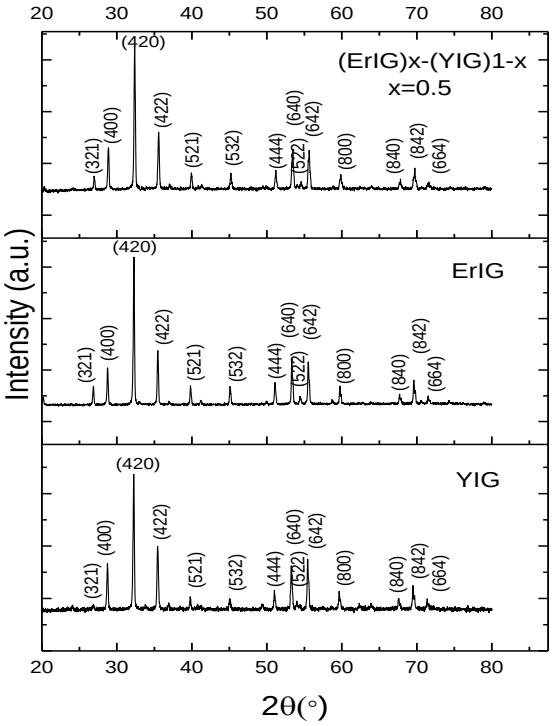

Figure 4.34 XRD pattern of YIG, ErIG and ErIG(x)-YIG(1-x)

Table 4.14 Calculated crystallite size (D), lattice parameter (a) and micro strain calculated for YIG, ErIG and YE0.5

Sample	Sample Code	2θ(°)	β	hkl	D(nm)	a	Micro Strain
$Y_3Fe_5O_{12}$	YIG	32.4	0.22	420	38.2	12.41	3.3
$Er_3Fe_5O_{12}$	ErIG	32.3	0.21	420	39.4	12.40	3.2
$Er_3Fe_5O_{12}$ (x)/ $Y_3Fe_5O_{12}$ (1-x)	YE0.5	32.4	0.22	420	38.2	12.41	3.3

4.5.2 FESEM

The morphology of the samples has been studied with the help of FESEM analysis. **Figure 4.35** (a-c) represents the micrographs of the samples. It has been observed from micrographs that all the three samples have spherical shaped grains. It can be seen from the micrographs of YIG and ErIG that there is presence of pores. But the composite of both garnets (YE0.5) shows agglomeration. This agglomeration is due to magnetic attraction in nanocomposite, made up of soft ferrite **[133]**.

The gausian distributed histograms representing size distribution of the samples are as shown in **Figure 4.36** (a-c). The histograms were obtained using ImageJ software. Around 150 grains' diameter were selected to estimate size distribution of the samples **[177, 178]**. After that by using Origin Pro software gussian fitting was done. From histogram of sample YIG it has been found that the maximum number of grains lie between 0.30 μm to 0.59 μm. For ErIG sample the maximum number of grains lie between 0.6 μm to 1.1 μm . For $YE_{0.5}$ sample the maximum number of grains lie between 0.3 μm to 0.51 μm. The grain size of the samples is calculated by using line intercept method, which is as given in **Equation 4.57** and value is given in **Table 4.15**. Where "L" is the length of line, "n" is number of intercepts of grain and "m" is magnification of micrographs.

$$grain\ size = \frac{1.5\,L}{mn} \tag{4.57}$$

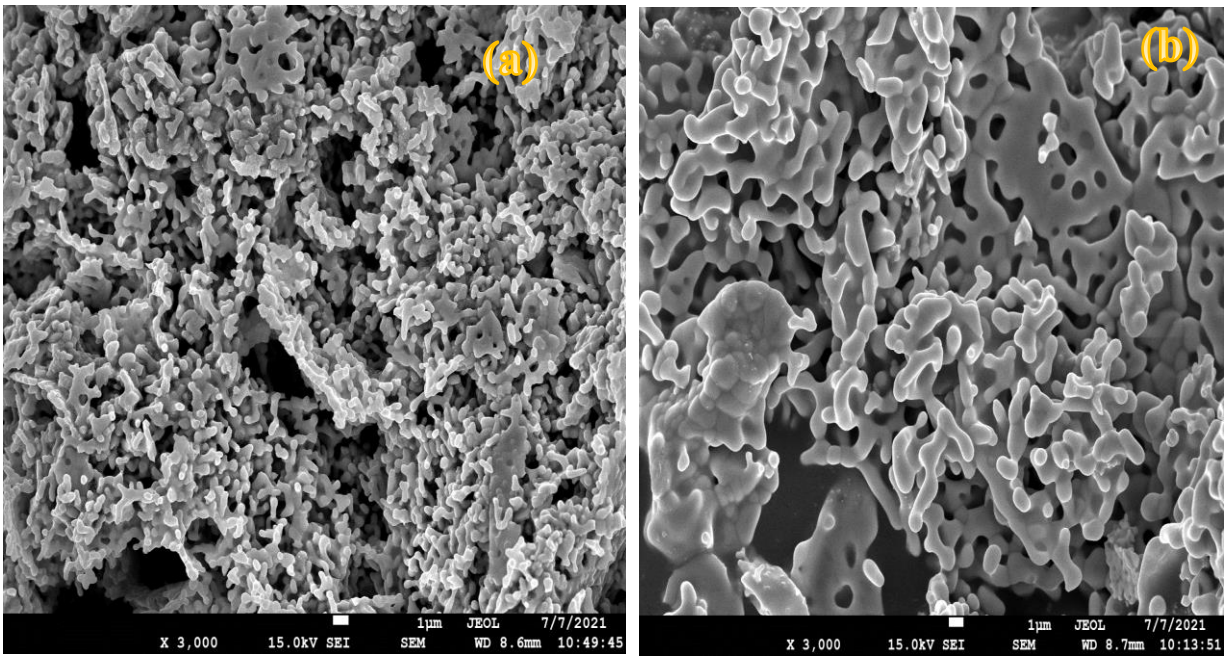

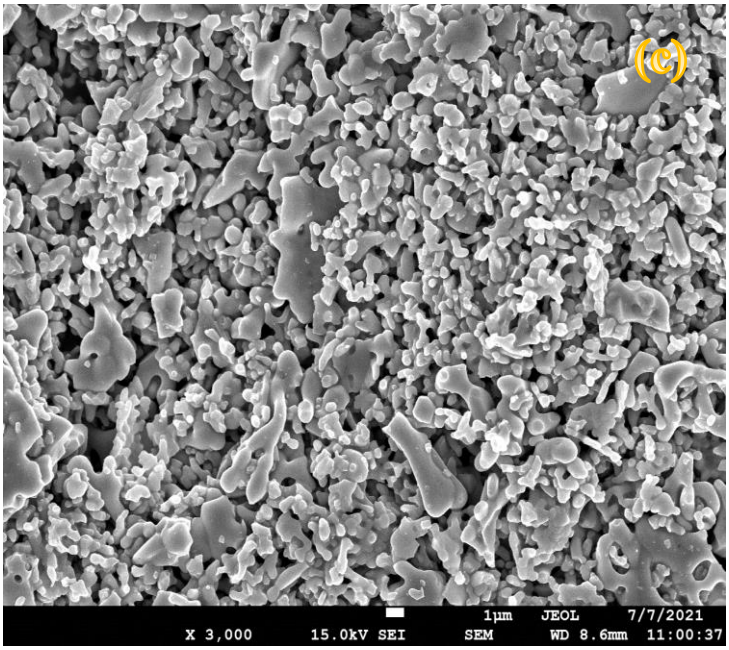

Figure 4.35 Micrograph of (a) YIG, (b) ErIG and (c) YE0.5 samples

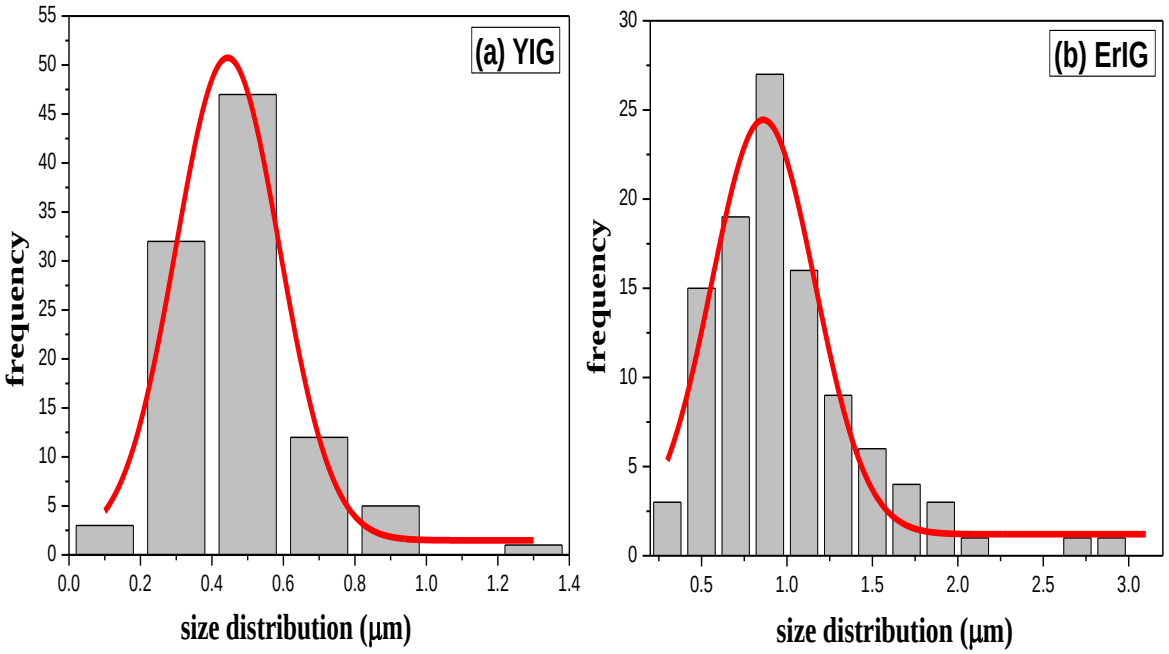

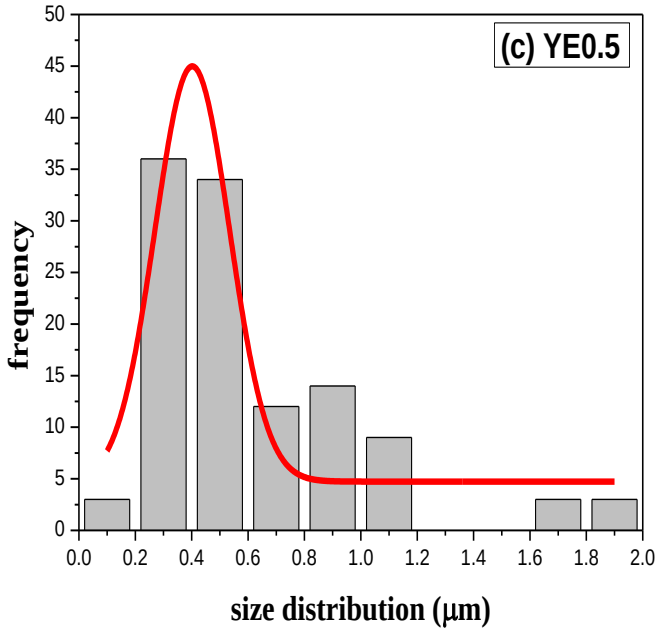

Figure 4.36 Size distribution histogram of (a) YIG, (b) ErIG and (c) YE0.5 samples

Table 4.15 Calculated grain size for YIG, ErIG and YE0.5 samples

Sample	Grain Size (μm)
YIG	0.30
ErIG	0.12
$YE_{0.5}$	1.0

4.5.3 Impedance Analyzer

The dielectric parameters of the samples were obtained by pressing samples into disc shaped pellets and applying conducting silver paste on both sides. **Figure 4.37** represents the equivalent circuit in which parallel-plate capacitor was used to analyse the dielectric parameters. This capacitor was filled with the pellets having dielectric constant ε', area A and diameter d.

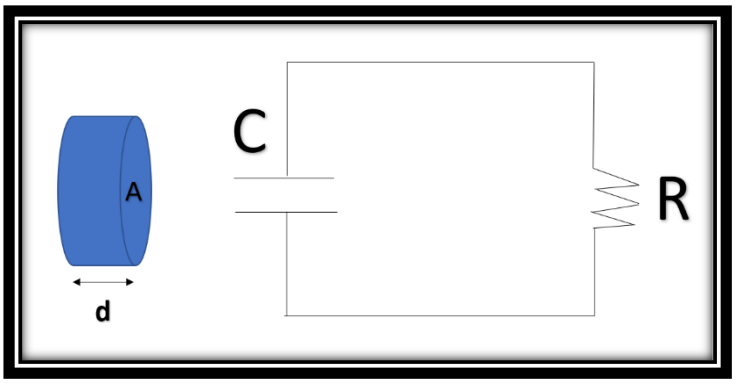

Figure 4.37 Parallel-plate capacitor used to analyse dielectric parameters

Dielectric Constant

Dielectric materials consist of complex permittivity. The complex permittivity (ε*) consist of real (ε') and imaginary part (ε") part. The real part signifies about the energy stored in dielectric material in presences of electric field. The imaginary part signifies about the loss in energy to AC field. **Figure 4.38** represent the variation of dielectric constant (ε') with frequency for all prepared samples. It has been observed that the value of dielectric constant decreases with increase in frequency and at higher frequency it become constant for all samples. This is obvious nature of ferrites and have studied many researchers **[179]**. This dielectric curve dispersion with frequency can be understand by using theory given by Koop's, which is based on the model of Maxwell-Wagner. This theory explains about in-homogeneous double layer structure of dielectric material. First layer is conducting (grains) and second layer is insulator (grain boundaries). According to theory grain boundaries are effective at lower frequencies and grain are effective in higher frequency. Although in superfine region, grain and grain boundaries are present in large amount as contrast to bulk region, due to which phenomena becomes complex. The value of dielectric constant is directly proportional to the value of grain boundaries. Due to which at higher frequency the values of dielectric constant do not vary.

It has been observed from **Figure 4.38** that YIG has lower values of dielectric constant as comparison to ErIG. The value of ε' for YIG was decreased from 14.2 at 100 Hz to 8 at 120 MHz. Whereas Musa et al., have reported that Al-YIG (x=0.2) sample gave the value of ε' in between 49.03 to 8.08 at 40 Hz to 1MHz **[102]**. Aakansha et al., have reported the value of ε' is 11.88 for YIG at 1MHz **[99]**. The value of ε' for ErIG was obtained in between 96 at 100 Hz to 13 at 120 MHz. The larger values of dielectric constant of YIG can explained on the basis of grain size. From FESEM analysis it has been observed that YIG has larger grain size as compare to ErIG. The sample with finer grain gives rise to higher dielectric constant because of larger

ratio of surface area to volume. The composite $Y_3Fe_5O_{12}$ (1-x)/ $Er_3Fe_5O_{12}$ (x) (x=0.5) gives moderate values of dielectric constant between 53 at 100Hz to 10 at 120MHz. Which implies that with incorporation of one soft ferrite into other soft ferrite influence the dielectric constant value. It can be concluded that the trend of curve of parent garnet ferrite produces the trend of their composites. The value of dielectric constant obtained by Shi et al., for Cu/YIG composite was near 50 at 1MHz, and 5 for YIG **[180]**. Factors like distribution of cations, structural homogeneity, synthesis methods, sintering temperature and size of the grain effects dielectric constant **[156]**.

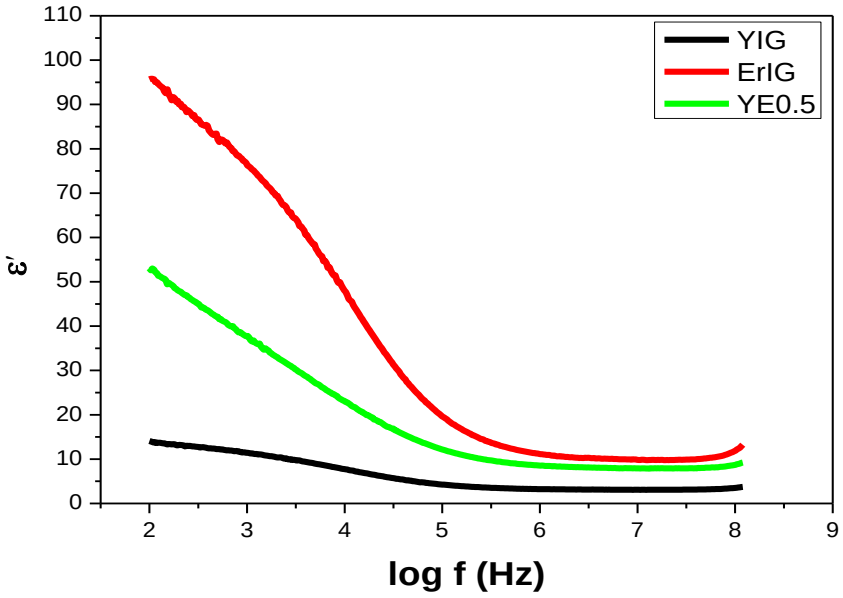

Figure 4.38 Variation of dielectric constant with frequency for YIG, ErIG and YE0.5 samples

Dielectric Loss

Figure 4.39 represent the dielectric loss (ε") in samples. It is clear from figure that ErIG is showing higher values of dielectric loss. It is observed that dielectric losses value firstly decreases up to 1KHz and then there is a rise in value near 1KHz to 10.5KHz for all sample. As the frequency increases the value of ε" start becoming almost constant or independent of frequency. Generally, the reason of dispersion can be clear by Iwauchi explanation. Which explains about the strong relation between dielectric nature of ferrites and conducting phenomena. The conducting phenomena in ferrites is due to hopping of electrons between ions of Fe^{2+} and Fe^{3+}. When hoping frequency becomes equal to external applied field then

maximum losses occurs in ferrites **[181]**. But in case of garnet ferrites there is no Fe^{2+} ions present. So, in our case the dielectric losses are due to internal friction which opposes the movement of all dipoles and hence losses are there in form of heat.

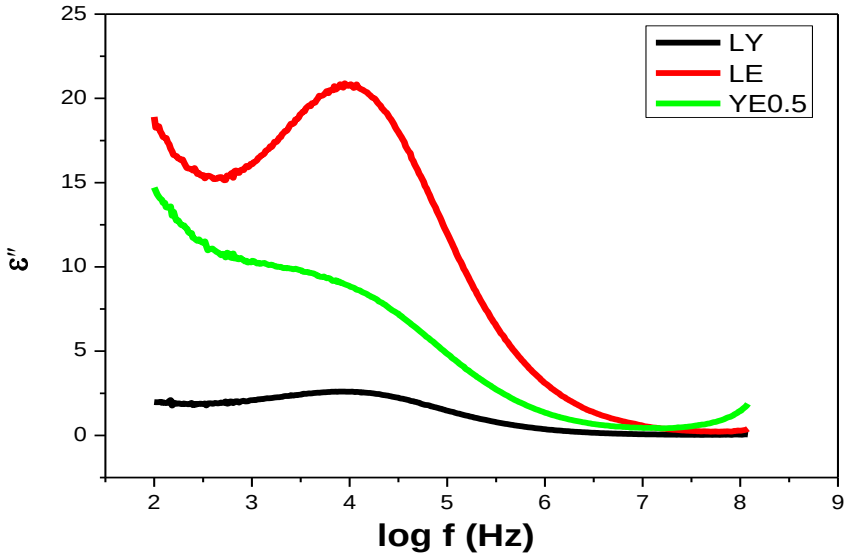

Figure 4.39 Variation of dielectric loss with frequency for YIG, ErIG and YE0.5 samples

Dielectric Tangent Loss

Dielectric tangent loss is the measure of loss of energy from externally applied field. This loss occurs due to domain wall resonance. The dielectric tangent loss in ferrites contributes largely in entire core loss and power loss. **Figure 4.40** represents the dielectric loss tangent in materials. When dielectric tangent loss is less than the core loss is also less **[182]**. **Figure 4.41** represent dielectric tangent loss for samples. The resonance peak has been observed for all samples with shifting in maxima beyond 10.5 KHz frequency. The reason of resonance frequency is that when natural frequency occurs the ions oscillate but as natural frequency approaches value of applied frequency, maximum power loss occurs and hence resonance in loss occurs. After that there is sharp fall in tangent loss at higher frequency. The values of losses for the LE0.5 composite are lesser than ErIG and are near to YIG at higher frequency. The value of tanδ~0.05 for YE0.5 composite at 1 MHz. Whereas YIG and ErIG has tanδ~0.02, 0.06 at 1MHz. The lower value of tangent loss is because of larger value of real part of dielectric constant ($\varepsilon^{'}$). It has been observed that ErIG has lower value of grain size but has high tangent losses as compared to YIG and YE0.5. This can be related with higher conductivity (explained in section 4.4.5) due to conduction of oxygen vacancies and this conduction is the reason of high tangent

losses **[183]**. Kotnala et al., have studied the dielectric properties of hexaferrite/spinel ferrite composite and found larger value of tanδ~ more than 20 at 100Hz and lower value of tanδ near 1 at 1MHz **[129]**. Paiva et al., have studied the dielectric properties of YIG/CTO composite and found that the value tanδ in between 0.2 to 0.1 **[184]**. Qureshi et al., have observed that for YIG/PMMA composite the value of tanδ lies in range 0.03 to 0.06 at 1MHz **[89]**. The lower value of dielectric loss tangent of YE0.5 implies that the material is suitable for microwave devices.

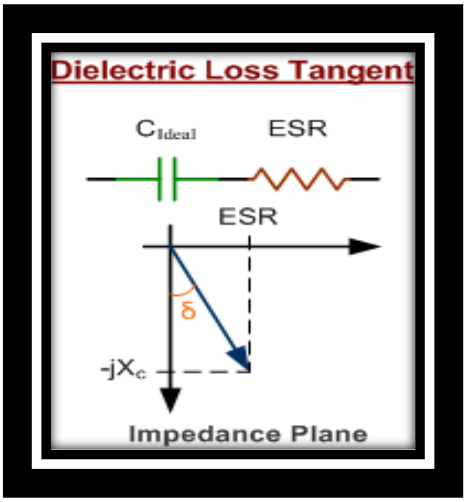

Figure 4.40 represents the dielectric loss tangent in materials

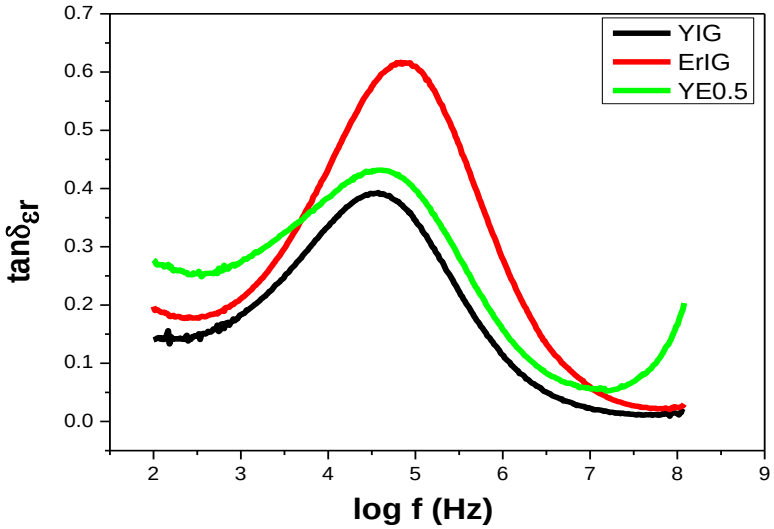

Figure 4.41 Variation of dielectric tangent loss with frequency for YIG, ErIG and YE0.5 samples

Electric Modulus

Complex electric modulus is described as inverse of complex permittivity. Electric modulus (M) is related to real part (M') which is resistive and imaginary part (M") which is reactive constituent of electric modulus and is given in **Equations (4.58)**, **(4.59)** and **(4.60) [185].**

$$M = M' - jM" \tag{4.58}$$

$$M' = \frac{\epsilon'}{(\epsilon')^2 + (\epsilon")^2} \tag{4.59}$$

$$M" = \frac{\epsilon"}{(\epsilon')^2 + (\epsilon")^2} \tag{4.60}$$

Figure 4.42 (a-b) represent real and imaginary part of complex electric modulus for all samples. It has been observed that YIG has higher value of real and imaginary part and ErIG has least values. Whereas YE0.5 composite have moderate values of real part and imaginary part. But YE0.5 gives least values of M" between100KHz to 1.5MHz. It has been noticed that at lower frequency range the value of real part (resistive) is low and with rise in frequency the values of M' also increases. And beyond 10 MHz there is a fall in value of M'. The electric modulus variation depends upon change in applied field and mobility of charge carriers.

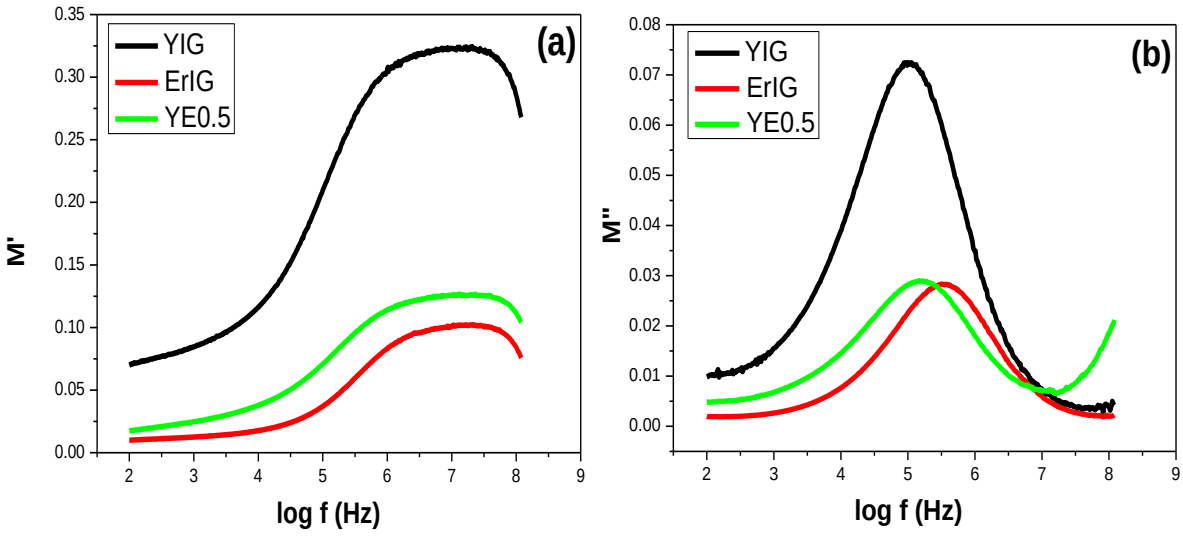

Figure 4.42 (a-b) represent real and imaginary part of complex electric modulus for YIG, ErIG and YE0.5

AC Conductivity

Inside a material the ability of conduction is specify by a conductivity of a material. Generally electrical conductivity inside ferrite materials is due to hopping of electron from ion to ion of same element present in different valence state (e.g., Fe^{2+}/Fe^{3+}). From **Figure 4.43** it has been clear that with increase in frequency AC conductivity also increases. But overall, all the three sample possesses very low conductivity. This low conductivity in garnet ferrites means high resistivity as in garnet ferrites there is no Fe^{2+} ion so hopping is not possible. It has been noticed that ErIG give larger value of conductivity as comparison to YIG and their composite give moderate values up to 1 MHz. The larger value of conductivity for ErIG is because it possesses larger permittivity ($\varepsilon^{'}$) values. The variation of AC conductivity can also be explained by **Equation (4.61) [185]**.

$$\sigma_{ac}(\omega, T, r) = \omega \varepsilon_0 \varepsilon'(\omega, T, r)\, tan\delta(\omega, T, r) \tag{4.61}$$

Where ω is angular frequency of applied field, ε_0 is absolute permittivity, ε' is dielectric constant or relative permittivity, T is temperature, r is compositional ratio and $tan\delta$ is tangent loss. From the above equation it is clear that "σ_{ac}" is dependent on the value of ε'. Which means higher the value of ε' higher will be the conductivity. In case of composite the factor "r" will also play an important role. For YE0.5 both composition ratio "r" and dielectric constant ε' contributes to the value of AC conductivity. This can be a reason of higher value of σ_{ac} for YE0.5 as compare to parent garnets at higher frequency.

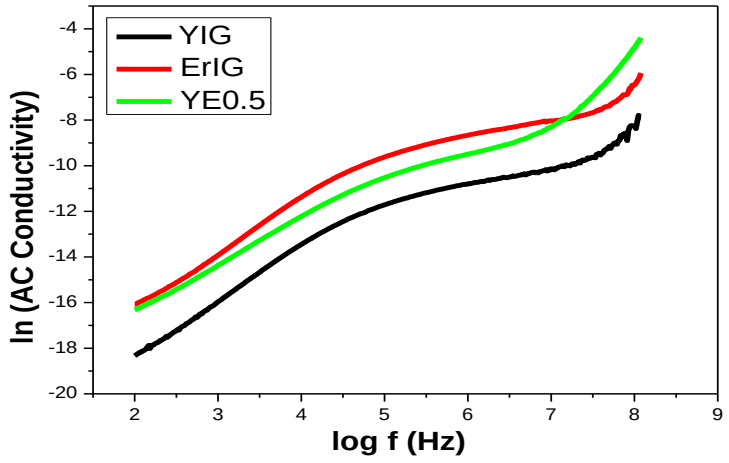

Figure 1.43 Variation of ln (AC conductivity) with log f for YIG, ErIG and YE0.5 samples

4.5.4 VSM

The smooth S shaped magnetization versus applied field loop (M-H) for samples is as shown in **Figure 4.44**. Such shape of curves implies the superparamagnetic nature of the samples. Important magnetic parameters such as magnetic remanence 'Mr', coercivity 'Hc', magnetic saturation 'Ms' and squareness ratio (SQR) are calculated from M-H loop and tabulated in **Table 4.16**. The value of anisotropy constant (K_{eff}), magneto crystalline anisotropy (H_a), microwave operation frequency (ω_m) was calculated using **Equation (4.62)**, **(4.63)** and **(4.64)** and tabulated in **Table 4.16**.

$$K_{eff} = \frac{H_c \times M_s}{0.96} \tag{4.62}$$

$$H_a = \frac{2K_{eff}}{Ms} \tag{4.63}$$

$$\omega_m = 8\pi^2 \gamma M_s \tag{4.64}$$

It has been observed that YE0.5 composite give least value of coercivity (161.8 Oe) as compare to individual garnet ferrites. Which depict more soft nature of composite as compare to YIG and ErIG. Jung et al., have reported the value of H_c equals to 26 for the composite of Ce: YAG-YIG (in ratio 0.5:0.5) **[186]**. The reason for this is larger grain size of YE0.5 (1μm). As the size of grain increases, the single domain structure changes to multi-domain structure. Therefore, domain wall effect dominates. This domain wall effect requires very less field to magnetize and as a result coercivity decreases. The value of magnetic saturation is large for YE0.5 composite (20.35 emu/g) as compare to YIG and ErIG. The reason for larger value of M_s is larger grain size **[186]** of composite. YIG and ErIG has lower grain size and due to this surface effect dominate. The surface layer is un-reactive and has less magnetization. Paiva et al., have found that the value M_s is 13.2 emu/g for $YIG_{0.75}/CTO_{0.25}$ composite **[184]**. The value of squareness ratio for samples is less than 0.5 suggest about the multi-domain structure. The calculated value of microwave operating frequency is large for YE0.5 composite is 4.5 GHz whereas for YIG and ErIG is 3.6 and 3 GHz respectively. This suggest that composite of YIG and ErIG i.e., (YE0.5) provides better magnetic properties.

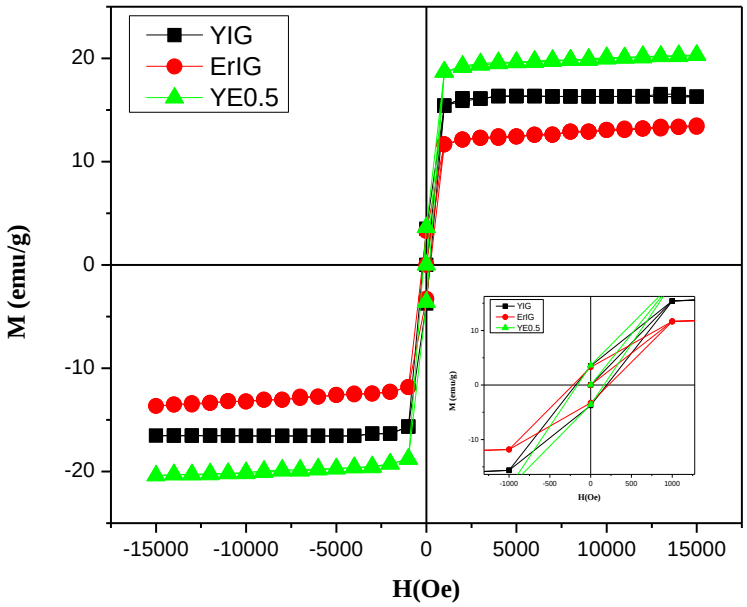

Figure 4.44 Magnetization versus applied field graph for YIG, ErIG and YE0.5 samples

Table 4.16 Calculated value of Hc, Mr, Ms, K_{eff}, H_a, SQR and ω_m for samples

Sample	H_c (Oe)	M_r(emu/g)	M_s(emu/g)	K_{eff}(erg/cm^3)	H_a	SQR	ω_m
YIG	189.4	3.62	16.55	3266	394.67	0.219	3.6 GHz
ErIG	218	3.27	13.6	3086	454.24	0.241	3.0 GHz
$YE_{0.5}$	161.8	3.61	20.35	3430.2	337.12	0.178	4.5 GHz

4.6 Yttrium iron garnet, Cd^{3+}- Co^{3+} substituted magnesium ferrite and their composite YIG/MgCdCoFe

4.6.1 XRD

The XRD pattern of the prepared samples i.e., YIG, $Mg_{0.4}Cd_{0.4}Co_{0.2}Fe_2O_4$ (MgCdCoFe) and YIG (*x*)/ MgCdCoFe (1-*x*) composites are shown in **Figure 4.45**. The obtained patterns were compared and matched with the JCPDS card no. 430507 for YIG and 221086 for MgCdCoFe respectively. Diffraction peaks in **Figure 4.45** (a) and (b) reveal the pure phase formation of cubic garnet ferrite with space group Ia3D and cubic spinel ferrite with space group Fd-227

respectively. **Figure 4.45** (c-e) represents the XRD patterns of composites. The diffraction peaks of YIG and MgCdCoFe are present in all composites. This implies that YIG and $Mg_{0.4}Cd_{0.4}Co_{0.2}Fe_2O_4$ exist independently without reacting with each other. However, for the *x* =0.3 composites, the highly intense peak of YIG at (420) becomes less intense implying that the spinel ferrite phase is dominating over the garnet ferrite phase in the composite. This disparity in intensity is obvious because the spinel ferrite phase is dominant for x = 0.3 composite, whereas for *x* = 0.6 and x = 0.9 composites the YIG phase dominates over MgCdCoFe phase. The number of corresponding phases of parent ferrites in the composite material determines the intensity and number of diffraction peaks **[188]**.

The extracted values of structural parameters like lattice constant '*a*', micro-strain '*ε*' and crystallite size '*D*' from the diffraction patterns are tabulated in **Table 4.17. Figure 4.46** represent the shift in *2θ* value of the highly intense diffraction peak with Miller indices (hkl) value (420) of YIG in YIG/MgCdCoFe (from x = 0.3 to x = 0.9) composites. From **Figure 4.46** and **Table 4.17**, it can be concluded that by incorporating spinel ferrite (MgCdCoFe) in garnet ferrite (YIG) the diffraction peak shift is towards the higher *2θ* values. This shift in angle further affects the value of lattice constant '*a*', which was calculated by using **Equation (4.65)** and is given in **Table 4.17**.

$$a = d(h^2 + k^2 + l^2)^{1/2} \tag{4.65}$$

Here 'd' is the interplanar spacing which is calculated with the help of Bragg's law **Equation (4.66)**:

$$d_{spacing}(\text{Å}) = \frac{n\lambda}{2\sin\theta} \tag{4.66}$$

He re the order of diffraction *n* is equal to 1 and hkl is the Miller indices. For YIG and MgCdCoFe, miller indices are corresponded to the highest intensity peaks and for composites, it corresponds to YIG peak).

From the above equation, we can write:

$$a = \frac{n\lambda}{2\sin\theta}(\mathrm{h}^2 + \mathrm{k}^2 + \mathrm{l}^2)^{1/2} \tag{4.67}$$

Equation (4.67) depicts that the lattice constant '*a*' is dependent on the angle (*θ*). The decrease in the value of '*a*' for YIG(*x*)/MgCdCoFe(1-*x*) (*x*=0.3, *x*=0.6 and *x*=0.9) composites is due to shift of angle towards higher side. Also, the fluctuation of the lattice constant of composite from

ideal YIG is due to variation in solubility between garnet and spinel ferrite **[189]**. The crystallite size '*D*' of the composites is calculated using Scherrer's formula (**Equation (4.68)**) **[190]**.

$$D = \frac{K\lambda}{\beta \cos\theta} \tag{4.68}$$

Where K, λ, β are the Scherrer's constant (=0.9), the wavelength X-ray source (=0.15406 nm) and full-width half maxima (FWHM, units are radians) respectively. Here the value of 'θ' for the composites is taken to correspond to the value of 'θ' for YIG. From **Table 4.17**, it is also clear that the composites have a larger value of '*D*' as compared to the parent ferrites. This is because of the nano dimensional particle sizes of the prepared composites **[191]**. With the addition of spinel ferrite in composite, the value of '*D*' increases for x = 0.3 to x =0.9 composites from 42.1 to 51.1 nm. The value of 'D' is less for x = 0.3 composites, which have a higher content of MgCdCoFe (70%) as compared to YIG (30%). The lesser value of '*D*' for x = 0.3 composite may be because the spinel ferrite is enhancing the crystal growth to a further extent. After that, it is restricting the crystal growth of YIG in the composite due to the presence of stress or strain. As the MgCdCoFe content start decreasing in x = 0.6 to x = 0.9 composites, the crystal growth is enhanced and the crystallite size increases. The micro-strain of the composites has been calculated by using **Equation (4.69)** and is summarized in Table 1.

$$\varepsilon = \frac{\beta}{4\tan\theta} \tag{4.69}$$

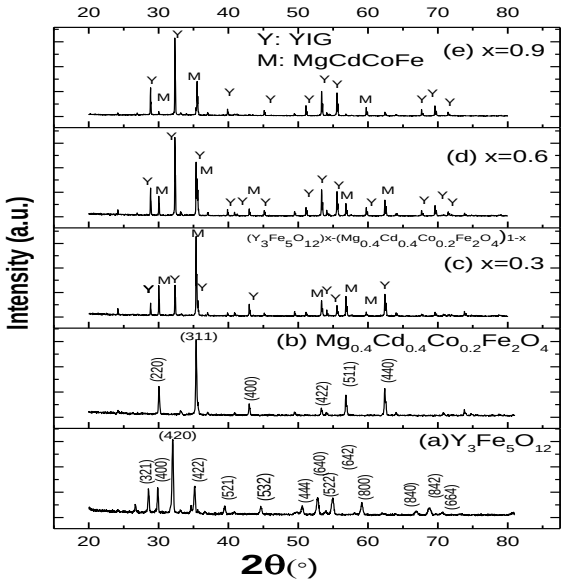

Figure 4.45 XRD pattern of the samples.

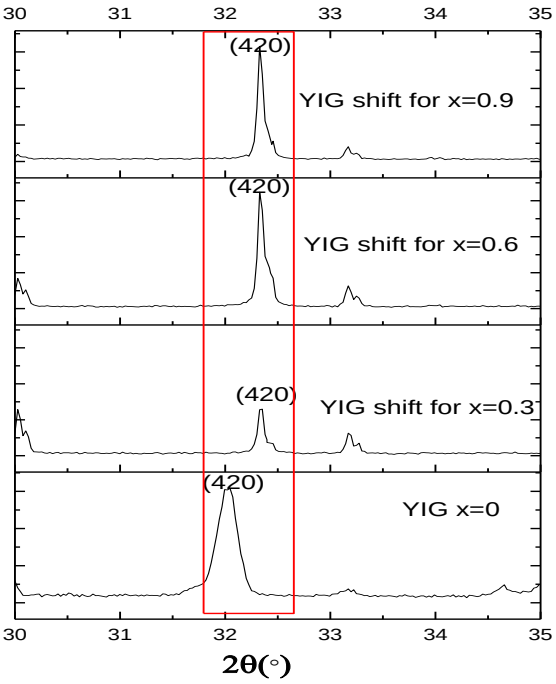

Figure 4.46 The shift in 2θ value with variation in composition

Table 4.17 Calculated values of 2θ, β, hkl, the crystallite size(D), lattice parameter(a) and micro stain (ε)

Sample	Sample Code	*2θ(°)*	*β*	*hkl*	*D(nm)*	*a*	*ε*
YIG	Y	32.01	0.25	420	32.1	12.49	-
$Mg_{0.4}Cd_{0.4}Co_{0.2}Fe_2O_4$	M	35.39	0.22	311	36.9	8.40	-
(YIG)x-($Mg_{0.4}Cd_{0.4}Co_{0.2}Fe_2O_4$)1-*x*(*x*=0.3)	YM0.3	32.46	0.17	420	42.1	12.32	2.8
(YIG)x-($Mg_{0.4}Cd_{0.4}Co_{0.2}Fe_2O_4$)1-*x* (*x*=0.6)	YM0.6	32.36	0.16	420	50.5	12.36	2.4
(YIG)x-($Mg_{0.4}Cd_{0.4}Co_{0.2}Fe_2O_4$)1-*x* (*x*=0.9)	YM0.9	32.35	0.16	420	51.4	12.36	2.3

Density and Porosity Study

The value of X-ray density *(D_x)*, bulk density *(D_b)*, Porosity *(P)* and relative density *(D_r)* was calculated using **Equations (4.70)**, **(4.71)**, **(4.72)** and **(4.73)** respectively **[114]** and tabulated in **Table 4.18**.

$$D_x = \frac{MZ}{N_A\, a^3} \tag{4.70}$$

Where *'M'* is the molecular weight of the sample, '*Z*' is the number of molecules per unit cell (for spinel and garnet ferrite Z is 8), *'N_A'* is Avogadro number (6.023×10^{-23}) and *'a'* is lattice constant.

$$D_b = \frac{M}{\pi r^2 d} \tag{4.71}$$

Where *'M'* is the mass of the pellet, *'r'* is the radius and *'d'* is the thickness of the pellet.

$$P = \left(\frac{D_x - D_b}{D_x}\right) \times 100 \tag{4.72}$$

$$D_r = \left(\frac{D_b}{D_x}\right) \times 100\% \tag{4.73}$$

From **Table 4.18**, it is clear that all the prepared composites have good bulk and relative density. This indicates that the sintering temperature is sufficient for the preparation of YIG and MgCdCoFe. The YM0.3 composite has the least porosity and high relative density. This implies that the presence of 70% of MgCdCoFe enhances the densification of YIG in the composite. The better densification in the composite is due to good packing.

Table 4.18 Calculated x-ray density (D_x), bulk density (D_b), porosity (P) and relative density (Dr) for samples

Sample	Sample Code	D_x	D_b (g/cm^3)	P%	D_r (%)
YIG	Y	5.03	4.82	4.05	96.0
$Mg_{0.4}Cd_{0.4}Co_{0.2}Fe_2O_4$	M	5.41	4.83	10.7	89.2
(YIG)x-($Mg_{0.4}Cd_{0.4}Co_{0.2}Fe_2O_4$)1-*x*(*x*=0.3)	YM0.3	5.53	5.31	3.95	96.0
(YIG)x-($Mg_{0.4}Cd_{0.4}Co_{0.2}Fe_2O_4$)1-*x* (*x*=0.6)	YM0.6	7.58	6.42	15.2	84.8
(YIG)x-($Mg_{0.4}Cd_{0.4}Co_{0.2}Fe_2O_4$)1-*x* (*x*=0.9)	YM0.9	9.67	8.25	14.7	85.3

4.6.2 FESEM

The morphological study is an important parameter to understand the shape and size of grains. The grain size and morphology of the samples further affect the magnetic, dielectric and many other physical properties. The morphological study was carried out with the help of FESEM micrographs. **Figures 4.47** (a-e) represents the FESEM micrograph of the prepared samples. **Figures 4.47** (a) and (b) represent the micrograph of YIG and MgCdCoFe samples respectively. It has been found that YIG has roughly spherical shaped grains. Whereas MgCdCoFe has cubic shaped grains. **Figure 4.47** (c-e) represents the micrographs of the YM0.3, YM0.6 and YM0.9

composites. It can be seen that two different morphologies of grains (spherical and cubic) are present in all the composites. The composite with x = 0.3 has very less porosity as compared to other composites due to the stronger packing of garnet and spinel ferrites. The spherical shaped YIG grains have some voids or spaces, which are further occupied by the grains of MgCdCoFe. For a higher packing mechanism, two conditions, (a) near about 30% fine and 70% coarse grains and (b) two different grain sizes should be there in the samples. In the synthesized samples the pores can be seen from micrographs. The calculated porosity matches FESEM images. The grain size was calculated by putting 10 intercept lines on the micrographs with the help of ImageJ software. The line intercept method was followed to get the values of grain sizes which is mentioned in **Equation (4.74)** and tabulated in **Table 4.19**. Where 'L' is the length of line, 'm' is magnetization and 'n' is number of intersects. The grain size of the materials lies between 0.57µm to 0.8 µm. The YM0.9 composite has a larger grain size, whereas YM0.3 has the least grain size. The composites have a difference in grain sizes due to the grain boundaries migration between two phases having restricted solubility **[136]**. So generally one ferrite influence the growth of the other, which further restricts the grain boundaries motions.

$$grain\ size = \frac{1.5\ L}{mn} \tag{4.74}$$

Table 4.19 Calculated grain size from the micrographs of the samples

Sample	Grain Size (µm)
Y	0.80±0.03
M	0.70±0.01
YM0.3	0.74±0.01
YM0.6	0.88±0.01
YM0.9	0.97 ±0.01

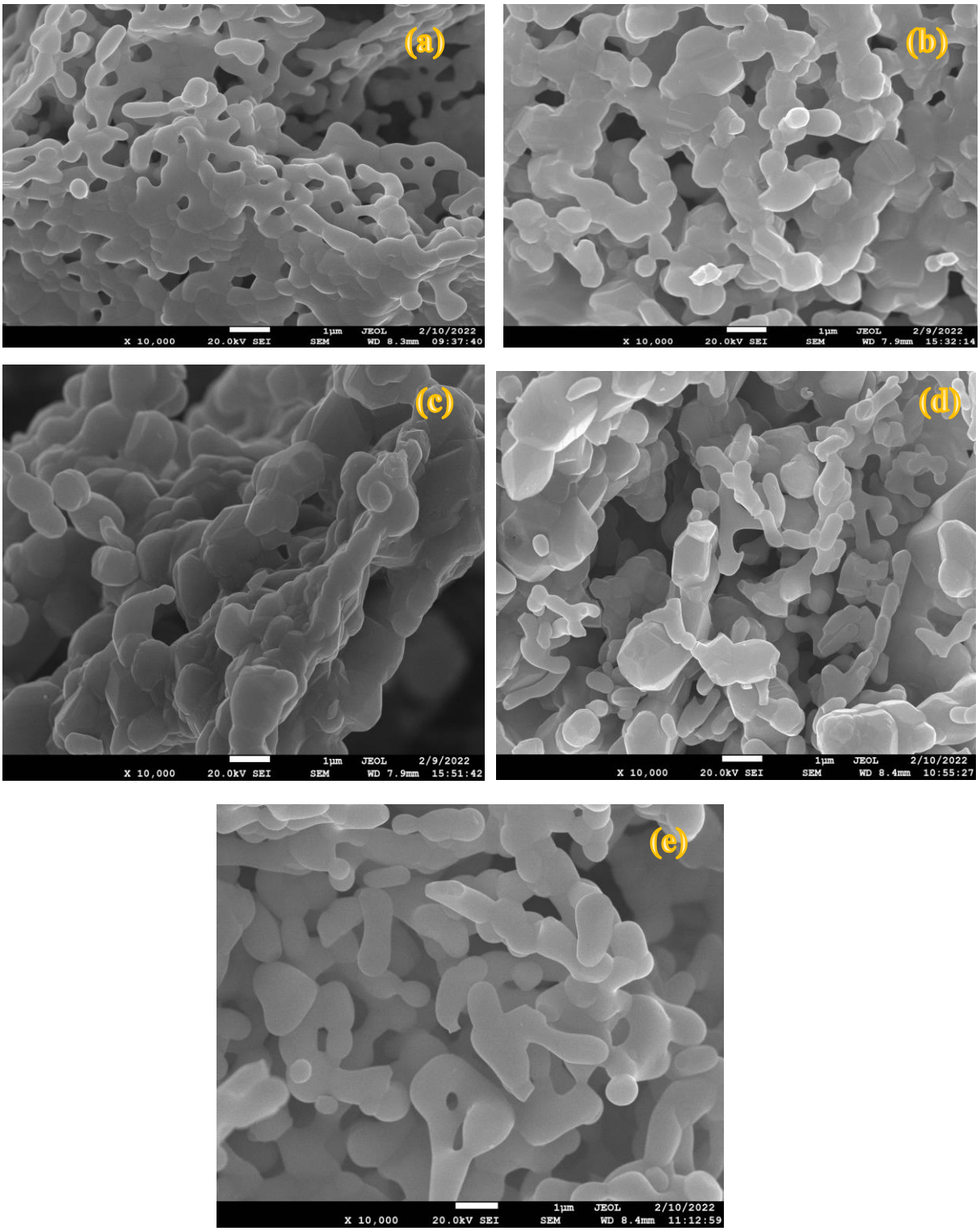

Figure 4.47 FESEM micrographs of (a) Y, (b) M, (c) YM0.3, (d) YM0.6 and (e) YM0.9 samples

4.6.3 EDX

To confirm the presence of all elements in the prepared nanocomposites, EDX has been carried out. The spectra of the two composites YM0.3 and YM0.6 are as shown in **Figure 4.48** (a-b). From this spectrum, it has been observed that both the composites have the presence of desired elements without any other undesirable elements. This confirms the successful synthesis of the phase pure nanocomposites.

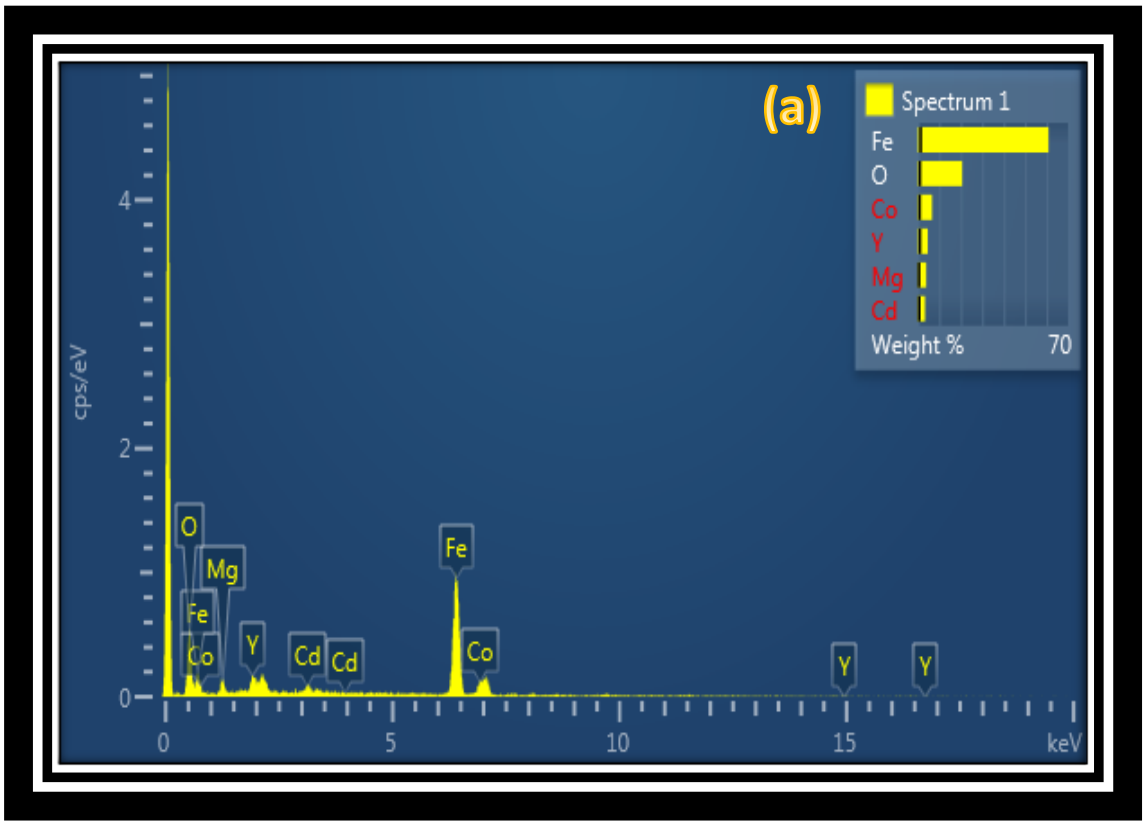

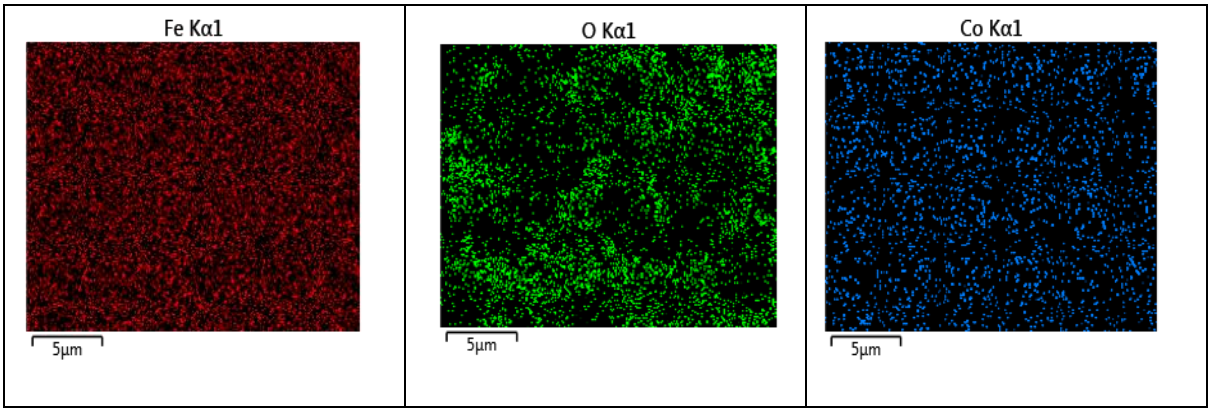

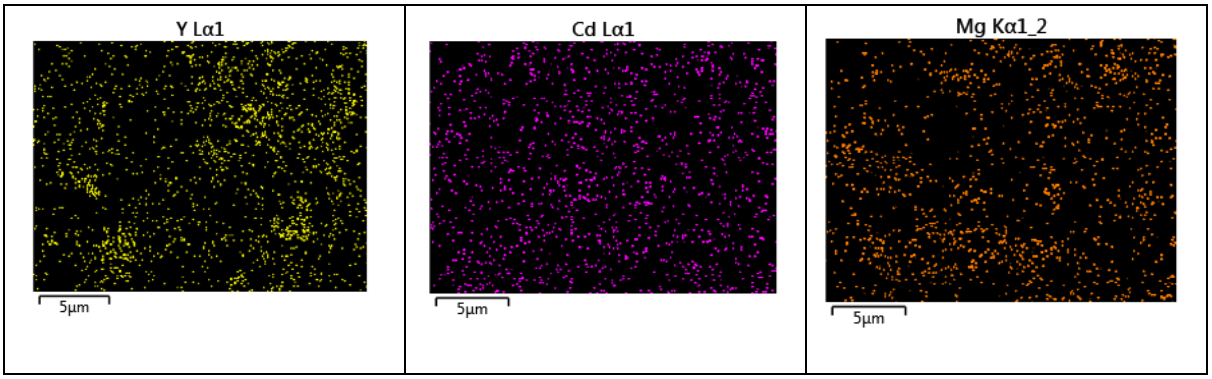
Y Lα1
5μm
Cd Lα1
5μm
Mg Kα1_2
5μm

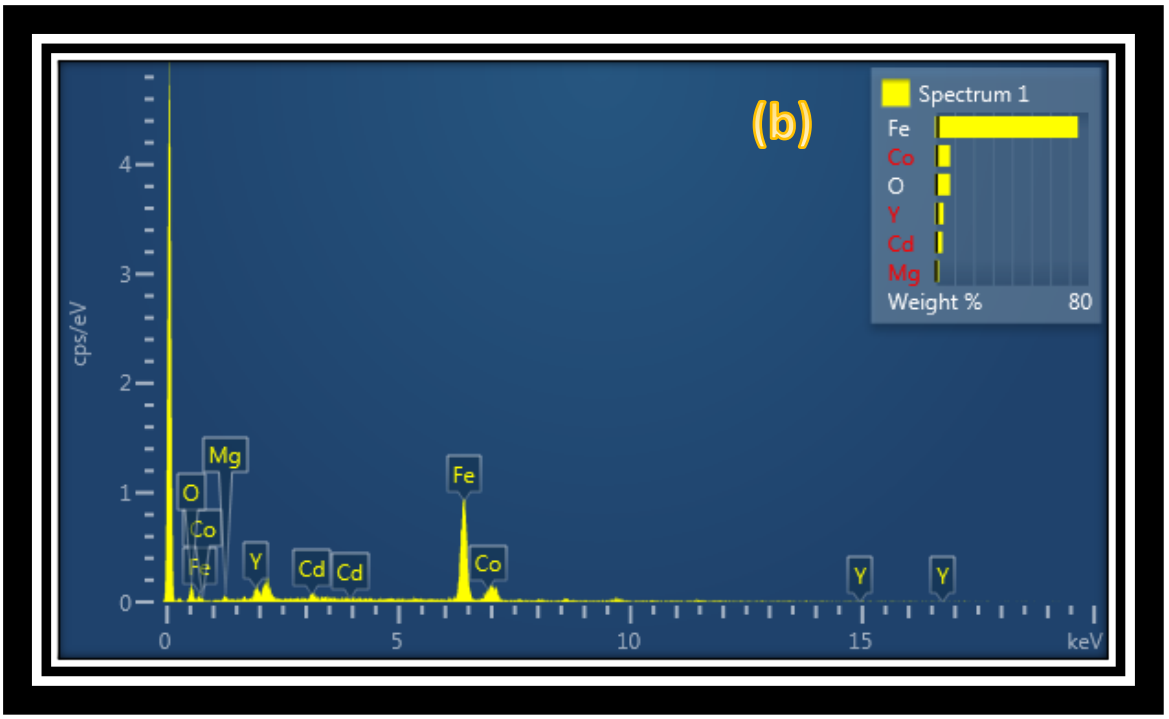
(b)
Spectrum 1
Fe
Co
O
Y
Cd
Mg
Weight %
80
cps/eV
0
1
2
3
4
0
5
10
15
keV
Mg
O
Co
Fe
Y
Cd
Cd
Fe
Co
Y
Y

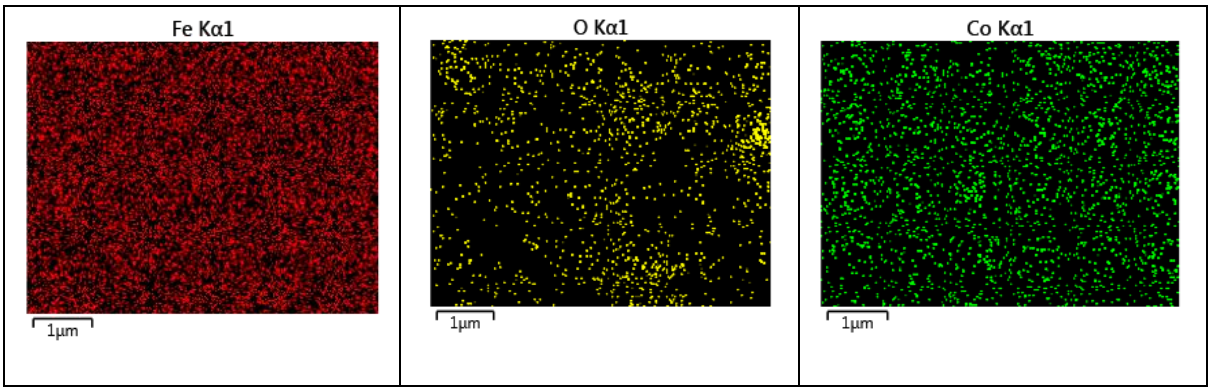
Fe Kα1
1μm
O Kα1
1μm
Co Kα1
1μm

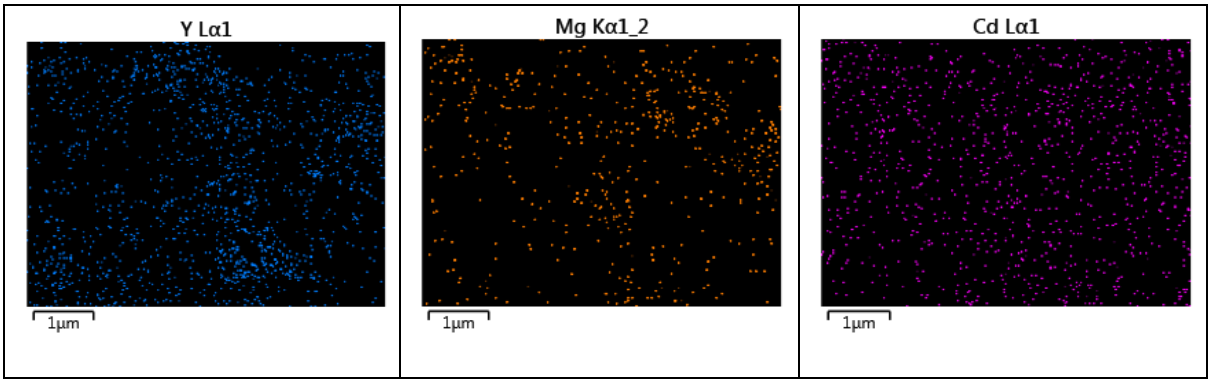

Figure 4.48 EDX spectra of (a) YM0.3 and (b) YM0.6 composites

4.6.4 VSM

The room temperature magnetic properties of the prepared samples were examined by using a vibrating sample magnetometer (VSM). The important magnetic parameters like remanence magnetization *(M_r)*, saturation magnetization *(M_s)*, coercivity *(H_c)*, squareness ratio (SQR), anisotropy *(K_{eff})* and magnetic crystalline anisotropy *(H_a)* were calculated from the Magnetization versus applied field curve **(Figure 4.49)**. These values are tabulated in **Table 4.20**. **Figure 4.21** depicts that all the prepared samples exhibit S-shaped M-H loop, which indicates the superparamagnetic behaviour. The prepared composites have single smooth M-H curves, this implies that the exchange coupling exists between the garnet and spinel ferrite **[192]**. The reason for the formation of a single magnetic curve is, that the mechanical blending method has provided the proper mixing of the two ferrites. The SQR value for all prepared samples is less than 0.5 and lies between 0.008 to 0.24, indicating the existence of multi-magnetic domain structures.

MgCdCoFe (M) has a higher value of H_c as compared to YIG (Y), because of higher magneto-crystalline anisotropy. The composites YM0.3 have a smaller grain size, so it has larger H_c as compared to other composites. With an increase in grain size, H_c decreases because the single domain size of the grain changes to a multi-domain structure and it requires a very less magnetic field for magnetic alignments. The M_s values for all composites are high as compared to YIG. This is because with the incorporation of MgCdCoFe, a disorder in spin, change in surface morphology and anti-phase disorder takes place **[149]**. The lower coercivity of YM0.9 composites is promising for the use in switching devices, whereas the larger coercivity of YM0.3 composite can be suitable for use in high-frequency device applications.

Table 4.20 Important magnetic parameters calculated from the M-H loop for samples

Sample	H_c (Oe)	M_r(emu/g)	M_s(emu/g)	K_{eff}(erg/cm^3)	H_a	SQR
Y	31.2	1.3	11.4	370.2	65.1	0.05
M	176	10.6	44	8075.8	367.1	0.24
YM0.3	99.2	5.3	41	4207.9	206.7	0.13
YM0.6	61.94	7.6	40.7	2625.9	129.0	0.08
YM0.9	9.64	0.41	27.1	271.8	20.1	0.01

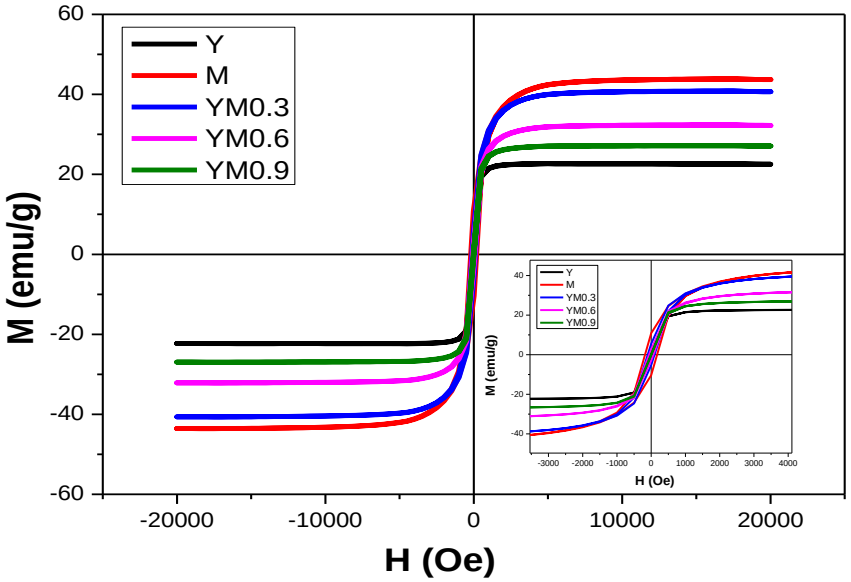

Figure 4.49 Magnetization (M) versus applied field curve for samples

4.6.5 VNA

Permittivity and Permeability:

The variations of the real part of dielectric permittivity (ε') and magnetic permeability (μ') with frequency in the Ku-band for composites are shown in **Figure 4.50** and **Figure 4.51** respectively. From **Figure 4.50,** it has been observed that the dielectric spectra are not showing dispersion behaviour (as explained by Koop's theory) from the 12 GHz to 17 GHz range of frequency. The permittivity of the composites follows an oscillating trend which may be due to the fluctuation in the polarization of ferrites with variation in frequency. The dispersion behaviour of the composites occurs beyond 17GHz of frequency. The composite YM0.3 has a higher permittivity value as compared to YM0.6 and YM0.9. The values of ε' for composites at 14.5 GHz frequency are given in **Table 4.21**. For the YM0.3 composite the value of ε' is ~ 19.5. this is because of the lower porosity and high density of the composites **[18]**.

The frequency variations of the real part of permeability (μ') of the composites are shown in **Figure 4.51** and this study also does not exhibit frequency dispersion. Beyond 17GHz the value of permeability increases. From **Table 4.21** it can be concluded that the composite YM0.3 has a higher value of μ'∼2.8 as compared to other composites. The reason for the higher value of permeability is lower porosity and higher densification of the composite. The permeability is dependent on grain size (D), saturation magnetization M_s and magneto-crystalline anisotropy as per equation $\mu \sim M_s^2 D/(K_{eff})^{0.5}$. The YM0.3 composite has a higher value of M_s and moderate grain size.

Dielectric and Magnetic Losses

The dielectric losses in samples occur due to vibrations of dipoles. Dielectric tangent loss is the measure of loss of energy from an externally applied field. This loss occurs due to domain wall resonance, due to pores, grain boundaries and impurities present in the structure of ferrites **[49]**. The dielectric loss tangent in ferrites contributes largely to entire core loss and power losses. The magnetic loss in the samples is due to losses in hysteresis, domain wall displacement (also known as resonance relaxation loss) and eddy current loss. At Higher frequencies, losses are dependent on morphology or grain sizes. **Figure 4.52** and **Figure 4.53** represent the dielectric and magnetic losses in the composite from 12 GHz to 18 GHz. It has been observed that all the composites offer less value of dielectric and magnetic losses. But it has been noticed that losses are approaching the negative values which is due to less signal to noise ratio or fixture error. **Table 4.21** summarizes the dielectric and magnetic loss tangents of all the composites at 14.5 GHz. The composite YM0.3 has the minimum value ∼0.009 of dielectric loss tangent and ∼0.002 of magnetic loss tangent at 14.5 GHz. The reason for lower losses is that the higher content of MgCdCoFe in the YIG composite suppresses the overall grain growth. This decreases the porosity and increases the density as the spinel ferrites segregate at grain boundaries of YIG, due to which grain size reduces and hence losses also decrease.

Miniaturization Factor of Antenna

The miniaturization factor decides the compactness of the antenna. The higher is the miniaturization factor, the more the compact size of the antenna is. The miniaturization factor is calculated using **Equation (4.75) [193]**.

$$\eta_i = \sqrt{\varepsilon' \mu'} \tag{4.75}$$

From the above equation, it is clear that the miniaturization factor η_i depends upon permittivity and permeability values. From **Figure 4.54**, it has been clear that the YM0.3 sample has larger values of η_i as compared to other composites. The values of η_i for all samples at 14.5 GHz are tabulated in **Table 4.21**. The sample YM0.3 has a higher value of η_i*~7.2* at 14.5 GHz.

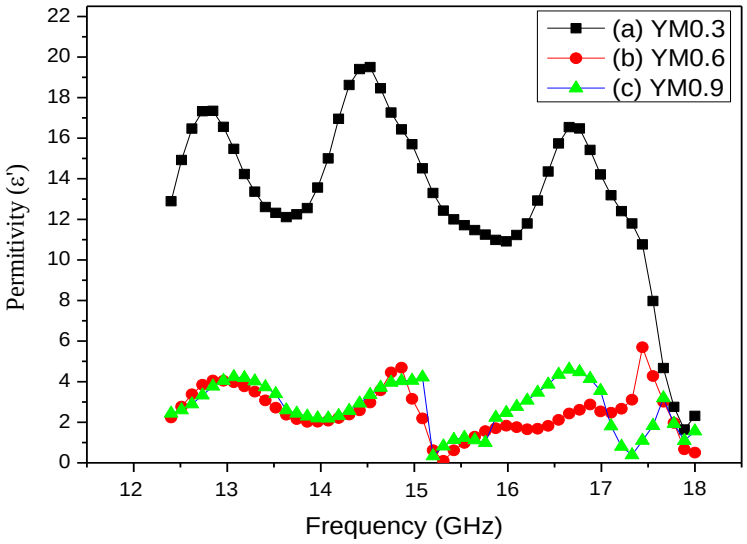

Figure 4.50 Variation of Permittivity with frequency (12-18GHz) for samples

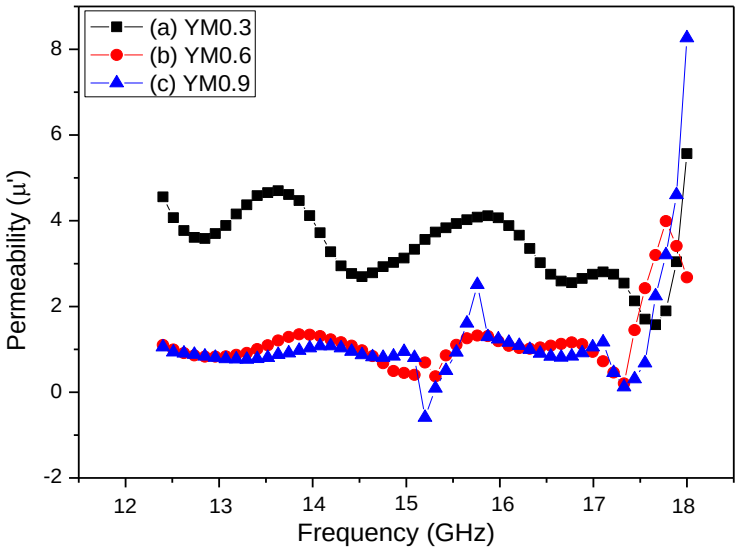

Figure 4.51 Variation of Permeability with frequency (12-18GHz) for samples

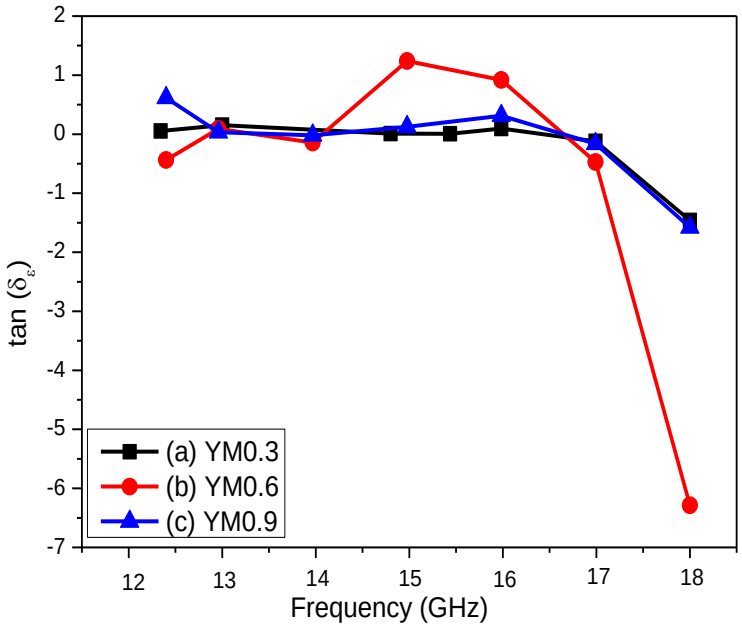

Figure 4.52 The obtained dielectric loss tangent for samples at a frequency from 12-18GHz

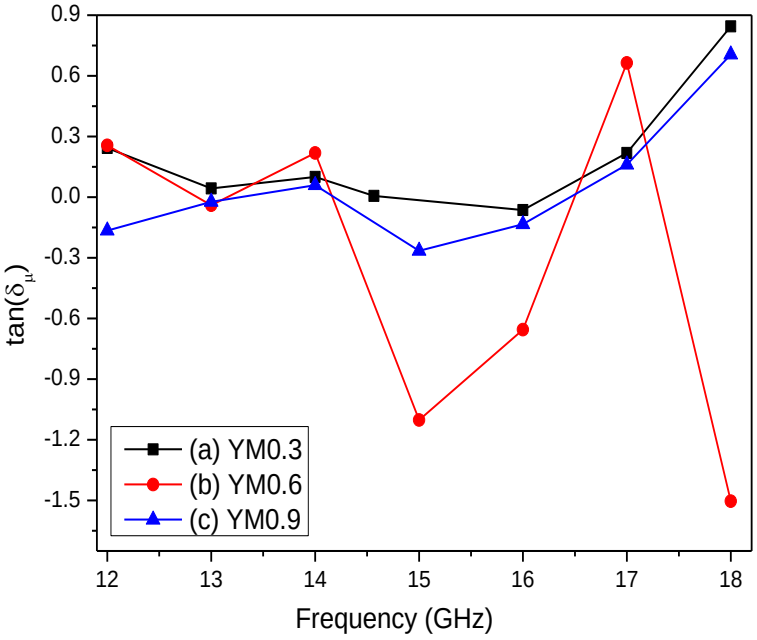

Figure 4.53 The obtained magnetic loss tangent for samples at frequency from 12GHz-18GHz

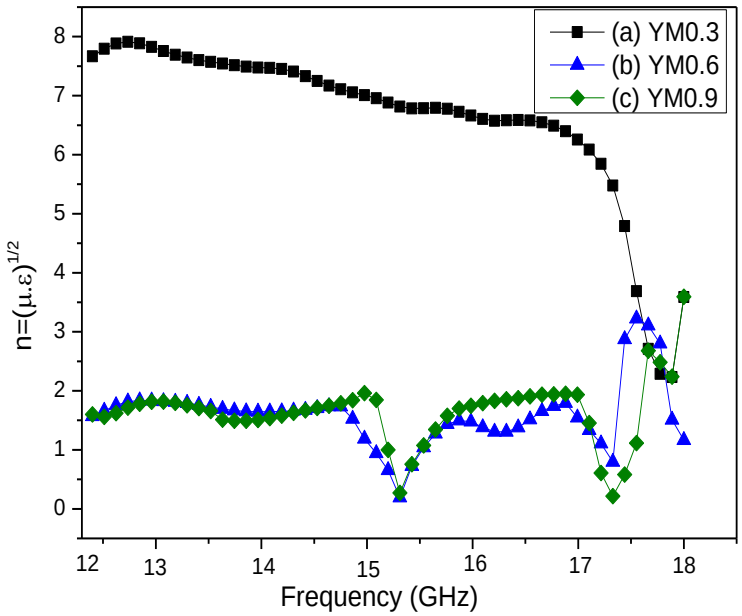

Figure 4.54 The obtained miniaturization factor for the composites at the frequency range of 12GHz-18GHz

Table 4.21 Calculated Permittivity, permeability, dielectric and magnetic loss tangent and miniaturization parameters at 14.5GHz for composites

Sample	ε'	μ'	$tan\delta_\varepsilon$	$tan\delta\mu$	η_i
YM0.3	19.5	2.8	0.009	0.002	7.2
YM0.6	3.57	1.2	0.5	Negligible	1.7
YM0.9	3.90	1.1	0.12	Negligible	1.8

4.7 Pr^{3+} substituted gadolinium garnet ferrite (GdIG)

4.7.1 XRD

X-ray diffraction pattern was used to study the structural properties of praseodymium doped gadolinium iron garnet ($Pr_xGd_{3-x}Fe_5O_{12}$ for x=0.5, 1.0 and 1.5). **Figure 4.55** represents the XRD pattern of $Pr_xGd_{3-x}Fe_5O_{12}$ (x=0.5,1.0, 1.5 represent by P1, P2 and P3 respectively). From pattern it has been clear that garnet phase is dominant for all samples. The obtain results of the samples were further compare with JCPDS no. 72-0141 of pure GdIG. The cubic structure of prepared samples with space group Ia3d has been assured by miller indices values at (321), (400), (420),

(422), (521), (532), (444), (640), (642), (800), (840), (842), and (664) **[167]**. With more addition of Pr in samples i.e., from x=0.5 to 1.5 the impurity phase (Fe_2O_3) has been observed. This impurity phase is due to stoichiometric modification in dodecahedral site **[178]**. Also, the higher intense peak (420) became less sharp with increase in Pr content in samples. This implies that the sample is becoming less crystalline with higher substitution of Pr.

The calculated value of crystallite size "D", lattice constant "a", micro strain "ε" and dislocation density "δ" is tabulated in **Table 4.22**. It has been observed that the crystallite size decreases with increases in Pr substitution. The variation in crystallite size with substitution is due to presence of impurities. These impurities further affect the growth of crystal **[170]**. Second reason of variation can be stress and strain due to Pr substitution which produce defect in lattice.

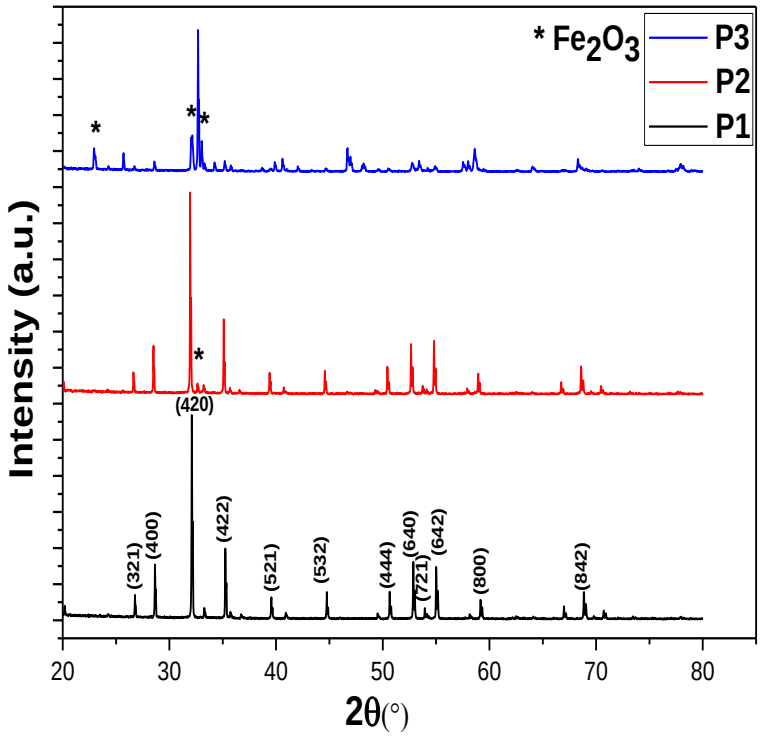

Figure 4.55 represents the XRD pattern of PrxGd3-xFe5O12 (a) x=0.5 (b) 1.0 and (c) 1.5

Table 4.22 The calculated values of 2 θ, FWHM (β), crystallite size (D), lattice constant (a), micro strain (ε) and dislocation density (δ) for samples

Sample	Sample Code	2θ(°)	β	hkl	D(nm)	a	ε	δ (nm^{-2})
$Pr_xGd_{3-x}Fe_5O_{12}$ (x=0.5)	P1	32.12	0.15	420	52.8	12.45	2.7	0.35
$Pr_xGd_{3-x}Fe_5O_{12}$ (x=1.0)	P2	31.90	0.17	420	46.6	12.51	2.6	0.46
$Pr_xGd_{3-x}Fe_5O_{12}$ (x=0.5)	P3	32.70	0.18	420	44.1	12.23	2.8	0.51

4.7.2 FESEM

FESEM was used to study the morphology of the Pr substituted samples. **Figure 4.56** (a-c) represent the micrographs of the sample P1, P2 and P3. From deep analysis of micrographs, it has been observed that all the samples have spherical shape grains which is in accordance with literature **[194]**. With increase in Pr^{3+}substitution, agglomeration has been observed. **Figure 4.57** (a-c) represent size distribution histogram of the samples. The maximum number of grains lies in 0.71μm, 1.1 μm, 77 nm for P1, P2 and P3 sample respectively. The ionic radii of substituted element, temperature, porosity and method of preparations affects the grain size of the samples.

Line intercept method **(Equation 4.76)** was used to calculate grain size of the samples and tabulated in **Table 4.23**.

$$grain\ size = \frac{1.5\,L}{mn} \tag{4.76}$$

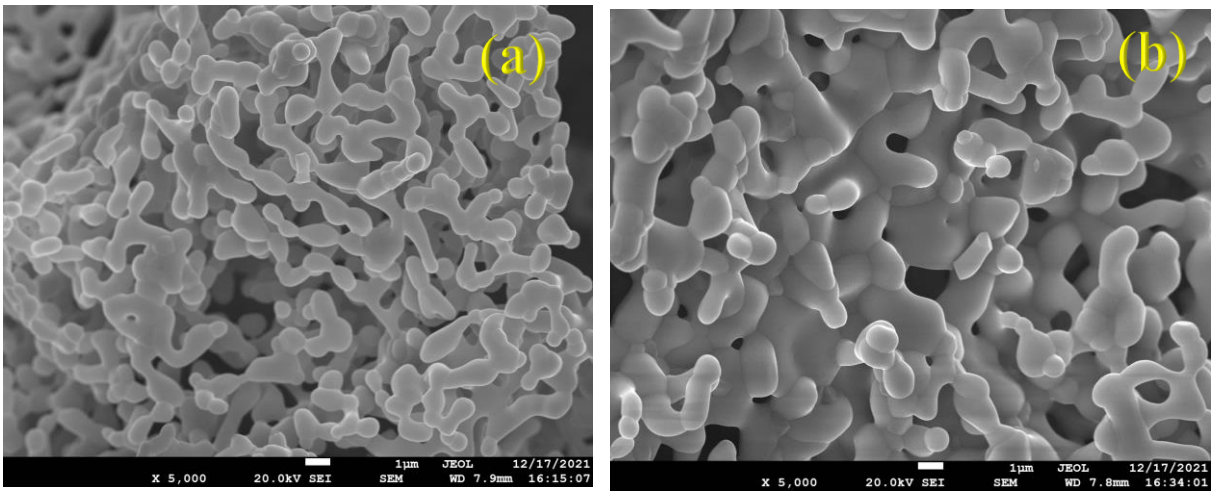

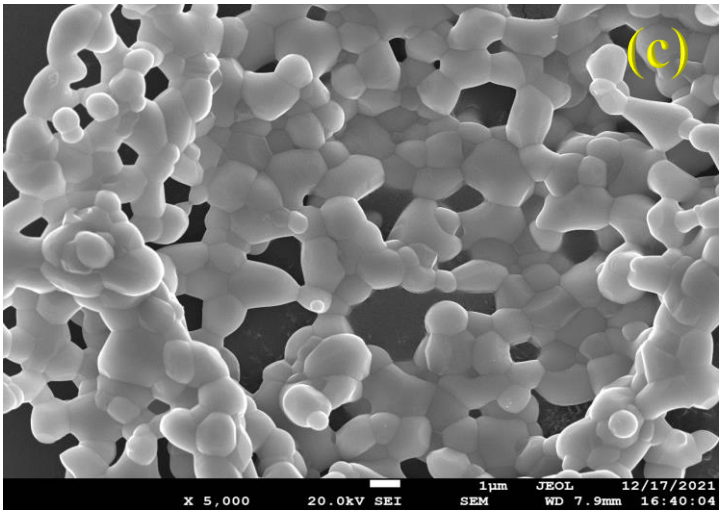

Figure 4.56 Micrographs of sample (a) P1, (b) P2 and (c) P3

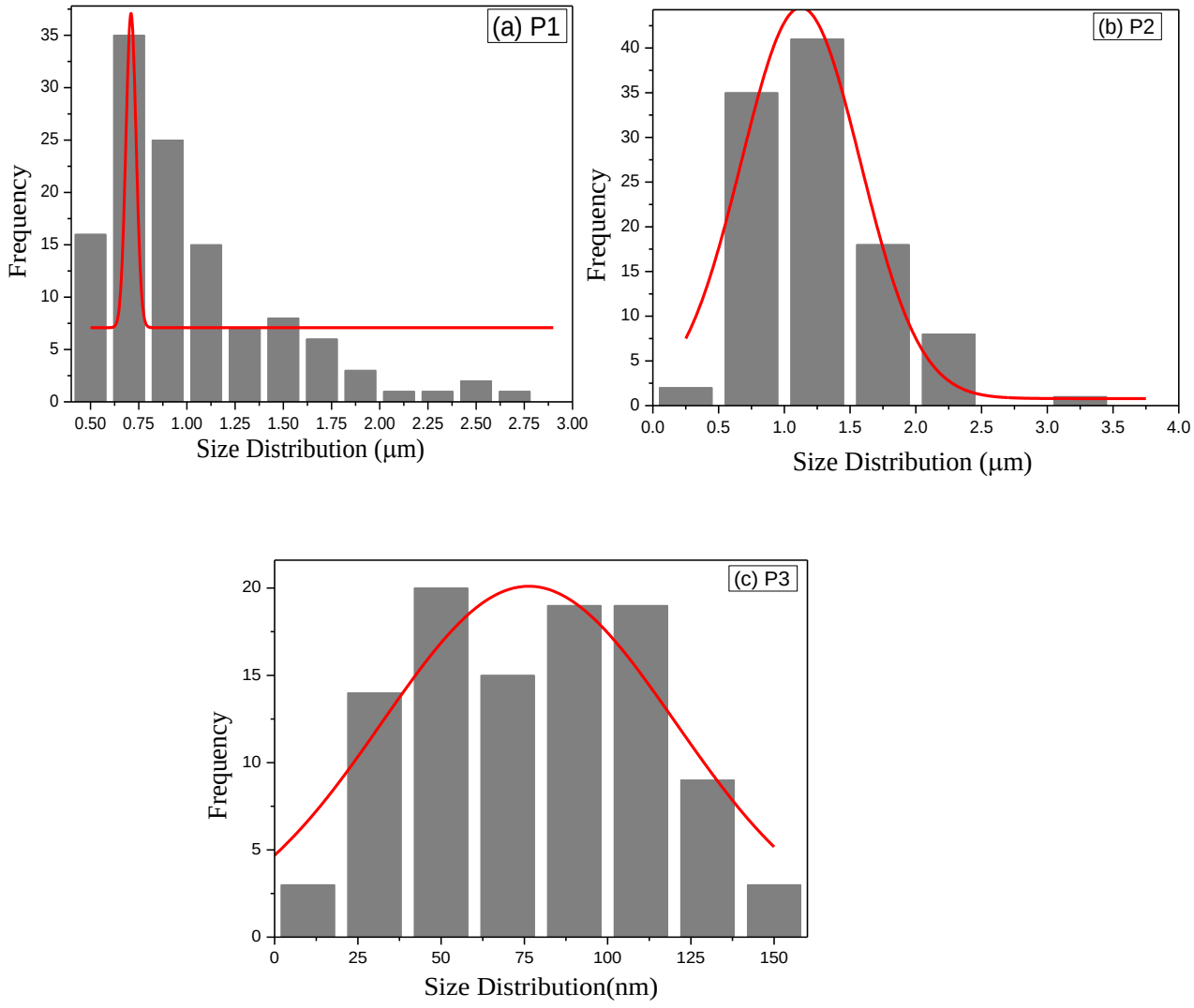

Figure 4.57 Gaussian fit histogram of samples (a) P1, (b) P2 and (c) P3

Table 4.23 Calculated grain size of sample (a) P1, (b) P2 and (c) P3

Sample	Grain Size (μm)
P1	0.271
P2	0.401
P3	0.308

4.7.3 UV-Vis

Absorption coefficient (α) and energy band gap (Eg) both are the special optical features. These features decide the use of ferrites for optoelectronic applications. UV-Vis spectroscopy was used to study optical property of $Pr_xGd_{3-x}Fe_5O_{12}$. **Figure 4.58** represents the absorption versus wavelength graph for samples P1, P2 and P3. The absorbance in all has been observed up to 280 nm, after that samples show transmittance. A shift in absorbance has been noticed with change in composition from x= 0.5 to 1.5. The absorbance in the materials depend upon factors like energy band and uneven surface **[195]**. **Figure 4.59** (a-c) represent $(\alpha h\nu)^2$ versus (hν) graphs which are plotted to calculate band gap of the samples. It has been observed that band gap of sample $Pr_xGd_{3-x}Fe_5O_{12}$ first decreases from 4.6 eV to 4.5 eV for x=0.5 to 1.0. After that the band gap increases from 4.5 eV to 4.7 eV. The change in bandgap depends upon several factors like crystallite size, impurity, concentration of substituents and morphology **[196]**.

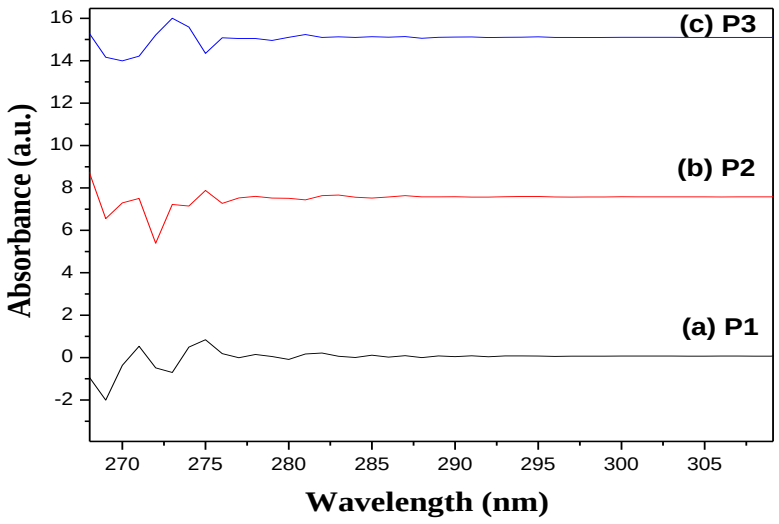

Figure 4.58 UV-Vis spectra of samples (a) P1, (b) P2 and (c) P3

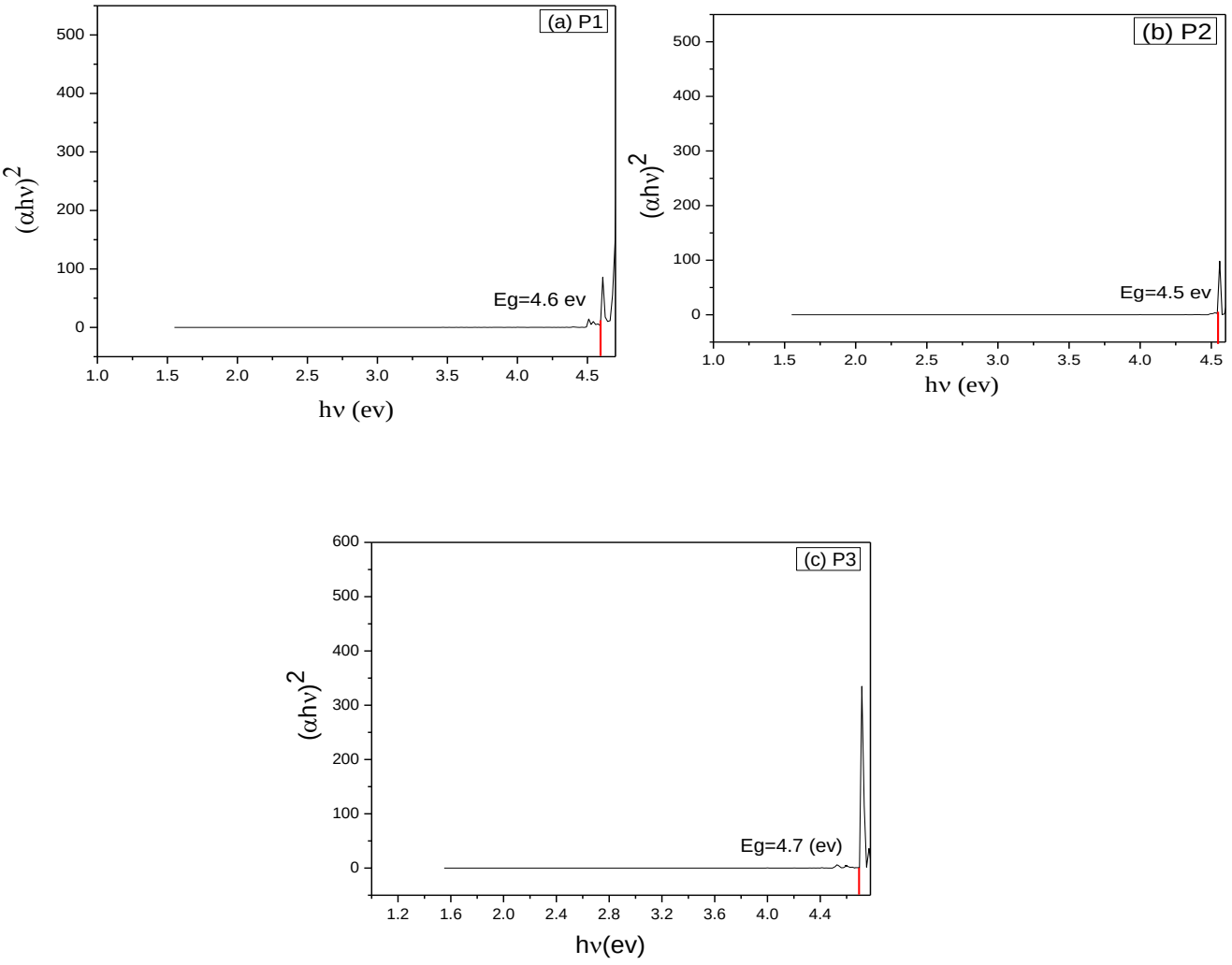

Figure 4.59 Calculated band gap of sample (a) P1, (b) P2 and (c) P3

4.7.4 Fluorescence

In order to study the luminescence property and to analyse the energy band gap with related to most strong position of sub band gap fluorescence spectroscopy was studied. **Figure 4.60** represent the fluorescence spectroscopy of $Pr_xGd_{3-x}Fe_5O_{12}$ sample. The excitation wavelength is around 270 nm which is choose from the obtained UV spectroscopy. At this excitation wavelength it has been observed that all three samples emit red colour i.e., at 650nm region. The reason of such emission is presence of nitrates group in prepared samples **[195]**. A shift has been observed with increases in Pr concentration in $Pr_xGd_{3-x}Fe_5O_{12}$. The intensity of the sample increases with increase in Pr concentration. The reason of increase in fluorescent intensity is because of increase in distance between GdIG and dopant (Pr) **[197]**. This implies

that increases in concentration of dopant increase the emission property. Such properties of $Pr_xGd_{3-x}Fe_5O_{12}$ makes it suitable to be used in optical storage and optical devices.

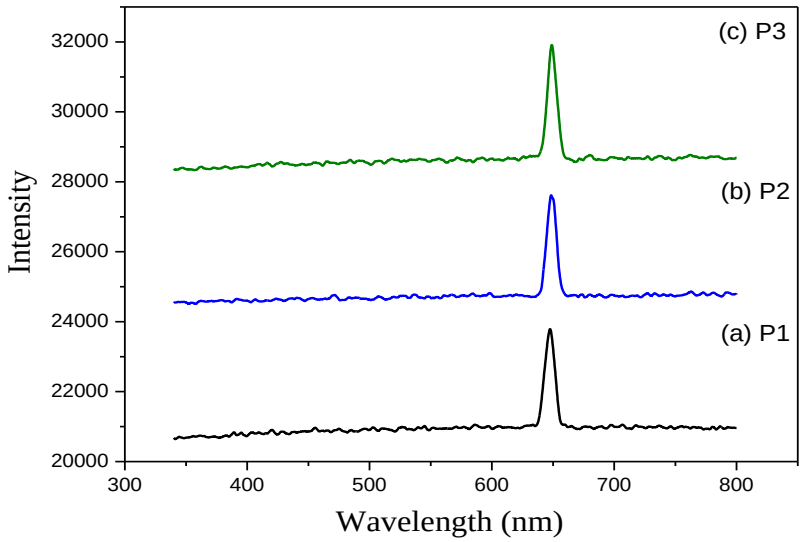

Figure 4.60 Fluorescence emission spectra of sample (a) P1, (b) P2 and (c) P3

Chapter 5

Summary and Conclusion

The novelty of the presented work is the choice of the composites. An attempt has been made to synthesis the composites of soft/soft ferrites (garnet/spinel ferrites). These ferrites individually do not yield good results for antenna application according to literature. But as per our observation it has been found that the combination of the garnet and spinel ferrites yield lower losses in microwave region, sustainable at higher temperatures with good structural, magnetic and dielectric properties.

This research work has attempted to address the problems faced in the fabrication, synthesis and characterization of nanocomposites for antenna miniaturization and microwave losses in antennas. The properties of nanocomposites of garnet ferrites such as structural, magnetic, dielectric and optical has been studied. The appropriateness of sol-gel auto-combustion method has been confirmed in this research. Most of the prepared nano-samples consist of single phase without any impurities with suitable time and sintering temperature.

By using sol -gel auto-combustion method $Gd_3Al_2Fe_3O_{12}$ has been prepared successfully. The sample further sintered at three different temperature that is at 900°C, 1000°C, 1100°C in order to study the effect of temperature on structural, morphology and magnetic properties of the garnet ferrite. From XRD of sintered sample it has been observed that with increase in temperature $Gd_3Al_2Fe_3O_{12}$ tending toward single phase formation. The average crystallite size at different sintering temperature was obtained in range from 27-36 nm. The FTIR analysis confirms achievement of garnet phase because there is presence of asymmetric stretching bond formed between cations of metals and anions of oxygen. From FESEM it was confirmed at 900°C sintering temperature agglomeration occurs which vanishes up to 1100°C. Also, it revealed that sintering temperature effect porosity, grain size, and size distribution. The grain size of samples ranges from 25-450, 10-125 and 13-73 nm for 900, 1000 and 1100°C respectively. VSM revealed that with increase in temperature the magnetic properties get altered. Coercivity and saturation magnetization decreases which depict that use of these materials in switching devices. Least value of H_c is 62.9 and least value of M_s is 2.46 noted at higher temperature (1100°C). The value of SQR of sample sintered at different temperature ranges between 0.007-0.055 which suggest about superparamagnetic nature. Also, the value of ω_m ranges from 500-700 MHz which shows that these materials have very good application in Ultra High frequency range.

The GdIG and MF were successfully prepared using the sol-gel auto-combustion method. GdIG composites (x=1.0,0.5,0.75) were prepared using mechanical blending according to wt%. The XRD pattern shows the presence of a pure phase of GdIG and MF. It is found that for x=0.5 composite both phases were present independently with sharper peaks, whereas at x=0.75 some GdIG peaks dominate. The crystallite size calculated from XRD data was found to be in the range 26-55 nm, which implies that samples are nanocrystalline. The average particle size obtained ranges from 0.24 to 0.42 μm for x=1,0.5 and 0.7. From the dielectric study, it has been observed that these composites show the variation of the real and imaginary part of the dielectric constant and loss tangent with frequency. Further from the M-H loop, it has been found that composites show better S-shaped curves as compared to GdIG which further tells about the superparamagnetic nature of composites. Value of M_s increases with increasing MF in GdIG, H_c decreases with the addition of MF in GdIG and M_r increases with the addition of MF. The calculated value of microwave operating frequency reveals that the addition of MF in GdIG enhances its operating frequency from MHz to GHz range which shows that alone GdIG is not sufficient to reach in GHz range its nanocomposites are the best option to operate in S-band.

Both $Gd_3Fe_5O_{12}$ and MFe_2O_4 were successfully prepared using sol-gel auto-combustion method. Further composite of both ferrites was formed by using mechanical blending method and then treated at 900°C and 1300°C. XRD reveals the presence of the phases in the composites for both samples. From FESEM it has been clear that temperature effects the morphology of both the samples. Impedance analyser study reveals that heat treatment gives larger value of dielectric constant in lower frequency range, which further decreases with increase in frequency. Whereas the dielectric loss tangent also increases with increase in temperature in higher frequency range. VSM study reveals that magnetic parameters varies with temperature which is due to change in microstructure with temperature. The calculated value of SQR suggests the single domain structure of the composites. The calculated value of microwave operating frequency reveals the uses of these composites in GHz range.

This work focuses to study variation in structural, optical and magnetic properties by substitution of Y^{3+}, Bi^{3+} and La^{3+} in GdIG. From XRD it has been clear that with change in substitution from x= 0 to 0.4 the value of crystallite size and lattice constant changes. From FESEM it has been notice that the samples have spherical grain shape. For sample x=0 maximum number of grains lie between 0.41μm to 0.58μm range, for sample x=0.2 lies between 0.61μm to 0.78μm range and for x=0.4 lies between 0.61μm to 0.92μm range. EDX confirms the dispersion of all ions in sample in desired amount without any other elements ions. The

value of band gap calculated from UV-VIS is in range from 3.7eV to 3.9eV which implies prepared samples are wide-bandgap semiconductors. The value of H_c is larger for x=0 and with substitution of La^{3+} from x=0.2 to x=0.4 it decreases from 40.42 to 39.14. This is because change in grain size with substitution. Also, the value of saturation magnetization varies with substitution. The value of operating microwave frequency also varies with substitution and suggests the use of these materials in 500 MHz to 1.1 GHz frequency range. The future scope of our work is that such materials can be use in high frequency devices and in communication devices especially for military applications.

Yttrium iron garnet (YIG) and Erbium iron garnet (ErIG) samples were prepared by sol gel auto combustion method. Mechanical blending method was adopted to form ErIG(x)-YIG(1-x) (x=0.5) composite. XRD confirmed proper formation of garnet phase in samples. The calculated lattice constant for YIG, GdIG and for their composite is almost same as they are garnet ferrites. From FESEM it has been noticed that composite YE0.5 showed agglomeration which is due to magnetic interaction between two ferrites. From size distribution histogram it has been found that the maximum number of grains lie between 0.30 μm to 0.59 μm, 0.6 μm to 1.1 μm, 0.3 μm to 0.51 μm for YIG, ErIG, YE0.5 respectively. From impedance spectroscopy it has been found that dielectric properties of the samples varies with frequency. ErIG gives larger value of dielectric constant and YIG give least value of dielectric constant but their composite YE0.5 give moderate value of dielectric constant. Whereas dielectric losses in YIG is least and ErIG is large. But if ErIG is incoperated with YIG than lesser value of losses has been obtained. These values of losses are almost near to the losses in YIG. YE0.5 composite give moderate value of dielectric constant, dielectric loss tanget, electrical modulus, ac conductivity. From VSM it has been observed that YE0.5 composite give good value of magnetic parameters. The compoite YE0.5 has higher value of microwave operating frequency near about 4.5GHz. From obtained results it can be concluded that YE0.5 composite is suitable to operate in microwave devices as it provide better dielectric and magnetic property as compare to parent garnet ferrite (YIG and ErIG).

The garnet ferrite (YIG) and spinel ferrite (MgCdCoFe) samples have been synthesized by using the sol-gel auto combustion method. The composites of YIG/MgCdCoFe with composition x = 0.3 (30% YIG, 70 % MgCdCoFe), x=0.6 (60% YIG, 40 % MgCdCoFe) and x=0.9 (90% YIG, 10 % MgCdCoFe) were prepared by facile mechanical blending method. The phase study reveals that both phases of YIG and MgCdCoFe are present independently in the composites. The composite at x = 0.3 has good compactness because of the enhanced packing

of the grains of two ferrites. The composite with x=0.3, also results in higher densification and lower bulk density as compared to other composites prepared. The magnetic properties of all the composites vary with the change in the composition of ferrites. The composite at x = 0.3 has a maximum H_c value whereas the composite at x =0.9 has the minimum value of H_c which suggests its potential application in switching devices. All the composites offer a high value of saturation magnetization (M_s). Among the composite studied, x = 0.3 composites offer very good magneto-dielectric properties with high ε' (~19.5) and μ' (~2.8). It has to be noted here also that for this composite the dielectric and magnetic losses are of the order of 10^{-2} only. The miniaturization factor is also high for the composite at x=0.3. So, we conclude that the composite of YIG/MgCdCoFe can be an excellent candidate for Ku band antenna applications.

Sol-gel auto-combustion process was carried out to prepare $Pr_xGd_{3-x}Fe_5O_{12}$ for x=0.5,1.0 and 1.5. XRD confirms the formation of garnet phase in Pr substituted GdIG. It has been observed that with increase in Pr content in garnet ferrite impurity phases were formed. Crystallite size, lattice constant, micro strain and dislocation density also varies with change in Pr content. From FESEM it has been observed that maximum number of grains lies in 0.71μm, 1.1 μm, 77 nm for x=0.5, 1.0 and 1.5 sample respectively. The bandgap evaluated from UV-Vis spectra was found in 4.5eV to 4.7eV range. From fluorescence spectroscopy it has been found that with increases in concentration of dopant, emission property enhances.

Future Work

Cancer is the second-highest mortality rate in the world and is also linked to drastically reduced life expectancy. New, promising methods for treating malignant neoplasms are now being explored, magnetic hyperthermia (MH) receiving a lot of attention. Magnetic nanoparticles (MNPs) are when exposed to an alternating magnetic field (AMF), they produce heat. As a result of the MNP is used to treat the tumor, the tumor is gradually heated to temperatures over 42°C, finally causing cell death. The performance of MH depends on the elemental composition, size, structure, anisotropic magnetic properties, stability, and other characteristics of the MNPs. MNPs based on iron oxides are now being investigated as a potential material for MH applications. They have good control over size and shape, and high magnetization, but lower magnetic anisotropy; yet, they are prone to aggregation and oxidation. Iron oxide MNPs should therefore be protected by shells, which could lead to a reduction in heating efficiency.

Ferrite-based MNPs have recently undergone significant research for biomedical use, specifically for MH. By adjusting the stoichiometry slightly, ferrite MNPs enable a wide range

of customized magnetization and magnetic anisotropy. As a result, the MHT parameters can be better matched, and smaller MNPs can be utilized for MH instead of the usual 20–25 nm iron oxide MNPs. They are typically coated with citrate ions to promote colloidal stability; however, this modification has little effect on MNPs' capacity for heating. The hysteresis loss in the B-H magnetic property was closely correlated with the heat generation in an AC magnetic field. The distortion of the cubic structure in the hysteresis loss contributed to the high heating ability. Such ferrite MNPs are thus attractive candidates for their usage in MH cancer therapy based on their physical and chemical characteristics. Currently, the US Food and Drug Administration has approved the use of iron oxide MNPs for cancer diagnosis, cancer hyperthermia, and iron deficiency anemia (FDA).

For cancer prospective the research will be elaborate to achieve following objectives:

1. Enhancing the heat generation ability in the AC magnetic field of garnet ferrites and their composites for cancer treatment.
2. To investigate the non-toxic ceramic oxides for cancer treatment.

Bibliography

[1] Ali T, Pathan S, Biradar RC. Multiband, frequency reconfigurable, and metamaterial antennas design techniques: Present and future research directions. Internet Technology Letters. 2018 Nov;1(6): e19.

[2] Basaran SC, Olgun U, Sertel K. Multiband monopole antenna with complementary split-ring resonators for WLAN and WiMAX applications. Electronics letters. 2013 Jun 13;49(10):636-8.

[3] Saini A, Kumar P, Ravelo B, Lallechere S, Thakur A, Thakur P. Magneto-dielectric properties of doped ferrite based nanosized ceramics over very high frequency range. Engineering Science and Technology, an International Journal. 2016 Jun 1;19(2):911-6.

[4] Andreou E, Zervos T, Alexandridis AA, Fikioris G. Magnetodielectric materials in antenna design: exploring the potentials for reconfigurability. IEEE Antennas and Propagation Magazine. 2018 Dec 28;61(1):29-40.

[5] Altunyurt N, Swaminathan M, Raj PM, Nair V. Antenna miniaturization using magneto-dielectric substrates. In2009 59th Electronic Components and Technology Conference 2009 May 26 (pp. 801-808). IEEE

[6] Xie F, Chen Y, Bai M, Wang P. Co-substituted LiZnTiBi ferrite with equivalent permeability and permittivity for high-frequency miniaturized antenna application. Ceramics International. 2019 Oct 1;45(14):17915-9.

[7] Zheng Z, Zhang H, Xiao JQ, Yang Q, Jia L. Low loss NiZn spinel ferrite–W-type hexaferrite composites from BaM addition for antenna applications. Journal of Physics D: Applied Physics. 2014 Feb 26;47(11):115001.

[8] Rajan A, Solaman SK, Ganesanpotti S. Cold Sintering: An Energy-Efficient Process for the Development of SrFe12O19–Li2MoO4 Composite-Based Wide-Bandwidth Ferrite Resonator Antenna for Ku-Band Applications. ACS Applied Electronic Materials. 2021 May 10;3(5):2297-308.

[9] Gan G, Zhang D, Zhang Q, Wang G, Huang X, Yang Y, Rao Y, Li J, Xu F, Wang X, Chen RT. Influence of microstructure on magnetic and dielectric performance of Bi2O3-doped MgCd ferrites for high frequency antennas. Ceramics International. 2019 Jun 15;45(9):12035-40.

[10] Su Z, Chang H, Wang X, Sokolov AS, Hu B, Chen Y, Harris VG. Low loss factor Co2Z ferrite composites with equivalent permittivity and permeability for ultra-high frequency

applications. Applied Physics Letters. 2014 Aug 11;105(6):062402.

[11] Stergiou CA, Litsardakis G. Y-type hexagonal ferrites for microwave absorber and antenna applications. Journal of Magnetism and Magnetic Materials. 2016 May 1; 405:54-61.

[12] Fechine PB, Rocha HH, Moretzsohn RS, Denardin JC, Lavin R, Sombra AS. Study of a microwave ferrite resonator antenna, based on a ferrimagnetic composite (Gd3Fe5O12) GdIGX–(Y3Fe5O12) YIG1− X. IET microwaves, antennas & propagation. 2009 Dec 1;3(8):1191-8.

[13] Kong LB, Li ZW, Lin GQ, Gan YB. Ni-Zn ferrites composites with almost equal values of permeability and permittivity for low-frequency antenna design. IEEE transactions on magnetics. 2006 Dec 19;43(1):6-10.

[14] Ramesh T, Raju P, Shinde RS, Murthy SR. Microwave hydrothermal synthesis and electromagnetic properties of nanocrystalline Y3-xDyxFe5O12 garnets for microwave antenna applications. Int. J. ChemTech. Res. 2014;7(2):539-46.

[15] Khan MI, Waqas M, Naeem MA, Hasan MS, Iqbal M, Mahmood A, Ramay SM, Al-Masry W, Abubshait SA, Abubshait HA, Mahmood Q. Magnetic behavior of Ga doped yttrium iron garnet ferrite thin films deposited by sol-gel technique. Ceramics International. 2020 Dec 1;46(17):27318-25.

[16] Akhtar MN, Saleem M, Khan MA. Al doped spinel and garnet nanostructured ferrites for microwave frequency C and X-band applications. Journal of Physics and Chemistry of Solids. 2018 Dec 1; 123:260-5.

[17] Zheng Z, Zhang H, Xiao JQ, Yang Q, Jia L. Low loss NiZn spinel ferrite–W-type hexaferrite composites from BaM addition for antenna applications. Journal of Physics D: Applied Physics. 2014 Feb 26;47(11):115001.

[18] Vinaykumar R, Prakash S, Roy PK, Bera J. Synthesis and characterization of Ba2Co2Fe12O22–NiFe2O4 ferrite composites: a useful substrate material in miniaturizing antenna. Journal of Materials Science: Materials in Electronics. 2021 Mar;32(6):7330-9.

[19] Lee J, Hong YK, Bae S, Jalli J, Abo GS, Park J, Seong WM, Park SH, Ahn WK. Low loss Co2Z (Ba3Co2Fe24O41)–glass composite for gigahertz antenna application. Journal of Applied Physics. 2011 Apr 1;109(7):07E530.

[20] Vinaykumar R, Bera J. Low-temperature sintering of SrCo1. 5Ti1. 5Fe9O19 ferrite and its characterization for X-band antenna application. Journal of Alloys and Compounds.

2019 Jun 25; 790:413-20.

[21] Xie F, Liu H, Bai M, Wen S, Xu F, Zhao J, Liu W. Flexible LiZnTiMn ferrite/PDMS composites with enhanced magnetic-dielectric properties for miniaturized application. Ceramics International. 2021 Jan 1;47(1):1121-5.

[22] He D, Li W, Zhang J, Wang G, Qiao L, Wang T. The preparation and high-frequency electromagnetic properties of Co80Ni20 alloy particles for potential antenna applications. Journal of Magnetism and Magnetic Materials. 2021 Nov 1; 537:168165.

[23] Polley K, Alam T, Bera J. Synthesis and characterization of BaFe12O19-CoFe2O4 ferrite composite for high-frequency antenna application. Journal of the Australian Ceramic Society. 2020 Dec;56(4):1179-86.

[24] Yang Y, Li J, Zhang H, Wang G, Rao Y, Gan G. TiO2 tailored low loss NiCuZn ferrite ceramics having equivalent permeability and permittivity for miniaturized antenna. Journal of Magnetism and Magnetic Materials. 2019 Oct 1; 487:165318.

[25] Lee W, Hong YK, Park J, LaRochelle G, Lee J. Low-loss Z-type hexaferrite (Ba3Co2Fe24O41) for GHz antenna applications. Journal of Magnetism and Magnetic Materials. 2016 Sep 15; 414:194-7.

[26] Wang Y, Edwards E, Hooper I, Clow N, Grant PS. Scalable polymer-based ferrite composites with matching permeability and permittivity for high-frequency applications. Applied Physics A. 2015 Aug;120(2):609-14.

[27] Kotnala RK, Ahmad S, Ahmed AS, Shah J, Azam A. Investigation of structural, dielectric, and magnetic properties of hard and soft mixed ferrite composites. Journal of Applied Physics. 2012 Sep 1;112(5):054323.

[28] Lee J, Hong YK, Bae S, Jalli J, Abo GS, Park J, Seong WM, Park SH, Ahn WK. Low loss Co2Z (Ba3Co2Fe24O41)–glass composite for gigahertz antenna application. Journal of Applied Physics. 2011 Apr 1;109(7):07E530.

[29] Primc D, Makovec D. Composite nanoplatelets combining soft-magnetic iron oxide with hard-magnetic barium hexaferrite. Nanoscale. 2015;7(6):2688-97.

[30] Skumryev V, Stoyanov S, Zhang Y, Hadjipanayis G, Givord D, Nogués J. Beating the superparamagnetic limit with exchange bias. nature. 2003 Jun;423(6942):850-3.

[31] Harris VG. Modern microwave ferrites. IEEE Transactions on Magnetics. 2011 Dec 21;48(3):1075-104.

[32] Bae S, Lee SW, Hirukawa A, Takemura Y, Jo YH, Lee SG. AC magnetic-field-induced heating and physical properties of ferrite nanoparticles for a hyperthermia agent in medicine. IEEE Transactions on nanotechnology. 2008 Oct 31;8(1):86-94.

[33] Sattar AA, Elsayed HM, Faramawy AM. Comparative study of structure and magnetic properties of micro-and nano-sized GdxY3− xFe5O12 garnet. Journal of Magnetism and Magnetic Materials. 2016 Aug 15; 412:172-80.

[34] Arun T, Vairavel M, Raj SG, Joseyphus RJ. Crystallization kinetics of Nd-substituted yttrium iron garnet prepared through sol–gel auto-combustion method. Ceramics International. 2012 Apr 1; 38(3):2369-73.

[35] Garskaite E, Gibson K, Leleckaite A, Glaser J, Niznansky D, Kareiva A, Meyer HJ. On the synthesis and characterization of iron-containing garnets (Y3Fe5O12, YIG and Fe3Al5O12, IAG). Chemical physics. 2006 Apr 21;323(2-3):204-10.

[36] Yousaf M, Noor A, Xu S, Akhtar MN, Wang B. Magnetic characteristics and optical band alignments of rare earth (Sm+ 3, Nd+ 3) doped garnet ferrite nanoparticles (NPs). Ceramics International. 2020 Jul 1;46(10):16524-32.

[37] Praveena K, Srinath S. Effect of Gd3+ on dielectric and magnetic properties of Y3Fe5O12. Journal of magnetism and magnetic materials. 2014 Jan 1; 349:45-50.

[38] Sharma V, Saha J, Patnaik S, Kuanr BK. Synthesis and characterization of yttrium iron garnet (YIG) nanoparticles-Microwave material. AIP Advances. 2017 May 22;7(5):056405.

[39] Hapishah AN, Hashim M, Syazwan MM, Idza IR, Rodziah N, Ismayadi I. Phase, microstructure and magnetic evaluation in yttrium iron garnet (YIG) synthesized via mechanical alloying. Journal of Materials Science: Materials in Electronics. 2017 Oct;28(20):15270-8.

[40] Ahniyaz A, Fujiwara T, Song SW, Yoshimura M. Low temperature preparation of β-LiFe5O8 fine particles by hydrothermal ball milling. Solid State Ionics. 2002 Nov 1;151(1-4):419-23.

[41] Raghavender AT, Pajic D, Zadro K, Milekovic T, Rao PV, Jadhav KM, Ravinder D. Synthesis and magnetic properties of NiFe2− xAlxO4 nanoparticles. Journal of Magnetism and Magnetic Materials. 2007 Sep 1;316(1):1-7.

[42] Mane DR, Birajdar DD, Shirsath SE, Telugu RA, Kadam RH. Structural and magnetic characterizations of Mn-Ni-Zn ferrite nanoparticles. physica status solidi (a). 2010 Oct;207(10):2355-63.

[43] Shirsath SE, Toksha BG, Kadam RH, Patange SM, Mane DR, Jangam GS, Ghasemi A. Doping effect of Mn2+ on the magnetic behavior in Ni–Zn ferrite nanoparticles prepared by sol–gel auto-combustion. Journal of Physics and Chemistry of Solids. 2010 Dec 1;71(12):1669-75.

[44] Akhtar MN, Islam MU, Niazi SB, Rana MU. Effect of Mg^{2+} substitutions on the structural and magnetic properties of Co–Mg W-type hexagonal ferrite. International Journal of Modern Physics B. 2011 Mar 30;25(08):1149-60.

[45] Makovec D, Kodre A, Arčon I, Drofenik M. Structure of manganese zinc ferrite spinel nanoparticles prepared with co-precipitation in reversed microemulsions. Journal of Nanoparticle Research. 2009 Jul;11(5):1145-58.

[46] Gyergyek S, Makovec D, Kodre A, Arčon I, Jagodič M, Drofenik M. Influence of synthesis method on structural and magnetic properties of cobalt ferrite nanoparticles. Journal of Nanoparticle Research. 2010 May;12(4):1263-73.

[47] Auwal IA, Güngüneş H, Güner S, Shirsath SE, Sertkol M, Baykal A. Structural, magneto-optical properties and cation distribution of SrBixLaxYxFe12− 3xO19 (0.0≤ x≤ 0.33) hexaferrites. Materials Research Bulletin. 2016 Aug 1; 80:263-72.

[48] Ahmadipour M, Ain MF, Ahmad ZA. A short review on copper calcium titanate (CCTO) electroceramic: synthesis, dielectric properties, film deposition, and sensing application. Nano-Micro Letters. 2016 Oct;8(4):291-311.

[49] Pullar RC. Hexagonal ferrites: a review of the synthesis, properties and applications of hexaferrite ceramics. Progress in Materials Science. 2012 Sep 1;57(7):1191-334.

[50] Wu T, Su H, Ding Q, Zhang H, Jing Y, Tang X. Aluminum substituted low loss Z-type hexaferrites for antenna applications. Physica B: Condensed Matter. 2013 Nov 15; 429:85-9.

[51] Chan KC, Liew XT, Kong LB, Li ZW, Lin GQ. Ni1− xCoxFe1. 98O4 Ferrite Ceramics with Promising Magneto-Dielectric Properties. Journal of The American Ceramic Society. 2008 Dec;91(12):3937-42.

[52] Mosallaei H, Sarabandi K. Magneto-dielectrics in electromagnetics: Concept and applications. IEEE Transactions on antennas and propagation. 2004 Jun 7;52(6):1558-67.

[53] Lodhi MY, Khan MA, Akhtar MN, Warsi MF, Mahmood A, Ramay SM. Role of Nd-Ni on structural, spectral and dielectric properties of strontium-barium based nano-sized X-type ferrites. Ceramics International. 2018 Feb 15;44(3):2968-75.

[54] Anderson EE, Cunningham Jr JR. High-Permeability Garnets. Journal of Applied Physics. 1960 Sep;31(9):1687-8.

[55] Craik DJ, Tebble RS. Ferromagnetism and ferromagnetic domains. North-Holland Publishing Company; 1965.

[56] Dionne GF. Effect of pore size on remanence ratios of magnetic materials. Journal of

Applied Physics. 1969 Jan;40(1):431-2.

[57] Pardavi-Horvath M. Microwave applications of soft ferrites. Journal of Magnetism and Magnetic Materials. 2000 Jun 2; 215:171-83.

[58] Özgür Ü, Alivov Y, Morkoç H. Microwave ferrites, part 1: fundamental properties. Journal of Materials Science: Materials in Electronics. 2009 Sep;20(9):789-834.

[59] Goldman A. Chemical aspects of ferrites. Modern ferrite technology. 2006:71-110.

[60] Dionne GF. A review of ferrites for microwave applications. Proceedings of the IEEE. 1975 May;63(5):777-89.

[61] Batlle X, Labarta A. Finite-size effects in fine particles: magnetic and transport properties. Journal of Physics D: Applied Physics. 2002 Mar 5;35(6): R15.

[62] Goodenough JB. Summary of losses in magnetic materials. IEEE Transactions on magnetics. 2002 Dec 10;38(5):3398-408.

[63] Spark M, Loudon R, Kittle C. Ferromagnetic Relaxation. L'Ph) s. Ree. 1961; 122:791.

[64] Sparks M. Ferromagnetic-relaxation theory. McGraw-Hill; 1964.

[65] Karami MA, Shokrollahi H, Hashemi B. Investigation of nanostructural, thermal and magnetic properties of yttrium iron garnet synthesized by mechanochemical method. Journal of magnetism and magnetic materials. 2012 Sep 1;324(19):3065-72.

[66] Dionne GF. Magnetic oxides. New York: Springer; 2009 Oct 14; 15.

[67] Yahya N, Akhtar MN, Nasir N, Shafie A, Jabeli MS, Koziol K. Carbon nanotubes fibres/aluminium-NiZnFe2O4 based electromagnetic transmitter for improved magnitude versus offset (MVO) in a scaled marine environment. Journal of nanoscience and nanotechnology. 2012 Oct 1;12(10):8100-9.

[68] Bertaut F, Forrat F, Fang P. Comptes Rendus Acad. Fr. 1956;242:382.

[69] Xu H, Yang H, Xu W, Feng S. Magnetic properties of Ce, Gd-substituted yttrium iron garnet ferrite powders fabricated using a sol–gel method. Journal of Materials processing technology. 2008 Feb 1;197(1-3):296-300.

[70] Harris VG. Modern microwave ferrites. IEEE Transactions on Magnetics. 2011 Dec 21;48(3):1075-104.

[71] Tatarenko AS, Srinivasan G, Bichurin MI. Magnetoelectric microwave phase shifter. Applied Physics Letters. 2006 May 1;88(18):183507.

[72] He Y, He P, Harris VG, Vittoria C. Role of ferrites in negative index metamaterials. IEEE transactions on magnetics. 2006 Sep 25;42(10):2852-4.

[73] He P, Parimi PV, He Y, Harris VG, Vittoria C. Tunable negative refractive index metamaterial phase shifter. Electronics Letters. 2007 Dec 18;43(25):1440-1.

[74] He P, Gao J, Chen Y, Parimi PV, Vittoria C, Harris VG. Q-band tunable negative refractive index metamaterial using Sc-doped BaM hexaferrite. Journal of Physics D: Applied Physics. 2009 Jul 17;42(15):155005.

[75] Hong JS, Lancaster MJ. Microstrip filters for RF/microwave applications. John Wiley & Sons; 2004 Apr 7.

[76] Tsai CS, Qiu G, Gao H, Yang LW, Li GP, Nikitov SA, Gulyaev Y. Tunable wideband microwave band-stop and band-pass filters using YIG/GGG-GaAs layer structures. IEEE transactions on magnetics. 2005 Oct 17;41(10):3568-70.

[77] Gillette SM, Geiler AL, Chen Z, Chen Y, Arruda T, Xie C, Wang L, Zhu X, Liu M, Mukerjee S, Vittoria C. Active tuning of a microstrip hairpin-line microwave bandpass filter on a polycrystalline yttrium iron garnet substrate using small magnetic fields. Journal of Applied Physics. 2011 Apr 1;109(7):07A513.

[78] Ganne JP, Lebourgeois R, Paté M, Dubreuil D, Pinier L, Pascard H. The electromagnetic properties of Cu-substituted garnets with low sintering temperature. Journal of the European Ceramic Society. 2007 Jan 1;27(8-9):2771-7.

[79] Krishnaveni T, Kanth BR, Raju VS, Murthy SR. Fabrication of multilayer chip inductors using Ni–Cu–Zn ferrites. Journal of alloys and compounds. 2006 Apr 13;414(1-2):282-6.

[80] Chénais S, Druon F, Forget S, Balembois F, Georges P. On thermal effects in solid-state lasers: The case of ytterbium-doped materials. Progress in quantum electronics. 2006 Jan 1;30(4):89-153.

[81] Khazanov E. Faraday isolators for high average power lasers. InAdvances in Solid State Lasers Development and Applications 2010 Feb 1. IntechOpen.

[82] Kagamitani Y, Pawlak DA, Sato H, Yoshikawa A, Machida H, Fukuda T. Annealing effect in terbium–scandium–aluminum garnet single crystal. Japanese journal of applied physics. 2002 Oct 1;41(10R):6020.

[83] Yoshikawa A, Kagamitani Y, Pawlak DA, Sato H, Machida H, Fukuda T. Czochralski growth of Tb3Sc2Al3O12 single crystal for Faraday rotator. Materials research bulletin. 2002 Jan 1;37(1):1-0.

[84] Tan LR, Wu RX, Wang CY, Poo Y. Magnetically tunable ferrite loaded SIW antenna. IEEE Antennas and Wireless Propagation Letters. 2013 Feb 21;12:273-5.

[85] Anupama AV, Kumar R, Choudhary HK, Sahoo B. Synthesis of coral-shaped yttrium-aluminium-iron garnets by solution-combustion method. Ceramics International. 2018 Feb 15;44(3):3024-31.

[86] Tholkappiyan R, Vishista K. Tuning the composition and magnetostructure of dysprosium iron garnets by Co-substitution: An XRD, FT-IR, XPS and VSM study. Applied Surface Science. 2015 Oct 1; 351:1016-24.

[87] Zhao DL, Lv Q, Shen ZM. Fabrication and microwave absorbing properties of Ni–Zn spinel ferrites. Journal of Alloys and Compounds. 2009 Jul 8;480(2):634-8.

[88] Xu H, Yang H, Xu W, Feng S. Magnetic properties of Ce, Gd-substituted yttrium iron garnet ferrite powders fabricated using a sol–gel method. Journal of Materials processing technology. 2008 Feb 1;197(1-3):296-300.

[89] Qureshi A, Mergen A, Aktaş B. Dielectric and magnetic properties of YIG/PMMA nanocomposites. InJournal of Physics: Conference Series 2009 Mar 1 (Vol. 153, No. 1, p. 012061). IOP Publishing.

[90] Mallmann EJ, Sombra AS, Goes JC, Fechine PB. Yttrium iron garnet: properties and applications review. InSolid State Phenomena 2013 (Vol. 202, pp. 65-96). Trans Tech Publications Ltd.

[91] Zheng Z, Zhang H, Xiao JQ, Bai F. Low Loss NiZn/Co2Z Composite Ferrite with Almost Equal Values of Permeability and Permittivity for Antenna Applications. IEEE Transactions on Magnetics. 2013 Jul 15;49(7):4214-7.

[92] Varouti E, Rongas DK, Manios E, Kakoyiannis CG, Zervos T, Pissas M, Fikioris G. Properties of aluminum-substituted YIG with applications in tunable notched UWB antennas. In2014 Loughborough Antennas and Propagation Conference (LAPC) 2014 Nov 10 (pp. 713-716). IEEE.

[93] Akhtar MN, Khan MA, Ahmad M, Murtaza G, Raza R, Shaukat SF, Asif MH, Nasir N, Abbas G, Nazir MS, Raza MR. Y3Fe5O12 nanoparticulate garnet ferrites: comprehensive study on the synthesis and characterization fabricated by various routes. Journal of magnetism and magnetic materials. 2014 Nov 1; 368:393-400.

[94] Zhang T, Su H, Tang X, Zhang H, Jing Y, Li Y. Low loss Co2Z hexaferrite with matched permeability and permittivity in HF and VHF bands. Journal of Magnetism and Magnetic Materials. 2015 May 15; 382:283-7.

[95] Hasan IH, Hamidon MN, Ismail I, Osman R, Ismail A. Yttrium iron garnet thick film inclusion for enhanced microstrip patch antenna performance. In 2017 IEEE Regional

Symposium on Micro and Nanoelectronics (RSM) 2017 Aug 23 (pp. 131-134). IEEE.

[96] Fechine PB, Fontgalland G, Sombra AS. New materials for miniaturized magneto-dielectric antennas based on GdIGxYIG1-x composite. In2016 IEEE International Symposium on Antennas and Propagation (APSURSI) 2016 Jun 26 (pp. 1939-1940). IEEE.

[97] Andreou E, Zervos T, Varouti E, Pissas M, Christides C, Alexandridis AA, Fikioris G. Magneto-dielectric substrate influence on the efficiency of a reconfigurable patch antenna. In2017 International workshop on antenna technology: small antennas, innovative structures, and applications (iWAT) 2017 Mar 1 (pp. 191-194). IEEE.

[98] Akhtar MN, Ali K, Umer A, Ahmad T, Khan MA. Structural elucidation, and morphological and magnetic behavior evaluations, of low-temperature sintered, Ce-doped, nanostructured garnet ferrites. Materials Research Bulletin. 2018 May 1; 101:48-55.

[99] Aakansha, Deka B, Ravi S. Magnetic and Dielectric Properties of $Y_{3-x}Fe_5O_{12}$ (x = 0.0 to 0.3). Journal of Superconductivity and Novel Magnetism. 2018 31: 2121-2129.

[100] Bhalekar AR, Singh LN. Structural and magnetic studies of Al-doped Y2. 8 La0. 2 Fe5 O12 nanoferrites prepared by a sol-gel route. Journal of Superconductivity and Novel Magnetism. 2020 Jun;33(6):1859-70.

[101] Shafiee FN, Azis RA, Abdullah NH, Mustaffa MS, Nazlan R, Ismail I, Hamidon MN, Hasan IH. Potential patch antenna application with particle size variation in polycrystalline gadolinium iron garnet (GdIG). Journal of the Australian Ceramic Society. 2020 Sep;56(3):1097-105.

[102] Musa MA, Azis RA, Dong X, Osman NH, Hassan J, Muhammad FD, Mokhtar N. Influence of aluminum substitution on microstructural, electrical, dielectric, and electromagnetic properties of sol-gel synthesized yttrium iron garnet (YIG). AIP Advances. 2020 Apr 1;10(4):045128.

[103] Khalifeh MR, Shokrollahi H, Arab SM, Yang H. The role of Dy incorporation in the magnetic behavior and structural characterization of synthetic Ce, Bi-substituted yttrium iron garnet. Materials Chemistry and Physics. 2020 Jun 1; 247:122838.

[104] Gao F, Li J, Su H, Sun Y, Yang Y, Wang G, Han X, Li Q. Low dielectric loss and narrow FMR linewidth of Ca-Ge co-substituted YInIG ferrites for microwave device application. Journal of Alloys and Compounds. 2021 Dec 10; 885:160965.

[105] Li J, Sun Y, Gao F, Su H, Han X, Liang Z, Zhang H, Li Q. Enhanced FMR linewidth and magnetic properties of In3+-doped YIG ferrite materials for microwave devices applications. Journal of Magnetism and Magnetic Materials. 2021 Nov 15; 538:168318.

[106] Sibi N, Ganesanpotti S. Magnetodielectric response of composites based on a natural garnet and spinel ferrites for sub-GHz wireless applications. Ceramics International. 2021 Aug 1;47(15):21404-13.

[107] Dewi SH, Mulyawan A, Sarwanto Y, Winatapura DS, Adi WA. Effect of La3+ substitution on structural, microstructure, magnetic properties, and microwave absorbing ability of yttrium iron garnet. Journal of Rare Earths. 2022 Mar 14.

[108] Ji X, Zhou K, Zhao Y, Sun M, Dong S, Zhang H, Cao H, Zheng H, Wu Q, Zhang Y. Crystal Structure, Magnetic, Dielectric and Ferromagnetic Resonance Properties of Pr-Zn-Zr Co-Doped Yttrium Iron Garnet. Journal of Electronic Materials. 2022 Jan 2:1-9.

[109] Fu R, Li Y, Peng R, Lu Y, Wen Q. High Dielectric Constant YIG Ferrites with Low Sintering Temperature. Journal of Materials Science: Materials in Electronics. 2022 Jan 13:1-0.

[110] Mohd Shahrani NM, Hashim M, Hassan J, Azmi Z, Daud N. Effect of variation sintering temperature on magnetic permeability and grain sizes of Y3Fe5O12 via mechanical alloying technique. InMaterials Science Forum 2016 (Vol. 846, pp. 395-402). Trans Tech Publications Ltd.

[111] Mustaffa MS, Shahrani NM. Sintering temperature effect on microstructure and magnetic evolution properties with nano-and micrometer grain size in ferrite polycrystals. InSintering Technology-Method and Application 2018 Nov 5. IntechOpen.

[112] Thakur P, Sharma R, Sharma V, Sharma P. Structural and optical properties of Mn0. 5Zn0. 5Fe2O4 nano ferrites: effect of sintering temperature. Materials Chemistry and Physics. 2017 Jun 1; 193:285-9.

[113] Rastogi AC, Moorthy VN. Magnetic properties of multilayers of nano thin Co, Ce-doped

and undoped yttrium iron garnet films for magneto-optic applications. Materials Science and Engineering: B. 2002 Aug 1;95(2):131-6.

[114] Azis RS, Syazwan MM, Shahrani NM, Hapishah AN, Nazlan R, Idris FM, Ismail I, Zulkimi MM, Ibrahim IR, Abbas Z, Saiden NM. Influence of sintering temperature on the structural, electrical and microwave properties of yttrium iron garnet (YIG). Journal of Materials Science: Materials in Electronics. 2018 May;29(10):8390-401.

[115] Chen C, Cheng J, Yu S, Che L, Meng Z. Hydrothermal synthesis of perovskite bismuth ferrite crystallites. Journal of Crystal Growth. 2006 May 15;291(1):135-9.

[116] Singh V, Sharma S, Jha PK, Kumar M, Dwivedi RK. Effect of Y3+ substitution on structural, electrical and optical properties of BiFeO3 ceramics. Ceramics International. 2014 Jan 1;40(1):1971-7.

[117] Chen R, Zhou J, Zheng L, Zheng H, Zheng P, Ying Z, Deng J. Two-step sintering behavior of sol–gel derived dense and submicron-grained YIG ceramics. Journal of Electronic Materials. 2018 Apr;47(4):2411-6.

[118] Nazlan R, Hashim M, Abdullah NH, Ibrahim IR, Ismail I. Influence of milling time on the crystallization, morphology and magnetic properties of polycrystalline yttrium iron garnet. InAdvanced Materials Research 2012 (Vol. 501, pp. 324-328). Trans Tech Publications Ltd.

[119] Ramesh T, Rao GN, Suneetha T, Shinde RS, Rajendar V, Murthy SR, Kumar SA. Microwave-hydrothermal synthesis of Y3Fe5O12 nanoparticles: sintering temperature effect on structural, magnetic and dielectric properties. Journal of Superconductivity and Novel Magnetism. 2018 Jun;31(6):1899-908.

[120] Mousavi Ghahfarokhi SE, Mohammadzadeh Shobegar E, Zargar Shoushtari M. Effects of sintering temperature on structural, morphological and magnetic properties of strontium ferrite nanoparticles. Journal of Superconductivity and Novel Magnetism. 2019 Apr;32(4):1067-76.

[121] Fernandes C, Pereira C, Fernandez-Garcia MP, Pereira AM, Guedes A, Fernandez-Pacheco R, Ibarra A, Ibarra MR, Araujo JP, Freire C. Tailored design of Co x Mn 1− x Fe 2 O 4 nanoferrites: a new route for dual control of size and magnetic properties. Journal of Materials Chemistry C. 2014;2(29):5818-28.

[122] Su J, Lu X, Zhang C, Zhang J, Peng S, Wu X, Min K, Huang F, Zhu J. The effect of sintering temperature on magnetic and dielectric properties of Ho3Fe5O12 ceramics. Journal of materials science. 2011 May;46(10):3488-92.

[123] Popa PD, Rezlescu E, Doroftei C, Rezlescu N. Influence of calcium on properties of strontium and barium ferrites for magnetic media prepared by combustion. J. Optoelectron. Adv. Mater. 2005 Jun 1; 7:1553-6.

[124] Mürbe J, Töpfer J. High permeability Ni–Cu–Zn ferrites through additive-free low-temperature sintering of nanocrystalline powders. Journal of the European Ceramic Society. 2012 May 1;32(5):1091-8.

[125] Lin Q, He Y, Xu J, Lin J, Guo Z, Yang F. Effects of Al3+ substitution on structural and magnetic behavior of CoFe2O4 ferrite Nanomaterials. Nanomaterials. 2018 Oct;8(10):750.

[126] Kumar L, Kar M. Influence of Al3+ ion concentration on the crystal structure and magnetic anisotropy of nanocrystalline spinel cobalt ferrite. Journal of Magnetism and Magnetic Materials. 2011 Aug 1;323(15):2042-8.

[127] KUO MF, HUNG YH, HUANG JY, HUANG CC. Structure and magnetic properties of Mn and Al doped magnesium ferrite. China Steel Technical Report. 2016; 29:44-8.

[128] Smit J, Wijn HP. Physical properties of ferrites. InAdvances in Electronics and Electron Physics 1954 Jan 1 (Vol. 6, pp. 69-136). Academic Press.

[129] Kotnala RK, Ahmad S, Ahmed AS, Shah J, Azam A. Investigation of structural, dielectric, and magnetic properties of hard and soft mixed ferrite composites. Journal of Applied Physics. 2012 Sep 1;112(5):054323.

[130] Rahman MA, Gafur MA, Hossain AA. Structural, magnetic and transport properties of magnetoelectric composites. Journal of magnetism and magnetic materials. 2013 Nov 1; 345:89-95.

[131] Mohamed MB, El-Sayed K. Microstructure, magnetic and electric properties of BaTiO3–Ni0. 5Zn0. 5Fe1. 5Cr0. 5O4 nanocomposite. Materials Research Bulletin. 2013 May 1;48(5):1778-83.

[132] Torkian S, Ghasemi A, Razavi RS. Magnetic properties of hard-soft SrFe10Al2O19/Co0.

8Ni0. 2Fe2O4 ferrite synthesized by one-pot sol–gel auto-combustion. Journal of Magnetism and Magnetic Materials. 2016 Oct 15; 416:408-16.

[133] López-Ortega A, Estrader M, Salazar-Alvarez G, Roca AG, Nogués J. Applications of exchange coupled bi-magnetic hard/soft and soft/hard magnetic core/shell nanoparticles. Physics Reports. 2015 Feb 1; 553:1-32.

[134] Mohammed J, Suleiman AB, Carol TT, Hafeez HY, Sharma J, Maji PK, Kumar SG, Srivastava AK. Enhanced dielectric and optical properties of nanoscale barium hexaferrites for optoelectronics and high frequency application. Chinese Physics B. 2018 Dec 1;27(12):128104.

[135] Roy D, Shivakumara C, Kumar PA. Observation of the exchange spring behavior in hard–soft-ferrite nanocomposite. Journal of magnetism and magnetic materials. 2009 Mar 1;321(5):L11-4.

[136] Rai BK, Wang L, Mishra SR, Nguyen VV, Liu JP. Synthesis and magnetic properties of hard-soft SrFe10Al2O19/NiZnFe2O4 ferrite nanocomposites. Journal of Nanoscience and Nanotechnology. 2014 Jul 1;14(7):5272-7.

[137] Reetu, Agarwal A, Sanghi S, Ashima, Ahlawat N. Improved dielectric and magnetic properties of Ti modified BiCaFeO3 multiferroic ceramics. Journal of Applied Physics. 2013 Jan 14;113(2):023908.

[138] Garcia-Fernandez P, Aramburu JA, Barriuso MT, Moreno M. Key role of covalent bonding in octahedral tilting in perovskites. The Journal of Physical Chemistry Letters. 2010 Feb 4;1(3):647-51.

[139] Mizokawa T, Khomskii DI, Sawatzky GA. Interplay between orbital ordering and lattice distortions in LaMnO 3, YVO 3, and YTiO 3. Physical Review B. 1999 Sep 1;60(10):7309.

[140] Raghuvanshi S, Mazaleyrat F, Kane SN. Mg1-xZnxFe2O4 nanoparticles: Interplay between cation distribution and magnetic properties. AIP Advances. 2017 Oct 17;8(4):047804.

[141] Wright JP, McLaughlin AC, Attfield JP. Partial frustration of magnetic order in synthetic angelellite, Fe 4 As 2 O 11. Journal of the Chemical Society, Dalton Transactions.

2000(20):3663-8.

[142] Guo M, Liu W, Xu X, Wu P, Zhang H, Han Y, Rao G, Wang S. The effect of Fe–O–Fe bond angle on modulating multiferroic properties of Ba–K-codoped BiFeO3 nanoparticles. Journal of Nanoparticle Research. 2015 Nov;17(11):1-8.

[143] Rahman MT, Vargas M, Ramana CV. Structural characteristics, electrical conduction and dielectric properties of gadolinium substituted cobalt ferrite. Journal of Alloys and Compounds. 2014 Dec 25; 617:547-62.

[144] Bammannavar BK, Naik LR, Chougule BK. Studies on dielectric and magnetic properties of (x) Ni 0.2 Co 0.8 Fe 2 O 4+(1− x) barium lead zirconate titanate magnetoelectric composites. Journal of Applied Physics. 2008 Sep 15;104(6):064123.

[145] Prodromakis T, Papavassiliou C. Engineering the Maxwell–Wagner polarization effect. Applied Surface Science. 2009 May 15;255(15):6989-94.

[146] Murthy VR, Sobhanadri J. Electrical conductivity of some nickel-zinc ferrites. physica status solidi (a). 1976 Dec 16;38(2):647-51.

[147] Algarou NA, Slimani Y, Almessiere MA, Rehman S, Younas M, Unal B, Korkmaz AD, Gondal MA, Trukhanov AV, Baykal A, Nahvi I. Developing the magnetic, dielectric and anticandidal characteristics of SrFe12O19/(Mg0. 5Cd0. 5Dy0. 03Fe1. 97O4) x hard/soft ferrite nanocomposites. Journal of the Taiwan Institute of Chemical Engineers. 2020 Aug 1; 113:344-62.

[148] Dagar S, Hooda A, Khasa S, Malik M. Rietveld refinement, dielectric and magnetic properties of NBT-Spinel ferrite composites. Journal of Alloys and Compounds. 2019 Oct 25; 806:737-52.

[149] Davies JE, Hellwig O, Fullerton EE, Jiang JS, Bader SD, Zimanyi GT, Liu K. Anisotropy dependence of irreversible switching in Fe⁄ Sm Co and Fe Ni⁄ Fe Pt exchange spring magnet films. Applied Physics Letters. 2005 Jun 27;86(26):262503.

[150] Zhang L, Li Z. Synthesis and characterization of SrFe12O19/CoFe2O4 nanocomposites with core-shell structure. Journal of alloys and compounds. 2009 Feb 5;469(1-2):422-6.

[151] Liu JP. Exchange-coupled nanocomposite permanent magnets. Nanoscale Magnetic Materials and Applications. 2009:309-35.

[152] Rong CB, Zhang HW, Chen RJ, He SL, Shen BG. The role of dipolar interaction in nanocomposite permanent magnets. Journal of magnetism and magnetic materials. 2006 Jul 1;302(1):126-36.

[153] Du HF, Du A. Effect of exchange and dipolar interactions on the hysteresis of magnetic nanoparticle systems. physica status solidi (b). 2007 Apr;244(4):1401-8.

[154] Pandey R, Pradhan LK, Kar M. Structural, magnetic, and electrical properties of (1–x) Bi0. 85La0. 15FeO3-(x) CoFe2O4 multiferroic composites. Journal of Physics and Chemistry of Solids. 2018 Apr 1; 115:42-8.

[155] Gan G, Zhang D, Li J, Wang G, Yang Y, Wang X, Zhang H. Effect of temperature on magnetic and dielectric properties of Mg-Cd-Ga ferrites for high-frequency-range antennas. InJournal of Physics: Conference Series 2021 Mar 1 (Vol. 1802, No. 2, p. 022078). IOP Publishing.

[156] Kolekar YD, Sanchez L, Rubio EJ, Ramana CV. Grain and grain boundary effects on the frequency and temperature dependent dielectric properties of cobalt ferrite–hafnium composites. Solid State Communications. 2014 Apr 1; 184:34-9.

[157] Nongjai R, Khan S, Asokan K, Ahmed H, Khan I. Magnetic and electrical properties of In doped cobalt ferrite nanoparticles. Journal of applied physics. 2012 Oct 15;112(8):084321.

[158] Zhang S, Priya S, Shrout TR, Randall CA. Low frequency polarization behavior of x BiScO 3–y BiGaO 3–(1− x− y) PbTiO 3 piezocrystals. Journal of applied physics. 2003 Mar 1;93(5):2880-3.

[159] Fawzi AS. Effect of sintering temperature on structural, electrical, magnetic hysteresis and magnetoelectric effect on (x) Ni0. 7Zn0. 3Fe2O4+(1− x) PLZT composite by co-precipitation method. Adv Appl Sci Res. 2011; 2:577-89.

[160] Liu J, Duan CG, Yin WG, Mei WN, Smith RW, Hardy JR. Large dielectric constant and Maxwell-Wagner relaxation in Bi 2⁄ 3 Cu 3 Ti 4 O 12. Physical review B. 2004 Oct 12;70(14):144106.

[161] Ortega N, Kumar A, Bhattacharya P, Majumder SB, Katiyar RS. Impedance spectroscopy of multiferroic Pb Zr x Ti 1− x O 3⁄ Co Fe 2 O 4 layered thin films. Physical Review B.

2008 Jan 28;77(1):014111.

[162] Bharathi KK, Markandeyulu G, Ramana CV. AIP Adv. 2, 012139 (2012).

[163] Sinclair DC, Adams TB, Morrison FD, West AR. CaCu 3 Ti 4 O 12: one-step internal barrier layer capacitor. Applied Physics Letters. 2002 Mar 25;80(12):2153-5.

[164] Anand M, Banerjee V, Carrey J. Relaxation in one-dimensional chains of interacting magnetic nanoparticles: Analytical formula and kinetic Monte Carlo simulations. Physical Review B. 2019 Jan 3;99(2):024402.

[165] Šepelák V, Menzel M, Bergmann I, Wiebcke M, Krumeich F, Becker KD. Structural and magnetic properties of nanosize mechanosynthesized nickel ferrite. Journal of magnetism and magnetic materials. 2004 May 1; 272:1616-8.

[166] Patankar KK, Nipankar RP, Mathe VL, Mahajan RP, Patil SA. Role of sintering on magneto-electric effect in CuFe1. 8Cr0. 2O4–Ba0. 8Pb0. 2Ti0. 8Zr0. 2O3 composite ceramics. Ceramics international. 2001 Jan 1;27(8):853-8.

[167] Mohaidat QI, Lataifeh M, Hamasha K, Mahmood SH, Bsoul I, Awawdeh M. The structural and the magnetic properties of aluminum substituted yttrium iron garnet. Materials Research. 2018 Mar 15;21.

[168] Anupama MK, Rudraswamy B. Effect of Gd3+-Cr3+ ion substitution on the structural, electrical and magnetic properties of Ni-Zn ferrite nanoparticles. InIOP Conference Series: Materials Science and Engineering 2016 Sep 1 (Vol. 149, No. 1, p. 012194). IOP Publishing.

[169] Sharma V, Kuanr BK. Magnetic and crystallographic properties of rare-earth substituted yttrium-iron garnet. Journal of Alloys and Compounds. 2018 Jun 5; 748:591-600.

[170] Basavad M, Shokrollahi H, Ahmadvand H, Arab SM. Structural, magnetic and magneto-optical properties of the bulk and thin film synthesized cerium-and praseodymium-doped yttrium iron garnet. Ceramics International. 2020 Jun 1;46(8):12015-22.

[171] Leoni M, Martinez-Garcia J, Scardi P. Dislocation effects in powder diffraction. Journal of Applied Crystallography. 2007 Aug 1;40(4):719-24.

[172] Manikandan A, Vijaya JJ, Sundararajan M, Meganathan C, Kennedy LJ, Bououdina M.

Optical and magnetic properties of Mg-doped ZnFe2O4 nanoparticles prepared by rapid microwave combustion method. Superlattices and Microstructures. 2013 Dec 1; 64:118-31.

[173] Shokrollahi HE, Janghorban K. Soft magnetic composite materials (SMCs). Journal of Materials Processing Technology. 2007 Jul 6;189(1-3):1-2.

[174] Raad NA, Shokrollahi H, Basavad M, Arab SM. Magnetic performance and structural evaluation of La, Ce, Bi-substituted yttrium iron garnets. Ceramics International. 2020 Sep 1;46(13):21551-9.

[175] Tadic M, Panjan M, Damnjanovic V, Milosevic I. Magnetic properties of hematite (α-Fe2O3) nanoparticles prepared by hydrothermal synthesis method. Applied Surface Science. 2014 Nov 30; 320:183-7.

[176] Khan RA, Mizukami S, Khan AM, Ismail B, Khan AR, Miyazaki T. Static and dynamic magnetic characteristics of Mg substituted Ba–Co2 W-type hexaferrites. Journal of Alloys and Compounds. 2015 Jul 15; 637:197-202.

[177] Shafiee FN, Mustaffa MS, Abdullah NH, Hamidon MN, Ismail I, Nazlan R, Ibrahim IR, Idris FM, Shafie MS. Effect of microstructural evolution from nano to micron grain size regime towards structural, magnetic, electrical and microwave properties of gadolinium iron garnet (Gd3Fe5O12). Journal of Materials Science: Materials in Electronics. 2021 Apr;32(8):10160-79.

[178] Sharma A, Godara SK, Maji PK, Srivastava AK. Influence of Temperature on Structural and Magnetic Properties of Gd3AlxFe5− xO12 (x= 2). Crystal Research and Technology. 2022 Feb;57(2):2100109.

[179] Qindeel R, Alonizan NH. Improved structural and magnetic properties of Polypyrrole substituted spinel ferrites composites. Materials Science and Engineering: B. 2019 May 1; 244:43-8.

[180] Shi ZC, Fan RH, Wang XA, Zhang ZD, Qian L, Yin LW, Bai YJ. Radio-frequency permeability and permittivity spectra of copper/yttrium iron garnet cermet prepared at low temperatures. Journal of the European Ceramic Society. 2015 Apr 1;35(4):1219-25.

[181] Haijun Z, Zhichao L, Xi Y, Liangying Z, Mingzhong W. Dielectric and magnetic

properties of ZnCo-substituted X hexaferrites prepared by citrate sol–gel process. Materials research bulletin. 2003 Jan 25;38(2):363-72.

[182] Sadiq I, Ali I, Rebrov EV, Naseem S, Ashiq MN, Rana MU. Influence of Nd-Co substitution on structural, electrical, and dielectric properties of x-type hexagonal nanoferrites. Journal of materials engineering and performance. 2014 Feb;23(2):622-7.

[183] Sivakumar N, Narayanasamy A, Ponpandian N, Govindaraj G. Grain size effect on the dielectric behavior of nanostructured Ni 0.5 Zn 0.5 Fe 2 O 4. Journal of applied physics. 2007 Apr 15;101(8):084116.

[184] Paiva DV, Silva MA, Ribeiro TS, Vasconcelos IF, Sombra AS, Góes JC, Fechine PB. Novel magnetic–dielectric composite ceramic obtained from Y3Fe5O12 and CaTiO3. Journal of Alloys and Compounds. 2015 Sep 25; 644:763-9.

[185] Sharif MK, Khan MA, Hussain A, Iqbal F, Shakir I, Murtaza G, Akhtar MN, Ahmad M, Warsi MF. Synthesis and characterization of Zr and Mg doped BiFeO3 nanocrystalline multiferroics via micro emulsion route. Journal of Alloys and Compounds. 2016 May 15; 667:329-40.

[186] Jung HK, Kim CH, Hong AR, Lee SH, Kim TC, Jang HS, Kim DH. Luminescent and magnetic properties of cerium-doped yttrium aluminum garnet and yttrium iron garnet composites. Ceramics International. 2019 Jun 1;45(8):9846-51.

[187] Khan RA, Mizukami S, Khan AM, Ismail B, Khan AR, Miyazaki T. Static and dynamic magnetic characteristics of Mg substituted Ba–Co2 W-type hexaferrites. Journal of Alloys and Compounds. 2015 Jul 15; 637:197-202.

[188] Rahman MA, Gafur MA, Hossain AA. Structural, magnetic and transport properties of magnetoelectric composites. Journal of magnetism and magnetic materials. 2013 Nov 1; 345:89-95.

[189] Torkian S, Ghasemi A, Razavi RS. Magnetic properties of hard-soft SrFe10Al2O19/Co0. 8Ni0. 2Fe2O4 ferrite synthesized by one-pot sol–gel auto-combustion. Journal of Magnetism and Magnetic Materials. 2016 Oct 15; 416:408-16.

[190] Sharma A, Godara SK, Srivastava AK. Effect of Y3+, Bi3+, La3+ substitution on structural, optical and magnetic properties of gadolinium iron garnets. Materials Today:

Proceedings. 2022 Jan 1; 50:1867-77.

[191] Mohamed MB, Karimat ES. Structural, magnetic and dielectric properties of (PANI)–Ni0. 5Zn0. 5Fe1. 5Cr0. 5O4 nanocomposite. Composites Part B: Engineering. 2014 Jan 1; 56:270-8.

[192] Jacobo SE, Bercoff PG, Herme CA, Vives LA. Sr hexaferrite/Ni ferrite nanocomposites: magnetic behavior and microwave absorbing properties in the X-band. Materials Chemistry and Physics. 2015 May 1; 157:124-9.

[193] Bhongale SR. Mg-Nd-Cd ferrite as substrate for X-band microstrip patch antenna. Journal of Magnetism and Magnetic Materials. 2020 Apr 1; 499:165918.

[194] Akhtar MN, Sulong AB, Ahmad M, Khan MA, Ali A, Islam MU. Impacts of Gd–Ce on the structural, morphological and magnetic properties of garnet nanocrystalline ferrites synthesized via sol–gel route. Journal of Alloys and Compounds. 2016 Mar 5; 660:486-95.

[195] Chavan P. Facile Synthesis, Diffused Reflectance Spectroscopy & Fluorescence Studies of Ni0. 5− xMg0. 5CuxFe2O4 Nanoparticles. Journal of Fluorescence. 2021 Jul;31(4):1023-8.

[196] Chavan P, Naik LR, Belavi PB, Chavan GN, Kotnala RK. Synthesis of Bi3+ substituted Ni-Cu ferrites and study of structural, electrical and magnetic properties. Journal of Alloys and Compounds. 2017 Feb 15; 694:607-12.

[197] Talukdar S, Rakshit R, Krämer A, Müller FA, Mandal K. Facile surface modification of nickel ferrite nanoparticles for inherent multiple fluorescence and catalytic activities. RSC advances. 2018;8(1):38-43.

[198] Karilainen AO, Ikonen PM, Simovski CR, Tretyakov SA, Lagarkov AN, Maklakov SA, Rozanov KN, Starostenko SN. Experimental studies on antenna miniaturisation using magneto-dielectric and dielectric materials. IET microwaves, antennas & propagation. 2011 Mar 21;5(4):495-502.

[199] Bolivar PH, Brucherseifer M, Rivas JG, Gonzalo R, Ederra I, Reynolds AL, Holker M, De Maagt P. Measurement of the dielectric constant and loss tangent of high dielectric-constant materials at terahertz frequencies. IEEE Transactions on Microwave Theory and

Techniques. 2003 Apr 8;51(4):1062-6.

[200] Huitema L, Reveyrand T, Mattei JL, Arnaud E, Decroze C, Monediere T. Frequency tunable antenna using a magneto-dielectric material for DVB-H application. IEEE Transactions on Antennas and Propagation. 2013 Jun 18;61(9):4456-66.

Anjori Sharma

Female

Email: anjori.sharma1995@gmail.com

M: +91-7986150413

ACADEMIC QUALIFICATIONS

Year	Degree	Institute	CGPA / Percentage
2022	Ph.D. (Physics)	Lovely Professional University, Phagwara	9.34/10
2019	M.Sc. (Physics-Honors)	Lovely Professional University, Phagwara	8.35/10
2016	B.Sc. (General)	Guru Nanak Dev University, Amritsar	61%
2013	XII (CBSE)	Jawahar Navodaya Vidyalaya, Kapurthala	65%
2011	X (CBSE)	Jawahar Navodaya Vidyalaya, Kapurthala	9/10

PROJECT

Lovely Professional University *Jan2018-2019*

- **Effect of C^{+6} 80 MeV on Ferrous Chloride doped PVC blend.:** Undergone the dissertation of twelve months. The main objective of the project was to check whether heavy swift ion exposers tailors the property of polymer sample better than doped samples or not. The methodology that has being followed is Nano-Technology. The major outcome which has been obtained: enhancement in the absorption coefficient, strength, conductivity of exposed sample with less cost. Results shows that after exposer of Carbon ion the conductivity as well strength of the sample enhances. The major applications of the prepared samples are solar cells.

CARRIER OBJECTIVE

Seeking a position to utilize my good research skills and industry that offers professional growth while being resourceful, innovative and flexible.

RESEARCH INTEREST

Ceramics materials, polymers, garnet ferrites, hexaferrites, spinel ferrites, ceramics composites, microwave losses, communication devices miniaturization, structural properties, morphological properties, electrical properties, dielectric properties, magnetic properties, optical properties

PUBLISHED RESEARCH ARTICLES

- "Effect of Y^{3+}, Bi^{3+}, La^{3+} substitution on structural, optical and magnetic properties of gadolinium iron garnets", Mater. Today: Proceed. (2021).
- "Influence of temperature on structural and magnetic properties of $Gd_3Al_xFe_{5-x}O_{12}$ (x=2)", Journal of Crystal Growth Technology. (2021).
- "Influence of composition variations on structural, magnetic and dielectric properties of $Gd_3Fe_5O_{12}$(x)/$MgFe_2O_4$(1-x) composite", Indian Journal of physics. (2022).
- "Influence of Mn^{2+}-substitution on structural, morphological and magnetic properties of CO_2Y strontium hexaferrites", Mater. Today: Proceed. (2022).
- "Structural, morphological, optical, magnetic, and microwave properties of La^{3+}- Mn^{2+} substituted Zn_2-Y-type barium-strontium hexaferrite", Chinese Journal of Physics. (2022).
- "Low dielectric losses and enhanced magnetic property of ErIG(x)/YIG(1-x) (x=0.5) composite for antenna applications", Bulletin of Materials Science. (2022)
- "Structural Morphological and Electrochemical Investigation of Mn0.3Co0.2Zn0.5Fe2O4-Polyaniline Nanocomposite for Supercapacitor Application", Journal of Materials Science: Materials in electronics. (2022)
- "Effect of sintering temperature on structural, morphological, magnetic, and electrochemical properties of Mn0.3Co0.2Zn0.5Fe2O4 Ferrite", Journal of Sol-Gel Science and Technology. (2022)

SKILL SET

Good in MS Office, Good in Excel, Power Point Presentation, Good communication and writing skills, Leadership, Teamwork, Good interpersonal Skills

SOFTWARE

Origin, X-Powder, ZSimpWin, ImageJ, Rietveld Refinement

DATA INTERPRETATION STRENGTH

X-ray Diffractogram (XRD), Fourier Transform Infrared spectroscopy (FTIR), Field Emission Scanning Electron Microscope (FESEM), Energy Dispersive X-ray spectroscopy (EDX), Ultraviolet-Visible (UV-vis) spectroscopy, Impedance analyzer, Vector Network Analyzer (VNA), LCR meter, Fluorescence spectroscopy, Vibrating Sample Magnetometer (VSM) and Thermogravimetric Analysis (TGA)

POSITIONS OF RESPONSIBILITY

- Coordinator, Indian Science Congress, Lovely Professional University *2019*
- Coordinator, Science Quiz Competition, Lovely Professional University *2018*
- Coordinator, Science Debate Competition, Lovely Professional University *2018*

EXTRA CURRICULAR ACTIVITIES

Workshops/Seminars

- Presented research paper in International Conference on Recent Advances in Materials, Manufacturing and Machine Learning, *2022*
- Presented research paper in International Conference on Recent Advances in Mechanical Engineering and Nanomaterials, *2022*
- Presented research paper in 2nd International Conference Functional Materials, Manufacturing and Performances, *2021*
- Attended workshop on **"Research Foundation"** Lovely Professional University, *2018*
- Attended workshop on **"Life of Saha, Fermi, Maxwell"** Lovely Professional University, *2018*
- Attended talk on **"Future application of spectroscopy"** Lovely Professional University, *2018*
- Attended talk on **"Spectroscopy and Laser"** Lovely Professional University, *2018*

Achievements/Participation

- Awarded "**Best Paper Presentation Award"** International Conference on Recent Advances in Mechanical Engineering and Nanomaterials, *2022*
- Awarded **"Best Paper Presentation Award"** International Conference on Recent Advances in Materials, Manufacturing and Machine Learning, *2022*
- Awarded **"3rd Prize in Poster Presentation"** Lovely Professional University, *2019*
- Participated in **"Gunnies World Bhangra Record"** Lovely Professional University, *2018*
- Awarded **"2nd Prize in Physpank"** Lovely Professional University, *2017*
- Participated in **"Folk Song, Spectra"** Lovely Professional University, *2017*

STRENGTH

- Investigation of properties of new materials
- Paper Writing
- Hardworking
- Loyal
- Patient
- Honest and punctual
- Flexibility in multi-tasking

LANGUAGE PROFICIENCY

- English, Punjabi, Hindi

PERSONAL DETAILS

- Date of Birth : 22nd October 1995
- Nationality : Indian
- Address : H. No 9, Mohallan Upplan, Sultanpur Lodhi, Kapurthala, Punjab-144626, India

RESEARCH ARTICLE

CRYSTAL Research & Technology

www.crt-journal.org

Influence of Temperature on Structural and Magnetic Properties of $Gd_3Al_xFe_{5-x}O_{12}$ ($x = 2$)

*Anjori Sharma, Sachin Kumar Godara, Pradip K. Maji, and A. K. Srivastava**

This research work explores the effect of sintering temperature on morphology and magnetic properties of aluminum substituted gadolinium iron garnet $Gd_3Al_xFe_{5-x}O_{12}$ ($x = 2$). Sol–gel autocombustion method is adopted to prepare $Gd_3Al_xFe_{5-x}O_{12}$, and further sintered at 900, 1000, and 1100 °C. X-ray diffraction (XRD) confirms the formation of garnet phase structure. Fourier transformation infrared ray further stands with result of XRD that reveals the presence of garnet phase. Field emission scanning microscope analysis shows the formation of average grain size 4, 6, and 13 nm for 900, 1000, and 1100 °C, respectively. Vibrating sample magnetometer results show that the coercivity decreases with increases in temperature, which indicates that this material can be used in switching devices. The calculated value of microwave operating frequency reveals that these materials can be used in ultrahigh-frequency region.

1. Introduction

Magnetic materials are always in the top list of researchers due to their vast number of applications.[1–3] From these magnetic materials ferrites exhibit ferrimagnetism are continuously attracting the focus of many researchers and industrialist due to their good magnetic as well as dielectric properties.[4,7] These iron containing ferrites has numerous applications in communication, microwave devices, miniaturization of devices, sensors, radio frequency circuits, switching cores, high-frequency application, and many more.[5–12] Ferrites are categories as soft ferrites such as spinel and garnet having cubic structure, and hard ferrite that is hexaferrite having hexagonal structure.

Garnet ferrites are best known for their very good magnetic, electromagnetic, dielectric, magneto optical and thermal properties.[14,16] These ferrites are superior than spinel ferrite and hexaferrite because of very high resistance, low magnetic and dielectric losses better stability in structure which is due to presence of rare earth ion on the interstitial sites.[17,18] Formula of iron garnets are generally represented by $R_3Fe_5O_{12}$, where R is any rare earth. Garnet ferrites have cubic crystal structure with *Ia3d* space group and depending upon the occupancy of cations of both iron and rare earth, magnetic properties can be altered. There are three sites present in garnet ferrites name as dodecahedral site 24c, this site is the largest site and occupied by ion of rare earth $\{R^{3+}\}$, octahedral site 16a occupied by iron ion $[F^{3+}]$ and tetrahedral site 24d occupied by iron ion (F^{3+}). Even though the net magnetic moment of a and d sublattice which are antiferromagnetically coupled is equal and opposite to that of c sublattice[19] but there is some net magnetization because of unequal magnitude of magnetic moments which do not properly cancel out each other. The properties of ferrites can be altered by substitution. By substitution of scandium in octahedral site increases the magnetization where by substitution of aluminum and gallium in tetrahedral site decreases the magnetization.[46] By substituting nonmagnetic aluminum in place of magnetic iron ion in YIG provides large number of applications.[59] Besides the magnetic property other properties like microstructure dielectric properties of garnet ferrites depend upon fabrication techniques and temperature.[20,21] Higher temperature provides grain growth which further increase grain size. This increase in grain size affects the magnetic properties like coercivity (H_c), squareness ratio (SQR), $4\pi M_s$, and others.[34] This can be understood as with increases in temperature grain size increase this means that single domain size is changing into multiple-domain size. So, at higher temperature dominant domain wall effects is observed. The magnetization field required for domain wall motion is very less. This means that temperature can alert both structural as well as magnetic properties of ferrites.

There are many synthesis methods for garnet ferrites. Ball milling method is the method which requires very high temperature, this method is widely used but have disadvantage in the form of inhomogeneity in product.[27] Hydrothermal technique is also become one of the interests of many researchers as this method provide very high speed of heating with good reaction kinetics which give high yield.[28] Another promising method is the sol–gel method[13,15] which provide better homogeneity in garnet

A. Sharma, A. K. Srivastava
Department of Physics
Lovely Professional University
Phagwara, Punjab 144411, India
E-mail: srivastava_phy@yahoo.co.in
S. K. Godara
Department of Chemistry
Guru Nanak Dev University
Amritsar, Punjab 143005, India
P. K. Maji
Department of Polymer and Process Engineering
IIT Roorkee
Saharanpur Campus, Uttar Pradesh 247001, India

The ORCID identification number(s) for the author(s) of this article can be found under https://doi.org/10.1002/crat.202100109

DOI: 10.1002/crat.202100109

Indian J Phys
https://doi.org/10.1007/s12648-022-02365-5

ORIGINAL PAPER

Influence of composition variation on structural, magnetic and dielectric properties of $Gd_3Fe_5O_{12}$(x)/$MgFe_2O_4$(1−x) composite

A Sharma[1], S K Godara[2] and A K Srivastava[1]*

[1]Department of Physics, Lovely Professional University, Phagwara, Punjab 144411, India

[2]Department of Chemistry, Guru Nanak Dev University, Amritsar, Punjab 143005, India

Received: 21 September 2021 / Accepted: 05 April 2022

Abstract: Sol–gel auto-combustion method was used to prepare $Gd_3Fe_5O_{12}$ and $MgFe_2O_4$. Mechanical blending was used to form the composites of $Gd_3Fe_5O_{12}$ (x)−$MgFe_2O_4$ (1−x) (x = 1.0, 0.5, 0.75 in wt.%). X-ray diffraction (XRD) study reveals the pure phase formation of $Gd_3Fe_5O_{12}$ and $MgFe_2O_4$ and the presence of both phases in composites. The average crystallite size lies in the range of 26–56 nm. Field emission scanning electron microscope (FESEM) study reveals that the grains of $Gd_3Fe_5O_{12}$ have a spherical morphology and its composites show agglomeration due to presence of magnetic interaction between ferrites nanoparticles. The dielectric study reveals that the real and imaginary parts of complex permittivity of the composites vary with the change in the composition of $Gd_3Fe_5O_{12}$ and $MgFe_2O_4$. For $x = 0.5$, the low dielectric tangent loss ($\tan\delta$) $\sim$ 0.35 with high dielectric constant (ε') $\sim$ 612 was obtained at 1 MHz frequency. This suggests the use of these composites for dielectric substrate antennas. Further, the magnetic property reveals that the magnetic parameter of $Gd_3Fe_5O_{12}$ composites varies by addition of $MgFe_2O_4$, i.e. at $x = 0.5$ and 0.75. The values of microwave operating frequency (ω_m) are 3.5 GHz and 2.5 GHz for $x = 0.5$ and $x = 0.75$, respectively. These values suggest that the composites can be used in S-band.

Keywords: Garnet ferrite; Spinel ferrite; Sol–gel auto-combustion; Composite, Dielectric loss

1. Introduction

The word ferrites are now becoming a brand for many researchers and industrialist, because of its never-ending applications [1, 2]. Ferrites are ceramic oxides. Rather than ferrites, other oxides like ferroelectric metal oxides are used in electric and optical devices as they have good ferroelectric and opto-electrical properties [3]. Transition metal oxides have application in energy storage devices and sensor [4]. But due to good insulating and magnetic properties [5], a large number of researches are still going on complex oxides based on iron. Ferrites have very good insulating and magnetic properties so they are used in many devices like isolators, antennas, switches, filters, magnetic sensors, transformer core, drug carriers, memory devices, filters, microwave absorption, humidity gas sensor, and many more applications [6–11]. The properties of these ferrites are strongly dependent on the microstructure, materials, formation methods, and type of compositions. The advanced functioning composites having controlled magnetic and dielectric property are the challenge for modern physics. Materials showing low loss with good application in the high-frequency range can provide a better option for many communication-based devices.

The ferrites are ferromagnetic materials and are divided into two categories based on their crystal structure—hexagonal (for example hexaferrites) and cubic (for examples spinel and garnet ferrites). Each ferrite has its individual properties. Hexaferrites possess very good magnetic properties and have a higher value of imaginary part of complex permittivity which provides higher losses in the material [12], but many devices require low losses with good magnetic properties where hexaferrites are of no use. Garnet ferrite is soft ferrite that easily gets magnetized and demagnetized [13, 14]. The general formula of garnet ferrite is $R_3Fe_5O_{12}$, where R is rare earth having three sites. The cation of rare earth $\{R^{+3}\}$ is present in dodecahedral site 24c, whereas both 16a octahedral and 24d tetrahedral sites are occupied by iron ions $[Fe^{+3}]$, (Fe^{+3}), respectively.

*Corresponding author, E-mail: srivastava_phy@yahoo.co.in

Published online: 24 May 2022

Bull. Mater. Sci. (2022) 45:248
https://doi.org/10.1007/s12034-022-02810-5

Low dielectric losses and enhanced magnetic property of ErIG(x)/YIG($1-x$) (x = 0.5) composite for antenna applications

ANJORI SHARMA[1], IBRAHIM MOHAMMED[1], SACHIN KUMAR GODARA[2] and AJEET KUMAR SRIVASTAVA[1,*]

[1]Department of Physics, Lovely Professional University, Phagwara 144411, India
[2]Department of Chemistry, Guru Nanak Dev University, Amritsar 143005, India
*Author for correspondence (srivastava_phy@yahoo.co.in)

MS received 7 April 2022; accepted 24 July 2022

Abstract. The composite of yttrium iron garnet (YIG) and erbium iron garnet (ErIG; i.e., ErIG(x)/YIG($1-x$) (x = 0.5)) was prepared by facile mechanical blending method. X-ray diffraction study reveals the pure phase formation of YIG, ErIG and ErIG(x)/YIG($1-x$). Field-emission scanning electron microscope micrographs were used to calculate grain size of the samples. Impedance analyser was used to study dielectric property of YIG, ErIG and ErIG(x)/YIG($1-x$). The composite ErIG(x)/YIG($1-x$) has larger values of dielectric constant and lower values of tangent losses $\sim$0.05 at 1 MHz. Calculated ac conductivity of ErIG(x)/YIG($1-x$) composite is low, which implies its resistive nature. The value of coercivity (H_c) is lesser and value of magnetic saturation (M_s) is high for composite as compare to parent YIG and ErIG. The calculated value of microwave operating frequency (ω_m) for composite was found to be 4.5 GHz. The good dielectric property, low dielectric losses and enhanced magnetic property of ErIG(x)/YIG($1-x$) composite suggest a better option over parent garnet ferrites to be used in microwave devices such as dielectric antennas.

Keywords. Garnet ferrites; composite; dielectric constant; dielectric loss; magnetic property.

1. Introduction

Electrical insulator materials that can be operated in high frequency region, and have least losses are the key ingredient for microwave technology [1]. Ferrites are ferrimagnetic materials that have excellent magnetic and dielectric properties. Based on the structure, ferrites are categorized into two types: hexagonal and cubic ferrites. Hexaferrites have hexagonal structure, whereas spinel and garnet ferrites have cubic structure.

The fascinating properties of garnet ferrites $R_3Fe_5O_{12}$ (R is rare earth) like excellent dielectric, electromagnetic, magnetic, magneto-optical, high resistivity, thermal properties, low magnetic and dielectric losses make them fascinating for new technologies [2–6]. Garnet ferrites are used in many devices like: microwave high frequency devices, phase shifter, oscillator, communication devices, optical electronics devices, isolator, etc. [7–9]. Garnet ferrites are soft by nature. Generally, garnet ferrites have three sites, dodecahedral site 24c occupied by ions of rare earth, octahedral 16a and tetrahedral site 24d occupied by iron ions [10].

Large number of research have been carried out on rare-earth garnet ferrites because of their unique dielectric and magnetic properties. Bhalekar and Singh [1] have prepared Al-doped $Y_{2.8}$ $La_{0.2}$ $Fe_{5-x}O_{12}$ by sol–gel auto-combustion method and found use of the materials in high frequency microwave devices. Mallmann *et al* [11] have worked on $GdIG_xYIG_{1-x}$ composite and found that the composite is appropriate for microwave resonator antenna. Shi *et al* [12] have studied RF permeability and permittivity pattern of Cu/YIG and found that negative permittivity in composites implies that materials are suitable for microwave attenuation and electromagnetic cloaking applications. Soleimani *et al* [13] have studied reflection and transmission coefficient of YIG filled with polyvinylidene fluoride composite and found that with increase of YIG in polymer, reflection as well as transmission coefficient increases. Fechine *et al* [14] have studied $GdIG_x$ YIG_{1-x} composite for miniaturize magneto-dielectric antenna applications. Zheng *et al* [15] studied the dielectric property of erbium iron garnet (ErIG; $Er_3Fe_5O_{12}$) prepared by solid-state reaction method and found higher value of dielectric constant.

Based on the above discussion we have found that yttrium iron garnet (YIG) is known for very good thermal stability, low dielectric losses and narrow ferromagnetic resonance [16]. Whereas ErIG possesses very good dielectric property. In this research work, we have reported the improved morphological, dielectric and magnetic properties of the composite ErIG(x)/YIG($1-x$) (x = 0.5). YIG is known for its least losses and also its dielectric constant is

Published online: 13 December 2022

Materials Today: Proceedings xxx (xxxx) xxx

Contents lists available at ScienceDirect

Materials Today: Proceedings

journal homepage: www.elsevier.com/locate/matpr

Effect of Y^{3+}, Bi^{3+}, La^{3+} substitution on structural, optical and magnetic properties of gadolinium iron garnets

Anjori Sharma [a], Sachin Kumar Godara [b], A.K. Srivastava [a,*]

[a] Department of Physics, Lovely Professional University, Phagwara, Punjab 144411, India
[b] Department of Chemistry, Guru Nanak Dev University, Amritsar, Punjab 143005, India

ARTICLE INFO

Article history:
Received 17 August 2021
Received in revised form 10 September 2021
Accepted 14 September 2021
Available online xxxx

Keywords:
Garnet ferrites
Substitution
Band gap
Coercivity
Magnetic saturation
Ultra high frequency

ABSTRACT

The samples of $Y_{0.2}Bi_{0.2}La_xGd_{2.6-x}Fe_5O_{12}$ (x = 0, 0.2 and 0.4) were successfully prepared by sol–gel auto combustion method. X-ray diffraction (XRD) study reveals that garnet phase is dominant in all prepared samples. The crystallite size of the samples is in 33–54 nm range. The crystallite size varies with varying La^{+3+}substitution in the samples. The calculated grain size of the samples is in 0.100 to 0.116 μm range. Energy dispersive X-ray (EDX) mapping confirms the presence of all elements in the formed samples. From Ultraviolet– Visible (UV–VIS) spectroscopy it has been found that the samples have wide band gap (3.7 eV to 3.9 eV) which suggests that such materials can be operated in higher temperature, voltage and frequency. This makes these materials suitable in military application. From vibrating sample magnetometer (VSM) it has been clear that addition of La^{3+} changes the value of coercivity (H_c) and magnetic saturation (M_s) which make these materials suitable for switching devices and for antenna applications. The value of operating microwave frequency (ω_m) suggests the use of such materials in devices operated in Ultra High frequency region.

Selection and peer-review under responsibility of the scientific committee of the 2nd International Conference on Functional Material, Manufacturing and Performances

1. Introduction

The vast number of applications of Ferrites make them very important in this era of technology [1–5]. Ferrites have good magnetic, optical and insulating properties. So, these materials are used in, antennas, isolators, Faraday rotation devices, switches, military applications, magnetic sensor, drug carriers, memory devices, microwave absorption, humidity gas sensor and many more [6–11]. Ferrites are ferrimagnetic material and categorised into two types based on their structure. Hexagonal ferrites possess hexagonal shape, garnet ferrite and spinel ferrite having cubic structure.

Among these all-ferrites garnet ferrites are very fascinating materials. Garnet ferrites possess excellent magnetic, magneto-optical, dielectric, electromagnetic and thermal properties along with low magnetic and dielectric losses [12–16]. These properties make garnet ferrites more important than spinel and hexagonal ferrite. These ferrites have large number of applications such as in communication devices, phase shifter, oscillator, optical isolator, electronics devices etc [17,18]. Garnet ferrites are represented by chemical formula $R_3Fe_5O_{12}$, where R is any rare earth for example Y^{3+}, Gd^{3+}, Dy^{3+} etc. Garnet ferrites have *Ia3d* space group. The magnetic property of the garnet ferrite is depending upon the arrangement of ions in lattice site. There are three sites present in garnet structure named as dodecahedral site 24c, octahedral site 16a and tetrahedral site 24d. Rare earth cation $\{R^{3+}\}$ occupies dodecahedral site because of its large size. Two out of five iron ion $[F^{3+}]$ occupies octahedral site and three out of five iron ion (F^{3+}) occupies tetrahedral site. These cations present in the garnet ferrite interact with each other through oxygen anion. This further cause superexchange interaction which is deciding factor of magnetic moment in garnet ferrite [19]. The magnetic, structural and optical properties of garnet ferrites depend upon composition, sintering temperature, microstructure and method of preparation.

Many researchers have studied the effect of substitution in different site on garnet ferrite properties. Cheng et al. [20,21] studied the effect of La^{3+} substitution in YIG and noticed maximum value of saturation magnetization at x = 0.2. Cheng et al. [22] studied the effect of Dy^{3+} in YIG and noticed that with substitution, single

* Corresponding author.
E-mail address: srivastava_phy@yahoo.co.in (A.K. Srivastava).

https://doi.org/10.1016/j.matpr.2021.09.234
2214-7853/
Selection and peer-review under responsibility of the scientific committee of the 2nd International Conference on Functional Material, Manufacturing and Performances

Materials Today: Proceedings xxx (xxxx) xxx

Contents lists available at ScienceDirect

Materials Today: Proceedings

journal homepage: www.elsevier.com/locate/matpr

Influence of Mn^{2+}-substitution on the structural, morphological and magnetic properties of Co_2Y strontium hexaferrites

Ibrahim Mohammed [a], J. Mohammed [b], Anjori Sharma [a], Hamnesh Mahajan [a], Amarjeet Kaur [c], A.K. Srivastava [a,*]

[a] Department of Physics, School of Physical Sciences and Chemical Engineering, Lovely Professional University, Phagwara 144411, Punjab, India
[b] Department of Physics, Faculty of Science, Federal University Dutse, P.M.B. 7156, Dutse, Jigawa State, Nigeria
[c] Central Instrumentation Facility, Lovely Professional University, Phagwara 144411, Punjab, India

ARTICLE INFO

Article history:
Available online xxxx

Keywords:
Y-type hexaferrites
Coercivity
Saturation magnetization
Remnant magnetization
Morphology

ABSTRACT

This research focus on using sol-gel auto combustion method to synthesize Co_2Y strontium hexaferrite with chemical composition $Sr_2Mn_xCo_{2-x}Fe_{12}O_{22}$ (x = 0.0, 0.5, 1.0). Samples were calcinated at 1150 for 6 h. The XRD analysis revealed a single crystalline phase Co_2Y strontium hexaferrites with the absence of secondary phase or impurity. Values of lattice parameters as well as unit cell volume rise with addition of Mn^{2+}. The emergence of two peaks at 422 and 580 cm^{-1} in FTIR analysis suggests the formation of hexaferrites. The morphological analysis show an agglomerated network of grains which is caused by magnetic interaction. EDX spectra shows the entire host as well as substituted elements, this confirm the purity and stoichiometry of the prepared Co_2Y strontium hexaferrites samples. Magnetic parameters: coercivity, saturation magnetization, squareness ratio as well as remnant were calculated using M-H hysteresis loop obtained from the VSM.

Selection and peer-review under responsibility of the scientific committee of the International Conference on Recent Advances in Mechanical Engineering and Nanomaterials.

1. Introduction

Magnetic materials are widely employed in technological and industrial applications, including but not limited to the automobile sector, electronics, data storage and microwave (MW) devices [1]. Hexaferrites are among the most important materials nowadays due to the low cost, ease of manufacture, and fascinating electrical and magnetic properties [2]. Many researchers are interested in Y-type hexaferrites with planar magnetic anisotropy because they have the advantage of having a higher magnetic permeability in the GHz frequency range over other hexagonal ferrites with uniaxial magnetic anisotropy [3]. Also, because they develop good magnetic characteristics in the hyper frequency region when sintered at low temperature, Y-type hexaferrites are considered the best choice [4]. Crystalline structure of the Y-type hexagonal ferrites was said to be an alternating stacking of the S and T blocks along c-axis with space group R-3m [5–9]. Based on the relative direction of magnetic moments in each layer, two distinct magnetic blocks may be described: small (S) and large (L) magnetic moment and within each block, the magnetic moments of the Fe ions were organized in a collinear manner [10]. Two of Fe_3O_4 formula units formed S block, which has a spinel structure with 2-tetrahedral and also 4-octahedral cation sites [11]. Magnetic as well as structural properties of Y type hexaferrite are substantially influenced by a number of parameters, including sintering duration, chemical composition, ingredient purity, and substitution amount [12–14]. Several researchers have improved the magnetic as well as electric properties of Y-type nanohexaferrites to make them appropriate for microwave applications, including dielectric permittivity, dielectric losses, saturation magnetization, coercivity, and so on [4]. In hyper-frequency, Y-type hexaferrite has good magnetic characteristics and it is expected to address the demand for soft magnetic materials in high frequency chip components [15]. This research work aimed to study influence of Mn^{2+} on morphological and also magnetic properties of $Sr_2Mn_xCo_{2-x}Fe_{12}O_{22}$ (x = 0.0, 0.5, 1.0). The produced samples were analysed by XRD, FESEM/EDX, and VSM. Furthermore, this composition has never been studied before.

2. Material and method

Analytical grade chemicals from LOBA Chemie Pvt Ltd: strontium nitrate, $[Sr(NO_3)_2{\cdot}6H_2O]$, Ferric nitrate, $[Fe(NO_3)_2{\cdot}9H_2O$

* Corresponding author.
E-mail address: srivastava_phy@yahoo.co.in (A.K. Srivastava).

https://doi.org/10.1016/j.matpr.2021.12.514
2214-7853/
Selection and peer-review under responsibility of the scientific committee of the International Conference on Recent Advances in Mechanical Engineering and Nanomaterials.

Chinese Journal of Physics 78 (2022) 377–390

Contents lists available at ScienceDirect

Chinese Journal of Physics

journal homepage: www.sciencedirect.com/journal/chinese-journal-of-physics

Structural, morphological, optical, magnetic, and microwave properties of La^{3+}- Mn^{2+} substituted Zn_2-Y-type barium-strontium hexaferrite

Ibrahim Mohammed [a], J. Mohammed [b], Anjori Sharma [a], Hamnesh Mahajan [a], Shweta Sharma [a], Manisha Thakur [a], Amarjeet Kaur [c], Neha Aggarwal [d], A.K. Srivastava [a,*]

[a] Department of Physics, School of Physical Sciences and Chemical Engineering, Lovely Professional University, Phagwara-144411, Punjab, India
[b] Department of Physics, Faculty of Science, Federal University Dutse, P.M.B. 7156, Dutse, Jigawa, Nigeria
[c] Central Instrumentation Facility, Lovely Professional University, Phagwara-144411, Punjab, India
[d] Department of Electronics Technology, Guru Nanak Dev University, Amritsar, 143005, India

ARTICLE INFO

Keywords:
Y-type hexaferrites
UV-Vis spectroscopy
M-H hysteresis
EMI shielding

ABSTRACT

This experimental study examines the effects of the La^{3+}-Mn^{2+} substitution on structural, morphological, optical, magnetic, and microwave properties of $Ba_{1.7-x}Sr_{0.3}La_xZn_2Fe_{12-x}Mn_xO_{22}$ (x = 0.0, 0.1, 0.2) using sol-gel auto combustion. We characterize the as-prepared nanoparticles structurally using XRD and FTIR, and the morphology is determined using FESEM micrographs. Elemental analysis (EDX) verifies the presence of the entire experimental elements. The optical band gap was determined using UV Visible spectroscopy with the help of Tauc theory. VSM and VNA analyses determine the magnetic and microwave properties, respectively. The small coercivity and small area under the hysteresis loop show that the materials are soft magnetic. The microwave properties of the prepared material were affected by the grain size and saturation magnetization. A single absorption peak from the reflection loss graph and high shielding effectiveness of the synthesized nanoparticles indicates that the material may have the potential as an effective EMI shielding material in Ku-band.

1. Introduction

Wireless communication technology has steadily advanced in the information era, and electronic gadgets nearly surround every part of human existence, bringing in overwhelming electromagnetic waves (EMW). Excessive electromagnetic waves pollute the environment and potentially endanger human health [1–5]. Although electromagnetic wave has provided enormous advantages to humanity, the devastation it has caused is immeasurable [6]. There are significant efforts to develop high-performance EMW absorbers to prevent the harm caused by EM pollution to individuals and the environment while also meeting the criteria for electronic security and defensive stealth [7,8]. Due to their wide range of applications and great absorption capacity, EMW absorbers are protective agents against EMW concerns since they can convert EMW to thermal energy and subsequently dissipate it [9–12]. Thus, to convert EMW energy to thermal energy, various absorbers with superior EM wave attenuation performance were investigated [13]. In general,

* Corresponding author.
E-mail address: srivastava_phy@yahoo.co.in (A.K. Srivastava).

https://doi.org/10.1016/j.cjph.2022.06.025
Received 11 April 2022; Received in revised form 8 June 2022; Accepted 28 June 2022
Available online 30 June 2022

J Mater Sci: Mater Electron

Structural, morphological, and electrochemical investigation of $Mn_{0.3}Co_{0.2}Zn_{0.5}Fe_2O_4$-polyaniline nanocomposite for supercapacitor application

Hamnesh Mahajan[1], Shammi Kumar[2], Anjori Sharma[1], Ibrahim Mohammed[1], Manisha Thakur[1], Simrandeep Kour[1], Amarjeet Kaur[3], and Ajeet Kumar Srivastava[1,*]

[1] Department of Physics, Lovely Professional University, Phagwara, Punjab 144411, India
[2] Department of Physics, GCET, Chak Bhalwal, Jammu 181122, India
[3] Central Instrumentation Facility, Lovely Professional University, Phagwara, Punjab 144411, India

Received: 1 June 2022
Accepted: 12 October 2022

ABSTRACT

The present research deals in preparing $Mn_{0.3}Co_{0.2}Zn_{0.5}Fe_2O_4$ (spinel ferrite) by sol–gel procedure, polyaniline (PANI) by chemical oxidative method, and $Mn_{0.3}Co_{0.2}Zn_{0.5}Fe_2O_4$-PANI nanocomposite by physical blending method. X-ray diffraction (XRD) study affirms the formation of $Mn_{0.3}Co_{0.2}Zn_{0.5}Fe_2O_4$-PANI nanocomposite owing to the appearance of two different types of peaks: sharp $Mn_{0.3}Co_{0.2}Zn_{0.5}Fe_2O_4$ peaks, and broader PANI peaks. Fourier transform infrared spectroscopy (FTIR) of $Mn_{0.3}Co_{0.2}Zn_{0.5}Fe_2O_4$-PANI nanocomposite shows all characteristic vibrational bands, which are observed in the $Mn_{0.3}Co_{0.2}Zn_{0.5}Fe_2O_4$ and PANI spectra. Field emission scanning electron microscopy (FESEM) micrographs have been employed for measuring the average particle size by using ImageJ software. The encapsulation of the synthesized ferrite nanoparticle with the PANI matrix is exhibited by the FESEM micrograph of $Mn_{0.3}Co_{0.2}Zn_{0.5}Fe_2O_4$-PANI nanocomposite. The electrochemical activity of the novel $Mn_{0.3}Co_{0.2}Zn_{0.5}Fe_2O_4$-PANI nanocomposite is manifested to be higher as compared to their counterparts on account of synergistic impact, continual movement of electrons toward the electrode, and multiple redox reactions. AQ1

1 Introduction

The tremendous upgrades in ecological contamination and the ineluctable lack of fossil fuels are compelling researchers to foster perfect and economical energy storage gadgets [1]. At the present juncture, the most used energy storage gadgets are batteries, fuel cells, conventional capacitors, and supercapacitors [2]. The usage of batteries and fuel cells for high-energy applications is principally a direct result of their higher energy density. Nevertheless, it has the deficiencies of significant expense, short cycle life,

A2 Address correspondence to E-mail: srivastava_phy@yahoo.co.in

https://doi.org/10.1007/s10854-022-09335-x

Journal : 10854 - Large 10854 | Dispatch : 29-10-2022 | Pages : 14
Article No. : 9335 | LE | TYPESET
MS Code : JMSE-D-22-02151R1 | CP | DISK

Journal of Sol-Gel Science and Technology
https://doi.org/10.1007/s10971-022-06022-5

ORIGINAL PAPER: NANO-STRUCTURED MATERIALS (PARTICLES, FIBERS, COLLOIDS, COMPOSITES, ETC.)

Effect of sintering temperature on structural, morphological, magnetic, and electrochemical properties of $Mn_{0.3}Co_{0.2}Zn_{0.5}Fe_2O_4$ Ferrite

Hamnesh Mahajan[1] · Shammi Kumar[2] · Anjori Sharma[1] · Ibrahim Mohammed[1] · Manisha Thakur[1] · Amarjeet Kaur[3] · A. K. Srivastava[1]

Received: 22 August 2022 / Accepted: 13 December 2022

Abstract

The sol-gel methodology was exploited for the production of $Mn_{0.3}Co_{0.2}Zn_{0.5}Fe_2O_4$ ferrite nanoparticles, at different sintering temperatures (750, 950, and 1150 °C). The nanometer size crystallites were evaluated utilizing the Debye Scherrer formulae in the X-ray diffraction (XRD) study. The two bands manifested in Fourier transform infrared (FTIR) spectra near 600 cm^{-1} (tetrahedral site) and 400 cm^{-1} (octahedral site) ratify the formation of spinel structure for all sintering temperatures. Field emission scanning electron microscopy (FESEM) micrographs estimate the average size of the particle by using ImageJ software and reveal the agglomerated grains, which are inhomogeneous in shape and size. Energy dispersive X-ray (EDX) study confirms the stoichiometry and composition of the synthesized specimens. For an enhancement in the sintering temperature, the enhancement in the saturation magnetization was perceived in the magnetic studies by using a vibrating sample magnetometer (VSM). With regard to all incorporated samples, the squareness ratio was assessed to be under 0.5 which assimilates to a multi-domain structure. For all scan rates and current densities, the prepared $Mn_{0.3}Co_{0.2}Zn_{0.5}Fe_2O_4$ (1150 °C) had the higher value of the specific capacitance as portrayed through the electrochemical study.

✉ A. K. Srivastava
srivastava_phy@yahoo.co.in

[1] Department of Physics, Lovely Professional University, Phagwara, Punjab 144411, India

[2] Department of Physics, GCET, Chak Bhalwal, Jammu 181122, India

[3] Central Instrumentation Facility, Lovely Professional University, Phagwara, Punjab 144411, India

Published online: 31 December 2022

Effect of sintering temperature on the structural, dielectric and magnetic properties of garnet-spinel ferrite composites for the use in L-band devices

Journal:	*Materials Performance and Characterization*
Manuscript ID	MPC-2022-0084.R1
Manuscript Type:	Technical Manuscript
Date Submitted by the Author:	n/a
Complete List of Authors:	Sharma, Anjori; Lovely Professional University Mahajan, Hamnesh; Lovely Professional University Mohammed, Ibrahim; Lovely Professional University Godara, Sachin; Guru Nanak Dev University Sinha, Subhojyoti; Lovely Professional University Srivastava, Ajeet; Lovely Professional University,
Keywords:	Garnet ferrite, Dielectric constant, Temperature, Sol-gel auto-combustion, Spinel ferrite
ASTM Committees and Subcommittees:	A06.02 Material Specifications < A06 Committee on Magnetic Properties
Abstract:	Herein we have reported the influence of sintering temperature on the structural, dielectric and magnetic properties of garnet ferrite composite. The composite of gadolinium iron garnet and magnesium ferrite (Gd3Fe5O12(x)/MgFe2O4(1-x) at x=0.75)) was synthesized by the mechanical blending method and then sintered at 900°C and 1300°C. X-ray diffraction (XRD) study suggests that both the phases of ferrites are present in the composites without any impurities. Field emission scanning electron microscopy (FESEM) images indicate the change in microstructure with sintering temperature. Dielectric study reveals that the sample sintered at 900°C has higher value of dielectric constant (ε'r). The grain and grain boundary contributions in the composites have been elucidated by fitting the Nyquist plot with an electrical equivalent circuit. The extracted grain boundary resistance found to be increased from 64.7 MΩ to 2 ×1018 MΩ and grain resistance has been decreased to 1.78×10-22 Ω from 293.5 Ω with increase in temperature. From the M-H loop we have calculated the anisotropy constant (Keff)= 770, anisotropy field (Ha)=168.5 Oe, SQR= 0.07 and microwave operating frequency (ωm)= 2GHz for the sample sintered at 1300 °C. These parameter values suggest the potential use of these composites for microwave devices operating in the L band.

Applied Physics A

Investigation of miniaturization parameter and losses of YIG/MgCdCoFe composites for antenna applications in the Ku band

--Manuscript Draft--

Manuscript Number:	
Full Title:	Investigation of miniaturization parameter and losses of YIG/MgCdCoFe composites for antenna applications in the Ku band
Article Type:	Regular papers
Corresponding Author:	Ajeet Kumar Srivastava, Ph.D. Lovely Professional University Phagwara, Punjab INDIA
Corresponding Author Secondary Information:	
Corresponding Author's Institution:	Lovely Professional University
Corresponding Author's Secondary Institution:	
First Author:	Anjori Sharma
First Author Secondary Information:	
Order of Authors:	Anjori Sharma
	Hamnesh Mahajan
	Ibrahim Mohammed
	Amarjeet Kaur
	Neha Aggarwal
	Sukhleen Bindra Narang
	Subhojyoti Sinha
	Ajeet Kumar Srivastava, Ph.D.
Order of Authors Secondary Information:	
Funding Information:	
Abstract:	Herein we report the synthesis and enhanced magnetodielectric properties of Y3Fe5O12(x) and Mg0.4Cd0.4Co0.2Fe2O4 (1-x) (x = 0.3, 0.6, 0.9) composites for miniaturized antenna applications. X-ray diffraction confirms that the spinel ferrite phase dominates over the garnet ferrite phase for the x=0.3 composites whereas it is the opposite for x=0.6 and x=0.9 composites. The grains are spherical for the garnet phase and cubic for the spinel ferrite phase. Magnetic study reveals that the composite with x = 0.3 has the highest coercivity value of 99.2 Oe and magnetization value of 41 emu/g. The composite with x = 0.3, also has the highest permittivity value of ~19.5, permeability value of ~ 2.8 but low dielectric and magnetic losses of ~0.009 and ~0.002 respectively. These low losses and a high miniaturization factor of ~7.2 at 14.5 GHz make it a potential candidate for high-speed antenna applications.